Development and Implementation of Various Speed Controllers for Wide Speed Range Operation of IPMSM Drive

By

Md. Muminul Islam Chy.

A thesis submitted in partial fulfilment of the requirement for the of Masters of Science

at

Lakehead University

Thunder Bay, Ontario

July 2007

Your file Votre référence
ISBN: 978-0-494-31850-8
Our file Notre référence
ISBN: 978-0-494-31850-8

Abstract

Despite many advantageous features of interior permanent magnet synchronous motor (IPMSM), the precise speed control of an IPMSM drive becomes a complex issue due to nonlinear coupling among its winding currents and the rotor speed as well as the nonlinearity present in the electromagnetic developed torque due to magnetic saturation of the rotor core particularly, at high speeds (above rated speed). Fast and accurate response, quick recovery of speed from any disturbances and insensitivity to parameter variations are some of the important characteristics of high performance drive system used in robotics, rolling mills, traction and spindle drives. The conventional controllers such as PI, PID are sensitive to plant parameter variations and load disturbance. For the purpose of obtaining high dynamic performance, recently researchers developed several non-linear as well as intelligent controllers. Most of the reported works on controller design of IPMSM took an assumption of d-axis stator current (i_d) equal to zero in order to simplify the development of the controller. However, with this assumption it is not possible to control the motor above the rated speed and the reluctance torque of IPMSM can not be utilized efficiently. Furthermore, this assumption leads to an erroneous result for motor at all operating conditions. In this thesis, some controllers are developed for the IPMSM drive system incorporating the flux-weakening technique in order to control the motor above the rated speed. A detailed analysis of the flux control based on various operating regions is also provided in this thesis.

In order to get the optimum efficiency, an adaptive backstepping based nonlinear control scheme incorporating flux control for an IPM synchronous motor drive is

developed in this thesis. The system parameter variations as well as field control are taken into account at the design stage of the controller. Thus, the proposed adaptive nonlinear backstepping controller is capable of conserving the system robustness and stability against all mechanical parameters variation and external load torque disturbance. To ensure stability the controller is designed based on Lyapunov's stability theory.

A novel fuzzy logic controller (FLC) including both torque and flux control is also developed in this work. The proposed FLC overcomes the unknown and nonlinear uncertainties of the drive and controls the motor over a wide speed range. For further improvement of the FLC structure, the membership function of the controller is tuned online. An integral part of this work is directed to develop an adaptive-network based fuzzy interference system (ANFIS) based neuro fuzzy logic controller. In this work, an adaptive tuning algorithm is also developed to adjust the membership function and consequent parameters.

In order to verify the effectiveness of the proposed IPMSM drive, at first simulation model is developed using Matlab/Simulink. Then the complete IPMSM drive incorporating various control algorithms have been successfully implemented using digital signal processor (DSP) controller board-DS1104 for a laboratory 5 hp motor. The effectiveness of the proposed drive is verified both in simulation and experiment at different operating conditions. The results show the robustness of the drive and it's potentiality to apply for real-time industrial drive application. This thesis also provides through knowledge about development and various speed real-time applications of controllers for IPMSM drive, which will be useful for researchers and practicing engineers.

Acknowledgements

I would like to acknowledge and thank those people who have supported and helped me in the preparation of this thesis. Dr M. N. Uddin, my thesis supervisor, has been vital in the completion of this thesis and success of the project. He always endowed me with the strength to finish this work. This work might not be possible without his guidance. I am also indebted to other members in my department through the numerous discussion and encouragements.

I am also grateful to Manfred Klein, technologist of Electrical Engineering for his help in installing the experimental set up in power electronics laboratory. I want to give many thanks to other graduate students and staff of my department at Lakehead University. Numerous people and innumerable instances, which I cannot enumerate in a single page, have helped me to accomplish this project. My parents and friends have always been patient and supportive to me, understanding and allowing me to be 'workaholic'. I would like to appreciate all the circumstances around me, which have been so generous to this humble being.

Contents

List of Symbols

V_a	Maximum phase voltage amplitude
I_a	Maximum line current amplitude
v_a, v_b, v_c	a, b and c phase voltages
v_a^*, v_b^*, v_c^*	command a, b and c phase voltages
i_a, i_b, i_c	a, b and c phase currents
v_d, v_d^r	d-axis voltage
v_q, v_q^r	q-axis voltage
i_d, i_d^r	d-axis current
i_q, i_q^r	q-axis current
i_q^*	q-axis command current
R	stator resistance per phase
L_d	d-axis inductance
L_q	q-axis inductance
L_l	Leakage inductance
L_{md}	d-axis magnetizing inductance
L_{mq}	q-axis magnetizing inductance
ω_s	Stator angular frequency
ω_r	rotor speed
ω_r^*	motor command speed

e	Error between actual and command speed
Δe	Change of speed error
Θ_r	rotor position
p	differential operator *d/dt*
P	number of pole pairs
T_e	developed electromagnetic torque
T_L	load torque
J	rotor inertia constant
B_m	friction damping coefficient
ψ	magnetic flux linkage
V_B	DC bus voltage for the inverter

List of Acronyms

AB	Adaptive Backstepping
ALRM	Axially laminated reluctance motor
ANFIS	Adaptive-network-based fuzzy inference system
ANN	Artificial neural network
AOC	Analog to digital converter
BJT	Bipolar junction transistor
BLDC	Brushless DC
DSP	Digital signal processor
EKF	Extended Kalman Filter
FBFN	Fuzzy basis function network
FLC	Fuzzy logic controller
FW	Flux weakening
GFLC	Genetic based fuzzy logic controller
HPD	High Performance Drive
HPVSD	High performance variable speed drive
IGBT	Inverted gate bipolar transistor
IM	Induction motor
IPMSM	Interior Permanent Magnet Synchronous Motor

LCR	Linguistic control rule
MIMO	Multi-input-multi-output
MOSFET	Metal-oxide-semiconductor field-effect transistor
MRAC	Model Reference Adaptive Controller
MTPA	Maximum torque per ampere
NNC	Neural network controller
NFC	Neuro-fuzzy logic controller
OLS	Orthogonal least square
PDF	Pseudo-derivative-feedback
PI	Proportional Integral
PID	Proportional Integral Derivative
PM	Permanent Magnet
PMSM	Permanent Magnet Synchronous Motor
PWM	Pulse Width Modulation
RBFN	Radial basis function network
RTI	Real-time Interface
SISO	Single-input-single-output
SMC	Sliding Mode Control
STR	Self tuning regulator
TI	Texas Instruments
TSK	Takagi-Sugeno-Kang
VSC	variable structure controller
VSI	Voltage Source Inverter

Chapter 1

Introduction

1.1 Electric Motors

Once electric power became available, researchers were seeking a mean to use the energy in the application to rotate an object. Then the researchers developed different kinds of electric motors to achieve their requirements. One of the first electromagnetic rotary motors was consisted of a free-hanging wire dipping into a pool of mercury. A permanent magnet was placed in the middle of the pool of mercury. When a current was passed through the wire, the wire rotated around the magnet, showing that the current gave rise to a circular magnetic field around the wire. This is the simplest form of a class of electric motors called homopolar motors. A later refinement is the Barlow's Wheel. Earlier electric motors were used only in rail transportation. Nowadays the electric motors have been utilized starting from various industrial drives, tools, etc. to household appliances.

The modern dc motor was invented in 1873. The Gramme machine was the first industrially useful electric motor; earlier inventions were used as toys or laboratory

curiosities. Due to the decoupled nature of the field and armature, control of dc motor is relatively easy and hence utilized for high performance variable speed drive (HPVSD) applications for long time. However, these days dc motor is not widely used as it was in the past due to some of its disadvantages such as, limited range of operation, power loss in the field circuit, lack of overload capability, lack of ruggedness, high weight to power ratio, low torque density and frequent maintenance requirement as well as high cost due to brushes and commutators [1]. Fast and precise speed response, quick recovery of speed from any disturbances and parameter insensitive, robust in variable speed domain and maintenance free operations are the main concern for HPVSD. In order to overcome the disadvantages of dc motors, researchers developed ac motors such as induction motors (IM) and synchronous motors (SM). As compared to dc motor the advantages of IM are simple and rugged construction, reliability, low cost, low maintenance and direct connection to ac power source [2]. These days IM has been used as workhouse in industry. However, they have some limitations associated with their use in HPVSD applications. One of the limitations of IM is that it always operates at lagging power factor as the rotor induced current is supplied from the stator side. Another problem of IM is that it always runs at a speed lower than the synchronous speed and rotor quantities depend on slip speed. Thus the control of this motor is very complex. Furthermore, the real-time implementation of the IM drive depends on sophisticated modeling and estimation of machine parameters with complex control circuitry. Some other disadvantages are low torque density and the required inverter over sizing [2-3]. The disadvantages of IM encouraged researchers to develop SM.

In SM, the rotor coils fed by a field current from a separate dc source to create a continuous magnetic field. The rotating magnetic field attracts the rotor field. So the rotor will rotate in synchronism with the rotating magnetic field. Hence its control is less complex and it removes the slip power loss. But still there are some disadvantages exist such as the requirement of extra power suply, slip ring and brush at the rotor side. Permanent magnet synchronous motor (PMSM) developed to triumph over some drawbacks of conventional wire-wound SM. In PMSM, extra power supply, slip ring brush and the power loss due to excitation is eliminated.

It is proved that PMSM gives more torque density than the IM and the inverter size is also greatly reduced within the constant torque and power speed range [4]. The permanent magnet (PM) machine can be suitable for field weakening if it is properly designed. The interior permanent magnet synchronous motor (IPMSM) is a kind of PM motors in which these kinds of anisotropy characteristics are incorporated. The IPMSM is smaller, lighter and compact as compared to the conventional ac motor. Motor air flow of IPMSM is reduced as compared to IM which means that the noise level of IPMSM is significantly lower than that of IM. There is no copper wear on the rotor of the motor. So it gets rid of excessive shaft heating and doubling bearing grease packing life. As shown in the product comparison between IPMSM and IM in Fig.1 for Yaskawa Electric Inc. product (15 kw, 200 V, 1750 min), one can easily understood that efficiency is improved and inverter size is reduced by using IPMSM instead of IM [5]. Due to these advantageous features of IPMSM, researchers have looked into the application of this kind of motors for HPVSD.

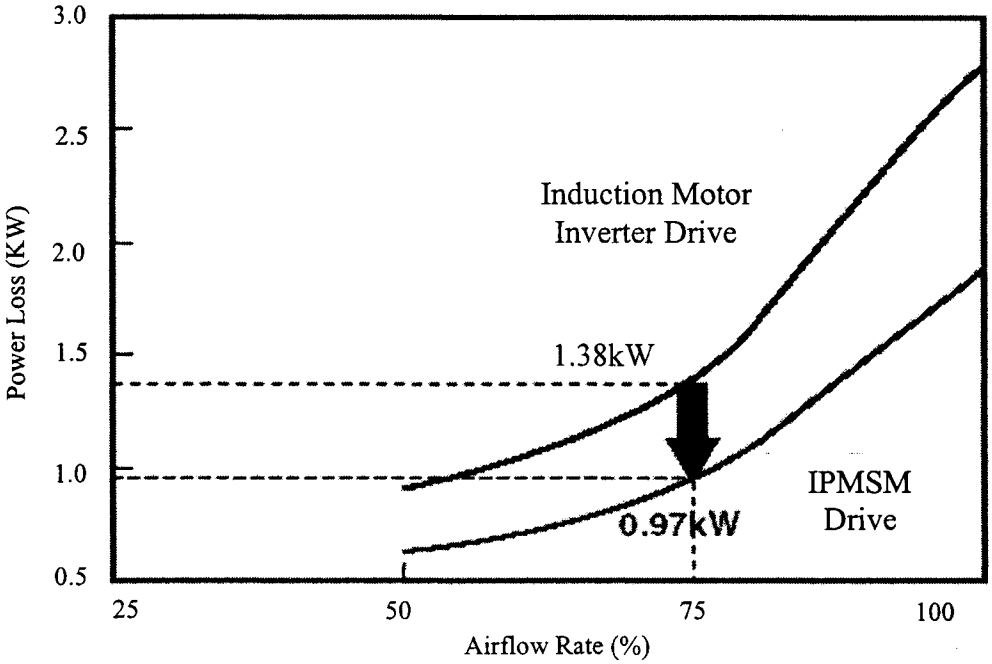

Fig.1(a): Comparison of power loss of IPMSM inverter drive with Induction motor inverter drive at different airflow rate.

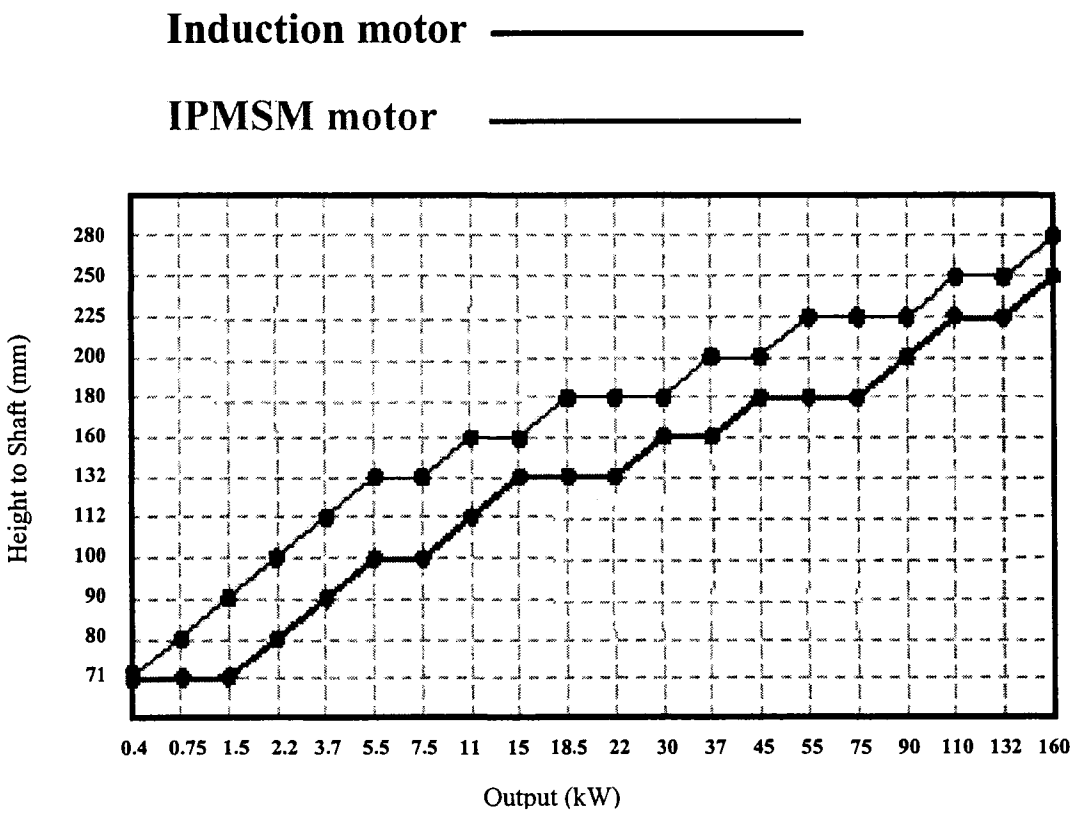

Fig.1 (b): Comparison of size of IPMSM with IM of different rating.

1.2 Permanent magnet synchronous motor

A PMSM is exactly similar to a conventional SM with the exception that the field winding and dc power supply is replaced by PMs. The PMSM has advantages of high torque to current ratio, large power to weight ratio, high efficiency, high power factor, low noise and robustness etc. Current improvement of PM motors is directly associated to the recent achievement in high energy permanent magnet material. Ferrite and rare earth/cobalt alloys such as neodymium-boron-iron (Nd-B-Fe), samarium-cobalt (Sm-Co) are widely used as magnetic materials. Rare earth/cobalt alloys have a high residual induction and coercive force than the ferrite materials. But the cost is also high. So rare earth magnets are usually used for HPVSD as high torque to inertia ratio is attractive. Depending on the position of PM, there are different types of PMSM which are discussed in the following subsection.

1.2.1 Classifications of PMSM

The classification for PMSM can be done based on some different principle such as design of the motor, driving power circuit configuration, position of magnet in the rotor, current regulation and the principal motor control method. The performance of a PMSM drive varies with the magnet material, placement of the magnet in the rotor, configuration of the rotor, the number of poles, EMF waveform and the presence of dampers on the rotor [6-7]. Depending on magnet configuration, it can be categorized into three divisions.

(a) Surface mounted PM motor: In this type of PM motor, the PMs are typically glued or banded with a non-conducting material to the surface of the rotor core as shown in Fig.2 (a). This type of motor is not suitable for high speed.

(b) Inset type PM motor: In this type of PM motor, the PMs are typically glued directly or banded with a non-conducting material inside the rotor core as shown in Fig.2 (b). This type of motor is not suitable for high speed.

(c) Interior type PM motor: In this type of PM motor, the PMs are imbedded in the interior of the rotor core as shown in Fig.2 (c). This is the most recently developed method of mounting the magnet. Interior magnet designs offer q-axis inductance larger than the d-axis inductance. The saliency makes possible a degree of flux weakening, enabling operation above nominal speed at constant voltage and should also help to reduce the harmonic losses in the motor. This kind of PM motor has the same advantages of inset PM motor as well as the advantages of mechanical robustness and a smaller magnetic air gap. Therefore the interior magnet design is better suited to applications where operation in the voltage limited high speed region is desired.

1.3 Literature review

Over the last few decades, semiconductor and microprocessor technologies have made evolutionary advancements on the design and control of electric motors. Low-cost microcontrollers for motor control applications encourage researchers to work with different techniques to implement high performance drive (HPD) in motion and speed control applications. The dynamics and control of ac drives are complex and their complexity increases for higher performance requirements. In addition, DSPs and their

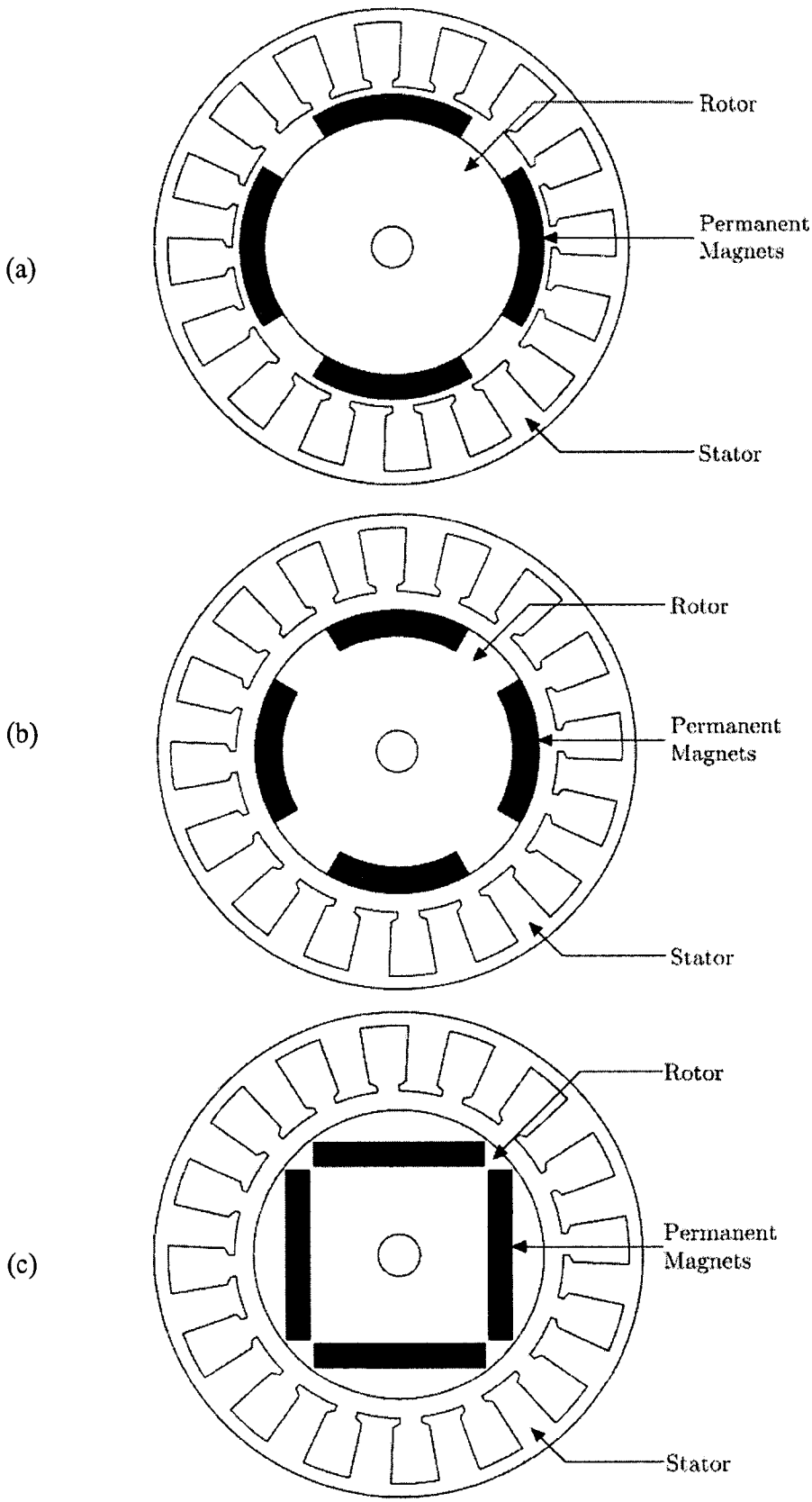

Fig.2: cross section of (a) surface mounted (b) inset and (c) interior type PM motor.

programming tools cater to determinism and predictability. So the researchers are working to implement their HPD using advanced semiconductor chips. Although straightforward open-loop volt/hertz (v/f) control method was employed for a long time in low performance drives. It is not a good choice for a HPD because of poor speed control accuracy, limitation in torque control and worse performance in any disturbance.

The scalar controller uses the magnitude of the current to vary the machine voltage which is developed with some transient frequency compensation included in the control loop. Scalar controller exhibits poor transient response. Boys and Walton [8] proposed a scalar control technique for inverter driven motors. It causes the air gap flux to vary over a wide range which is proportional to the load. In this work authors estimated the torque and implemented the speed controller based on the magnitude of the motor current. They developed the control algorithm based on the steady state motor model. However, the steady state motor model is not sufficient to handle the dynamic uncertainties as the nonlinearity presents in motor model. This causes slow responses which are unacceptable for HPD applications. Moreover, scalar control has limitations at the high and low ends of a motor's speed range.

To operate a polyphase motor at peak efficiency and at the desired torque, researchers have been utilizing closed loop vector control method, which uses feedback from the motor to maintain a desired speed or torque output. The principle of vector control is to eliminate the coupling between the direct (d) and quadrature (q) axes component of voltage/current. For vector control, a-b-c quantities can be transformed into the d-q quantities using Park's transformation [9]. In vector control, the q-axis current (i_q) is responsible to control the torque and d-axis current (i_d) is responsible for control of

the flux. Thus the ac motor can be controlled like a separately excited dc motor while keeping the advantages of ac over dc motors. Once the system determines the rotor-flux angle, a vector control algorithm determines the optimum timing and magnitude of the voltages to apply to the stator-phase windings. Thus the vector control provides significantly better performance and reduces torque ripple and current spikes.

In vector control many works have been reported [10-70]. These include some simple and easy fixed gain control techniques such as proportional integral (PI), proportional integral differential (PID) control technique. On the other hand, many other different control techniques of varying degree of complexity have appeared on the nature of drive applications such as pseudo-derivative-feedback (PDF) controllers, model reference adaptive controller (MRAC), sliding mode controller (SMC), self tuning regulator (STR), variable structure controller (VSC), fuzzy logic controller (FLC), neural network controller (NNC), neuro-fuzzy controller (NFC) etc. Major vector control works reported for IPMSM drive are briefly discussed below:

1.3.1 Fixed gain controller

B.K. Bose and P.M. Szczesny [10] developed a digital microcomputer-based and computer aided control system that describes control of an inverter fed IPMSM. They divide the operational region into a constant-torque region and a high-speed field-weakening constant-power region. For controlling purpose in constant-torque region, the vector or field-oriented control technique is used with the direct axis aligned to the stator flux. All the essential feedback signals for the control system are estimated. These signals include torque, stator flux, torque angle, rotor position and rotor temperature for magnet

flux compensation. Basically, the d axis and q axis components of stator flux are described respectively, as a function of stator d and q axis currents. PI controllers are used to generate command d and q axis currents to control the speed of the motor. This controller is sensitive to plant parameter variations and load disturbance. This controller used microcontroller based computer aided control system which is relatively costly for simple PI controller implementation and gives a good performance only in a particular range of speed. Gumaste and Slemon [11-12] proposed another vector control schemes with analyzing the steady state performance of voltage source inverter (VSI) and current source inverter (CSI) fed PMSM drives. They explored the total operating region into constant torque region and constant power region. They used the position feedback signal using encoder. In their work about steady state analysis of a VSI fed PMSM, they suggested removing damper winding which is necessary for motor stability and reduce harmonic current, whereas in case of CSI fed PMSM, they appreciated it to reduce commutating inductance. Macminn and Jahns [13] described another control technique to improve the performance of current regulators operating in the stationary reference frame. Speed-dependent back EMF and inductive voltage drops are compensated so that steady-state current errors are zeroed at all speeds until current regulator saturation limits are encountered. They proposed another technique that uses stator current components to prevent premature current regulator saturation, thereby improving the machine's torque production capabilities at high speeds. However, this technique does not work for a very wide range speed and the performance of this controller is not very good. Jahns et. al. [14] developed another speed controller based on controlling torque component of stator current. In this work, the author considered the effect of rotor configuration and current

regulator saturation. In another paper, Jahns [15] investigated the field weakening operation. But the analysis is very limited and this paper does not investigate the operation to use the full speed range. Pillay and Krishnan [16] proposed a high performance vector control scheme for IPMSM drive using state space model of IPMSM. They design the controller by forcing i_d to zero. In that way, they linearized the model of IPMSM. But it is not practical to design and predict the performance of the controller using linear model. However, the drawbacks of this work are, the speed controller is a PID controller and the reluctance torque was zero as i_d considered zero. Moreover the operating speed was limited as the flux cannot be controlled with i_d =0. Ogasawara and Akagi [17] described fixed gain control of an IPMSM, which is characterized by position estimation based on magnetic saliency. The real-time estimation algorithm detected motor current harmonics and determined the inductance matrix including rotor position information. However, PI controller suffers from lot of disadvantages which already mentioned earlier. Kazunori et. al. [18] worked with the effect of inner current control loops on the system performance of a position-sensorless IPM motor drive system. Authors estimated the position based on inductance matrix which can be calculated from current and voltage vectors. It was shown in this work that the inner current loops integrated in the control system make it possible to suppress interference between the q-axis voltage and the d-axis current and led to significant improvements in the stability of position control. However, authors didn't provide any experimental result to verify the feasibility of this controller in real field. This control method requires a lot of computation to implement in real-time, which makes it cumbersome to implement in real-time. Oyama et. al. [19] presented a carrier frequency control method for speed

control of IPM over a wide speed range including field weakening region. Authors estimated the position based on phase induction variation. In their control scheme, they extended flux-weakening regime, current regulator saturation and the worst degrading factor of torque production in the extended flux-weakening range is eliminated. This method has the drawback of torque ripple. Moreover it requires high frequency injection and difficulty in choosing the injected signal frequency between the carrier frequency and motor fundamental frequency. Mademlis and Agelidis [20] divided the operating region of IPM motor into three divisions, constant torque region with maximum torque to current ratio, voltage and current limited region, voltage limited region. The command d-axis current was determined based on the operating region. Command q-axis current was determined through a PI controller and a current limiter. The performance of this controller is parameter sensitive and affected by load disturbance. Furthermore, the ripple in q-axis current affects the d-axis current too, which will further increase the developed torque ripple at output. Chang et. al. [21] proposed a hall current sensor based IPMSM drive. To eliminate the cost of encoder in the motor drive the authors proposed a new way to sense the position without using encoder. The authors didn't consider the flux control in this work which not only reduces the range of operational speed but also gives non-optimum performance. The transient performance of the proposed controller is not good. Bolognani et. al. [22] developed another way to recognize the speed of the IPM motor with the experimental realisation of a sensorless IPMSM drive. They used an extended kalman filter (EKF) to estimate the rotor position. Position and angular speed of the rotor were obtained through an EKF. They developed a way to estimate the position of the rotor such that estimation algorithm does not require the knowledge of the

mechanical parameters and the initial rotor position. In that work, they developed a control algorithm that has been specifically studied to enhance the overall system performance. This controller is insensitive to mechanical parameters of the drive, but it requires high rate of computation to implement in real-time. Morimoto et. al. [23] proposed a V/F control system with a speed-control loop for position sensorless speed control of super high-speed permanent magnet (PM) motor of micro gas turbine generation system. This control is commanded by applied voltage. They claimed that by this strategy, the micro gas turbine generator system can be controlled without a high-speed current regulator. Morimoto et. al [24] did another work to control the speed of IPMSM over a wide range of speed. In that work they analyzed the current and voltage constraints for different operating regions. They developed some field weakening controllers for high speed. They have accounted and compensated for the magnetic saturation and demagnetization effect of permanent magnet to achieve high torque and high efficiency operation within maximum voltage and current limit of the inverter and motor. They studied different control techniques such as flux control, constant flux linkage control, unity power factor control with i_d=0. In this work, to overcome the effect of saturation, the d-axis command current is generated by calculating the d and q-axis inductances. However the speed controller is a fixed gain PI controller which is not suitable for HPD.

Rahman et. al., [25] presented direct torque control scheme for wide speed range operation of IPMSM drives, where both torque and stator flux linkage are directly controlled. Like conventional controllers, current controllers followed by pulse width modulation (PWM) or hysteresis comparators and coordinate transformation are not used

in that scheme. This eliminates the delays through these networks and offers the possibility of dispensing with the rotor position sensor for the electronic commutator, if the initial rotor position is known only approximately. The scheme incorporates all the usual control regimes, such as the maximum torque per ampere (MTPA) operation in constant torque region, the flux-weakening (FW) region, and operates the drive within the voltage and current limits of the motor/inverter. Command torque was calculated using PI controller and command flux was determined by using a look up table for both constant torque and constant power regions. As the look-up table cannot cover all the operating condition, the performance was limited by the operating region. Furthermore, only few experimental results were provided in that paper.

Although these fixed gain controllers have been using in industry for a long time because of simplicity and easy to implement in real-time. However, conventional controllers such as PI, PID are not suitable for HPD. Because these controllers are very sensitive to plant parameter variations, load disturbance and any other kinds of disturbances like temperature change, command speed change. So the parameters have to be adjusted online such that it gives optimum performance with dynamic condition. That is why researchers have been looking for different ways to adapt the parameters with changing situations to achieve the desired criteria of HPD.

1.3.2 Adaptive controller

For designing a HPD, gains have to be adapted to achieve fast transient response, accurate speed response, non-linear load handling capability and adaptability and quickest recovery from any kind of uncertainties. Researcher, worked on adaptive gain

controllers, developed different ways to achieve adaptations. Vaez et. al. [26] proposed an adaptive controller for IPM motor drives in order to achieve on-line loss minimization. In this work, a control strategy was developed by taking into account the inherent parameter variations of IPM motors. This loss minimization technique was developed in such a way that it works if the absolute value of speed error remains within a certain limit. However, the dynamic performance of the controller is not that good. Moreover, at steady state the ripple is high in this controller. It has a lot of computational burden as there are different controllers for dynamic and steady state regions. In [27], researchers developed a model reference adaptive control (MRAC) for position control of PMSM drive. The general idea is to create a closed loop controller with parameters that can be updated to change the response of the system. In this technique, the drive forces the response to follow the output of the reference model regardless of the drive parameter changes. The output of the system is compared to a desired response from a reference model. The control parameters are updated based on this error. In their work they used MRAC controller and PI controller in two loops. Steady state error of the PI controller is used to compensate the chattering problem due to discontinuous control inputs. However this still does not completely get rid of chattering problem. Cerruto et. al., [28] proposed another MRAC controller for PMSM drive in robotic application. The error between reference model and actual model is used to adjust system parameters such as inertia and torque constant. This type of controllers suffers from a lot of online computation to implement in industry. Sozer and Torrey [29] developed flux weakening control of the IPMSM drive by adjusting the d-axis current. They used direct model reference adaptive controller and direct adaptive flux weekener for controlling torque component and flux

component of current. However, they investigated the performance of the controller in very limited condition. Namudri and Sen [30] proposed another type of controller named sliding mode controller (SMC) for vector control of synchronous motor. It comprises a phase controlled chopper and GTO inverter to provide torque component current. Due to frequency limitation of GTOs this type of control cannot be utilized for HPDs. Consoli and Antonio [31] developed another SMC for torque control and investigated the performance above the base speed using FW technique. They used the actual current and line voltage as feedback to generate torque and flux. The effect of constant acceleration, constant speed and constant deceleration are counted for designing SMC. Variable bandwidth is used to reduce the chattering problem. However, the drive system has not been investigated in real-time where the unknown and unavoidable parameter variations and chattering problem exist. Ghirby and Le-Huy [32] proposed a variable structure controller for PMSM. They used current loop and speed loop for this controller. The drive does not get rid of chattering problem completely. The performance of the drive has not been investigated for wide speed range. Sepe and Lang [33] developed another adaptive controller with the estimation of mechanical parameters. Because of huge computational burden, the performance of the controller becomes worse in real field. Rahman et. al. [34] developed a nonlinear adaptive backstepping speed controller for IPMSM drive realizing that the conventional controller designed with the standard linear d-q axis IPMSM model with constant parameters will lead to an unsatisfactory prediction of the performance of an IPM motor owing to the magnetic saturation of these machines even during normal operation. In order to achieve high performance from an IPMSM, the vector control technique is utilized for their proposed drive. In this paper, authors

estimated the motor parameters as the d-q axes inductance and load torque. The most appealing point of this work is the use of virtual control variable to make original high order system simple, thus the final control output can be derived step by step through suitable Lyapunov functions ensuring global stability. In this work authors took an assumption of d-axis current equal to zero to simplify the controller design. This assumption leads to erroneous and/or non-optimal results for motors at all operating conditions. Furthermore, due to this assumption, the operating range of the IPMSM is reduced. Sometimes it cannot even reach the rated speed at rated load. Due to well-known disadvantages of adaptive controller such as steady-state chattering problem and dependency of motor model parameters, researchers looked into the application of intelligent computation algorithm for motor drive applications.

1.3.3 Intelligent controller

Despite many advantageous features of interior permanent magnet synchronous motor (IPMSM) the precise speed control of an IPMSM drive becomes a complex issue due to nonlinear coupling among its winding currents and the rotor speed as well as the nonlinearity present in the electromagnetic developed torque due to magnetic saturation of the rotor core [35]. The main advantages of intelligent controllers are: their designs do not need the exact mathematical model of the system and theoretically they are capable of handling any nonlinearity of arbitrary complexity. Over the last decade researchers [36-50] have done extensive research for application of fuzzy logic controller (FLC), artificial neural network (ANN) and neuro-fuzzy (NF) controllers for HPVSD systems. Simplicity and less intensive mathematical design requirements are the main features of intelligent

controllers, which are suitable to deal with nonlinearities and uncertainties of electric motors [36-40]. Therefore, the intelligent controllers demand particular attention for high performance nonlinear IPMSM drive systems. Among the intelligent controller FLC is the simplest for speed control of high performance IPMSM drive. In contrast to conventional control techniques, FLC is the best in complex ill-defined process that can be controlled by a skill human operator without much knowledge of their underlying dynamics. Recently researchers [34-46, 52, 53] have worked to develop FLCs for motor drives to mimic human thinking as closely as possible. Works have already been reported on the use of FLCs for conventional dc motors [54, 55], switched reluctance motors [52, 53] and IM drives [69]. In [38], the authors developed a direct FLC and an adaptive FLC which is based on MRAC. For the direct FLC, the controller normalizing gains are designed for certain situations, which would then prohibit the machine to achieve desired performance in case of large disturbances. The adaptive FLC uses adaptive model of the motor with FLC to control the motor. This paper did not show any experimental result for this controller. Because of two FLCs, there is a lot of computational burden to implement this system in real-time. Uddin and Rahman [41] proposed a FLC for IPMSM drive. In that work, the vector control technique incorporated with the FLC was used to obtain the highest torque sensitivity of the IPMSM drive. For that FLC, the speed error and the rate of change of speed error are considered as the input linguistic variables and the torque producing current component is considered as the output linguistic variable. This controller suffers from significant ripple in the developed torque. In [42], the authors proposed FLC based MTPA speed controller. They designed the controller to calculate command torque from which they derived the command q and d axes current to control

the speed motor. The command q and d axes current derived from command torque is dependent on motor parameters. This command torque has lot of ripple which makes the output speed with high ripple. So it is inappropriate for real-time implementation. Uddin et. al [43] developed a genetic based fuzzy logic controller (GFLC) for the IPM ac motor drive. In this work they reduced the number of membership functions for low computational burden of FLC. A performance index, J is tuned for the parameter of their proposed GFLC such that it reflects small settling time, small steady state error, and small overshoots. The tuning parameters are adjusted offline in order to minimize the index in a predetermined level utilizing genetic algorithm (GA). The optimization process is based on the rated conditions of the motor. Due to difficulties of binary representation when dealing with continuous search space with large dimension, they proposed to implement the optimization using a real-coded GA. Due to high computational burden of GA, it is almost impossible to apply GA in real-time. So the control requirements of IPM motor drive under significant uncertainty of disturbance can not be satisfied in this controller for all operating points. Zawirski developed an angular speed control scheme for PMSM [44]. The controller was constructed by combining a non-integral fuzzy and a PI algorithm. However, authors did not provide any experimental result to prove the feasibility of the controller in real field. Bolognani et. al. [45] proposed a FLC for switched reluctance motor. In this work, they designed a FLC which has only one input obtained from error, while the FLC output is integrated to produce the torque reference. This controller is not robust as it works only with error. As the output of the FLC is integrated to manipulate command torque, it gives high ripple. In [46], Lai et. al. proposed another hybrid FLC for direct torque control of IM drive. They used PI

controller for steady state condition and PI type FLC for transient condition. As it uses PI controller in steady state, it suffers with the disadvantages of PI controller. With any disturbance like load change the speed deviates from command speed and it switches from PI to PI types FLC which makes the controller complex. Stewart et. al. [47] investigates the potential of multi-objective control design with hardware in the loop. The authors tuned PI parameters on-line by multi-objective GA to apply in a sealed pump running on magnetic bearings. A DC motor dynamometer rig and a microcontroller were used as a platform to develop and assess the control algorithms. In particular, an on-line tuned type PI and an off-line designed type FLC and online tuned FLC were considered for performance investigation. The harmonic in PI and offline designed type FLC is reduced by online tuning of FLC. But online tuning of FLC needs a lot of computation. In [48], Uddin et. al developed another FLC for IM drive. They calculate the command torque component of current using FLC. But they didn't control the flux according to different operating condition.

The use of neural network in control systems is very attractive because of their ability to learn, to approximate functions, to classify patterns and their potential for massively parallel hardware implementation. In [49], ANN was implemented for online tuning of the gains of PI controller. In this work, radial basis function network (RBFN) based ANN is utilized to control speed of IPMSM. Like the counter propagation network, the RBFN is designed to perform input output mapping based on the concept of locally tuned. The input variables are each assigned to a node in the input layer and pass directly to the hidden layer without weight. The hidden layer nodes are the RBF units. Each node in this layer contains a parameter vector called a center. The node calculates the

Euclidean distance between the center and the network input vector and passes the result through a nonlinear function. For learning purpose the orthogonal least square (OLS) method is used in this work. Yi et. al. [50] proposed an ANN based adaptive controller for IPMSM drive. In that work, an ANN model was derived as the inverse dynamic model of IPMSM, Then they adapted the model based on speed error signal. In this controller, it is tough to get the training data that required for adapting ANN parameters to get the desired performance at all conditions. This controller didn't control flux to get optimum performance. Rahman et. al [51] proposed another ANN controller for PMSM drive. In that work, they used offline and online training to tune weights and biases of the ANN if the speed error signal is beyond a prescribed limit. This controller does not ensure the stability in all operating region. They didn't consider flux control either. Moreover, this controller requires a lot of computation. Elbuluk et. al [52] suggested another type of controllers with adaptation. This paper presented ANN-based model reference adaptive system (MRAS) to estimate the speed and position of a PMSM. An NN adaptation method was used as the optimization engine for a comprehensive parameter estimation strategy. Two NN-based MRASs were presented. First, the use of an NN adaptation for the estimation of the stator resistance and torque constant was presented. Second, a rotor-speed estimation algorithm with stator resistance adaptation was developed. The estimator used the back EMF to determine the motor position and speed. The adaptation was done based on speed error using back propagation technique. In adaptation process, Jacobian function for the system is simplified as unique, which may cause some error. The use of low pass filter in the training and adaptation process makes the system slow. Urasaki et. al [53] proposed another high efficiency NN

controller for IPMSM drive. The authors control the torque component current by PI controller. So this controller still suffers from the well known disadvantages of PI controllers. The flux is controlled by an NN controller. The NN controller was designed to control the actual flux component of the stator current to the desired flux component of the stator current. But it is tough to calculate the desired flux component of the current as it depends on parameters and operating conditions. This needs a lot of computation in calculating command d-axis current for implementing in real-time. In [54], Sarkawi et. al. proposed a multi-layer NN architecture for the identification and control of dc brushless motors operating in a HPD. But they didn't provide any experimental result to verify feasibility of the controller in real field.

The conventional FLC has a narrow speed operation and needs much more manual adjusting by trial and error if high performance is wanted [55]. On the other hand, it is extremely tough to create a serial of training data for ANN that can handle all the operating modes. The more advanced intelligent controller is NFC, which is the combination of FLC and ANN controller. The NFC utilizes the transparent, linguistic representation of a fuzzy system with the learning ability of artificial neural networks. Thus it takes advantages of both FLC and ANN. Uddin et. al [55] proposed a fuzzy basis function network (FBFN) based NFC to tune the parameters of PI controller. In this NFC, initially different operating conditions are obtained based on motor dynamics incorporating uncertainties. These are used to optimize the PI controller parameters in a closed-loop vector control scheme in order to get the initial PI controller parameters. In the optimization procedure a performance index is developed to reflect the minimum speed deviation, minimum settling time and zero steady-state error. However, the weights

and centres were trained offline in order to avoid computational burden. Thus, the controller cannot adapt with changing operating condition. Rubaai et.al. [56] proposed an adaptive fuzzy neural network controller (FNNC) for practical application of high-performance BLDC drives. The FLC scheme was implemented by using a multilayer neural network. The authors performed learning of the structure based on the partition of input space, whereas learning of the parameter was done on the supervised gradient decent method. To give better performance in all operating condition, it is necessary to tune the membership functions. C. T. Lin [57] proposed a new structure and parameter learning scheme for a NFC system. The disadvantages of this learning scheme are that it is suitable only for offline instead of online operation and a large amount of representative data must be collected in advance for the implementation of this scheme. Moreover, the independent realization of the structure and parameter learning is too time-consuming. Lin et.al [58] proposed a self-constructing fuzzy neural network for PMSM drive. They used structure learning and parameter learning. But it is not suitable to implement in industry because of a lot of computational burden. Furthermore, they didn't consider the flux control. Inoue et. al [59] have proposed a fuzzy algorithm for the brushless dc servo motor drive. The fuzzy algorithm is used to tune the gains of PI controller. However, the drive system incorporates a reference generator, the observer and fuzzy interferencers with two PI controllers which make the system complex.

Some researchers are working to combine intelligent controllers and adaptive controllers to give better performance. Cavallaro et. al.[72] have proposed another adaptive speed regulator scheme based on the MRAC approach, employing Fuzzy laws for adaptive process. The adaptation procedure is divided into two phases. Firstly, the

actual output of the process is compared with the output of the reference model to obtain an error. Consequently, the parameters of the control law are adjusted to nullify such error according to suitable adaptive algorithms. In this work they used a neuro-fuzzy approach for the optimization of the fuzzy adaptive laws in order to avoid one of the major drawbacks of the fuzzy control. The main drawback of this method is that it requires huge computation which is the major limitation for practical industrial applications. Koviac et. al., [73] have developed fuzzy logic based model reference controller for PMSM. They used the error between the output of MRAC and the actual output as the input to the FLC. A linearized model of PMSM is used as the model of the PM motor. But in real-time the motor is not a linear and the parameters of the model changes with operating condition. Thus the performance of the drives deteriorates in real-time.

1.4 Thesis motivation

As shown in literature review, most of the controller for IPMSM drive was designed for constant torque region with considering command d axis current equal to zero [16, 21, 24, 33, 50, 51, 58]. In that way, the researchers linearize the model which leads to an erroneous result. But one of the important advantages and superiorities of IPM motor is it's saliency which gives this machine significant reluctance torque [74-77]. Another advantage of this type of motors is its ability of a degree of flux weakening, enabling operation above nominal speed at constant voltage and should also help reduce the harmonic losses in the motor. So without controlling the flux component, the main

advantages of IPMSM over other PM motors can not be acquired. To get optimum performance from an IPMSM motor, flux component current must be controlled. Although IPMSM has lots of advantages over others, the precise speed control of an IPMSM drive is a complex issue because of nonlinear coupling among its winding currents and the rotor speed as well as the nonlinearity present in the electromagnetic developed torque due to magnetic saturation of the rotor core [24, 35]. At high speed, particularly above the rated speed, the system nonlinearity becomes severe as the voltage, current and power capability of the motor/inverter exceeds the rated limits. Thus, this thesis takes an attempt for the development of several speed control techniques of IPMSM in order to achieve high performance and wide speed range operation incorporating flux control. In the development stage of the controller, machine parameters, particularly, the characteristics current constraint, voltage constraint, proper flux control for both constant torque and constant power operations are considered.

1.5 Thesis organization

The remaining chapter of the thesis is organized as follows. In chapter 2 describes the derivation of the mathematical model of the IPMSM. Here it is shown that the vector control technique greatly simplifies the control of the motor. Then the operating region of IPMSM including both constant torque and constant power regions are analyzed. Next, chapter 3 shows the controller design procedure using adaptive backstepping technique in detail for speed control. The design is based on the motor model equations derived in chapter 2. In the development of the controller flux control is incorporated considering maximum torque per ampere (MTPA) technique. It describes the model development and

shows the simulation results of the complete drive system. Chapter 4 describes the real-time implementation of the complete drive system using dSPACE DSP in this chapter. The detailed experimental results of the adaptive based nonlinear controller are shown in this chapter. In chapter 5, the fundamental idea of the FLC including linguistic variables, membership function, fuzzification, rule evaluation and defuzzification are presented. Then a novel speed control scheme of IPMSM drive using a fuzzy logic algorithm is developed. The same FLC is used to control both flux and torque controls. Detailed simulation and experimental results are investigated to test the performance of the controller. Then a comparison between conventional FLC and the proposed FLC are also provided. In chapter 6, a new adaptive NFC is developed in which the membership functions and consequent parameters are tuned online. Then the performance of the controller is investigated both in simulation and experiment. Finally, a summary of the thesis and suggestions for future works are highlighted in chapter 7. After that, all pertinent references and appendices are listed.

Chapter 2

Modeling of IPMSM

2.1 Introduction

Analytically, the IPMSM is the same as the conventional wire-wound excited SM with the exception that the excitation is provided by the permanent magnets instead of wire wound dc rotor field. Therefore, the standard d-q axes model for synchronous machines can be used for the d-q axis model of the IPMSM by removing the equation related to field current and associated dynamics.

2.2 Mathematical model development

If ψ is the constant flux linkage provided by the permanent magnets, then the flux linkages in the three phase stator winding due to PM of the rotor can be given as,

$$\begin{bmatrix} \psi_{am} \\ \psi_{bm} \\ \psi_{cm} \end{bmatrix} = \psi \begin{bmatrix} \sin\theta_r \\ \sin(\theta_r - \frac{2\pi}{3}) \\ \sin(\theta_r + \frac{2\pi}{3}) \end{bmatrix} \tag{2.1}$$

where $\psi_{am}, \psi_{bm}, \psi_{cm}$ are the flux linkages in the three phase stator winding due to PM of the rotor and θ_r is the rotor position. So total air gap flux linkage for three phases are the summation of the flux linkage for the corresponding phase current, mutual flux linkage for the currents in other phases and the flux linkages in the three phase stator winding due to PM of the rotor. The equations for the air gap flux linkage for three phases are given as,

$$\begin{bmatrix} \psi_a \\ \psi_b \\ \psi_c \end{bmatrix} = \begin{bmatrix} L_{aa} & M_{ab} & M_{ac} \\ M_{ba} & L_{bb} & M_{bc} \\ M_{ca} & M_{cb} & L_{cc} \end{bmatrix} \begin{bmatrix} i_a \\ i_b \\ i_c \end{bmatrix} + \psi \begin{bmatrix} \sin\theta_r \\ \sin(\theta_r - \frac{2\pi}{3}) \\ \sin(\theta_r + \frac{2\pi}{3}) \end{bmatrix} \tag{2.2}$$

where ψ_a, ψ_a, ψ_a are the air gap flux linkage for the phase a, b, c, respectively; L_{aa}, L_{bb}, L_{cc} are the self inductances and M_{ab}, M_{bc}, M_{ca} are the mutual inductances, respectively. The phase voltage is the voltage drop in each phase plus the voltage drop due to the rate of change of flux linkage. The voltage equations of the three phases of the IPMSM can be defined as:

$$v_a = r_a i_a + \frac{d\psi_a}{dt} \tag{2.3}$$

$$v_b = r_b i_b + \frac{d\psi_b}{dt} \tag{2.4}$$

$$v_c = r_c i_c + \frac{d\psi_c}{dt} \tag{2.5}$$

where v_a, v_b, v_c are the three phase voltages, i_a, i_b, i_c are the three phase currents and r_a, r_b, r_c are the three phase stator resistances. These equations can be written in matrix form as,

$$\begin{bmatrix} v_a \\ v_b \\ v_c \end{bmatrix} = \begin{bmatrix} r_a & 0 & 0 \\ 0 & r_b & 0 \\ 0 & 0 & r_c \end{bmatrix} \begin{bmatrix} i_a \\ i_b \\ i_c \end{bmatrix} + \frac{d}{dt} \begin{bmatrix} \psi_a \\ \psi_b \\ \psi_c \end{bmatrix} \tag{2.6}$$

These voltage equations depend on the flux linkage components which are function of rotor position θ_r and the coefficients of the voltage equations are time varying with the exception of the motor is motionless. In order to keep away from the difficulty of calculations, all the equations have to be changed to the synchronously revolving rotor reference frame where the machine equations are no longer dependent on the rotor position. These transformations can be accomplished in two steps using Park's transformation equations [9]. In the first step, the machine equations are changed from the stationary a-b-c frame into the stationary d-q frame and in second step, from the stationary d-q frame to the synchronously rotating d^r-q^r frame. The phase variables in terms of d-q-0 variables can be written in matrix form as,

$$\begin{bmatrix} x_a \\ x_b \\ x_c \end{bmatrix} = \begin{bmatrix} \cos\theta_r & \sin\theta_r & 1 \\ \cos(\theta_r - \frac{2\pi}{3}) & \sin(\theta_r - \frac{2\pi}{3}) & 1 \\ \cos(\theta_r + \frac{2\pi}{3}) & \sin(\theta_r + \frac{2\pi}{3}) & 1 \end{bmatrix} \begin{bmatrix} x_q \\ x_d \\ x_0 \end{bmatrix} \tag{2.7}$$

The corresponding inverse relation can be written as,

$$\begin{bmatrix} x_q \\ x_d \\ x_0 \end{bmatrix} = \frac{2}{3}\begin{bmatrix} \cos\theta_r & \cos(\theta_r - \frac{2\pi}{3}) & \cos(\theta_r + \frac{2\pi}{3}) \\ \sin\theta_r & \sin(\theta_r - \frac{2\pi}{3}) & \sin(\theta_r + \frac{2\pi}{3}) \\ \frac{1}{2} & \frac{1}{2} & \frac{1}{2} \end{bmatrix}\begin{bmatrix} x_a \\ x_b \\ x_c \end{bmatrix} \tag{2.8}$$

The rotor location or rotor position angle is defined as,

$$\theta_r = \int_0^t \omega_r(\tau)d\tau + \theta_r(0) \tag{2.9}$$

For balanced three phase, '0' sequence component (x_0) does not exist, and it is convenient to set initial rotor position $\theta_r(0)=0$ so that the q axis coincides with a-phase. Under these condition the above equation can be written as,

$$\begin{bmatrix} x_a \\ x_b \\ x_c \end{bmatrix} = \begin{bmatrix} 1 & 0 \\ -\frac{1}{2} & -\frac{\sqrt{3}}{2} \\ -\frac{1}{2} & \frac{\sqrt{3}}{2} \end{bmatrix}\begin{bmatrix} x_q \\ x_d \end{bmatrix} \tag{2.10}$$

and

$$\begin{bmatrix} x_q \\ x_d \end{bmatrix} = \begin{bmatrix} \frac{2}{3} & -\frac{1}{3} & -\frac{1}{3} \\ 0 & -\frac{1}{\sqrt{3}} & \frac{1}{\sqrt{3}} \end{bmatrix}\begin{bmatrix} x_a \\ x_b \\ x_c \end{bmatrix} \tag{2.11}$$

The quantities in the stationary d-q frame can be converted to synchronously rotating d^r-q^r frame with the help of Fig.2.1 as,

$$\begin{bmatrix} x_q^r \\ x_d^r \end{bmatrix} = \begin{bmatrix} \cos\theta_r & -\sin\theta_r \\ \sin\theta_r & \cos\theta_r \end{bmatrix}\begin{bmatrix} x_q \\ x_d \end{bmatrix} \tag{2.12}$$

and inverse relation,

$$\begin{bmatrix} x_q \\ x_d \end{bmatrix} = \begin{bmatrix} \cos\theta_r & \sin\theta_r \\ -\sin\theta_r & \cos\theta_r \end{bmatrix} \begin{bmatrix} x_q^r \\ x_d^r \end{bmatrix} \tag{2.13}$$

assuming the eddy current and hysteresis losses are negligible, the induced emf is sinusoidal, the stator resistance of the three phases are balanced, neglecting the saturation and using equations (2.6),(2.8),(2.12), the d^r-q^r axis model of IPMSM

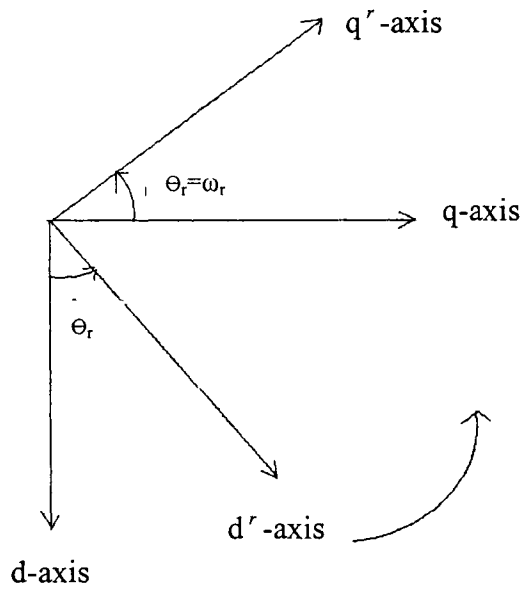

Fig.2.1: Relative position of stationary d-q axis to the synchronously rotating d^r-q^r axis.

can be derived as follows,

$$v_q^r = Ri_q^r + \frac{d\psi_q^r}{dt} + \omega_s \psi_d^r \tag{2.14}$$

$$v_d^r = Ri_d^r + \frac{d\psi_d^r}{dt} - \omega_s \psi_q^r \tag{2.15}$$

where v_d^r, v_q^r are d and q axis voltages and i_d^r, i_q^r are d,q axis currents, ψ_d^r, ψ_q^r are d,q axis flux linkages and R is the stator resistance per phase and ω_s is the stator frequency. ψ_d^r and ψ_q^r can be written as,

$$\psi_q^r = L_q i_q^r \tag{2.16}$$

$$\psi_d^r = L_d i_d^r + \psi \tag{2.17}$$

where, $L_q = L_l + L_{mq}$

$L_d = L_l + L_{md}$

L_d and L_q are d-q axis inductances, L_{md}, L_{mq} are d-q axis magnetizing inductances and L_l is the leakage inductance per phase. The stator frequency related to rotor frequency as,

$$\omega_s = P\omega_r$$

Using equations (2.14)-(2.17), the motor equations can be written as ,

$$v_q^r = L_q \dot{i}_q^r + R i_q^r + P\omega_r L_d i_d^r + P\omega_r \psi \tag{2.18}$$

$$v_d^r = L_d \dot{i}_d^r + R i_d^r - P\omega_r L_q i_q^r \tag{2.19}$$

In these equations all the stator voltages and currents are in rotor reference frame. The total average energy coming from the source which is also the developed power per phase is given by,

$$P_{phase} = \frac{1}{2}(-P\omega_r L_q i_q^r i_d^r + P\omega_r L_d i_q^r i_d^r + P\omega_r \psi i_q^r) \tag{2.20}$$

The total power developed by the machine is given by,

$$P_{mech} = \frac{3P\omega_r}{2}\{\psi i_q^r + (L_d - L_q) i_q^r i_d^r\} \tag{2.21}$$

According to (2.16)-(2.19), the d-q axis equivalent circuit diagram can be drawn as shown in Fig.2.2.

So the developed torque,

$$T_e = \frac{P_{mech}}{\omega_r} = \frac{3P}{2}\{\psi i_q^r + (L_d - L_q) i_q^r i_d^r\} \tag{2.22}$$

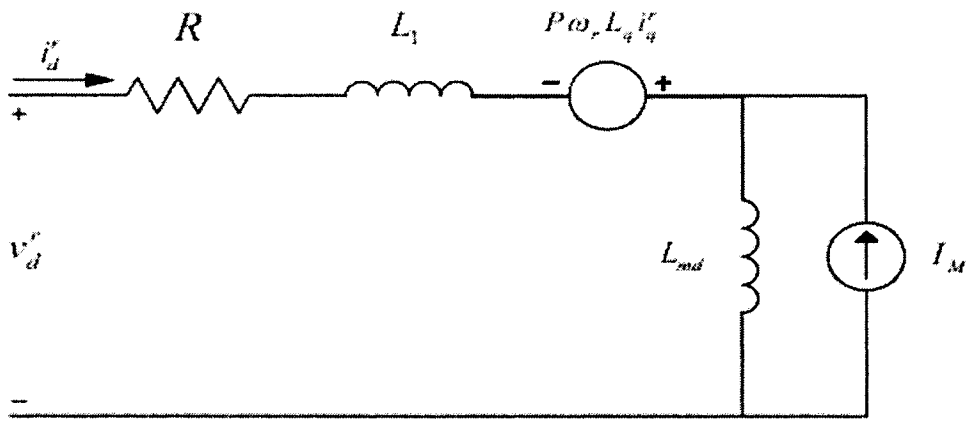

(a) d-axis equivalent circuit.

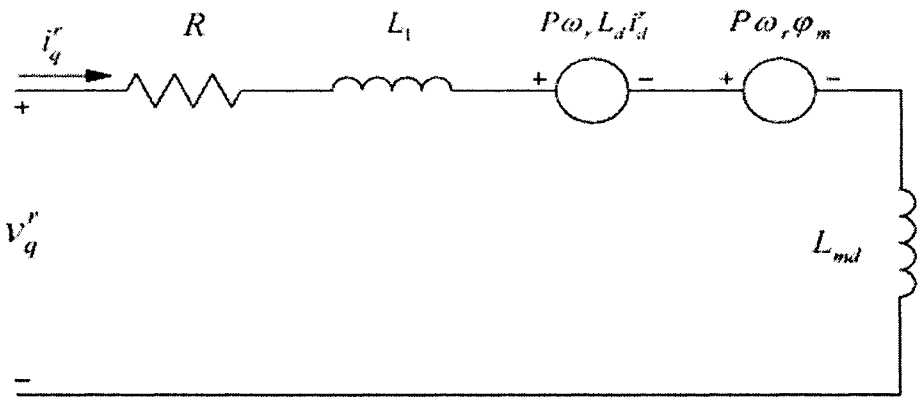

(b) q-axis equivalent circuit.

Fig.2.2: Equivalent circuit model of IPMSM.

The motor dynamic can be represented by the following equation:

$$T_e = T_L + B_m \omega_r + J\dot{\omega}_r \tag{2.23}$$

where T_L is the load torque in Nm, B_m is the friction damping coefficient in Nm/rad/sec and J is rotor inertia constant in kg-m^2.

2.3 Vector control of IPMSM

As mentioned earlier, the vector control technique is an effective technique for control of ac motors in HPD. The IPMSM can be vector controlled when the machine equations are transformed from the a-b-c frame to the synchronously rotating d-q frame where sinusoidal voltage become constant like a dc voltage. In case of dc motor, the developed torque is,

$$T_e = KI_aI_f \tag{2.24}$$

where I_a is the armature current, I_f is the field current and K is a constant. Both I_a and I_f are orthogonal and decoupled vectors. So the control becomes easier for separately excited dc motor. In case of PM motor the first term of torque equation (2.22) represents the magnet torque produced by the permanent magnet flux and q axis current and the second term represents the reluctance torque produced by the interaction of q and d axis inductances and the d-q axis currents. Most of the researchers consider the command d-axis current, i_d^r=0. So that the torque equation becomes linear with i_q and control task becomes easier.

$$T_e = \frac{3P}{2}\psi i_q = K_t i_q \tag{2.25}$$

However with the assumption of i_d^r=0, as per equation (2.17), the flux cannot be controlled in an IPMSM. Without a proper flux control, motor cannot be operated above the rated speed while maintaining voltage and current within the rated capacity of the motor/inverter. In the proposed work, the flux will be properly controlled so that the motor can be controlled efficiently below and above the rated speed. Thus, the IPMSM

can be controlled like a separately excited DC motor where i_q controls torque and i_d controls flux.

Using phasor notation and taking the d^r axis as the reference phasor, the steady state phase voltage V_a can be derived from steady state $d^r - q^r$ axis voltage using equation (2.18) and (2.19) as,

$$V_a = v_d^r + jv_q^r$$

$$= RI_a - \omega_s L_q i_q^r + j\omega_s L_d i_d^r + j\omega_s \psi \qquad (2.26)$$

The phase current $I_a = i_d^r + ji_q^r$ (2.27)

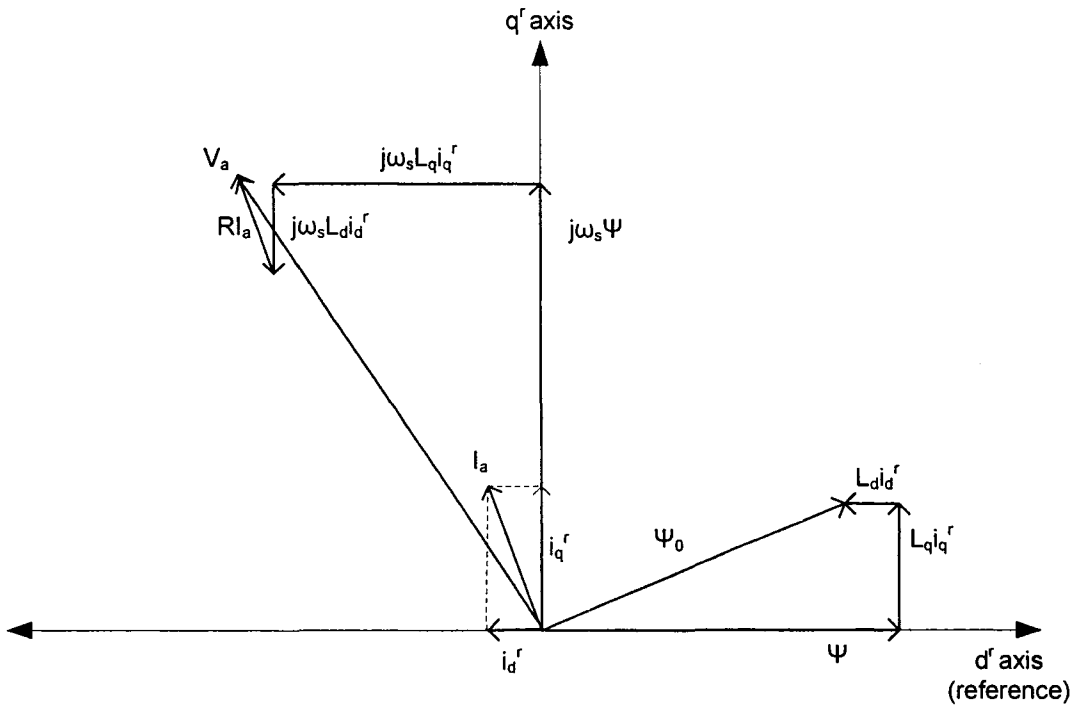

Fig.2.3: vector diagram of IPMSM.

In the case of IPM motor, the d^r axis current is negative and it demagnetizes the main flux provided by the permanent magnets. Thus in order to take the absolute value of i_d^r, we can rewrite the equation as,

$$V_a = RI_a - \omega_s L_q i_q^r - j\omega_s L_d i_d^r + j\omega_s \psi \qquad (2.28)$$

Based on equation (2.28), the basic vector diagram of the IPMSM is shown in Fig.2.3. The stator current vector can be controlled by controlling the individual d-q current components

2.4 Analysis of operating region

Precise control of the high performance IPMSM drive over the full range of speed is an engineering challenge. Selecting command i_d^r=0, in order to simplify the development of the controller, leads to erroneous and/or non-optimal results for motor at all operating conditions. With i_d^r=0, the resultant air gap flux remains constant as the direct control of flux is not possible for IPMSM. Without controlling the flux, sometimes the motor cannot even reach the rated speed at rated load. As the speed is inversely proportional to the air gap flux and proportional to the back emf, in order to drive the motor above the rated speed while maintaining voltage and current constraint, the flux has to be decreased which can be done by controlling i_d^r. Recently researchers reported on FW operation of IPMSM [74-78]. However, the efforts are at its initial stage as compared to the work done on IPMSM control, with the assumption of i_d^r=0. Soit is important to develop methods to control flux properly so that the IPMSM drive can be operative over for the whole wide speed range, namely, constant torque and constant power (field weakening) region. In the following subsection both constant torque and constant power regions are discussed in detail.

2.4.1 Constant torque region

For a practical inverter-fed motor drive, there exists an inverter output voltage limit, output current limit and power capacity limit. Assume that the maximum available phase voltage amplitude and the maximum line current amplitude are V_a and I_a, respectively. Then the feasible operation range is constrained by the following inequalities:

$$(v_d^r)^2 + (v_q^r)^2 \le {V_a}^2 \tag{2.29}$$

$$(i_d^r)^2 + (i_q^r)^2 \le {I_a}^2 \tag{2.30}$$

With the assumption of i_d^r=0, the reluctance torque of the IPMSM is not fully exploited. In the case where i_d^r is not equal to zero, then it is seen that T_e contains a nonlinear term, rendering the controller design much more difficult than a linear one. As far as achieving fast transient response and low loss is concerned, the MTPA control is rather attractive. The basic principle of MTPA is that for a given torque demand, the line current amplitude is minimized to achieve the maximum torque. The MTPA can be achieved by proper controlling of flux utilizing the armature reaction effect of i_d^r. Below the base speed, with the assumption of keeping the absolute value of stator current constant at its maximum value, I_a, i_d^r can be calculated in terms of i_q^r for MTPA control. This can be obtained by differentiating (2.22) with respect to i_q^r and setting it to zero as [74],

$$i_{dM}^r = \frac{\psi}{2(L_q - L_d)} - \sqrt{\frac{\psi^2}{4\left(L_q - L_d\right)^2} + i_q^{r^2}} \tag{2.31}$$

where i_{dM}^r is the value of i_d^r corresponding to MTPA. Then, one can obtain the maximum available torque as follows:

$$T_{eM} = \frac{3P}{2}\{\psi i_{\mathrm{qM}}^{\mathrm{r}} + (L_d - L_q) i_{\mathrm{qM}}^{\mathrm{r}} i_{dM}^r\} \tag{2.32}$$

where $$i_{qM}^r = \sqrt{I_a{}^2 - (i_{dM}^r)^2} \tag{2.33}$$

For clarity, the trajectory of the MTPA curve, the current limit curve, constant torque curves, voltage limit curves are shown in Fig.2.4. The constant torque curves are drawn for constant amount of torque T_1, T_2, T_{eM}, respectively, where $T_{eM} > T_2 > T_1$. So the maximum torque that can be generated (keeping i_d^r=0 and maintaining current constraint) is T_2, which can be obtained with MTPA technique at lower amount of current. The distance between any point of the constant torque curve and the point O indicates the stator current required to achieve the desired torque. The point at which the constant torque curve intersects with the MTPA curve is the lowest distance of that constant torque curve from the origin point O. Thus, the MTPA curve ensures the lowest current to achieve the desired torque. As seen from Fig.2.4, maintaining the current constraint, with MTPA technique, one can obtain T_{eM} amount of torque but with the same current one can get maximum T_2 torque with i_d^r=0 technique. Hence the operating limit of the drive can be extended by MTPA technique. Till now we have discussed the technique based on current constraint only. Now the voltage constraint will be discussed.

The voltage limiting curves V_m, V_1, V_C, V_2, V_E are corresponding to the motor speed ω_{rM}, ω_1, ω_{rC}, ω_2, ω_{rE}, respectively where $\omega_{rM} < \omega_1 < \omega_{rC} < \omega_2 < \omega_{rE}$. Although at the beginning of this section it was mentioned that T_2 is the maximum torque that can be achieved without controlling i_d^r as shown in Fig.2.4. Now if the voltage constraint is

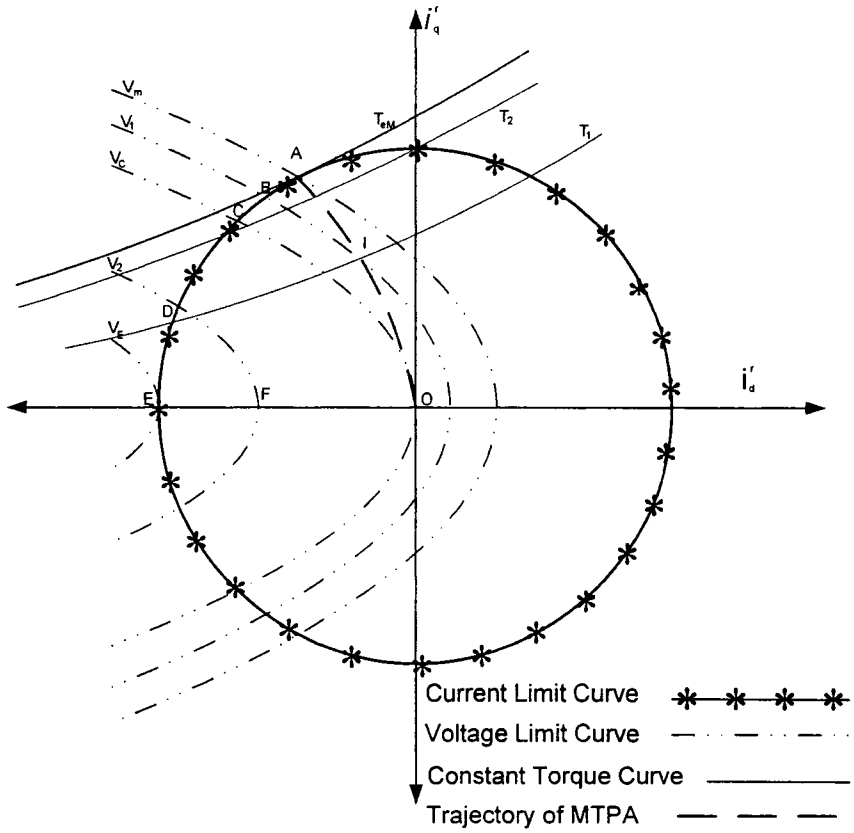

Fig.2.4: MTPA trajectory, Current limit curve, Voltage limit curves of IPMSM in d-q axes plane neglecting stator resistance.

considered then the maximum torque at speed ω_{rM} with $i_d^r=0$ control technique is even less than T_2. As shown in Fig.2.4, with voltage constraint if $i_d^r=0$ technique is used to control the motor, then the maximum torque that can be achieved is even less than T_1. With the increase of speed, the capability of torque decreases very quickly. The cause of the reduction of the torque production capability is that with $i_d^r=0$ control technique the rotor core becomes saturated to produce torque. So the above discussion specifies the necessity of flux control even in the constant torque region to achieve maximum torque. In summary, in region I when motor speed $\omega_r \leq$ rated speed, ω_{rM}, it is called constant

torque region and the motor should be run along MTPA curve to achieve maximum efficiency.

2.4.2 Constant power region

It has been discussed in the previous section that MTPA technique is used to control a motor below the rated speed in order to achieve maximum efficiency. Above the rated speed, the traditional control strategy is simply to reduce the magnetic flux intensity by applying negative i_d resulting in field weakening control. But the flux component of current still can be controlled by MTPA technique if the torque requirement is low enough to satisfy voltage constraint. The constant power region or FW region can be sub-divided into partial FW region and full FW region.

(a) Partial field weakening region:

From Fig.2.4, it can be observed that MTPA can be even applied but to maintain the current and voltage constraint, the produced torque decreases because of insufficient demagnetization. But as long as the produce torque is sufficient, it is a good choice to use MTPA. Otherwise FW control can be applied. Substituting (2.18) and (2.19) into (2.29) the voltage constraint can be defined as,

$$(Ri_d^r - P\omega_r L_d i_q^r + L_d \frac{di_d^r}{dt})^2 + (Ri_q^r + P\omega_r L_d i_d^r + L_q \frac{di_q^r}{dt} + P\omega_r \psi)^2 \le V_a^2 \qquad (2.34)$$

at steady state condition,

$$(Ri_d^r - P\omega_r L_d i_q^r)^2 + (Ri_q^r + P\omega_r L_d i_d^r + P\omega_r \psi)^2 \le V_a^2 \qquad (2.35)$$

At the same time the rotor angular frequency is less than the critical frequency, ω_{rc}. This can be obtained from (2.35) by setting both i_d and i_q to zero as,

$$\omega_{rC} = V_a /(P\psi) \tag{2.36}$$

From equation (2.35), neglecting armature resistance,

$$(P\omega_r L_d i_q^r)^2 + (P\omega_r L_d i_d^r + P\omega_r \psi)^2 \leq V_a^2 \tag{2.37}$$

However, depending on the load requirement (2.37) may not be satisfied even if the speed is below ω_{rc}.

When the motor follows MTPA trajectory it takes minimum amount of stator current. Thus, the copper loss is reduced and hence efficiency is increased for the drive. If the current controllers saturated due to voltage constraint, a flux weakening technique (explained in next subsection) will be used as shown by the arrow sign in Fig.2.5.

(b) **Full field weakening region:**

When the speed is above critical speed (ω_{rc}), it is called pure field weakening region. To control the motor above the critical speed considering both current and voltage constraints the operating region is limited by the d-axis current line, current constraint curve and voltage limit curve. It can be easily understood from Fig.2.6 that the intersecting point of voltage limit curve with constant torque curve gives the minimum current point to produce the required torque. Thus, it is the best choice for low copper loss. The relation between d and q axis command currents for field weakening while maintaining current and voltage constraints can be obtained as [74],

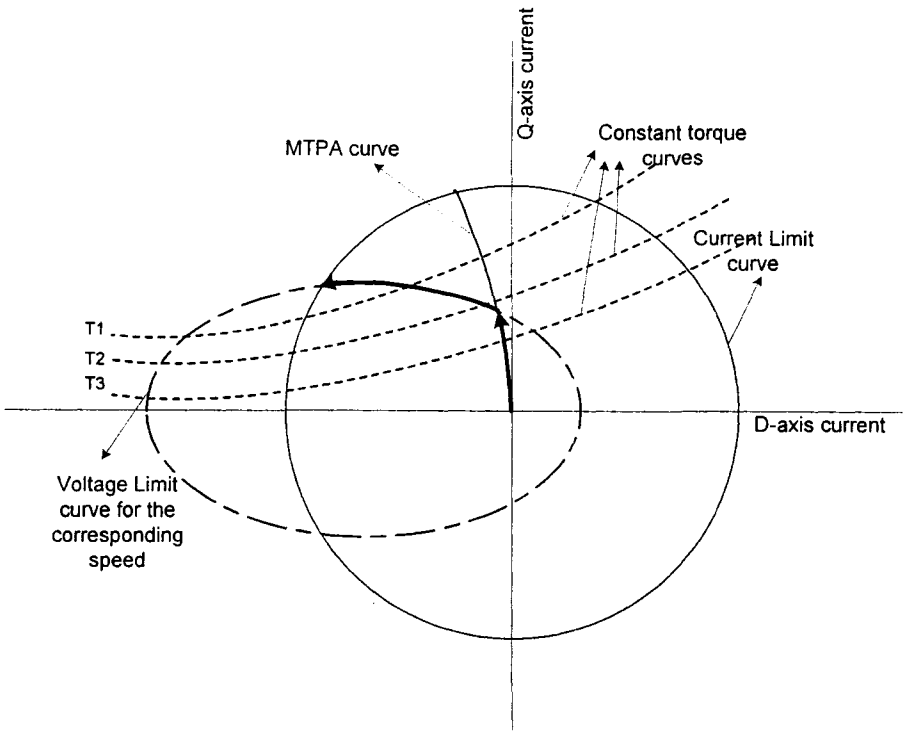

Fig.2.5: Control in partial flux weakening region

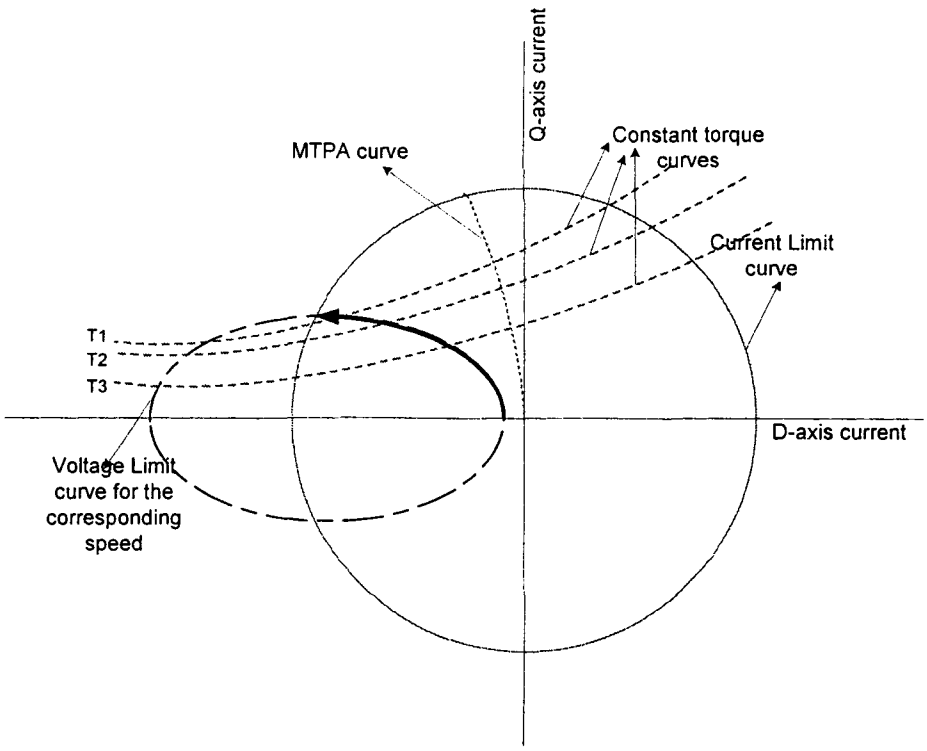

Fig.2.6: Control in constant power region

$$i_d^r = -\frac{\psi}{L_d} + \frac{1}{L_d}\sqrt{\frac{(V_a')^2}{P^2\omega_r^{\,2}} - L_q^2 i_q^2} \tag{2.38}$$

where V_a' is the maximum stator phase voltage neglecting the stator resistance voltage drop. From (2.38), one can obtain the maximum speed, called the extreme angular frequency ω_{rE} that a motor can achieve is,

$$\omega_{rE} = \frac{\sqrt{V_a^{\,2} - (RI_a)^2}}{P(L_d I_a + \psi)} \tag{2.39}$$

So in summary, constant power region or FW can be divided into two regions: one is partial FW region (IIA), another is full FW region (IIB). In region IIA, the maximum torque that can be developed using MTPA maintaining voltage and current constraint is shown in Fig.2.7. If the torque requirement is higher then the controller would increase

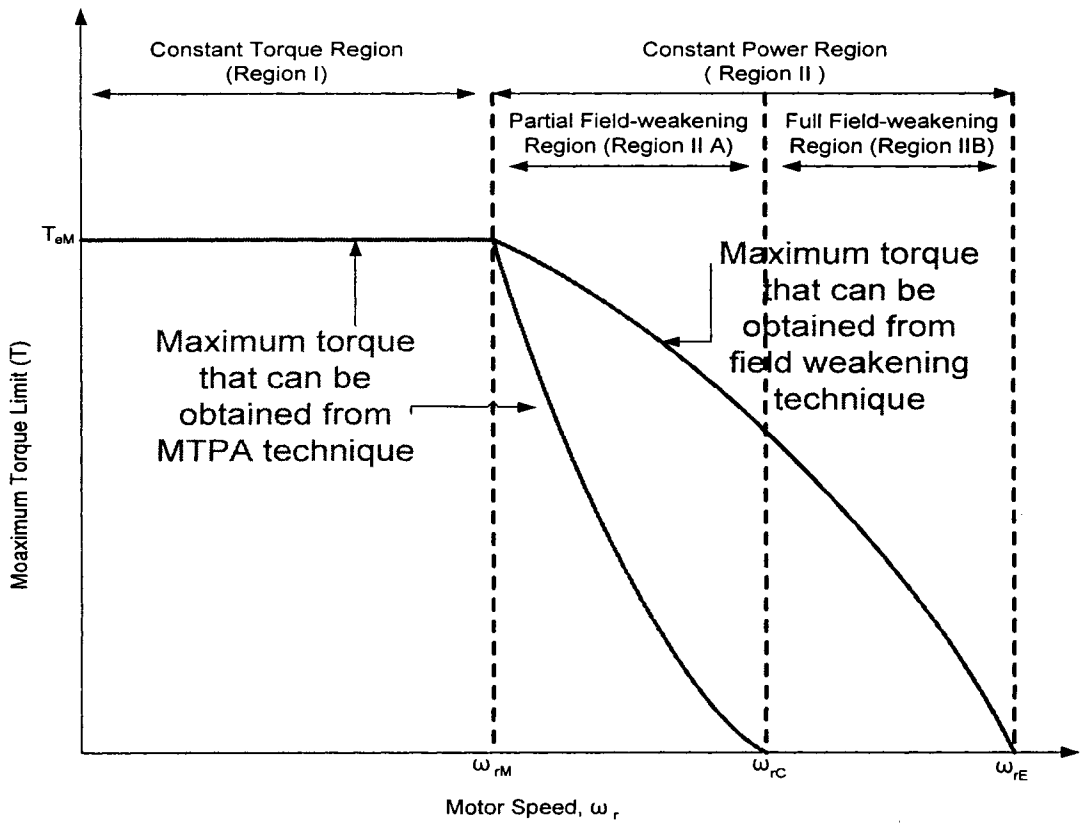

Fig.2.7: Maximum torque limit curve at different operating region.

its demagnetization component of current to prevent saturation at that speeds and increase its ability to give more torque. In region IIB, when the motor speed $\omega_{rC} < \omega_r < \omega_{rE}$, the maximum torque that can be obtained from a motor is shown in that figure.

2.5 Effect of stator resistance

The analysis that was done based on Fig.2.4, which is drawn by neglecting the stator resistance. The effect of considering the stator resistance will change the voltage limit curve. So if one considers the resistance voltage drop, this voltage should be

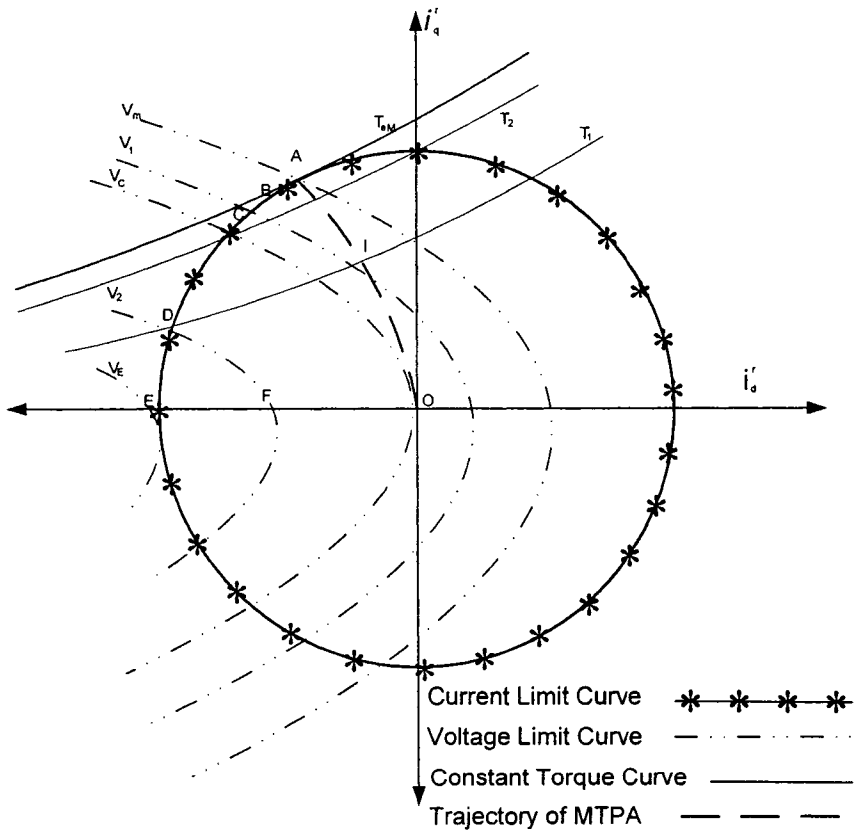

Fig.2.8: MTPA trajectory, Current limit curve, Voltage limit curves of IPMSM in d-q axes plane considering stator resistance.

deducted from the voltage limit curve in that part above the x-axis. That means in the motoring action this voltage will be reduced in voltage limit curve. On other case the resistance voltage drop should be added to the voltage limit curve in that part below the x-axis. That means in the braking action this voltage will be increased in voltage limit curve. The voltage limit curve in Fig.2.4 was an ellipse symmetric to the i_d axis. If the stator resistance is considered, the voltage limit curve will not be symmetric with i_d axis any more. This curve will be inclined toward i_d axis. The stator resistance drop will be increased with increase of current. So it will affect the voltage limit curve more when the operating point move from point 'O' to the near point to current circle of Fig.2.8. So the voltage limit for motoring action and braking/generating will be different as shown in Fig.2.8.

Chapter 3

Design and Development of a New Adaptive Backstepping Based Nonlinear Controller

3.1 Introduction

The conventional fixed gain PI and PID controllers are sensitive to plant parameter variations, load variations and other disturbances. For the purpose of obtaining high dynamic performance, several non-linear controllers have been developed for IPMSM [27-35]. Recently, feedback linearization control (FBLC) has been applied to IPMSM with an aim to design the nonlinear controller by changing the original dynamics into linear one, which has got limitations in terms of incorporating all system nonlinearities [34,81,82]. Thus, the performance of the system utilizing FBLC for reported works were not at the optimal level. Therefore, it is necessary to develop an adaptive controller which

incorporates system nonlinearities particularly, mechanical parameters, sometimes which are not possible to measure at all. These parameters may also vary with different operating conditions especially with mechanical load. In this chapter, a nonlinear controller for IPMSM is developed based on adaptive backstepping technique. In order to achieve high performance operation from an IPMSM, the vector control technique is utilized for the proposed drive. Most of the reported works on adaptive backstepping based nonlinear control of IPMSM took an assumption of d-axis current i_d=0 in order to simplify the development of the controller [34,80]. Because of the disadvantages of that type of control as mentioned in earlier chapter, i_d is controlled in such a way that the MTPA operation is achieved in this work. Researchers have made some efforts to develop the IPMSM drive system incorporating the field control technique ($i_d \neq 0$), where no uncertainties are considered in control technique [15,74-78]. To ensure stability, the proposed adaptive controller is designed based on Lyapunov's stability theory [80]. To ensure the robustness, all the mechanical parameters are estimated online based on adaptive backstepping technique [34,81,82]. Thus, the proposed adaptive nonlinear backstepping controller (ABNC) is capable of conserving the system robustness and stability against all mechanical parameter variations and external load torque disturbances. Moreover, the integrated drive system ensures efficient utilization of the developed torque as $i_d \neq 0$.

3.2 Controller design

The foundation of backstepping controller is the identification of a virtual control variable and forcing it to become a stabilizing function. Thus, it generates a

corresponding error variable which can be stabilized by proper input selection via Lyapunov's stability theory [80]. In order to derive the adaptive control algorithms the mathematical model of IPMSM as derived in chapter 2 is considered.

$$\dot{i}_q = \frac{1}{L_q}(v_q - Ri_q - P\omega_r L_d i_d - P\omega_r \psi) \tag{3.1}$$

$$\dot{i}_d = \frac{1}{L_d}(v_d - Ri_d + P\omega_r L_q i_q) \tag{3.2}$$

$$T_e = \frac{3P}{2}\left[\psi\, i_q + \left(L_d - L_q\right) i_d i_q\right] \tag{3.3}$$

$$T_e = T_L + B_m\omega_r + J\dot{\omega}_r \tag{3.4}$$

In order to achieve high performance from an IPMSM, the vector control technique is utilized for the proposed adaptive backstepping based nonlinear controller (ABNC) of IPMSM drive. Command d-axis and q-axis input voltages are developed in the proposed controller to guarantee high speed tracking performance of the IPMSM. The first step for the purpose of velocity tracking is to select the input variable with proper value in order to ensure the convergence of the motor speed to the command speed. The speed error is defined as,

$$e = \omega_r^* - \omega_r \tag{3.5}$$

Then from (3.3)-(3.5) one can get,

$$\dot{e} = -\dot{\omega}_r = \frac{1}{J}[B_m\omega_r + T_L - \frac{3P}{2}(\psi i_q + (L_d - L_q)i_d i_q)] \tag{3.6}$$

Considering the Lyapunov's function as, $V_2 = \frac{1}{2}e^2$, the derivative of the Lyapunov's function is given by,

$$\dot{V} = e\dot{e} = \frac{e}{J}(B_m\omega_r + T_L - \frac{3P}{2}\left[\psi i_q + \left(L_d - L_q\right) i_d i_q\right])$$

$$= -k_s e^2 + \frac{e}{J}\{(B_m\omega_r + T_L - \frac{3P}{2}\psi i_q + k_s Je) - \frac{3P}{2}\left(L_d - L_q\right) i_d i_q\} \tag{3.7}$$

where k_s is a closed loop feedback constant. In order to stabilize the motor speed the d-q-axes currents are identified as virtual control variables. Many researchers have focused their attention on the vector control of the IPMSM drive by forcing i_d, equal to zero, which essentially linearizes the torque equation [34,82]. However, in real-time, the electromagnetic torque is, in fact, nonlinear in nature. In order to incorporate this nonlinearity in a practical IPMSM drive, a simplified control technique for MTPA is derived to provide required motor torque with the minimum possible stator current. For MTPA technique, the relationship between i_d and i_q can be obtained as [74],

$$i_d = \frac{\psi}{2(L_q - L_d)} - \sqrt{\frac{\psi^2}{4\left(L_q - L_d\right)^2} + i_q^2} \tag{3.8}$$

For real-time implementation of the drive system with MTPA within rated speed, the proposed work presents a simplified relationship between the d-q axis currents by expanding the square root term of the equation (3.8) using Taylor's series around zero.

$$i_d = \frac{\psi}{2(L_q - L_d)} - \frac{\psi}{2(L_q - L_d)}\sqrt{1 + \frac{4\left(L_q - L_d\right)^2}{\psi^2} i_q^2}$$

$$= \frac{\psi}{2(L_q - L_d)} - \frac{\psi}{2(L_q - L_d)}(1 + \frac{2\left(L_q - L_d\right)^2}{\psi^2} i_q^2 + \text{ higher order of } \frac{4\left(L_q - L_d\right)^2}{\psi^2} i_q^2)$$

Neglecting the higher order of $\frac{4\left(L_q - L_d\right)^2}{\psi^2} i_q^2$, the expression of d-axis current can be written as,

$$i_d = -\frac{\left(L_q - L_d\right)}{\psi} i_q^2 \tag{3.9}$$

With this value of i_d, speed control tracking can be achieved from equation (3.7) by choosing the command q axis current as,

$$i_q^* = \frac{2}{3P\psi}[(T_L + B_m\omega_r + k_s Je) - \frac{3P}{2}(L_d - L_q)^2 \frac{i_q^3}{\psi}] \tag{3.10}$$

Since the value of load torque is unknown and the motor parameters are varying with different operating condition, these values should be estimated adaptively. So from equation (3.7) the command values of d and q axis currents can be chosen as,

$$i_d^* = -\frac{(L_q - L_d)}{\psi} i_q^2 \tag{3.11}$$

$$i_q^* = \frac{2}{3P\psi}[(\hat{T}_L + \hat{B}_m \omega_r + k_s \hat{J} e) - \frac{3P}{2}(L_d - L_q)^2 \frac{i_q^3}{\psi}] \tag{3.12}$$

where $\hat{T}_L$, $\hat{B}_m$ and $\hat{J}$ are the corresponding estimated parameter values.So if actual d-q axes current converge to command current, then the derivative of the Lyapunov's function becomes,

$$\dot{V} = -k_s e^2$$

Defining the load torque estimation error, $\tilde{T}_L = \hat{T}_L - T_L$, and friction and damping coefficient error, $\tilde{B}_m = \hat{B}_m - B_m$, d axis current error, $e_d = i_d^* - i_d$ and q-axis current error, $e_q = i_q^* - i_q$, the error dynamics from (3.6) can be rewritten as,

$$\dot{e} = \frac{1}{J}[B_m\omega_r + T_L - \frac{3P}{2}(\frac{2}{3P}(\hat{B}_m\omega_r + \hat{T}_L + K_s\hat{J}e - \frac{3P}{2}(L_q - L_d)^2 \frac{i_q^3}{\psi}) + \frac{3P}{2}(L_q - L_d) i_d i_q) + \frac{3P}{2}\psi e_q]$$

$$= \frac{1}{J}[-\tilde{T}_L - \tilde{B}_m\omega_r - K_s\hat{J}e + \frac{3P}{2}\psi e_q - \frac{3P}{2}(L_q - L_d) e_d i_q] \tag{3.13}$$

For stabilizing the d,q axis current vectors, the d,q axis current error dynamics can be defined as,

$$e_d = i_d^* - i_d = \frac{(L_d - L_q)2i_q}{\psi}\left(-\frac{Ri_q}{L_q} - \frac{P\omega_r L_d i_d}{L_q} + \frac{v_q}{L_q} - \frac{P\omega_r\psi}{L_q}\right) + \frac{Ri_d}{L_d} - \frac{P\omega_r L_q i_q}{L_d} - \frac{v_d}{L_d} \tag{3.14}$$

$$e_q = i_q^* - i_q = \frac{2}{3P\psi}\left(\hat{B}_m\frac{d\omega_r}{dt} + k_s\hat{J}\frac{de}{dt} - \frac{9P(L_q - L_d)^2 i_q^2}{2\psi}\frac{di_q}{dt}\right) - \frac{di_q}{dt}$$

$$= \frac{2}{3P\psi}\left(\hat{B}_m\frac{d\omega_r}{dt} + k_s\hat{J}\frac{de}{dt}\right) - \frac{3(L_q - L_d)^2 i_q^2}{\psi^2}\frac{di_q}{dt} - \frac{di_q}{dt}$$

$$= \frac{2}{3P\psi}\left(\hat{B}_m\frac{d\omega_r}{dt} - k_s\hat{J}\frac{d\omega_r}{dt}\right) - \left\{\frac{3(L_q - L_d)^2 i_q^2}{\psi^2} + 1\right\}\frac{di_q}{dt}$$

$$= \frac{2}{3P\psi}\left((\hat{B}_m - k_s\hat{J})\frac{d\omega_r}{dt}\right) - \left\{\frac{3(L_q - L_d)^2 i_q^2}{\psi^2} + 1\right\}\left(-\frac{Ri_q}{L_q} - \frac{P\omega_r L_d i_d}{L_q} + \frac{v_q}{L_q} - \frac{P\omega_r\psi}{L_q}\right)$$

$$= \frac{2(\hat{B}_m - k_s\hat{J})}{3P\psi J}\left(\frac{3P}{2}[\psi i_q + (L_d - L_q)i_d i_q] - B_m\omega_r - T_L\right) + \frac{3}{\psi^2}(L_d - L_q)^2 i_q^2\left(\frac{Ri_q}{L_q} + \frac{P\omega_r L_d i_d}{L_q} - \frac{v_q}{L_q}\right.$$

$$\left. + \frac{P\omega_r\psi}{L_q}\right) + \frac{Ri_q}{L_q} + \frac{P\omega_r L_d i_d}{L_q} - \frac{v_q}{L_q} + \frac{P\omega_r\psi}{L_q} \tag{3.15}$$

Besides the estimation of B_m and T_L, another mechanical parameter, J also need to be estimated online. Hence the corresponding error variable can be defined as,

$$\tilde{A} = \frac{1}{\hat{J}} - \frac{1}{J} \tag{3.16}$$

As the mechanical parameters of the system change at the different operating condition, those should be determined adaptively. Based on the error dynamics, new Lyapunov's function including the d-q axes current error variables and estimation error variables can de define as,

$$V_2 = \frac{1}{2}\left(e^2 + e_d^2 + e_q^2 + \frac{1}{\gamma_1}\tilde{A}^2 + \frac{1}{\gamma_2}\tilde{B}_m^2 + \frac{1}{\gamma_3}\tilde{T}_L^2\right) \tag{3.17}$$

By differentiating the Lyapunov's function and using the value of error dynamics one can get,

$$\dot{V}_2 = e\dot{e} + e_d\dot{e}_d + e_q\dot{e}_q + \frac{1}{\gamma 1}\tilde{A}\dot{\tilde{A}} + \frac{1}{\gamma 2}\tilde{B}_m\dot{\tilde{B}}_m + \frac{1}{\gamma 3}\tilde{T}_L\dot{\tilde{T}}_L$$

$$= -k_s e^2 - k_1 e_d^2 - k_2 e_q^2 + \frac{1}{\gamma_1}\tilde{A}\dot{\tilde{A}} + \frac{1}{\gamma_2}\tilde{B}_m\dot{\tilde{B}}_m + \frac{1}{\gamma_3}\tilde{T}_L\dot{\tilde{T}}_L + \frac{e}{J}[-\tilde{T}_L - \tilde{B}_m\omega_r - K_s\tilde{J}e + \frac{3P}{2}\psi e_q - \frac{3P}{2}(L_q$$

$$-L_d)e_d i_q] + e_d[\frac{(L_d - L_q)2i_q}{\psi}(-\frac{Ri_q}{L_q} - \frac{P\omega_r L_d i_d}{L_q} + \frac{v_q}{L_q} - \frac{P\omega_r\psi}{L_q}) + \frac{Ri_d}{L_d} - \frac{P\omega_r L_q i_q}{L_d} - \frac{v_d}{L_d} + k_1 e_d]$$

$$+e_q[\frac{2(\hat{B}_m - k_s\hat{J})}{3P\psi J}(\frac{3P}{2}[\psi i_q + (L_d - L_q)i_d i_q] - B_m\omega_r - T_L) + \frac{3}{\psi^2}(L_d - L_q)^2 i_q^2(\frac{Ri_q}{L_q} + \frac{P\omega_r L_d i_d}{L_q} - \frac{v_q}{L_q}$$

$$+\frac{P\omega_r\psi}{L_q}) + \frac{Ri_q}{L_q} + \frac{P\omega_r L_d i_d}{L_q} - \frac{v_q}{L_q} + \frac{P\omega_r\psi}{L_q} + \frac{2}{3P\psi}(\dot{\tilde{T}}_L + \dot{\tilde{B}}\omega_r + \dot{J}K_s e) + k_2 e_q] \qquad (3.18)$$

the control d-q voltages can be derived from (3.1) – (3.4) and (3.18) as follows [83],

$$v_d = Ri_d - P\omega_r L_q i_q + k_1 e_d L_d - \frac{3P}{2\hat{J}}L_d(L_q - L_d)i_q e\frac{(L_d - L_q)2i_q L_d\psi}{\psi^2 + 3(L_q - L_d)^2 i_q^2}$$

$$(\frac{2(\hat{B}_m - k_s\hat{J})}{3P\psi\hat{J}}(\frac{3P}{2}[\psi_m i_q + (L_d - L_q)i_d i_q] - \hat{B}_m\omega_r - \hat{T}_L) + k_2 e_q + \frac{3P}{2\hat{J}}\psi e) \qquad (3.19)$$

$$v_q = \frac{\psi^2}{\psi^2 + 3(L_q - L_d)^2 i_q^2}(\frac{2L_q(\hat{B}_m - k_s\hat{J})}{3P\psi\hat{J}}(\frac{3P}{2}[\psi_m i_q + (L_d - L_q)i_d i_q] - \hat{B}_m\omega_r - \hat{T}_L) + Ri_q + P\omega_r L_d i_d$$

$$+P\omega_r\psi + k_2 e_q L_q + \frac{3}{\psi^2}(L_q - L_d)^2 i_q^2(Ri_q + P\omega_r L_d i_d + P\omega_r\psi) + \frac{3P}{2\hat{J}}\psi e L_q] \qquad (3.20)$$

where k_s, k_1, k_2 are the closed loop feedback constants.

3.3 Development of mechanical parameters update laws

Choosing the values of these d and q axis voltages and substituting these values in equation (3.18) with further simplification, the Lyapunov's function becomes,

$$\dot{V}_2 = \frac{e}{J}[-\tilde{T}_L - \tilde{B}_m\omega_r + \frac{3P}{2}\psi e_q - \frac{3P}{2}(L_q - L_d)e_d i_q] + e_d\frac{3P(L_d - L_q)i_q e}{2\hat{J}} + e_q[(\frac{2(\hat{B}_m - k_s\hat{J})}{3P\psi J}$$

$$+\frac{2(\hat{B}_m - k_s\hat{J})}{3P\psi\hat{J}}(\tilde{B}_m\omega_r + \tilde{T}_L) - \frac{3P}{2\hat{J}}\psi e] - \frac{2(\hat{B}_m - k_s\hat{J})}{3P\psi\hat{J}})(\frac{3P}{2}[\psi i_q\psi i_q + (L_d - L_q)i_d i_q$$

$$-k_s e^2 - k_1 e_d^2 - k_2 e_q^2 + \frac{1}{\gamma_1}\tilde{A}\dot{\tilde{A}} + \frac{1}{\gamma_2}\tilde{B}_m\dot{\tilde{B}}_m + \frac{1}{\gamma_3}\tilde{T}_L\dot{\tilde{T}}_L \tag{3.21}$$

Equation (3.21) can be simplified in the following form:

$$\dot{V}_2 = -k_s e^2 - k_1 e_d^2 - k_2 e_q^2 + \tilde{T}_L[-\frac{e}{J} + \frac{2e_q(B_m - k_s J)}{3P\psi J} + \frac{1}{\gamma 3}\dot{\tilde{T}}_L]$$

$$+\tilde{B}_m[-\frac{e}{J} + \frac{2e_q(B_m - k_s J)}{3P\psi J} + \frac{1}{\gamma_2}\dot{\tilde{B}}_m\omega_r] + \tilde{A}[\frac{3P\psi e e_q}{2} - \frac{3P}{2}(L_q - L_d)i_q e e_d$$

$$+\frac{e_q(\hat{B}_m - k_s\hat{J})}{\psi}[\psi i_q + (L_d - L_q)i_d i_q] - \frac{1}{\gamma 1}\dot{\tilde{A}}] \tag{3.22}$$

where γ_1, γ_2, γ_3 are adaptive gains. The update laws for the estimated adaptive values can be derived as [83]:

$$\dot{\tilde{T}}_L = -\gamma_3[-\frac{e}{\hat{J}} + \frac{2e_q(\hat{B}_m - k_s\hat{J})}{3P\psi\hat{J}}] \tag{3.23}$$

$$\dot{\tilde{B}}_m = -\gamma_2\frac{1}{\omega_r}[-\frac{e}{\hat{J}} + \frac{2e_q(\hat{B}_m - k_s\hat{J})}{3P\psi\hat{J}}] \tag{3.24}$$

$$\dot{\tilde{A}} = \gamma_1[\frac{3P\psi e e_q}{2} - \frac{3P}{2}(L_q - L_d)i_q e e_d + \frac{e_q(\hat{B}_m - k_s\hat{J})}{\psi}[\psi i_q + (L_d - L_q)i_d i_q]] \tag{3.25}$$

The right hand side of update laws also contain the updated parameters. For the first sample nominal values of the parameters are used in the right side and then updated parameters are used from the next sample. Based on the algorithm mentioned earlier the block diagram of the proposed ABNC based IPMSM drive is shown in Fig.3.1.

3.4 Simulation result of the proposed ABNC based IPMSM drive

In order to verify the effectiveness of the proposed controller, a computer simulation model is developed using Matlab/Simulink software as per Fig.3.1 [84]. The gain used in the simulation model of ABNC drive system are k_s=25, k_1=500, k_2=1000. The detailed simulation results are presented after an explanation of the complete drive system. The dynamics of the IPMSM is complex because of its nonlinear nature and also the discrete time nature of the inverter and motor system. So the explanation of the complete drive system includes the mathematical model development of inverter and other parts of the drive system.

3.4.1 ABNC drive system

In order to predict the behaviour of the proposed drive a simulation model of the proposed drive has been tested before it is implemented in real-time. The complete simulink block diagram for the proposed ABNC drive is shown in Fig.3.2. The motor parameter used for this simulation is shown in Appendix A. The details of each subsystem are shown in Appendix B. The state space equation (3.1)-(3.4) for IPMSM is used for motor model in simulink. The command current of the controller is generated using equations (3.11)-(3.12). Adaptive controller is simulated in the controller block using control law equation (3.19)-(3.20) to give the command d and q axis voltages. The command voltages are applied to the inverse Clark and Park transformation *(dq/abc* block) to reverse into command *abc* coordinate values [9]. The Estimator block estimates

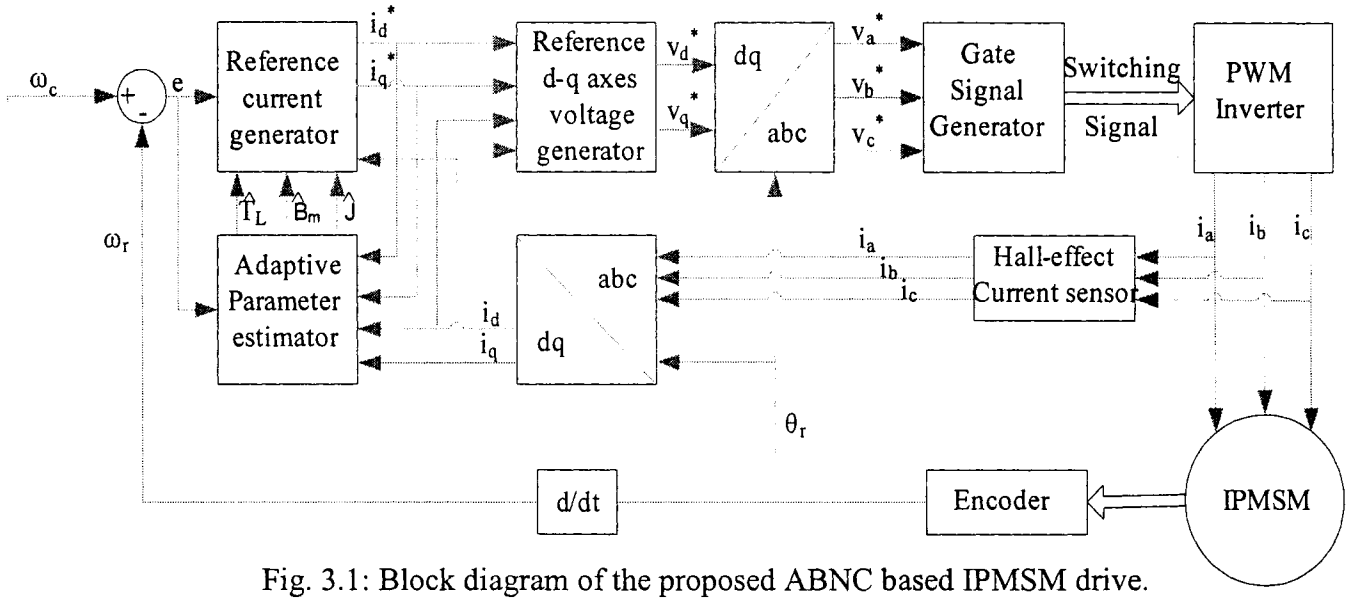

Fig. 3.1: Block diagram of the proposed ABNC based IPMSM drive.

the mechanical motor parameters using the update laws (3.23)-(3.25). The command abc voltages are the input to the pulse width modulation (PWM) signal generator. The PWM strategies considered in this thesis is hysteresis PWM. Three-phase reference voltages from the controller are compared with a common high frequency triangular carrier wave of fixed amplitude to generate PWM signals.

The switching logic of the corresponding inverter leg are given as follows,

if $v_{a,ref} > V_{triangle}$, SW1=1 (on) and SW4=0, State 1 for phase a

if $v_{a,ref} < V_{triangle}$, SW1=0 and SW4=1, State 0 for phase a

if $v_{b,ref} > V_{triangle}$, SW3=1 and SW6=0, State 1 for phase b

if $v_{b,ref} < V_{triangle}$, SW3=0 and SW6=1, State 0 for phase b

if $v_{c,ref} > V_{triangle}$, SW5=1 and SW2=0, State 1 for phase c

if $v_{c,ref} < V_{triangle}$, SW5=0 and SW2=1, State 0 for phase c

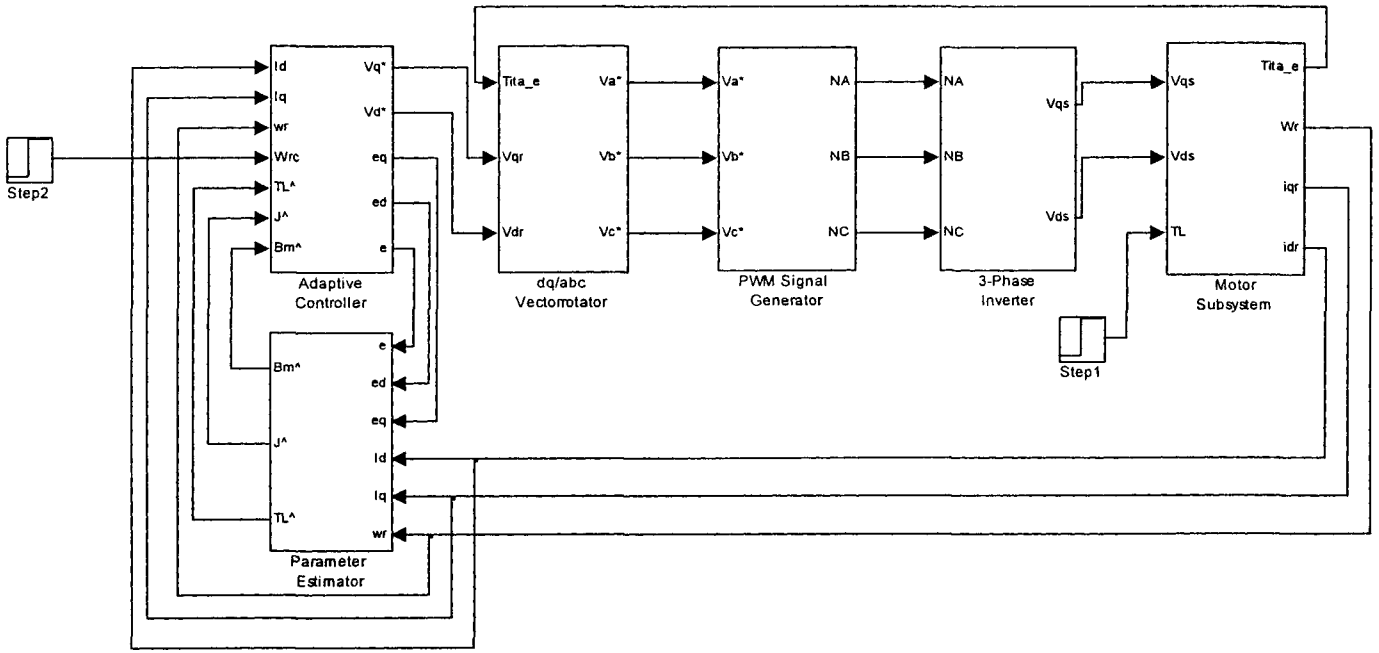

Fig.3.2: Simulink schematic of the complete ABNC drive for IPMSM.

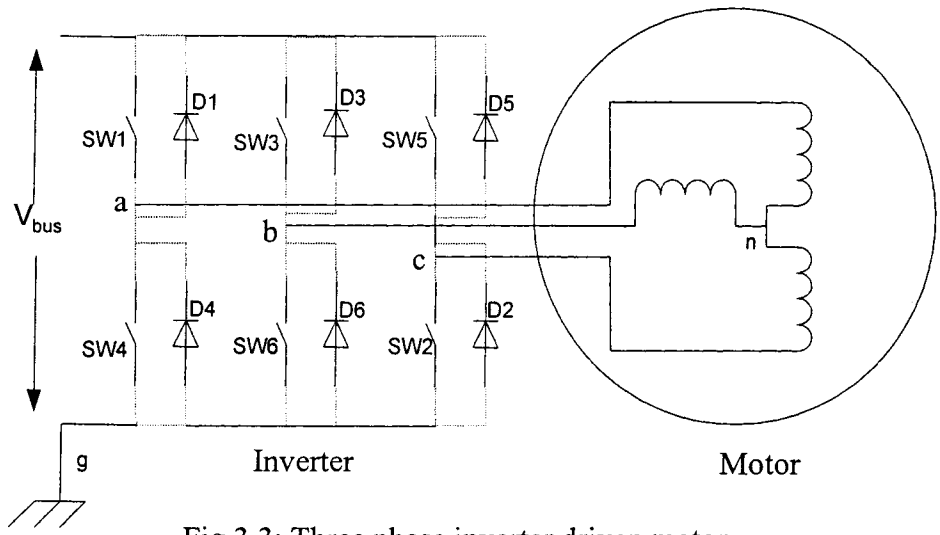

Fig.3.3: Three phase inverter driven motor.

The sinusoidal reference voltage establishes the desired fundamental frequency of the inverter output, while the triangular carrier wave establishes the switching frequency of the inverter.

To implement the simulink model of the 3-phase inverter, a relation has to be established between the phase voltages and switch signals. A 3-phase inverter consists of three legs, each having two switches and two anti-parallel freewheeling diodes as shown in Fig.3.3. The motor terminals *(a, b* and c) are connected to the mid-point of each inverter leg. The motor phase winding are Y-connected, 'n' is the neutral point which is not grounded and 'g' is the inverter ground. The inverter leg voltages (with respect to ground g) are denoted by v_{ag}, v_{bg} and v_{cg}.and the motor phase voltages (with respect to neutral n) are denoted by v_{an}, v_{bn} and v_{cn}. Application of Kirchhoff's voltage law to the inverter motor circuit it can be easily derived that

$$\begin{bmatrix} v_{an} \\ v_{bn} \\ v_{cn} \end{bmatrix} = \frac{1}{3}\begin{bmatrix} 2 & -1 & -1 \\ -1 & 2 & -1 \\ -1 & -1 & 2 \end{bmatrix}\begin{bmatrix} v_{ag} \\ v_{bg} \\ v_{cg} \end{bmatrix} \tag{3.26}$$

The values of v_{ag}, v_{bg} and v_{cg} depend on the switching logic signals SW1, SW2, SW3, SW4, SW5, SW6. As an example, if switch SW1 is on or logic '1' and switch SW4 is off or logic '0', the bus voltage would appear V_{bus} across terminals 'a' and 'g', therefore v_{ag} $=V_{bus}$. On the other hand, , if switch SW1 is off or logic '0' and switch SW4 is on or logic '1', the ground will be connected with terminals 'a'. therefore v_{ag} =0. Turning on both SW1 and SW4 would short the voltage bus to ground, Thus a dead time must be included in switching logic by intentionally delaying the all off-on transitions of the transistor switches. During the dead time, both SW1 and SW4 are simultaneously turned off and the direction of current i_a will determine the actual voltage. If $i_a < 0$, then $v_{ag}=V_{bus}$ and diode D1 will conduct. If $i_a > 0$, then v_{ag} =0 and diode D4 will conduct. Since the on-and-off states of the power switches in one inverter leg are always opposite without

Table 3.1: Inverter states and corresponding invert leg voltages and motor phase voltage.

Phase state 'abc'	v_{ag}	v_{bg}	v_{cg}	v_{an}	v_{bn}	v_{cn}
000	0	0	0	0	0	0
001	0	0	V_{bus}	-1/3 V_{bus}	-1/3 V_{bus}	2/3 V_{bus}
010	0	V_{bus}	0	-1/3 V_{bus}	2/3 V_{bus}	-1/3 V_{bus}
011	0	V_{bus}	V_{bus}	-2/3 V_{bus}	1/3 V_{bus}	1/3 V_{bus}
100	V_{bus}	0	0	2/3 V_{bus}	-1/3 V_{bus}	-1/3 V_{bus}
101	V_{bus}	0	V_{bus}	1/3 V_{bus}	-2/3 V_{bus}	1/3 V_{bus}
110	V_{bus}	V_{bus}	0	1/3 V_{bus}	1/3 V_{bus}	-2/3 V_{bus}
111	V_{bus}	V_{bus}	V_{bus}	0	0	0

considering the dead time, each inverter leg can be in either of two states. Therefore, the three-phase inverter as a whole can be in any of possible eight states. Table 3.1 summarizes these eight inverter states and corresponding invert leg voltages and motor phase voltage using the relations in (3.26).

3.4.2 Design of PI controller for comparison purpose

In order to prove the superiority of the proposed ABNC, a PI controller is designed for speed control. The input to the PI controller is the speed error and the output is the torque component of command current i_q^*. The PI type speed controller can be described as:

$$i_q^* = K_p \Delta \omega_r + K_i \int \Delta \omega_r dt$$

where $\Delta\omega_r$ is the speed error between actual and command speeds, K_p is the proportional gain and K_i is the integral gain for the PI controller. To determine the gains of PI controller, the following equations for second order system are used.

$$\zeta = \frac{B_m + K_p}{2\sqrt{K_i J_m}}$$

$$\omega_n = \sqrt{\frac{K_i}{J_m}}$$

At first the PI controller gains are selected as K_p=0.5 and K_i=3 to avoid overshoot but the controller becomes sluggish. In order to get a reasonable settling time, the PI speed controller parameters are played around these values by trial and error. The parameters of the PI controller are chosen by trail and error such that it gives the best performance such

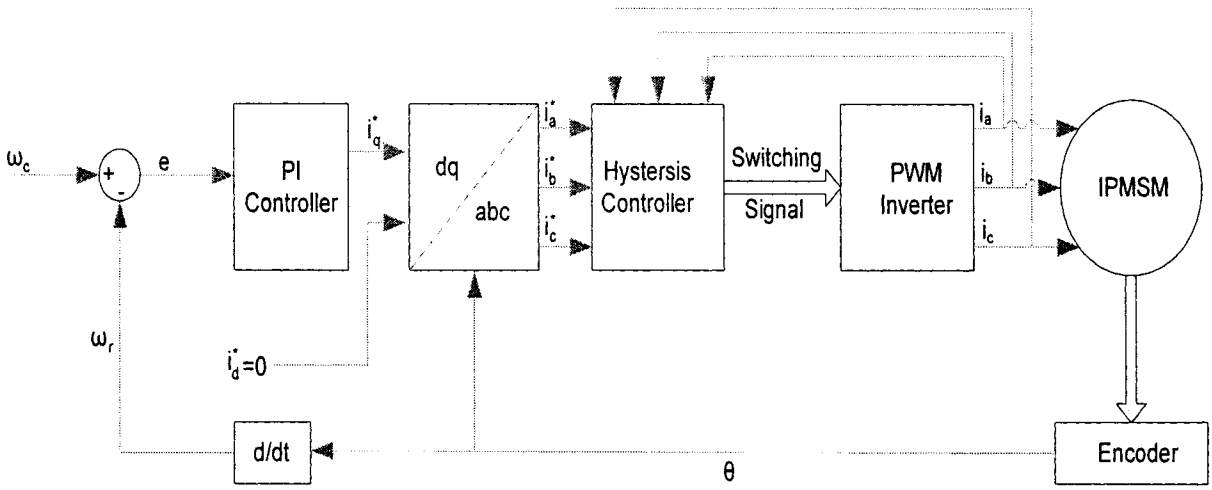

Fig.3.4: Block diagram of the PI controller based IPMSM drive.

as minimum overshoot, minimum settling time and zero steady state error based on simulation results. The constants are found to be, K_p=1 and K_i=8. The command d-axis current is considered as zero. These d and q axis command currents are transformed into abc coordinates and fed to a hysteresis current controller, which is used to generate the PWM gate signals for the inverter. The block diagram of the IPMSM drive with PI controller is shown in Fig.3.4.

3.4.3 Results and discussion

The performance of the proposed ABNC based IPMSM drive has been investigated extensively at different operating conditions. Sample results are presented below. In order to show the superiority a performance comparison of the proposed ABNC controller with a conventional PI controller is also provided. The simulated starting responses for the proposed ABNC and PI controller with full load (20Nm) at command

speed 183 rad/sec are shown in Figs.3.5-3.8. In Fig.3.5, the starting response of a PI controller is shown. The input to the PI controller is speed error and the output is command q-axis current. The values of the gains of PI speed controller are determined offline by trial and error such that it gives comparably better response for different condition. The proportional gain is selected equal to 8 and integral gain is selected at 1. In this case the motor speed can follow the command speed, the speed response has an overshoot and the starting current is also high. It is found in Fig 3.6 that settling time is less and the actual speed converges with the reference speed with no overshoot and steady state error. The line current is less for the same load torque as the proposed ABNC controller is designed with MTPA technique. For this particular motor as the saliency is not that significant, the effect of MTPA is not that high. The wave shape for d-axis and q-axis current are also shown for both PI and proposed ABNC controller. For the designing purpose of the proposed adaptive controller d and q axis currents are considered as virtual control variables. The d and q axis current errors and speed error and developed torque for the proposed controller are shown in Fig.3.7. All the current and speed errors converge to zero. Thus it ensures the global stability of the drive system and it was the goal in designing the controller. The estimated load torque, inertia constant and friction constant are shown in Fig. 3.8. These estimated values are not exactly following the nominal values but nearly nominal values. The reason is that the nominal values are measured with lot of assumptions and the purpose of adaptive controller is to adjust the parameter values with online changing condition. The speed response and corresponding line current, speed error of the PI controller at rated speed (183 rad/sec) with no load are shown in Fig.3.9. It is observed that it has high overshoot and long settling time at that

condition. The speed response and corresponding line current, d-q axes current of the proposed controller at rated speed (183 rad/sec) with no load are shown in Fig.3.10. The speed of the proposed drive can follow the reference speed negligible overshoot. But the settling time is little longer. The corresponding speed error, developed torque and virtual control variable errors are shown in 3.11. All the error variables converge to zero which indicate the stability of the drive system at no load. The corresponding estimated load torque and inertia and friction constant are shown in Fig.3.12. Although the only two cases, full load and no load conditions, are shown in this thesis, more simulations are done at different load conditions and satisfactory results are found.

One important property of a high performance drive is its robustness of the controller to the disturbance like change of load which is a very common type of disturbance. So this property should be tested and compared with PI controller. The speed response, line current and d-q axis currents with a step increase of load from no load to high load (15 N-m) at t=1.5 sec for PI controller and proposed ABNC controller are shown in Figs.3.13 and 3.14, respectively. In the case of PI controller, speed response has a high overshoot at start with no load and the speed deviation from the command speed is high with change of load. On other side, the proposed controller has a reasonably better performance for sudden change in load. Although there is a small deviation of speed with change of load but it converges within minimum time to the reference speed. The q axis current and d axis current converge to new value with change of load so that the motor actual speed follows the reference speed. The line current of the controller is shown in Fig.3.14(b). As the proposed controller maintains MTPA operation, it takes lowest line current to develop certain torque and hence the copper loss will be minimized. The

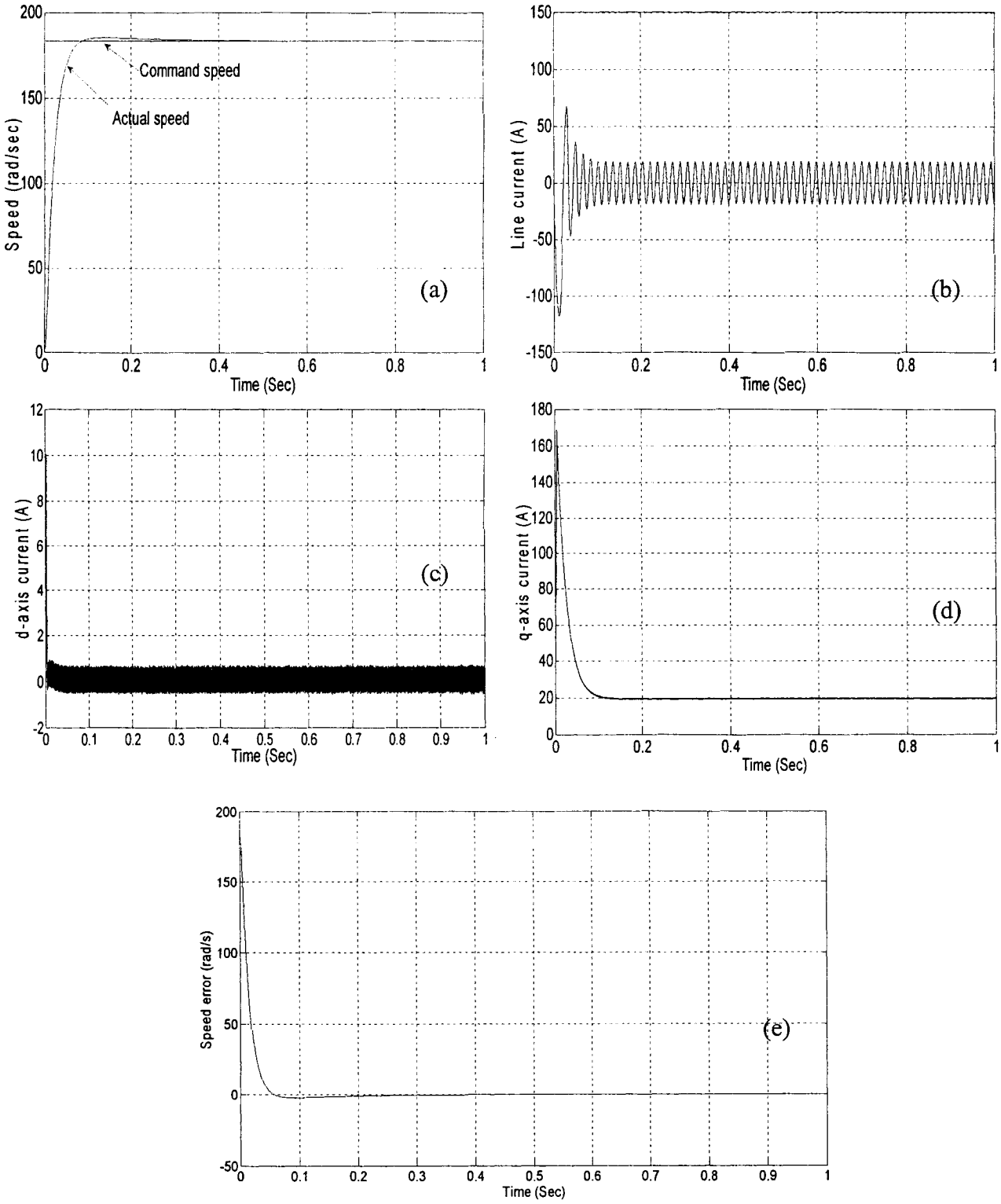

Fig.3.5. Simulated response of PI controller based IPMSM drive at full load (20Nm) and rated speed (183 rad/sec); (a) speed (b) line current (c) d-axis current (d) q-axis current (e) speed error.

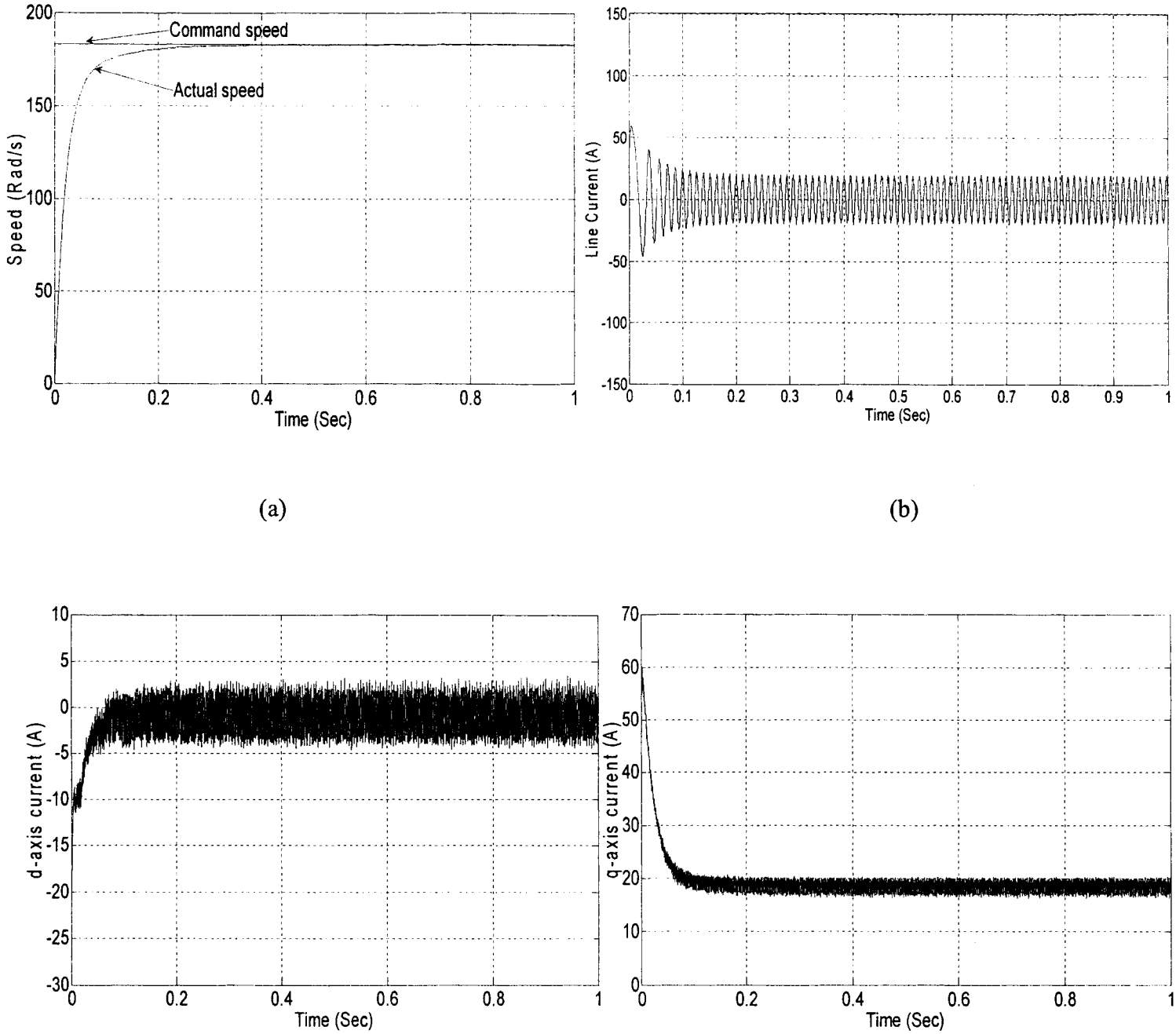

Fig.3.6: Simulated response of the proposed ABNC based IPMSM drive at full load (20Nm) and rated speed (183 rad/sec); (a) speed (b) line current (c) d-axis current (d) q-axis current.

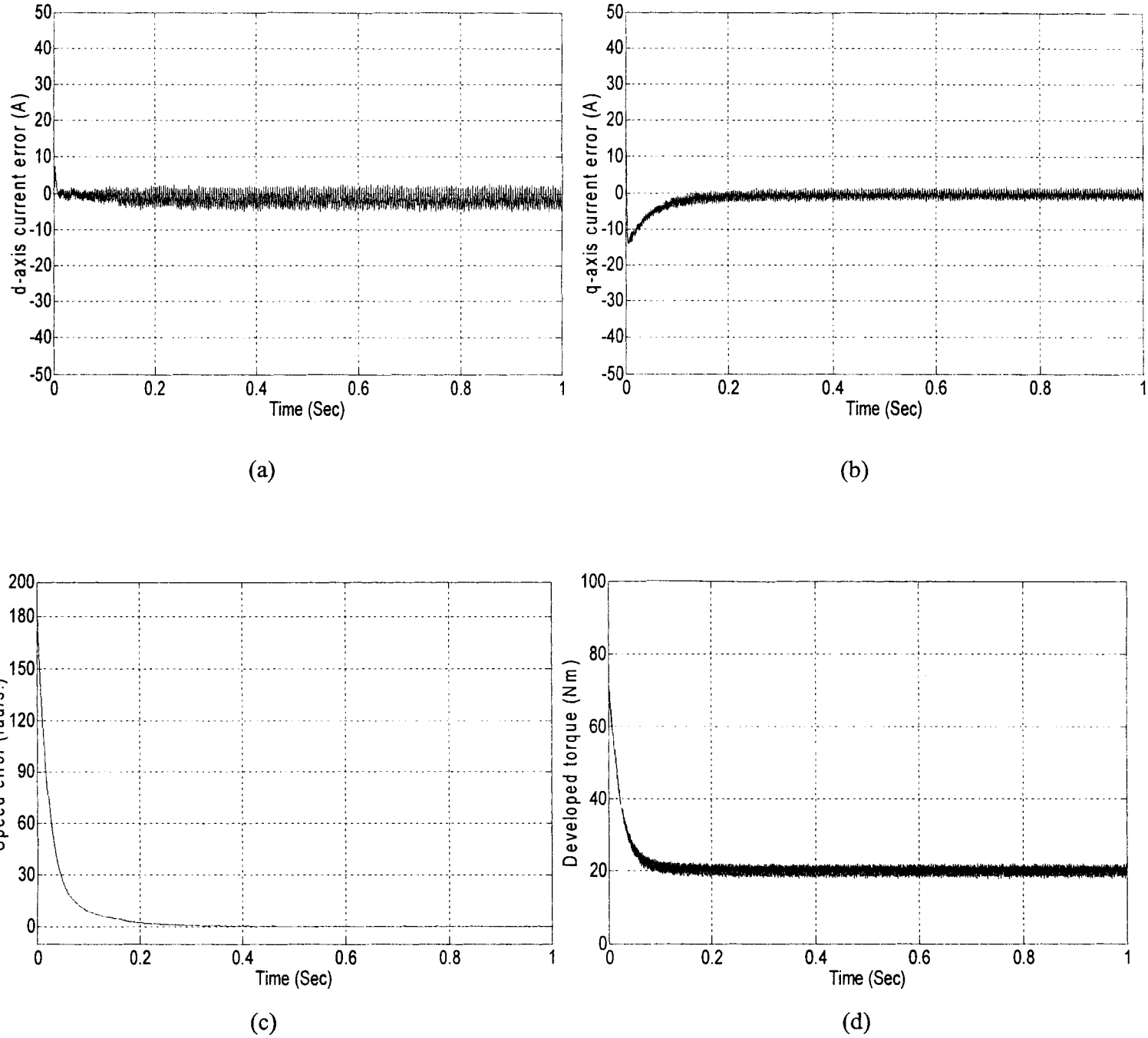

Fig.3.7: Simulated response of the proposed ABNC based IPMSM drive at full load (20Nm) and rated speed (183 rad/sec); (a) d-axis current error, e_d (b) q-axis current error, e_q (c) speed error, e_r (d) developed torque.

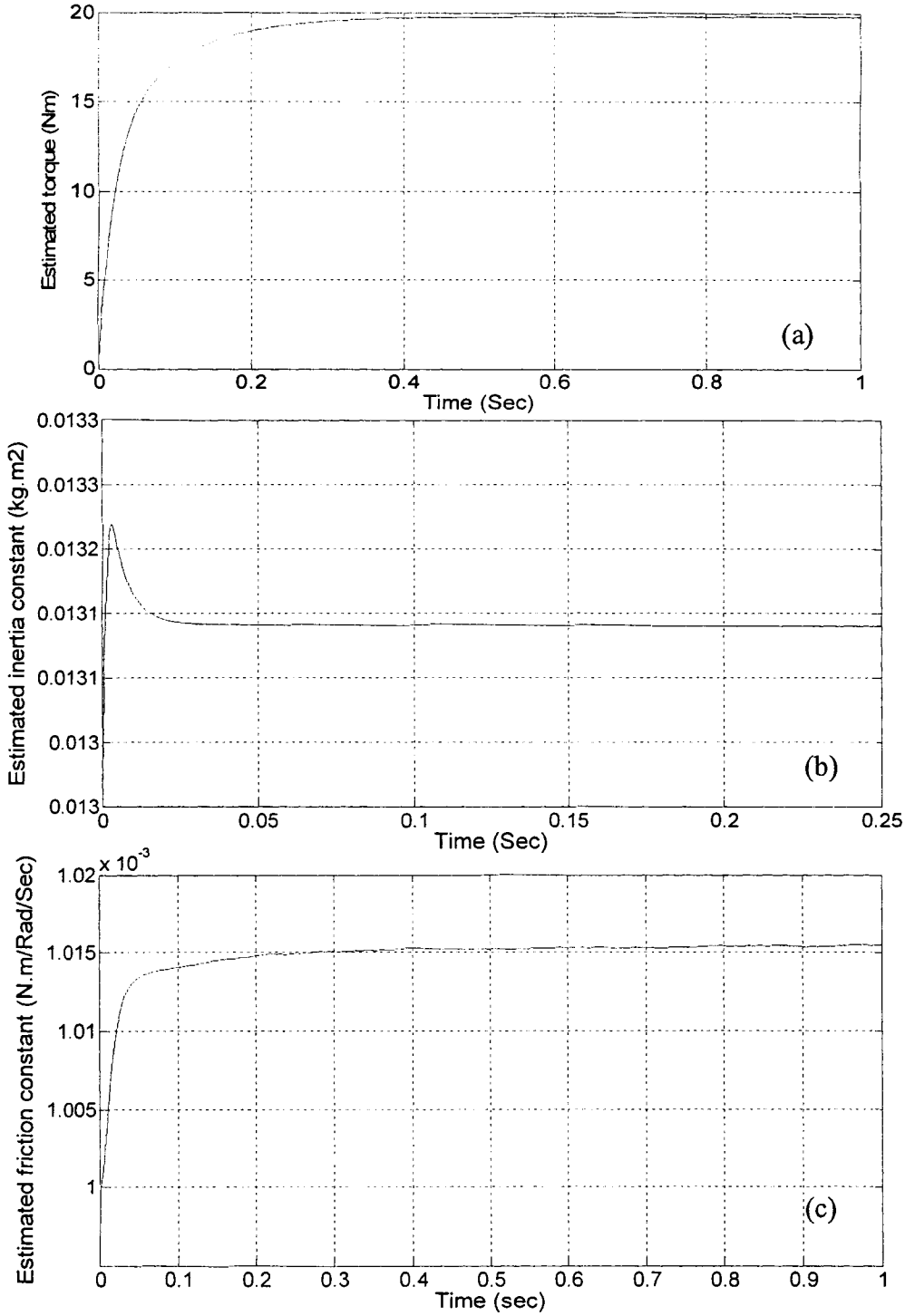

Fig.3.8: Simulated response of the proposed ABNC based IPMSM drive at full load (20Nm) and rated speed (183 rad/sec); (a) estimated load torque (b) estimated inertia constant (c) estimated friction constant.

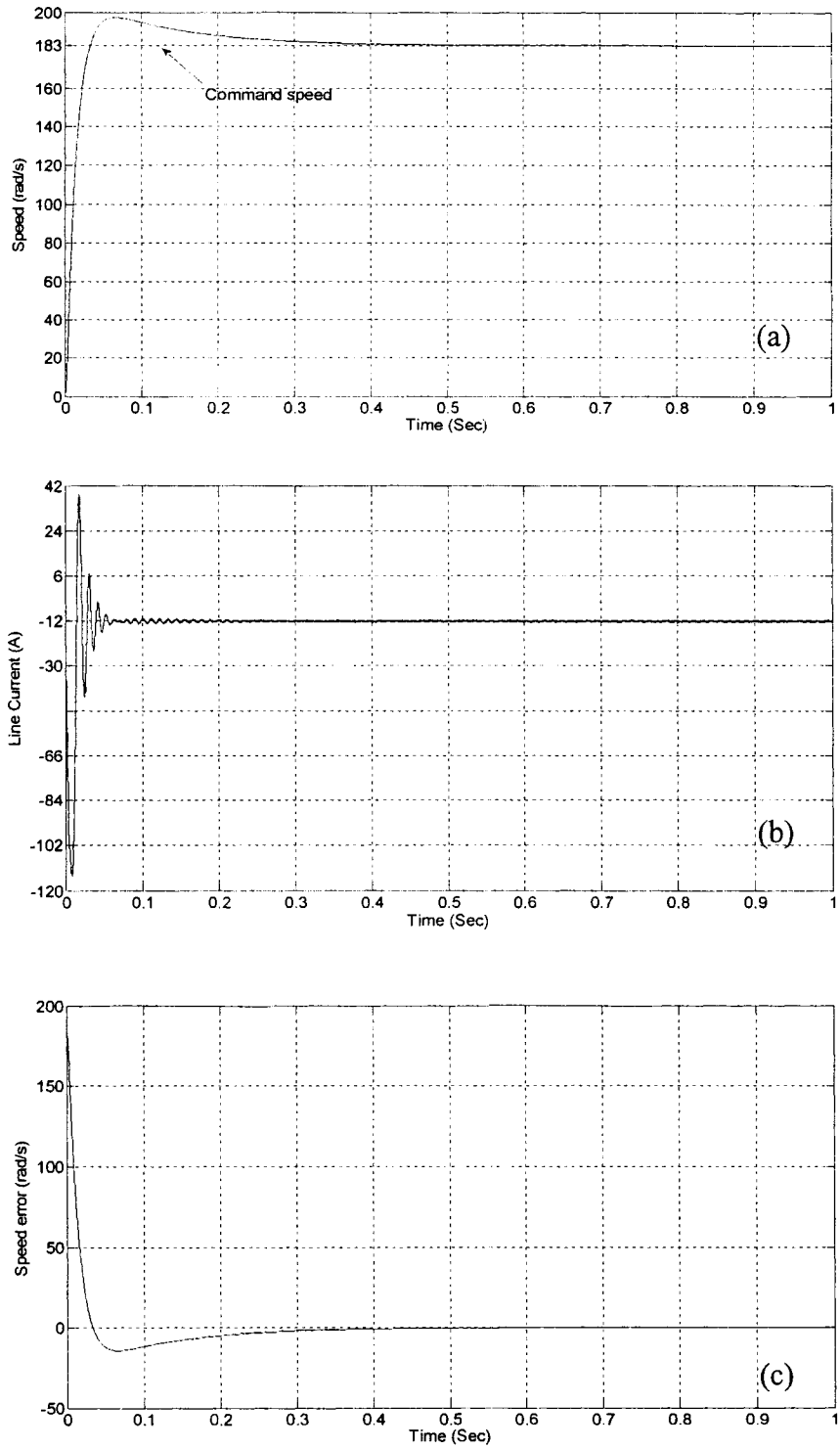

Fig.3.9: Simulated response of the PI based IPMSM drive at no load and rated speed (183 rad/sec); (a) speed (b) line current (c) speed error.

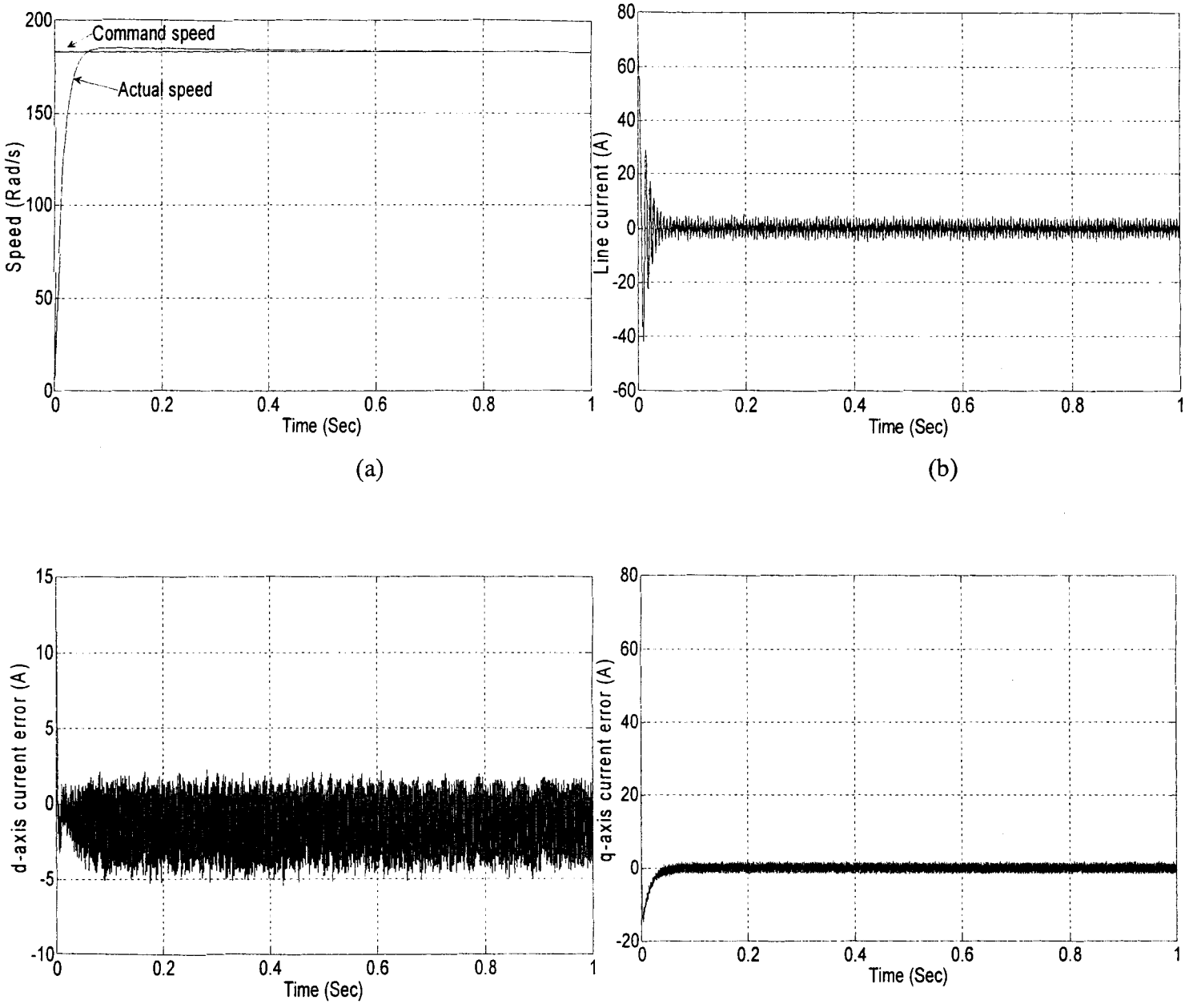

Fig.3.10: Simulated response of the proposed ABNC based IPMSM drive at no load and rated speed (183 rad/sec); (a) speed (b) line current (c) d-axis current (d) q-axis current.

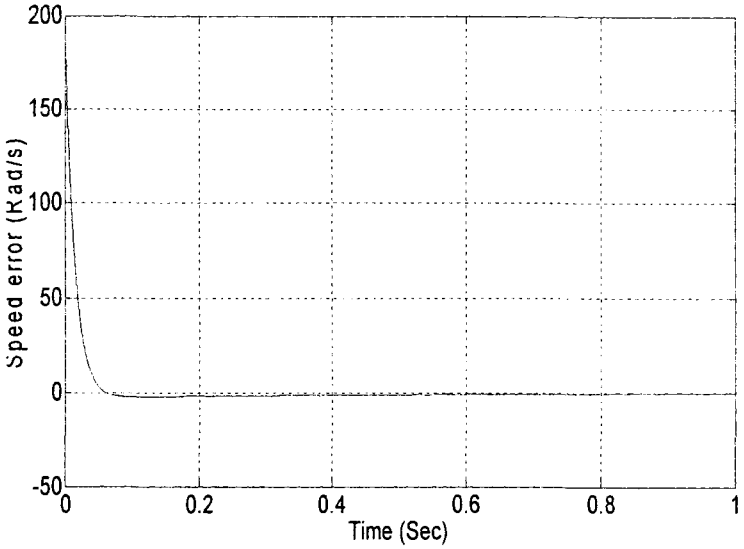

(a)

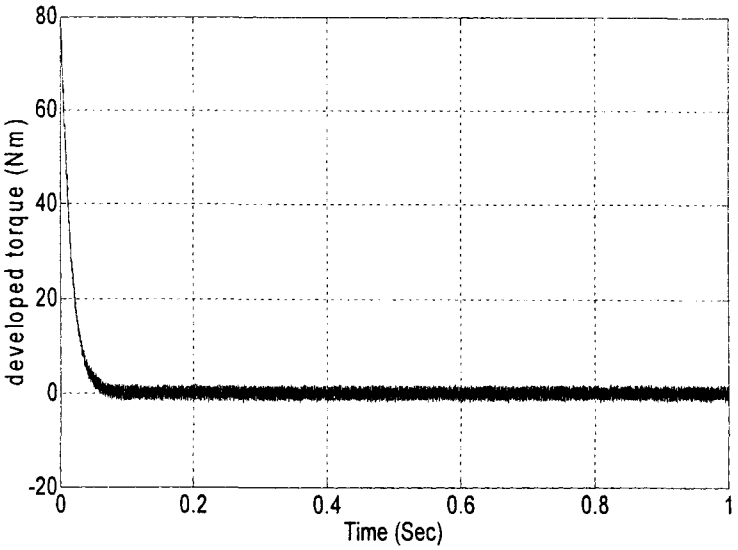

(b)

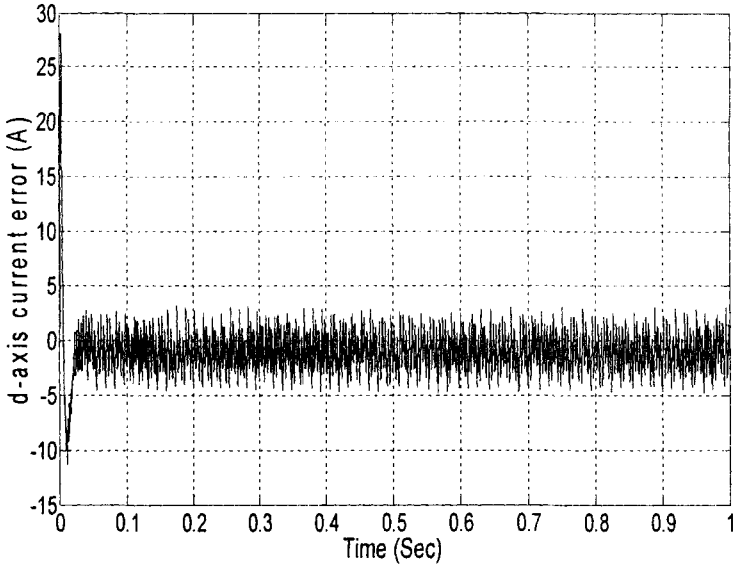

(c)

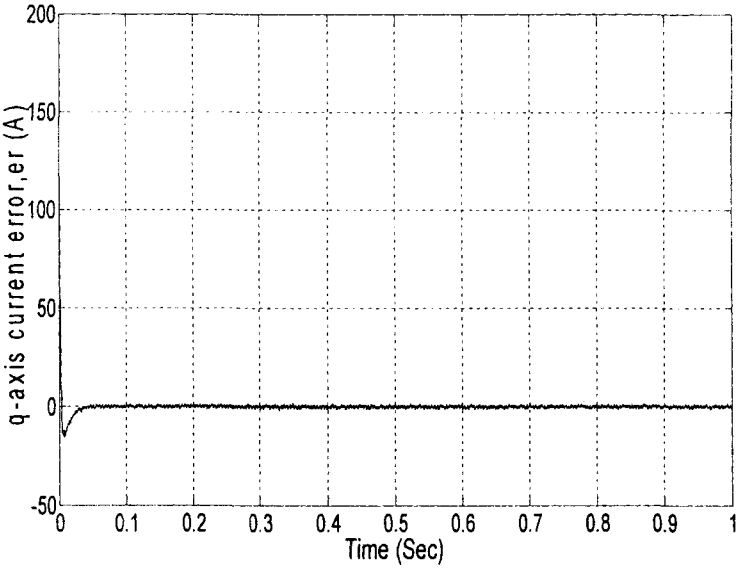

(d)

Fig.3.11: Simulated response of the proposed ABNC based IPMSM drive at no load and rated speed (183 rad/sec); (a) speed error, e_r (b) developed torque (c) d-axis current error, e_d (d) q-axis current error, e_q.

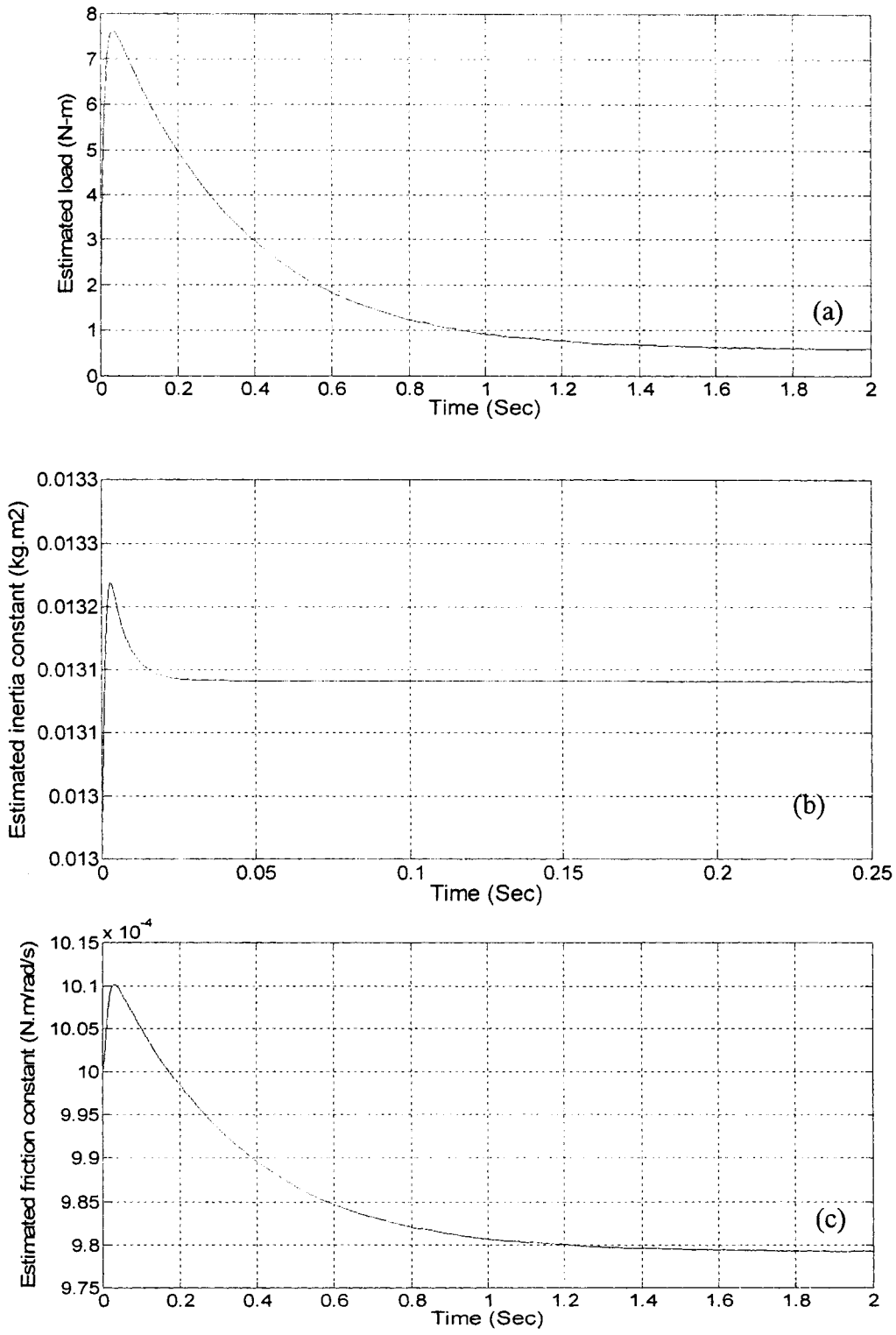

Fig.3.12: Simulated response of the proposed ABNC based IPMSM drive at no load and rated speed (183 rad/sec); (a) estimated load torque (b) estimated inertia constant (c) estimated friction constant.

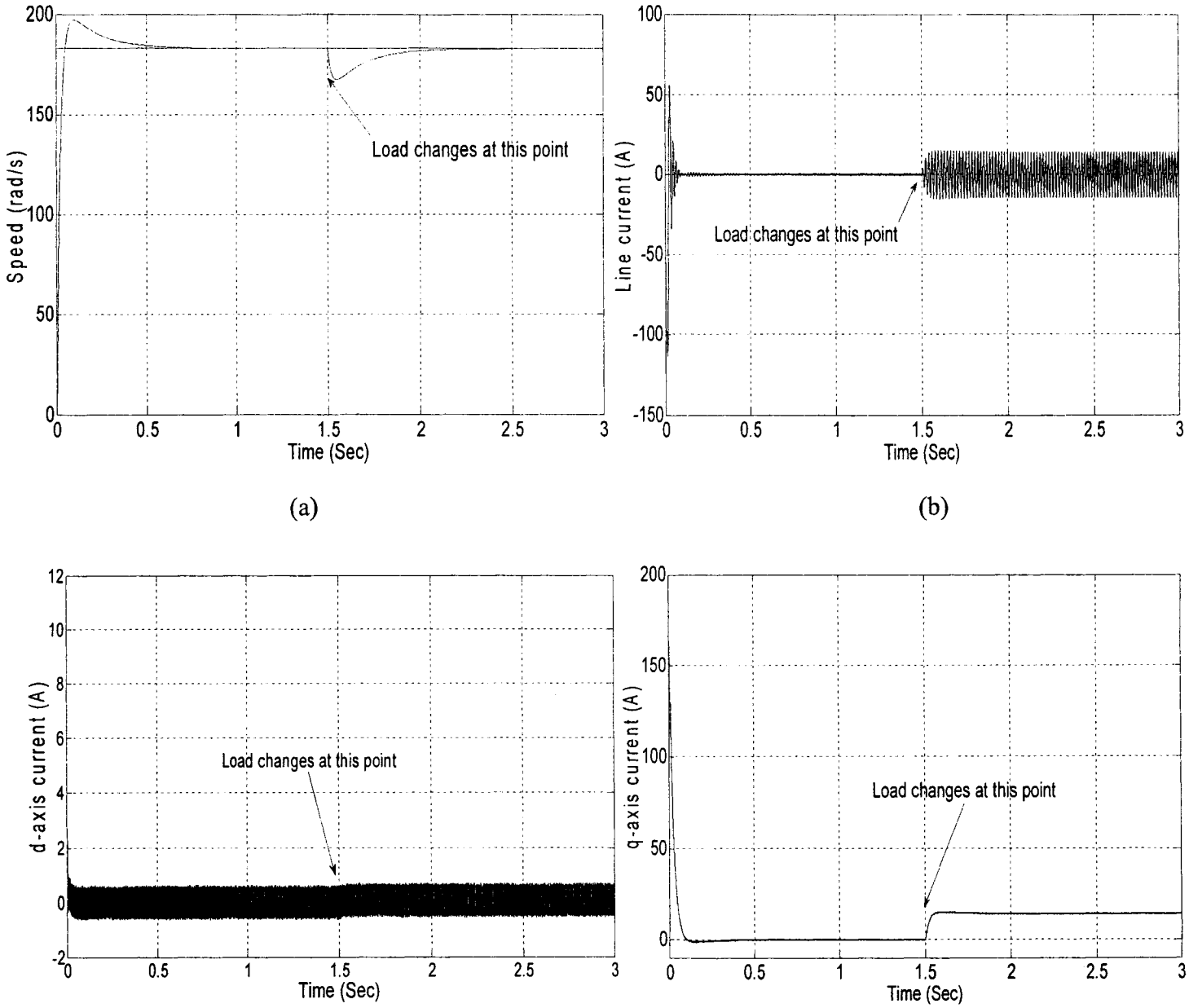

Fig.3.13: Simulated response of PI controller based IPMSM drive for a step increase of load from no load to high load (15Nm) and rated speed (183 rad/sec); (a) speed (b) line current (c) d-axis current (d) q-axis current.

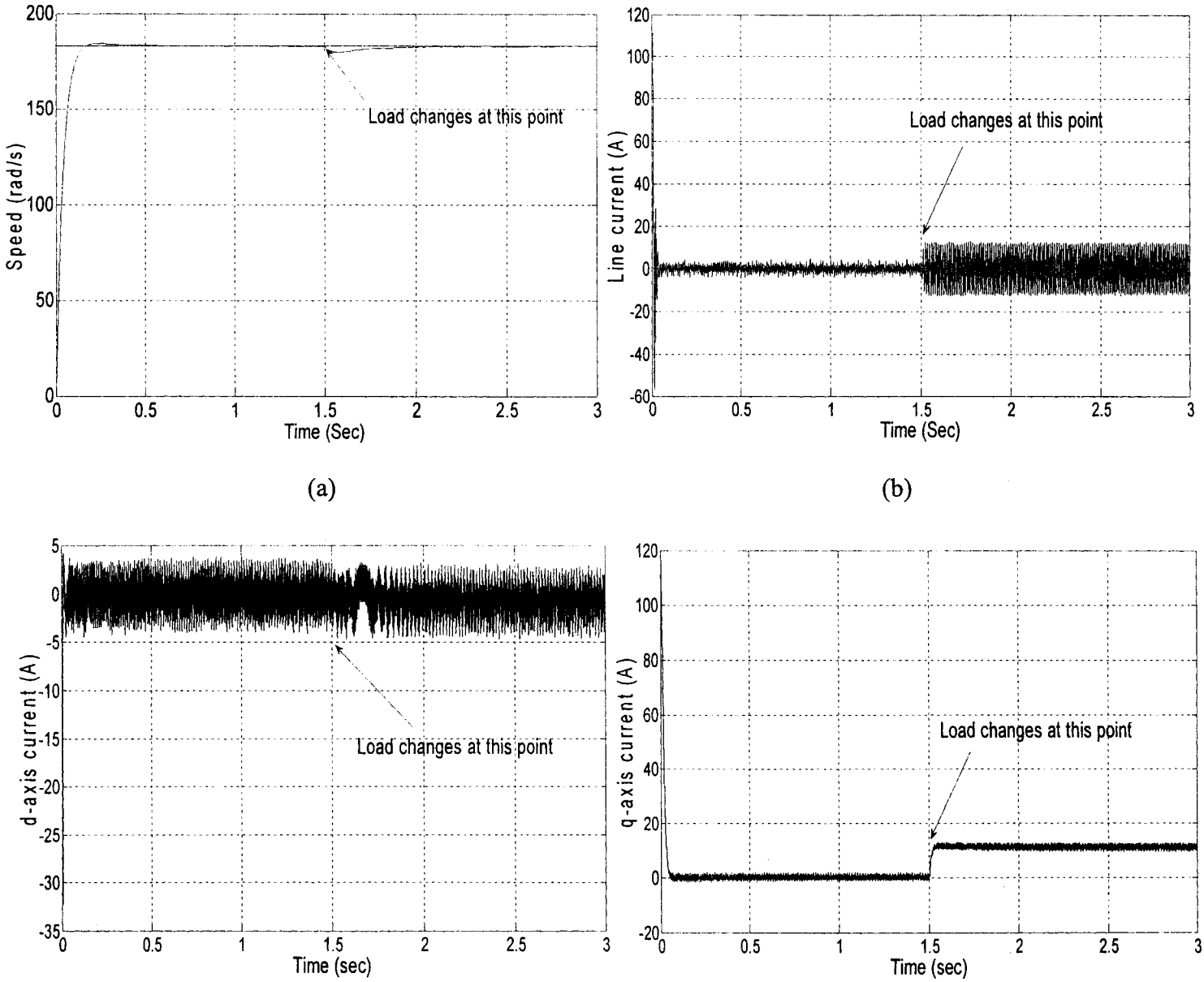

Fig.3.14: Simulated response of the proposed ABNC based IPMSM drive for a step increase of load from no load to high load (15Nm) and rated speed (183 rad/sec); (a) speed (b) line current (c) d-axis current (d) q-axis current.

corresponding d-q axis current is shown in Figs.3.14(c) and 3.14(d), respectively. If load increases from no load to full load, the torque component of the current increases and as the d-axis current depend on q-axis current to maintain MTPA, it also increases. Actually for the motor parameters used in this simulation, the difference between d and q axis inductance is very low, so the effect of reluctance torque, which is a result of interaction between d-q axis inductances is low as compared to magnetic torque. The speed error, developed torque and virtual control variable errors are shown in Fig.3.15. The developed torque converges to load torque with change of load and all error variables converge to zero. The estimated load torque can follow the actual load torque with the change of load as shown in Fig.3.16.

As the proposed controller use MTPA technique in controller design, it will enhance the operating region of the motor to constant power region upto ω_{cM} while maintaining voltage and current constraint as discussed in chapter 2. The value of ω_{cM} can be determined by using equation (2.36). So the speed range of this motor will be upto partial field weakening region (region IIA) with low load torque as shown in Fig.2.6. It is an essential property for high performance drive application to follow the reference speed with sudden change of reference speed according to the demand. The responses of the proposed controller for a change of command speed from constant torque region with speed 100 rad/sec to partially field weakening region with 200 rad/sec at no load are shown in the Fig.3.17. It shows that it can follow command speed with zero steady-state error and with very low overshoot. Thus, the drive can follow reference speed even above the rated speed with maintaining the voltage and current constraint. Fig.3.17(b) shows the corresponding line current and 3.17(c) and 3.17(d) show the d-q axis currents. Speed

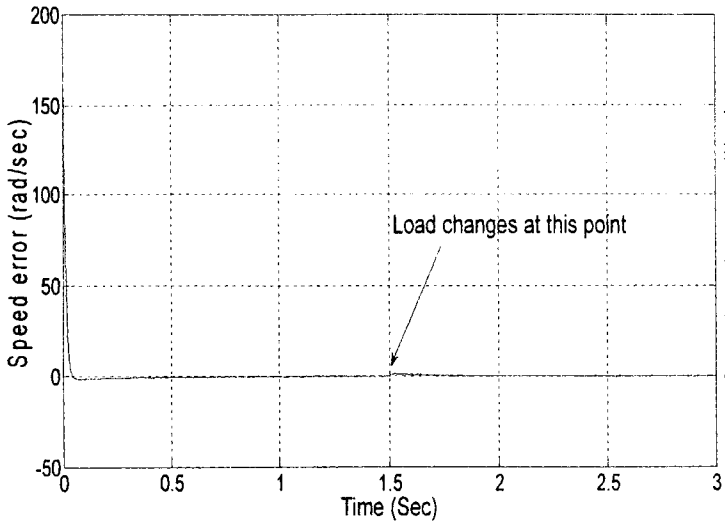

(a)

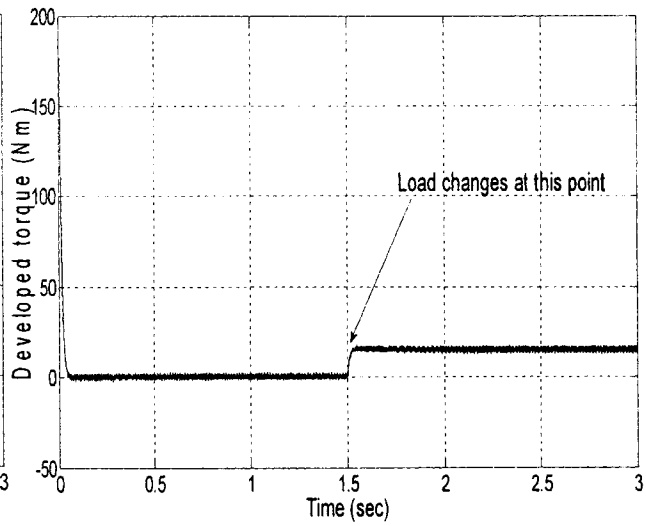

(b)

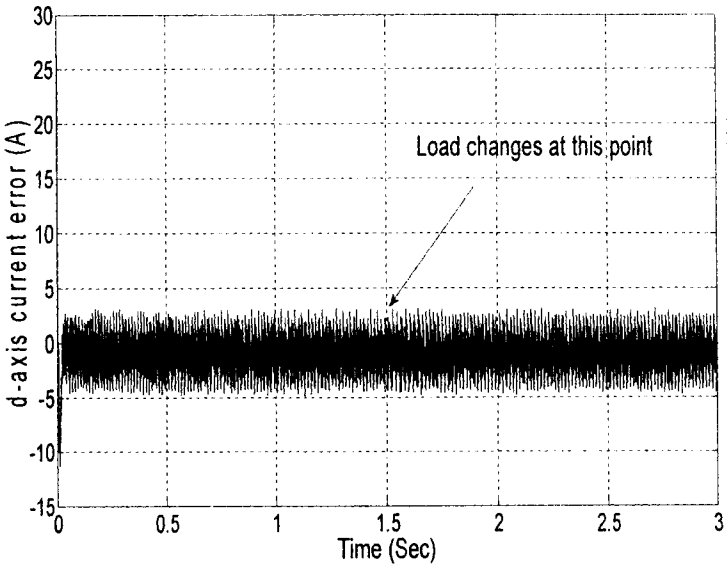

(c)

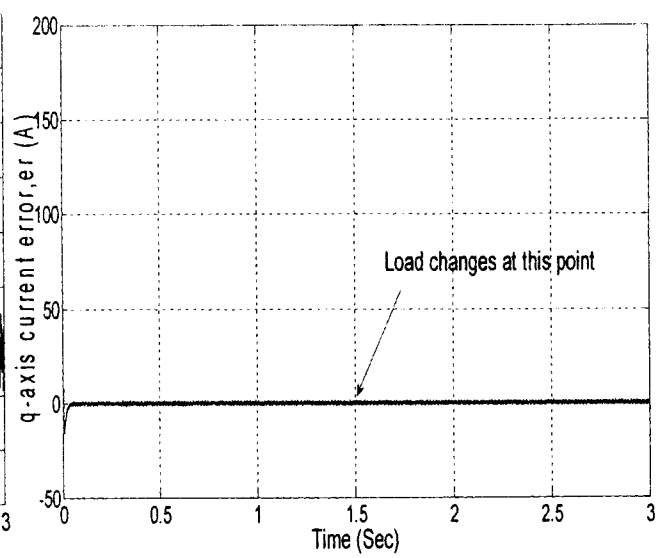

(d)

Fig.3.15: Simulated response of the proposed ABNC based IPMSM drive for a step increase of load from no load to high load (15Nm) and rated speed (183 rad/sec); (a) speed error, e_r (b) developed torque (c) d-axis current error, e_d (d) q-axis current error, e_q.

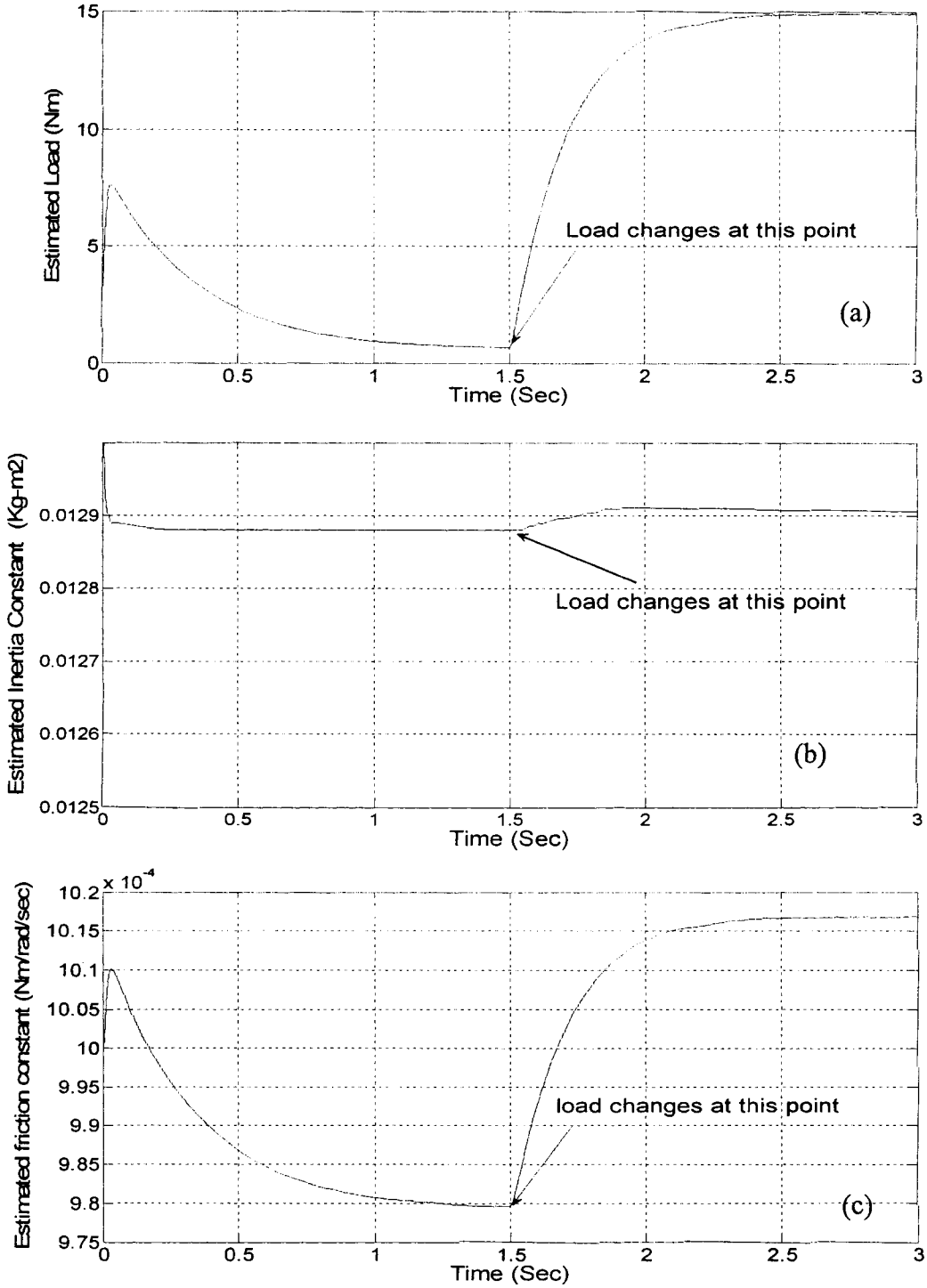

Fig.3.16: Simulated response of the proposed ABNC based IPMSM drive for a step increase of load from no load to high load (15Nm) and rated speed (183 rad/sec); (a) estimated load torque (b) estimated inertia constant (c) estimated friction constant.

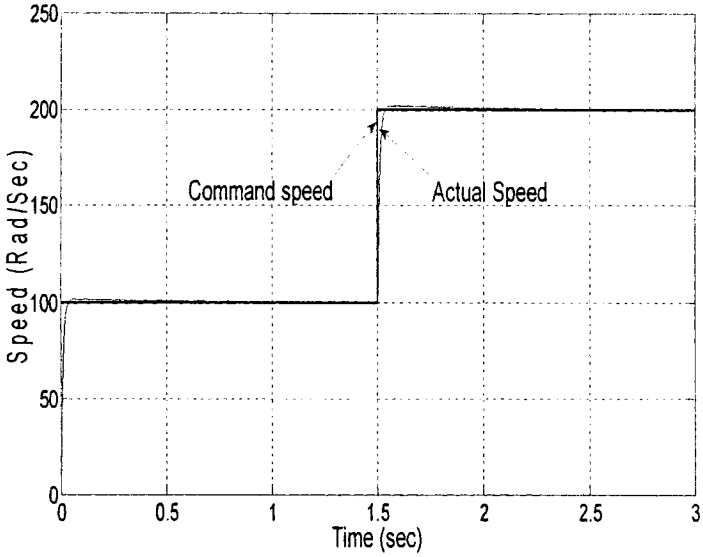

(a)

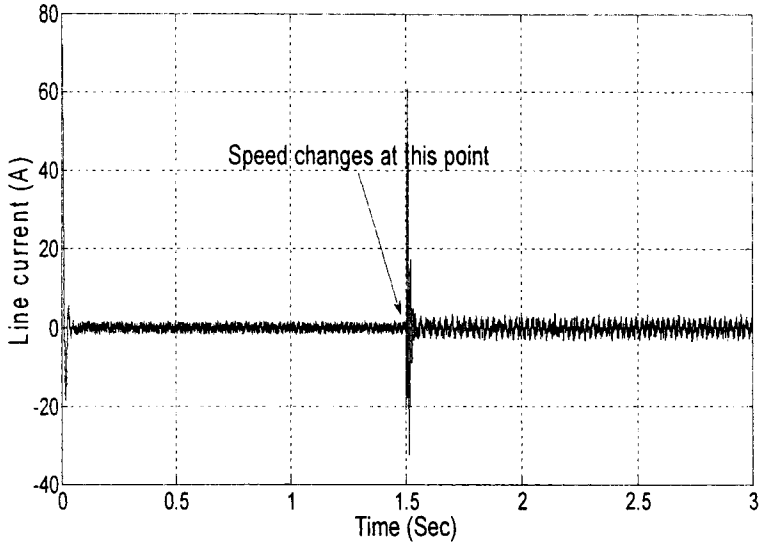

(b)

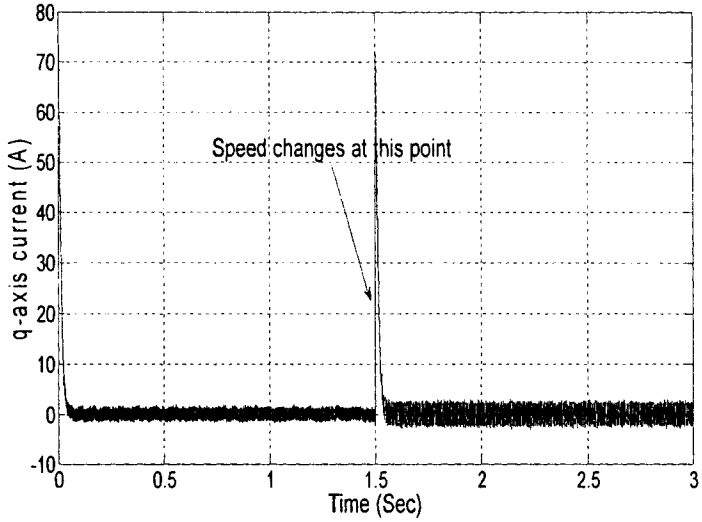

(c)

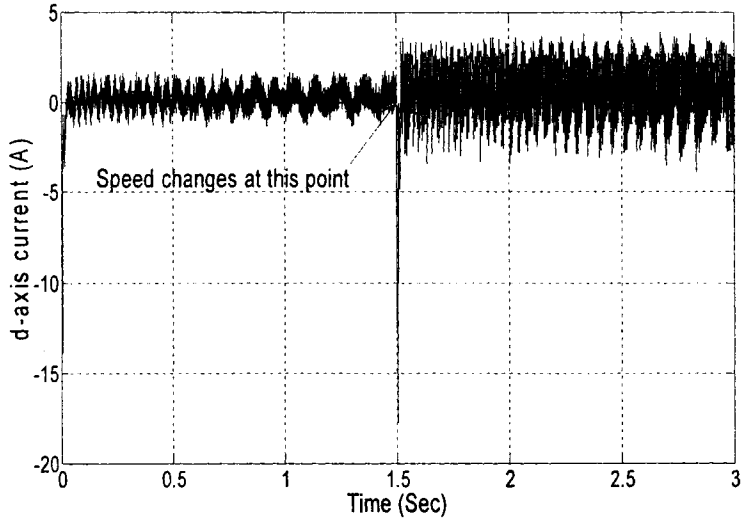

(d)

Fig.3.17: Simulated response of the proposed ABNC based IPMSM drive for a step increase speed command from 100 rad/sec to 200 rad/sec at no load; (a) speed (b) line current (c) d-axis current (d) q-axis current.

error for the proposed controller with change of reference speed from 100 rad/sec to 200 rad/sec at t=1.5 sec is shown in Fig.3.18(a). The developed torque and virtual control variable errors are shown in Figs.3.18(b),(c),(d), respectively. The estimated load torque, inertia and friction constant are shown in Fig.3.19. The speed response of a PI controller for step increase of speed from 100rad/sec to 183 rad/sec with 15 Nm load is shown in Fig.3.20. The motor can follow the reference speed with overshoot. As the MTPA was not used with PI, it was not possible to run the motor above the rated speed. The speed response of the proposed controller for step decrease of speed from 200rad/sec to 100 rad/sec with no load and change of speed from 100rad/sec to 183 rad/sec with 15N-m load is shown in Fig.3.21. The proposed drive can follow the reference speed without overshoot and with zero steady-state error. The proposed ABNC based drive has better performance than PI controller in the case of changing reference speed. The corresponding developed torque, line current and d-q axis currents are shown in Fig.3.22. Figs.3.23 and 3.24 show the speed response of the proposed ABNC based IPMSM drive under rated speed and rated load condition with doubled inertia ($J \rightarrow 2J$) and doubled friction constant ($B_m \rightarrow 2B_m$), respectively. It is evident from Figs.3.23 and 3.24 that the proposed controller based IPMSM drive can follow the command speed with increased inertia and friction constant smoothly without overshoot and steady state error. The summary of the results that obtained from these simulation results are stated briefly in the following table:

Comparison of performance between PI and proposed ABNC based IPMSM drive:

Operating Condition	Property	PI Controller	Proposed ABNC
Starting response for a step speed command at rated load	Overshoot	2 %	Less than 0.5 %
	Settling time	0.4 s	0.4s
	Starting maximum current	120 A	60 A
Starting response for a step speed command at no load	Overshoot	6 %	Less than 2%
	Settling time	0.65 s	0.65s
	Starting current	120 A	60 A
Response for a step change of load	Speed deviation	6 %	Less than 2.5%
	Settling time	0.7 s	0.7s
	Steady state current at full load	13.3 A	13.2 A
Response for a step change of command speed from 100 rad/s to 183 rad/s	overshoot	4 %	Less than 2%
	Settling time	0.4 s	0.5s
	Maximum current at the point of speed change	80 A	55A

3.5 Conclusion

A new nonlinear adaptive backstepping controller scheme has been developed and simulated utilizing the maximum torque capability. This proposed scheme both fully

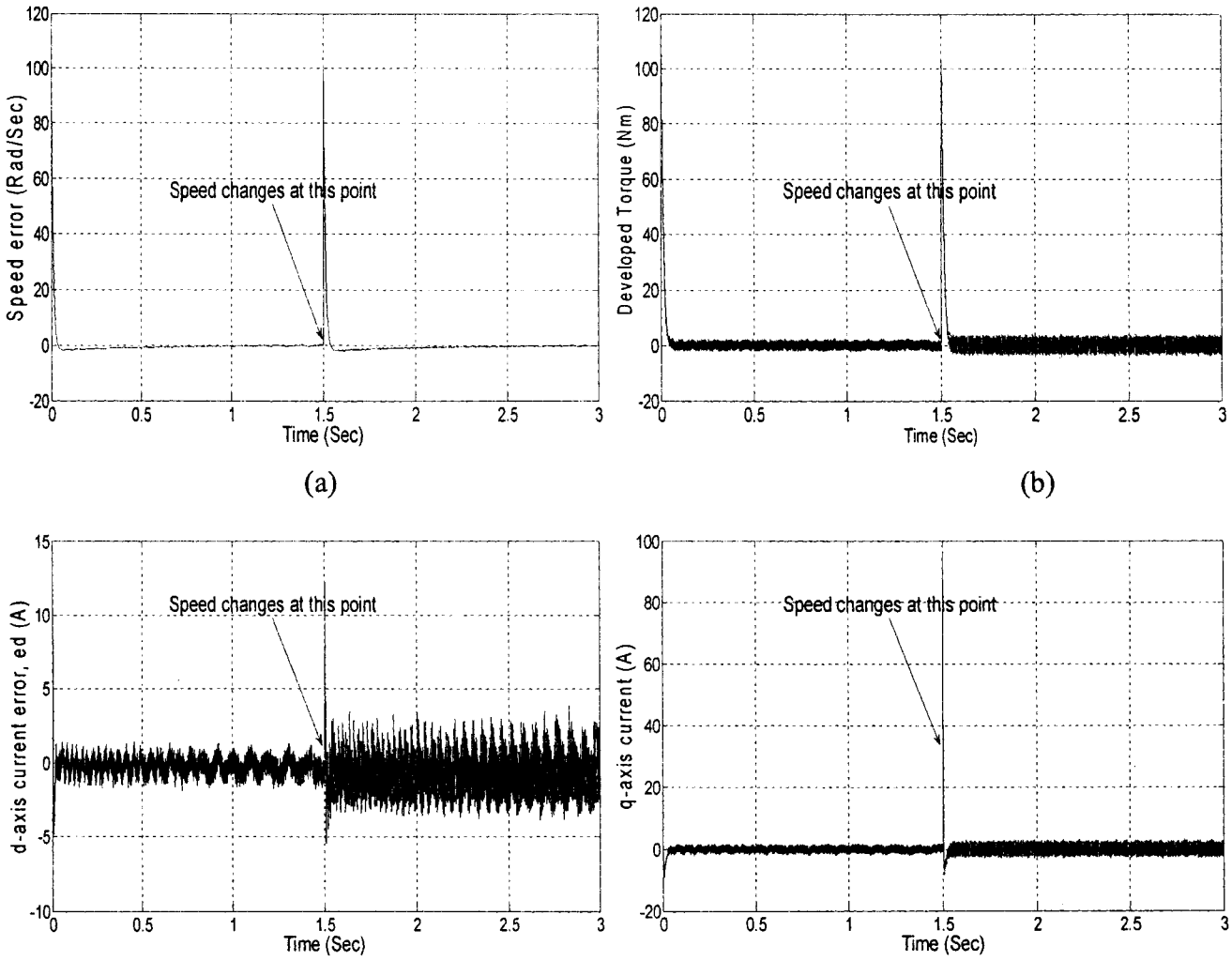

Fig.3.18: Simulated response of the proposed ABNC based IPMSM drive for a step increase speed command from 100 rad/sec to 200 rad/sec at no load; (a) speed error, e_r (b) developed torque (c) d-axis current error, e_d (d) q-axis current error, e_q.

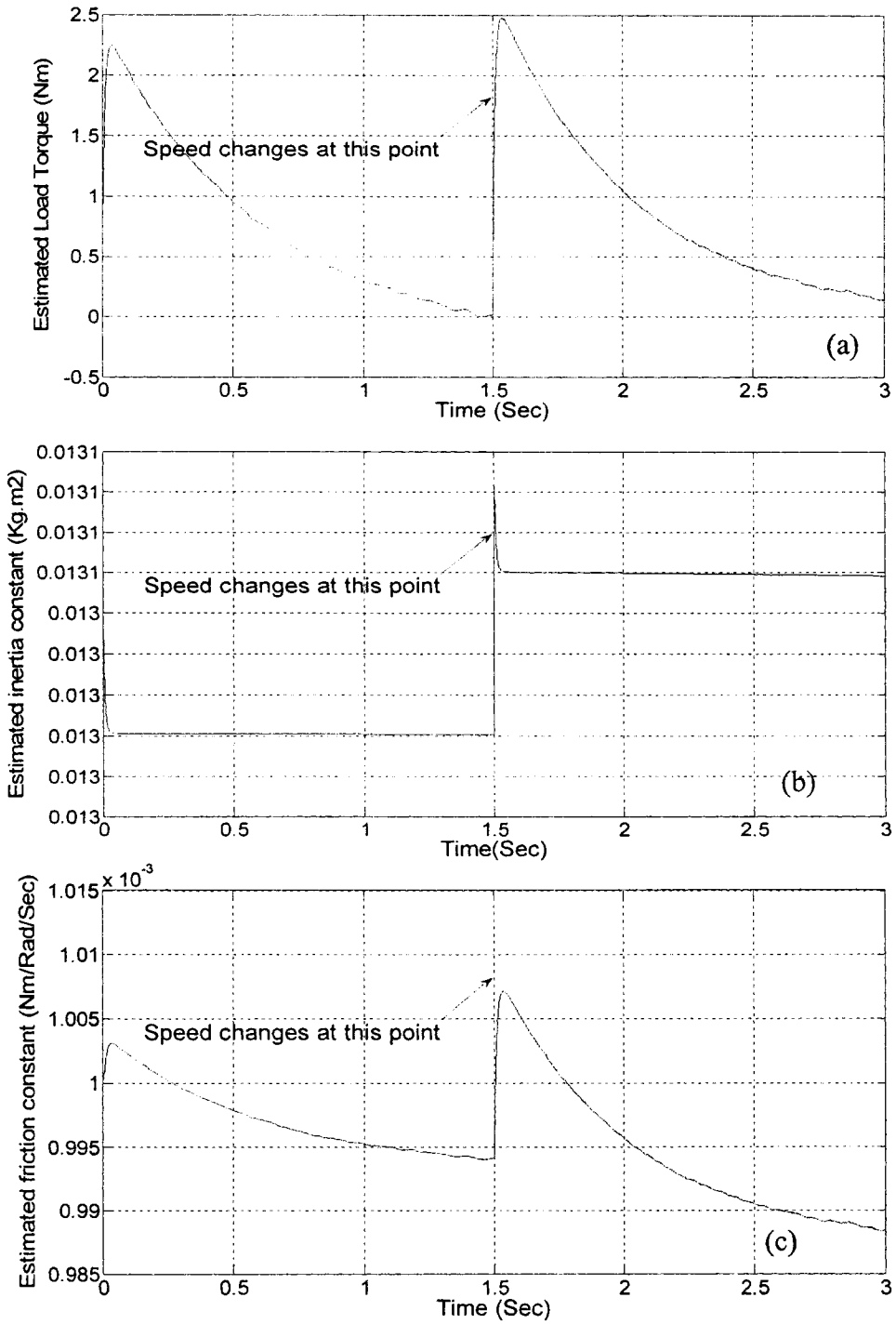

Fig.3.19: Simulated response of the proposed ABNC based IPMSM drive for a step increase of speed command from 100 rad/sec to 200 rad/sec at no load; (a) estimated load torque (b) estimated inertia constant (c) estimated friction constant.

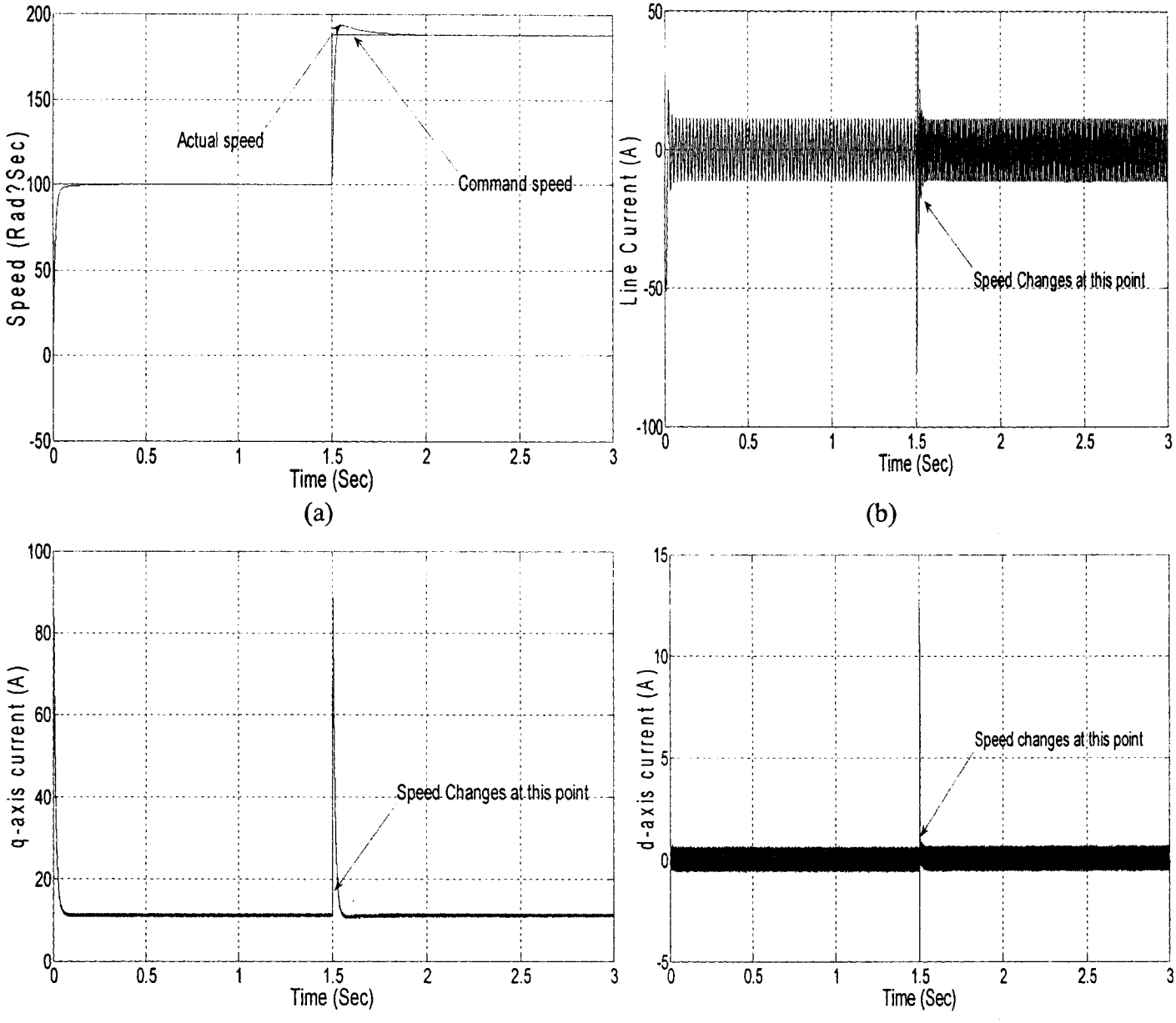

Fig.3.20: Simulated response of PI controller based IPMSM drive for a step increase of speed command from 100 rad/sec to 183 rad/sec at 15 Nm load; (a) speed (b) line current (c) d-axis current (d) q-axis current.

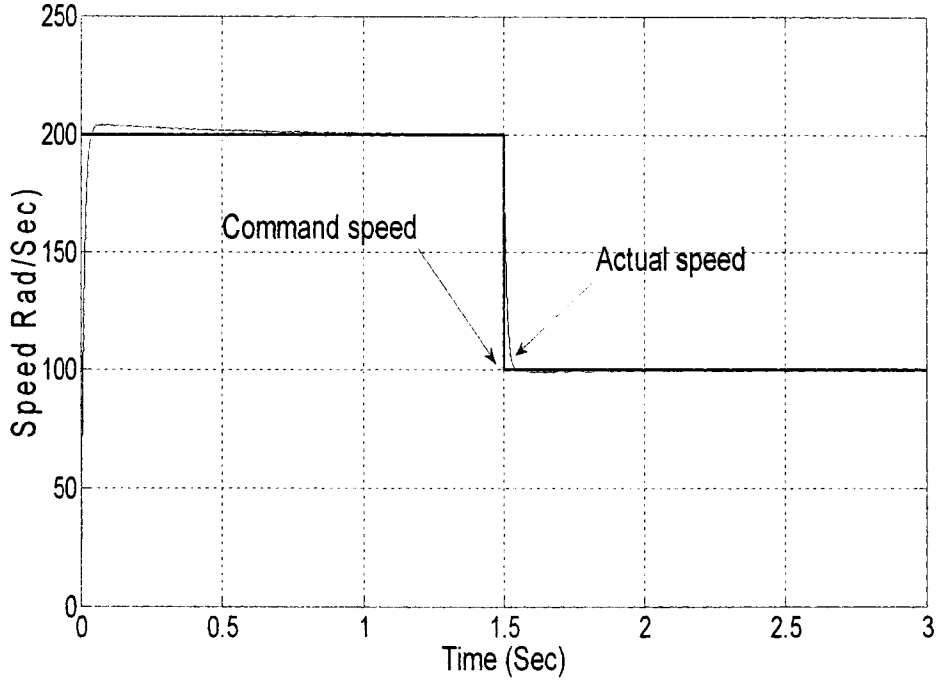

(a)

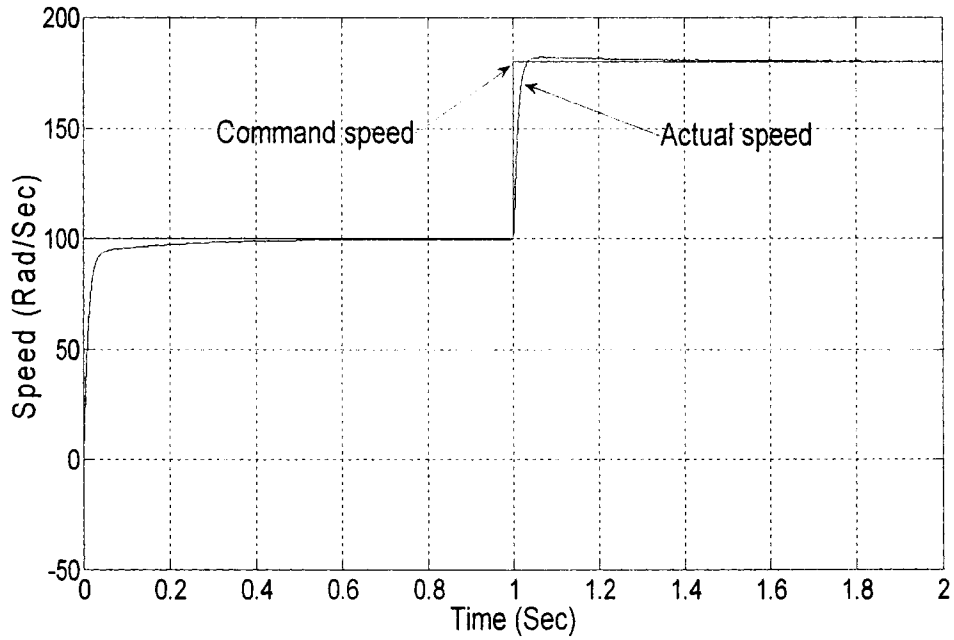

(b)

Fig.3.21: Simulated speed response of the proposed ABNC based IPMSM drive for a step increase of speed command from (a) 200 rad/sec to 100 rad/sec at no load (b) 100 rad/sec to 183 rad/sec at 15 Nm load.

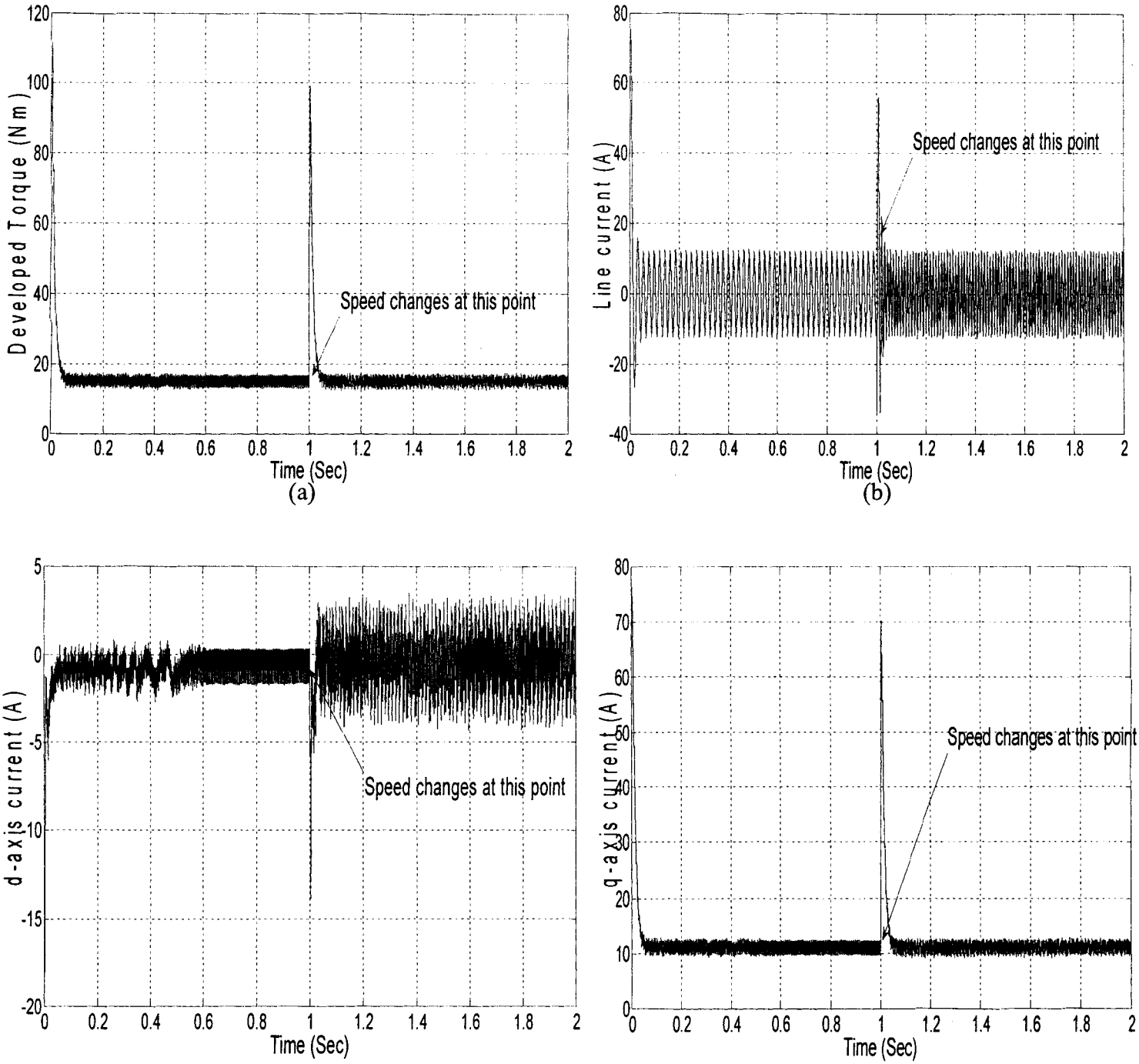

Fig.3.22: Simulated speed response of the proposed ABNC based IPMSM drive for a step increase of speed command from 100 rad/sec to 183 rad/sec at 15 Nm load (a) developed total torque (b) line current (c) d-axis current (d) q-axis current.

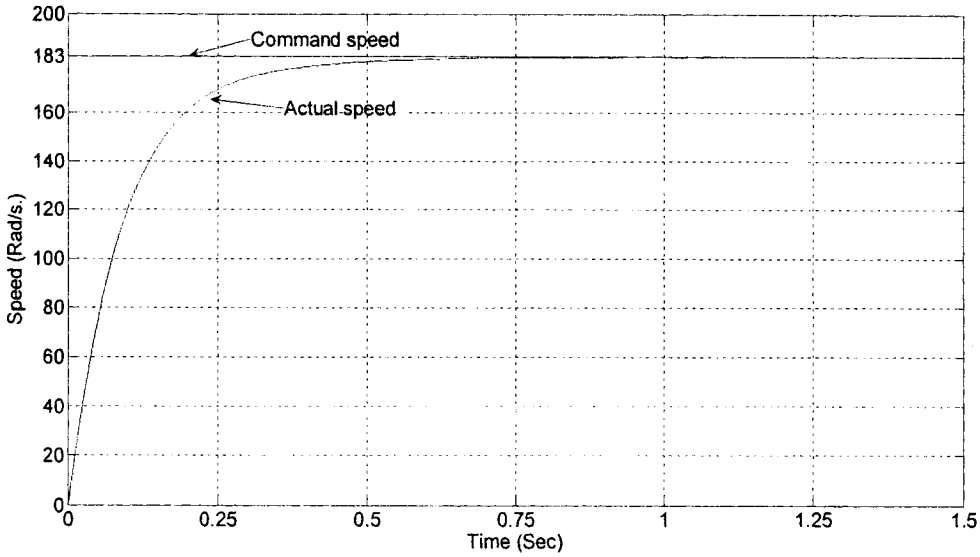

Fig.3.23: Simulated speed response of the proposed IPMSM drive system with doubled inertia (J→2J) under rated speed and load condition.

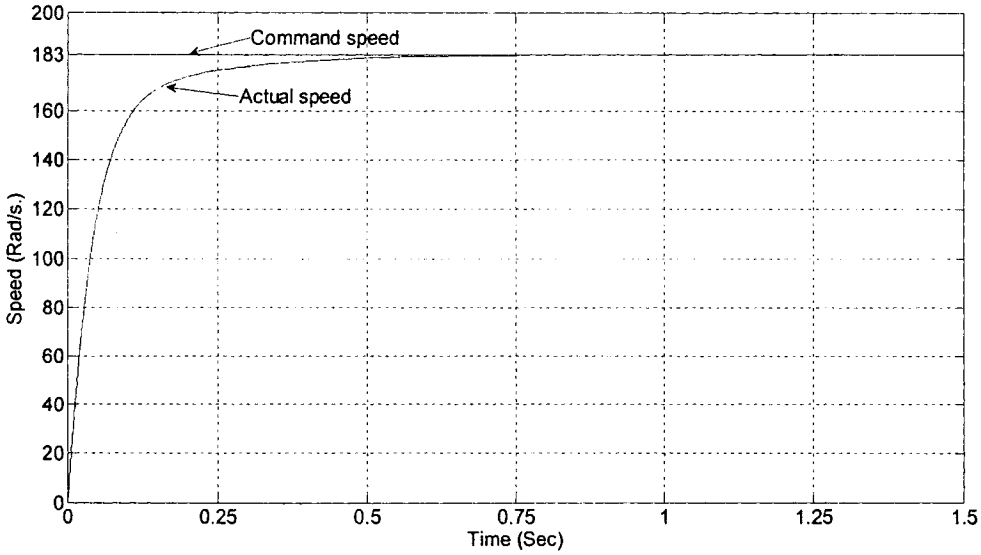

Fig.3.24: Simulated speed response of the proposed IPMSM drive system with doubled friction constant ($B_m \rightarrow 2B_m$) under rated speed and load condition.

utilize the reluctance torque and successfully estimate the parameter values at different operating conditions. The proposed ABNC based vector control of IPMSM enhances the operating speed limit to the partial field weakening region significantly which was not possible with conventional $i_d=0$ control technique. The performance of the proposed control technique has been tested in simulation at different operating conditions. In order to prove the superiority of the proposed ABNC, the performance of the proposed controller is compared with PI at different operating conditions. It has been found that the proposed adaptive backstepping based IPMSM drive is able to follow the command speed maintaining the global stability.

Chapter 4

Real-time Implementation

4.1 Introduction

The performance of the proposed drive was tested in real-time after getting some promising results in simulation. The complete vector control scheme of IPMSM incorporating the proposed ABNC is successfully implemented in real-time using DSP controller board DS 1104 on a laboratory 5 hp motor. The detailed real-time implementation is described in this chapter.

4.2 Experimental Setup

The experimental setup for the real-time implementation of the proposed controller is shown in Fig 4.1(a) and 4.1 (b). The test IPMSM is labelled as 'M'. The rotor

position of the test motor is measured by an optical incremental encoder which is labelled as 'E'. The encoder is directly connected to the rotor shaft. The motor is coupled with a DC machine (G) which works as a generator to act as loading machine to the motor. Some resistors (L) are connected to the output voltage terminals of the DC machine as load. The actual motor currents are measured by Hall-effect current transducers. The

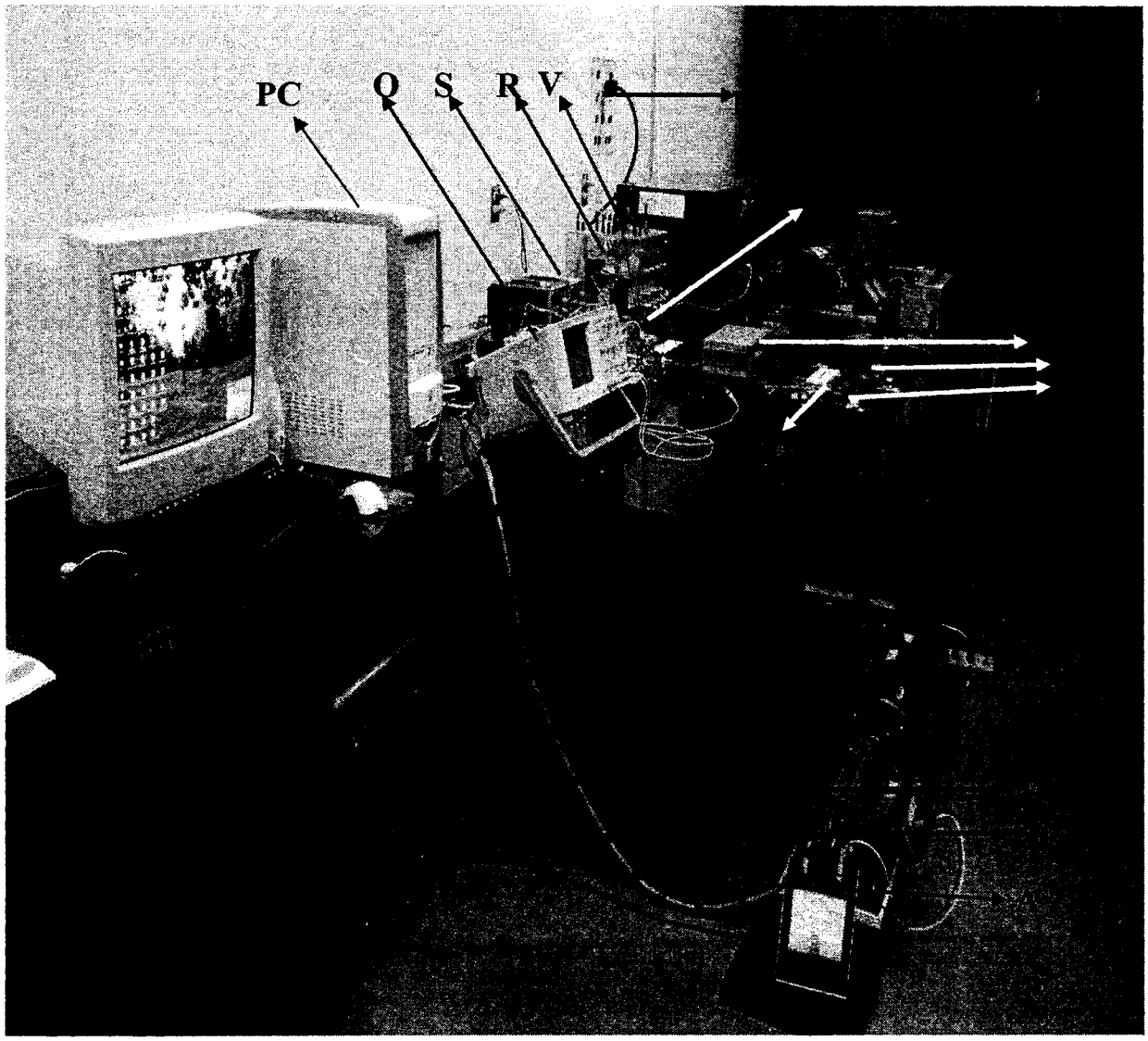

Fig.4.1(a): Experimental setup of the proposed controller of IPMSM drive.

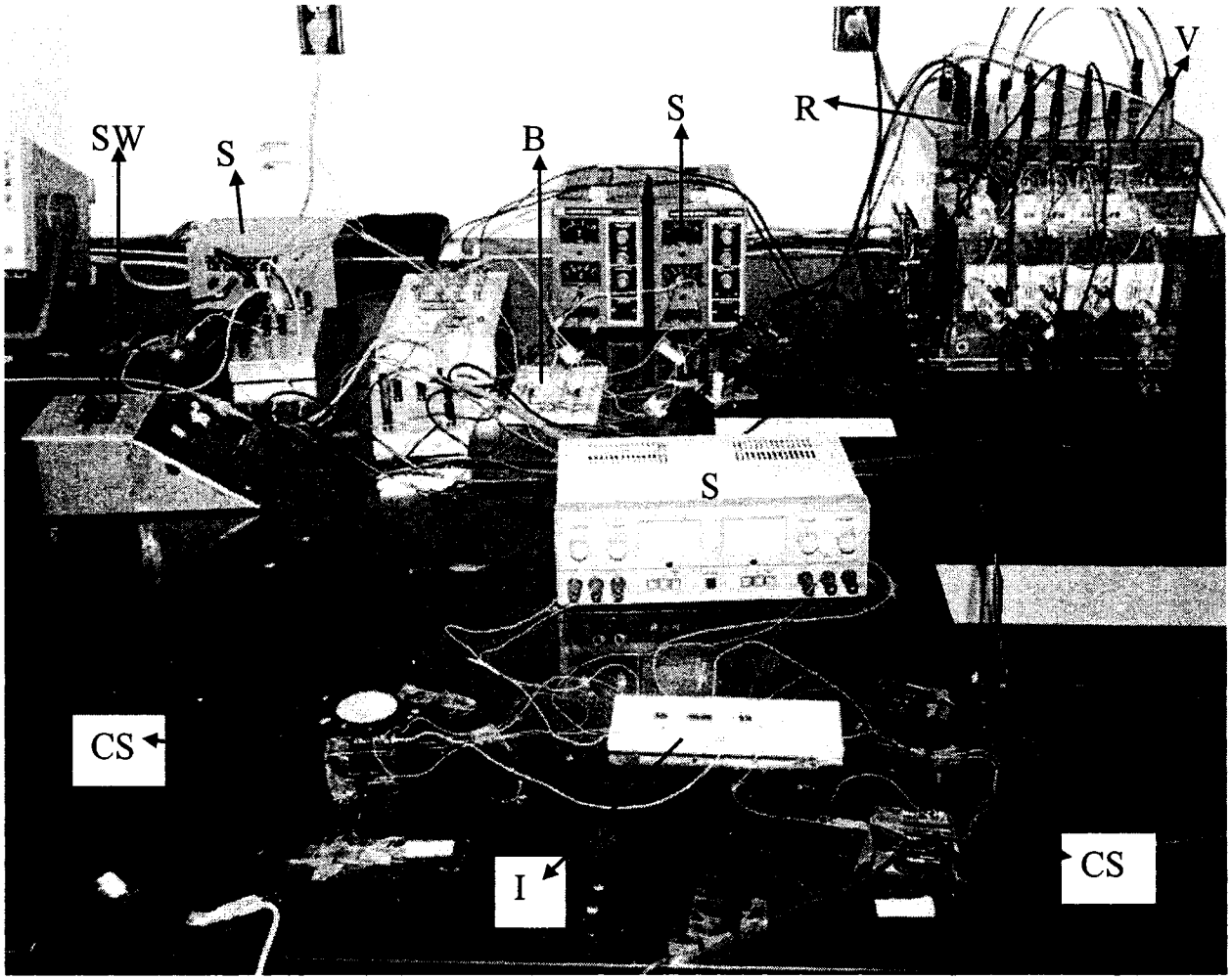

Fig.4.1(b): Experimental setup of the proposed controller (close-up view).

interface circuit (I) is located between the Hall-effect sensor and the A/D channel of DSP board. These transducers are labelled as 'CS'. These current sensors (CS) have a linear response over wide range of frequencies (up to 250 kHz). Another gate drive circuit is used to increase the power level of the firing pulses so that these are sufficient to drive the inverter insulated gate bipolar transistor (IGBT) switches. The gate drive circuit also provides isolation between low power control and the high power supply circuits. The

gate drive circuit is labelled as 'D'. The power circuits consist of a 3-phase variable ac autotransformer (A), power supply (PS), rectifier (R) and IGBT inverter (V). The DC bus voltage of the voltage source inverter (VSI) is obtained by rectifying ac voltage and filtered by a large capacitor (≈1000 uF). The ac voltage is supplied by the power supply through autotransformer. The rectifier enclosed within 3-phase (6 pulses) IGBT inverter is labelled as 'V'. This inverter has active security feature against short circuit, under voltage of power supply as well as built in thermal protection, which prohibits destructive heat sink temperatures. The variable ac power of the rectifier is supplied by autotransformer (A) through a single pole single throw (SPST) switch (SW). The personal computer, in which the DSP board DS1104 is installed, is labelled as 'PC'. A digital storage oscilloscope is used to capture the desired analog signal coming out

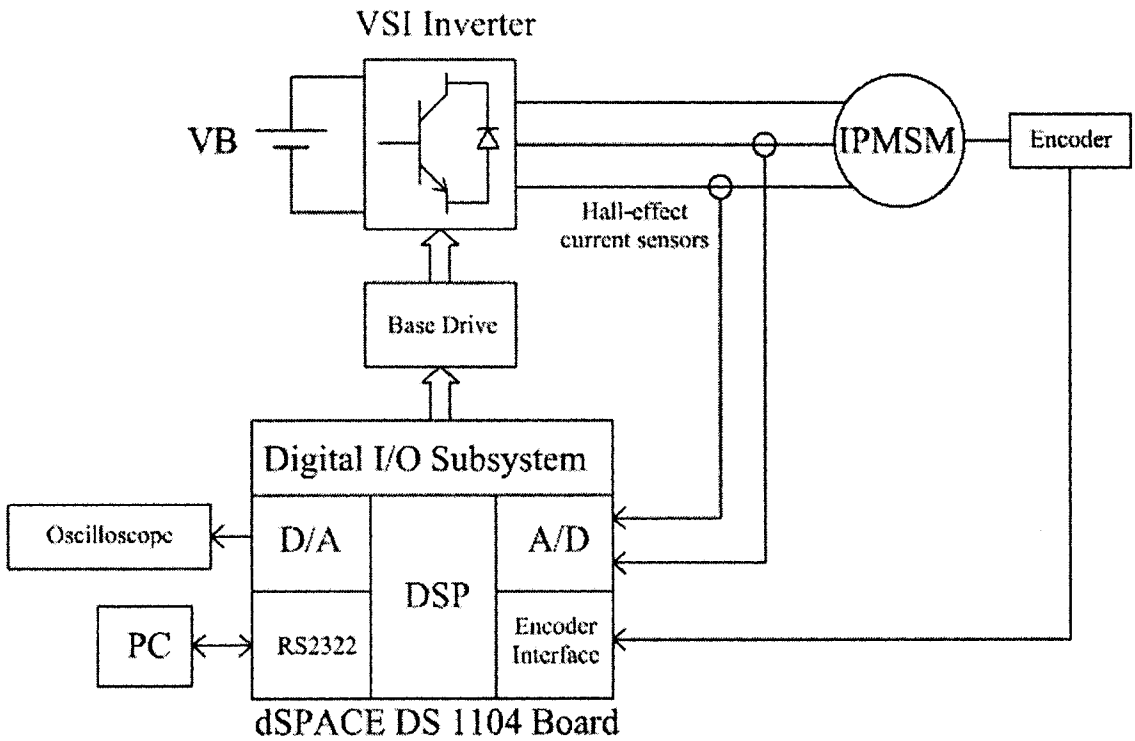

Fig.4.2: Block diagram of hardware schematic of VSI fed IPMSM drive.

through D/A port of the DSP board. The oscilloscope is labelled as 'O'. The complete drive has been implemented through both hardware and software which are discussed below.

4.3 Hardware implementation of the drive

The block diagram of hardware schematic of VSI fed IPMSM drive is shown in Fig.4.2. The DSP board DS1104 board is installed in an Intel PC with uninterrupted communication through dual port memory to implement the control scheme in real-time. The DS1104 board is mainly based on a Texas Instrument MPC8240 64-bit floating point digital signal processor. The block diagram of the DSP board is shown in Fig.4.3. The DS1104 board uses a PowerPC type PPC603e processor which operates at the clock of 250 MHz with 32 KB cache. This board has a 32 MB of SDRAM global memory and 8 MB of flash memory. The DSP is supplemented by a set of on-board peripherals used in digital control systems including analog to digital (A/D), digital to analog (D/A) converters and digital incremental encoder interfaces. This board is also equipped with a TI TMS320F240 16-bit micro controller DSP that acts as a slave processor and provides the necessary digital I/O ports configuration and powerful timer functions such as input capture, output capture and PWM generation. In this work, the slave processor is used for only digital I/O subsystem configuration. The block diagram of the hardware schematic is shown in Figure 4.2. Rotor position is sensed by an optical incremental encoder mounted at the rotor shaft and is fed back to the DSP board through the encoder interface. The encoder used in this work generates 1024 pulses per revolution. By using a built-in 4-fold pulse multiplication the output of the encoder is increased to 4x1024 pulses per

revolution in order to get a better resolution. So the resolution of the encoder is 0.087890625°. These pulses are fed to the one of two digital incremental encoder interface channels of the board. A 24-bit position counter is used to count the encoder pulses and is read by a calling function in the software. The counter is reset in each revolution by the index pulse generated from the encoder. The motor speed is computed from the measured rotor position angles using discrete difference equation. The actual motor currents are measured by the Hall-effect sensors, which have current range of 0 ~ ±200A and a frequency range of 0~250 KHz. The current signals are fed back to DSP board through A/D channels. The output current signal of these sensors is converted to a voltage across the resistor connected between the output terminal of the sensor and ground. One can scale the output voltage by selecting the value of the resistors. These resistors can be within the range 0~100Ω. As the output voltages due to these current sensors are low, interface circuit is used to amplify the output of the sensor and it also reduces the noises. The interface circuit consists of non-inverting amplifier with operational amplifier LM741CN as shown in Appendix C. As the motor neutral is not grounded, only two phases current are measured and third phase current is calculated using Kirchoff's Current Law in software. The command voltages are generated from the proposed controller and compared with the triangular carrier wave. This generates the logic signals which act as firing pulses for the inverter switches. Thus, these six logic signals are the output of the DSP Board and fed to the base drive circuit of the IGBT inverter power module. The outputs of the digital I/O subsystem of the DS 1104 are six pulses with a magnitude of 5 V. This voltage level is not sufficient for the gate drive of IGBTs. Therefore, the voltage level is shifted from +5 V to +15V through the base drive

circuit with the chip SN7407N as shown in Appendix C. At the same time it also provides isolation between low power and high power circuits.

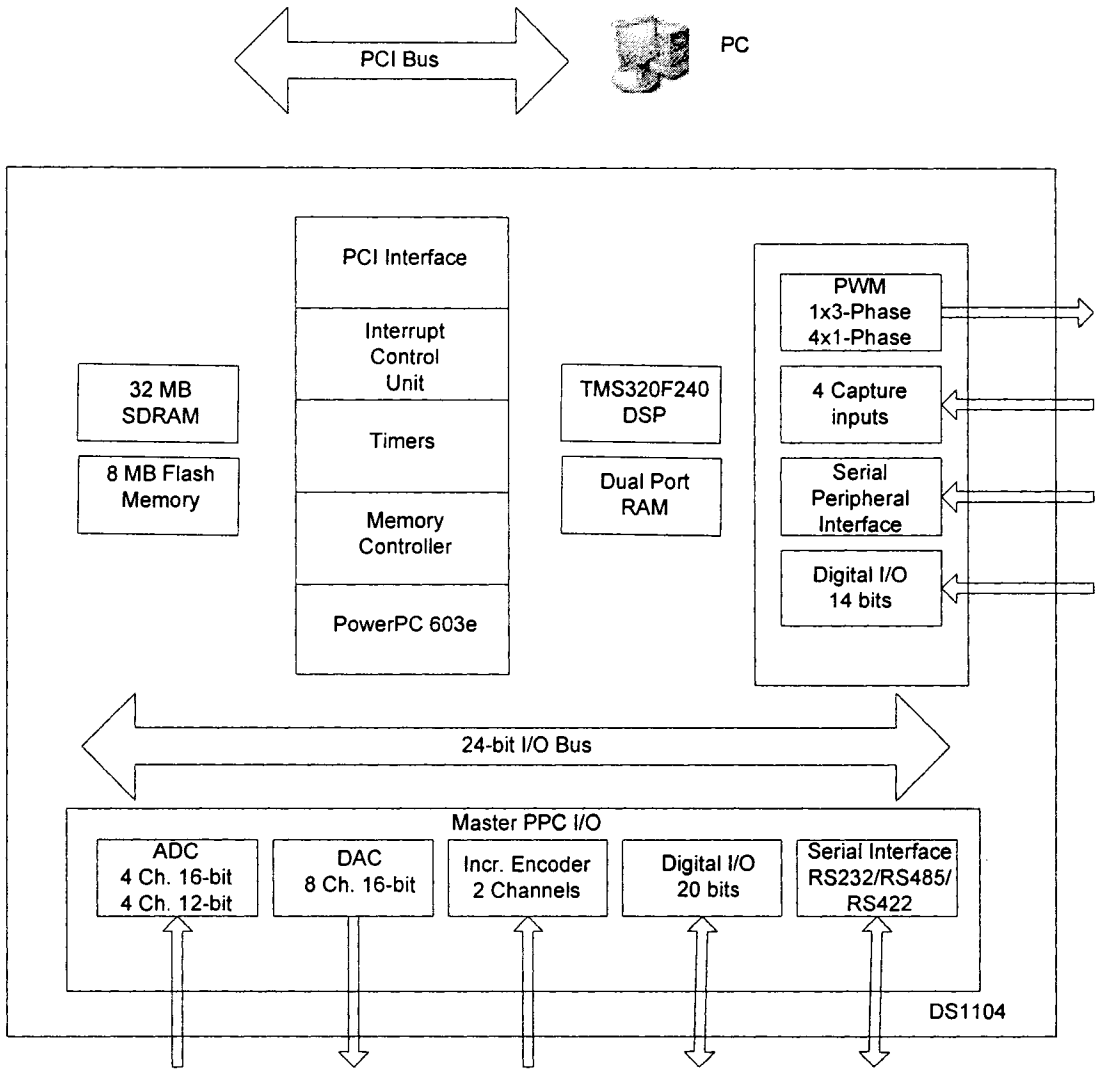

Fig.4.3: Block diagram of DS1104 board.

4.4 Software implementation of the drive

In order to implement the control algorithm, a real-time Simulink model is developed according to the complete drive system is shown in Appendix D.1. Then the

model is downloaded to the DSP board using the Control Desk software [85]. The dSPACE DS1104 board is a self-contained system, not an embedded system. This means the board installed in the lab computer through a PCI slot is its own entity and the host PC does none of the processing for a system implemented on the board. As a result, the board requires that software to be created and downloaded to the board for the system to function.

The ControlDesk software is used to download software to the DSP board, start and stop the function of the DS1104 as well as create a layout for interfacing with global variables in dSPACE programs. The sampling frequency used in this work is found to be 10 kHz. If the sampling frequency that is higher than 10 kHz is chosen, the 'overrun error' occurs, which indicates too much computational burden for the processor.

The flow chart of the software for real-time implementation is shown in Fig.4.4. After initializing all the required variables, the timer interrupt routine is set up to read the values of the currents and rotor position angle every 100 μS . The motor currents obtained through analog to digital converter (ADC) channels 1 and 2 are multiplied by the gain 18.814 and 16.6667, respectively in order to obtain the actual current values in software. These constants depend on the Hall-effect sensors specifications, the resistors used at the output node of these sensors and the resistors used in the interface circuit. After these digitalized currents in *abc* coordinates are converted into rotating reference frame of *d-q* axes coordinates.

The rotor position angle is measured by encoder and can be calculated in radian by the equation of $2\Pi/1024$ x P, where P is the number of pulses counted in the counter. Once the rotor position angle is calculated, the rotor speed is computed from the

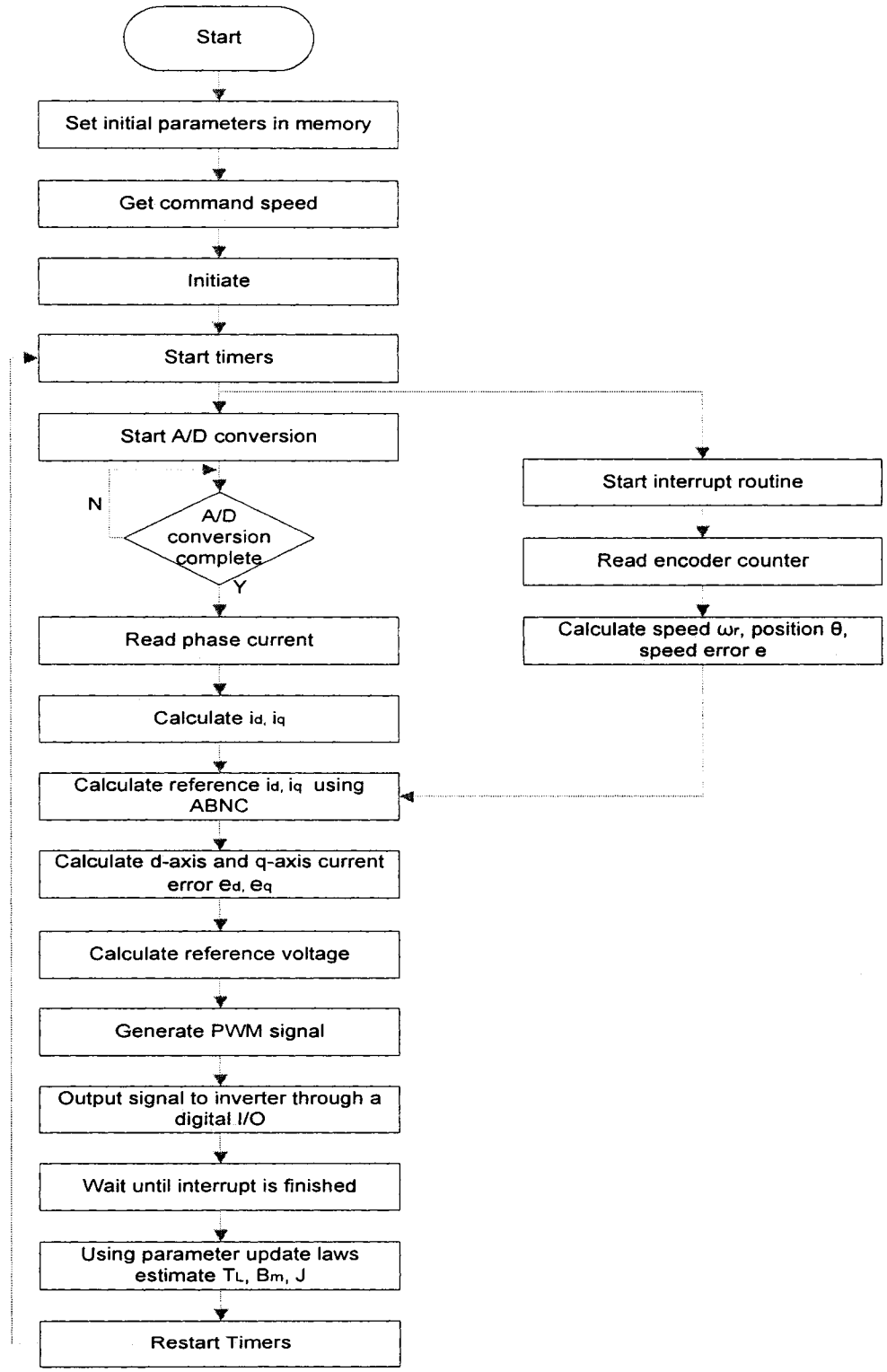

Fig.4.4: Flow chart of the software for real-time implementation of the proposed controller of IPMSM drive.

measured rotor position angles using numerical backward differentiation. Based on the calculated speed, the speed error between actual and reference speed is calculated. Using the speed error and virtual control dynamics error the reference d, q axis voltages are calculated according to the proposed MTPA technique explained in chapter 3. All the calculated and measured values as explained above such as d, q-axes currents, rotor speed along with initial parameters stored in memory are used to compute the tracking errors. Based on these tracking errors, mechanical parameters such as friction coefficient, damping factor and load torque are estimated by the parameter update laws developed in Chapter 3. The initial parameter values are required to estimate current values. In that case, the nominal measured parameter values are used as initial values. These newly estimated parameters will be used in the routine of control loop until next parameter adaptation occurs. Finally, the reference voltages are compared with the triangular carrier signal (1.2 kHz) to generate the six PWM pulses for the inverter switches. All off-to-on transitions of the PWM pulses are delayed by the dead time of 0.5 milliseconds in order to prevent the shorting of the dc bus voltage to ground. These pulses are sent to the inverter gate drive through a digital I/O subsystem of the board.

4.5 Experimental results

Experimental test were done to verify the effectiveness of the proposed ABNC based IPMSM drive scheme at different operating conditions. Experimental tests are also carried out for conventional fixed PI controller in order to prove the superiority of the ABNC. The starting response of the PI controller based IPMSM drive for a command speed 183 rad/sec is shown in Fig. 4.5(a). The gains of the controller are chosen as K_p=

0.15 and K_i= 0.2 by trial and error method in order to get minimum overshoot and settling time. It is shown that although the motor can follow the command speed, it has huge overshoot and it has higher settling time than the proposed controller. The experimental starting speed response of the proposed ABNC based IPMSM drive is shown in Fig. 4.5(b). It shows that it can follow command speed with reasonable steady-state error and without overshoot/undershoot. For the sake of safe operation, the voltage is applied to the inverter through variac and rectifier arrangement as quickly as possible. The performance for a step change of command speed is also investigated for a sudden change of speed command from 100 rad/s to 200 rad/s at light load. From Fig. 4.6 (a), it is shown that the motor can follow the command speed smoothly with reasonable steady state error and no overshoot. The corresponding q and d axis current are shown in Fig. 4.6 (b) and (c). In industrial application, sudden change of load is a common incident. The experimental speed response of PI controller for a step change of load at rated speed is shown in Fig.4.7. With change of load, the speed deviates from the command speed and it converges to the command speed slowly. It is found from Fig.4.8 (a) that the motor can follow the command speed for a step increase in load. It converges to its command speed very quickly without any overshoot or undershoot. The corresponding q and d axes current are shown in Figs.4.8 (b) and (c), respectively. With the increase of load the q-axis current increases to supply more torque and d axis current decreases to maintain MTPA technique. The speed response for a decrease of load is shown in Fig. 4.9. It is observed that the speed of the motor increases a little bit with decrease of load but it converges to command speed very fast. Thus, the performance of the proposed ABNC based IPMSM drive has been found to be robust and stable in real-time for different

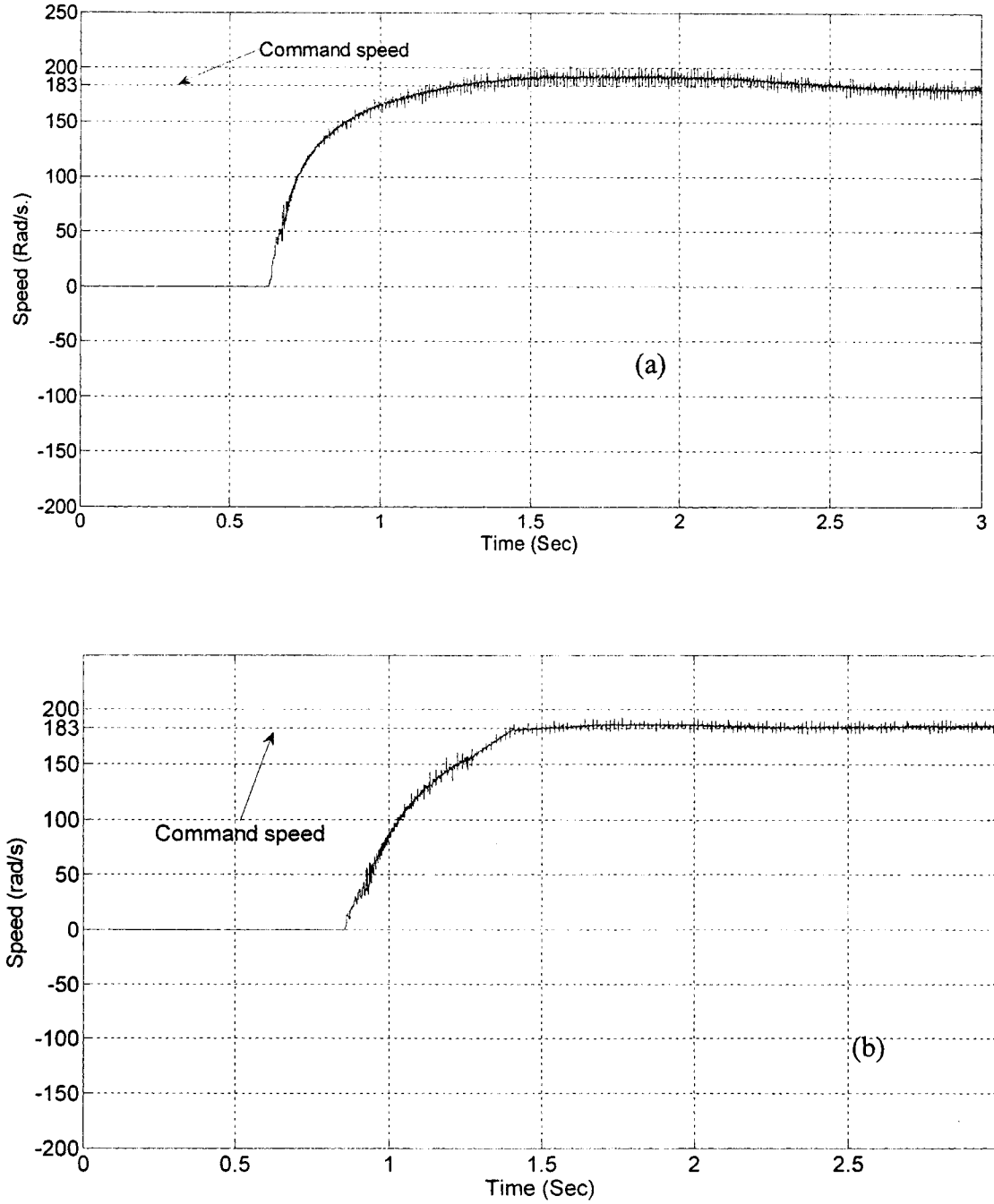

Fig.4.5: Experimental starting speed response for a step change of command speed (183 rad/s) for (a) PI controller (b) ABNC controller.

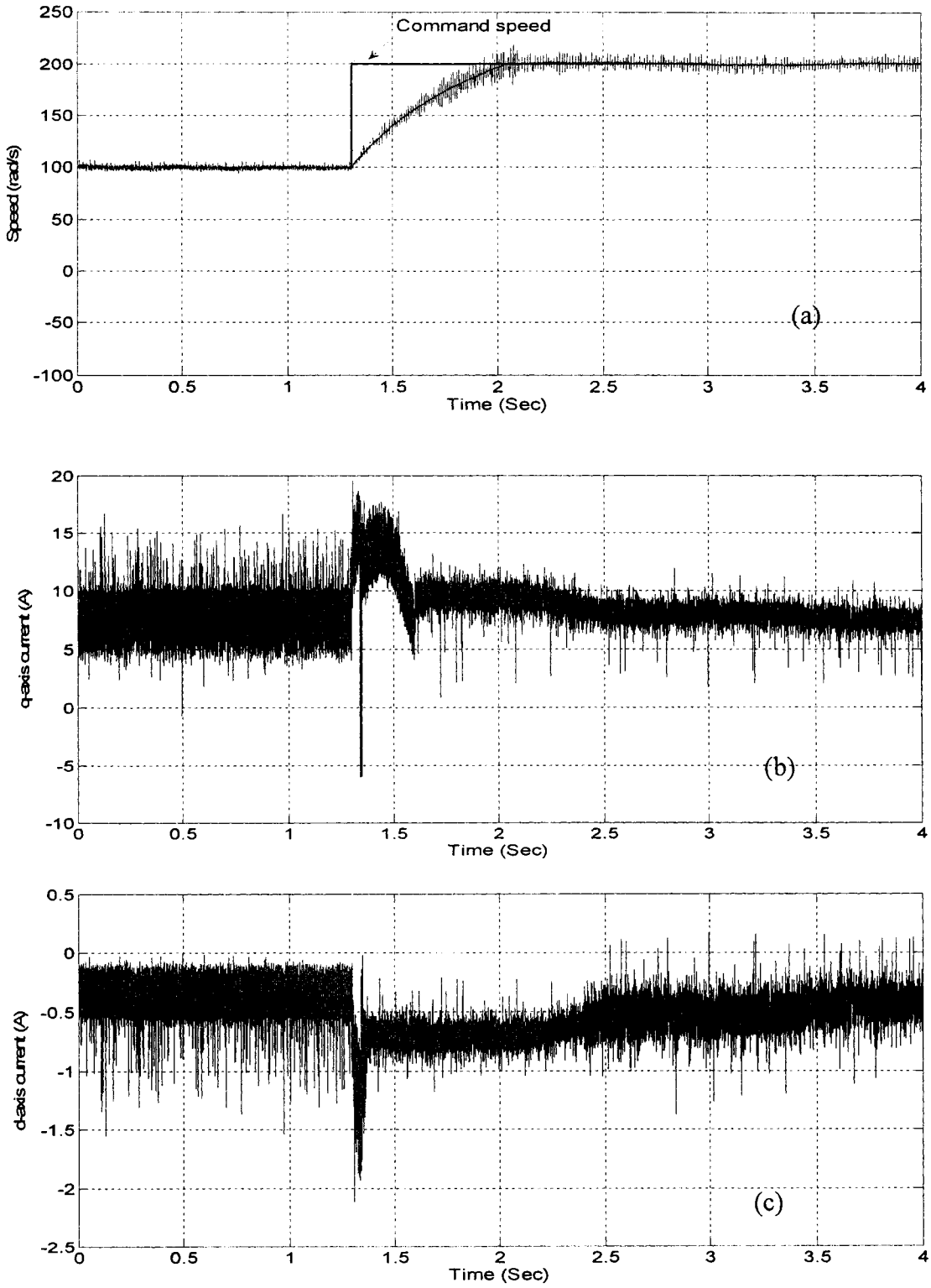

Fig.4.6: Experimental response of the proposed ABNC controller for a step increase in speed command (a) speed (b) q-axis current (c) d-axis current.

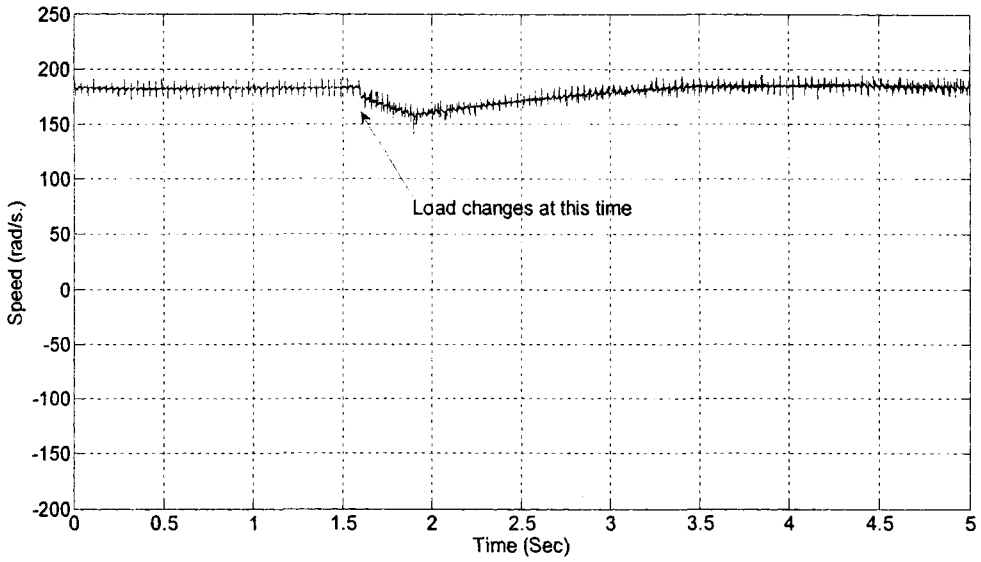

Fig. 4.7: Experimental speed response of the PI controller for a step increase in load at rated speed.

operating conditions. However, there is a ripple in i_d and i_q as well as the speed, which needs to be minimized. The steady state speed error of the proposed controller at rated speed and load is shown in Fig.4.10. It is observed that there is low steady state error of the speed response although it suffers with ripple. The experimental results obtained from this chapter are summarized in the following table.

Operating Condition	Property	PI Controller	Proposed ABNC
Starting response for a step speed command at rated load	Overshoot	9 %	Less than 5 %
	Settling time	1.2 s	1.2 s
Response for a step change of load	Speed deviation	12 %	Less than 6 %
	Settling time	2 s	0.8s

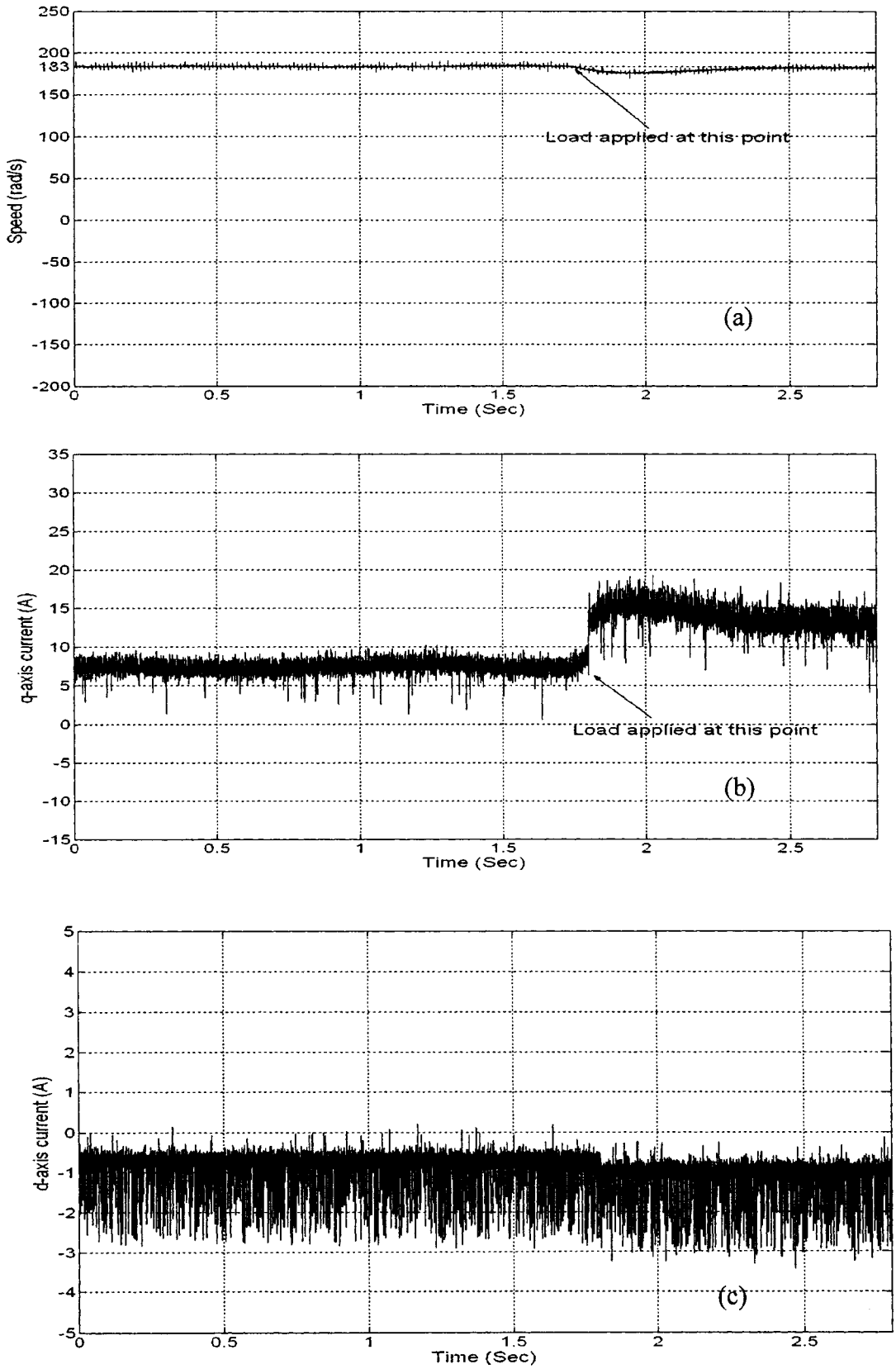

Fig. 4.8: Experimental response of the proposed ABNC controller for a step increase in load at rated speed; (a) speed response (b) q-axis current (c) d-axis current.

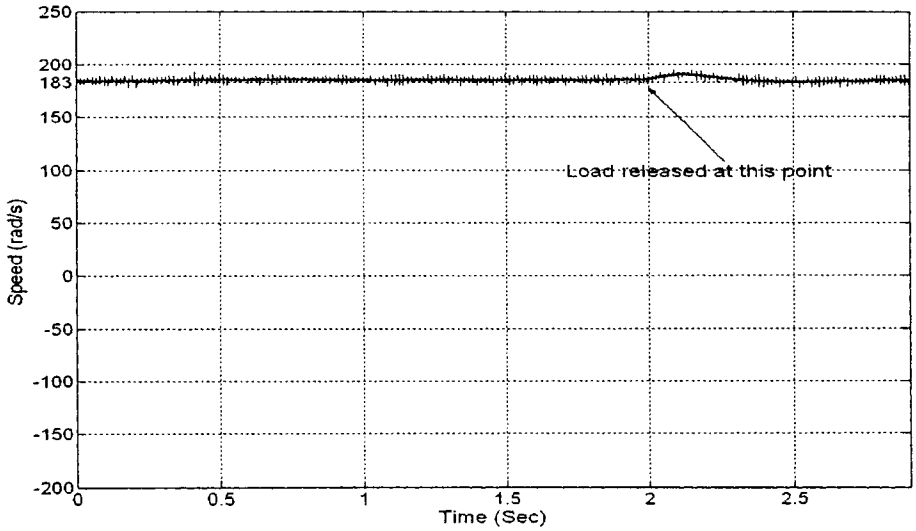

Fig. 4.9: Experimental speed response of the proposed ABNC controller for a step decrease in load at rated speed.

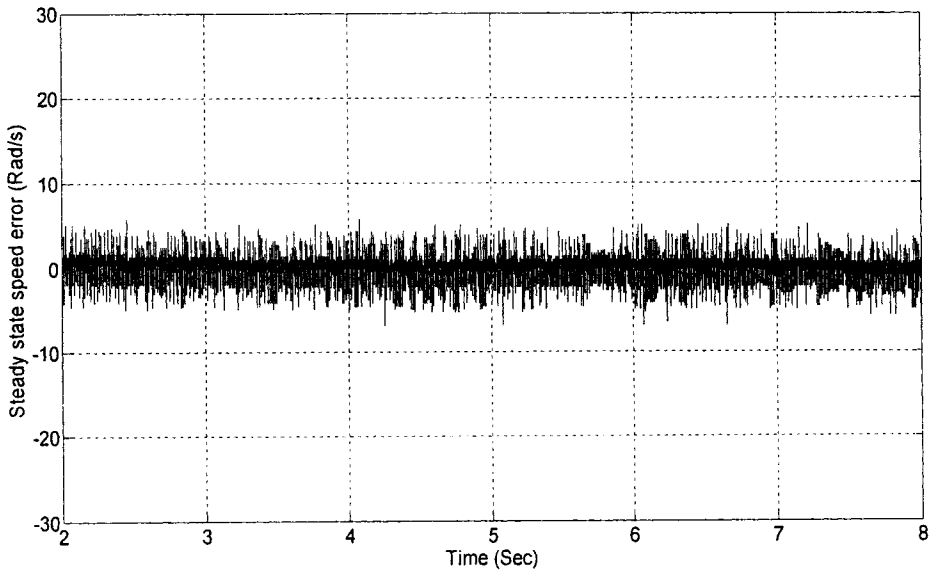

Fig. 4.10: Experimental steady state speed error of the proposed ABNC controller for a rated command (183 rad/s.) speed at rated load.

4.6 Conclusion

The detail experimental implementation of the proposed ABNC based vector control of IPMSM drive using dSPACE DSP board DS-1104 has been presented in this chapter. The performance of the proposed drive has been tested at different operating conditions such as sudden change of load, command speed etc. In order to prove the superiority, the performance of the proposed ABNC based drive has been compared with a conventional PI controller based drive. Due to incorporation of MTPA control technique, the operating speed region has been extended beyond the rated speed limit which was not possible with conventional i_d=0 control method. The performance of the proposed drive has been found to be robust.

Chapter 5

Design and Development of New Fuzzy Logic Controller Incorporating Flux Control

5.1 Introduction

Due to the well-known disadvantages of the conventional proportional integral (PI)), proportional integral derivative (PID) controllers and their adaptive versions recently researchers looked into the possibility of intelligent controllers application for IPMSM drives [38-69]. The main advantages of intelligent controllers are: their designs do not need the exact mathematical model of the system and theoretically they are capable of handling any nonlinearity of arbitrary complexity.

Among the various intelligent controllers, fuzzy logic controller (FLC) is the

simplest for speed control of high performance IPMSM drive. The FLC is better than the conventional controllers in terms of insensitivity to parameter and load variations, response time, settling time and robustness. It is based on the linguistic control rules which are also the basis of human logic. The reported FLC application in IPMSM drive did not consider the flux control as it assumed i_d=0 [41]. For an IPMSM the flux can be controlled indirectly by controlling the d-axis armature reaction current, i_d. In [42,44] the flux control is considered but the drawbacks of these works are either the operating speed is limited within the rated speed or the flux is controlled separately outside of the FLC block. In the case when flux is controlled outside of FLC block, it is dependent on motor parameters. So far none of the reported works considers the design of FLC incorporating flux control. In order to be completely independent of motor parameters, in this paper a novel FLC based speed control technique is developed for wide speed range operation of an IPMSM drive. The proposed FLC simultaneously controls both torque and flux of the motor while maintaining current and voltage constraints. Thus, a stand alone FLC is utilized whose outputs are d and q- axes currents. The FLC is designed based on conventional maximum torque per ampere (MTPA) operation [74] below the rated speed and the field weakening (FW) operation [74] above the rated speed. At first, the operating region of IPMSM is analyzed in d-q current plane. Then d,q current control algorithms are incorporated into the FLC. This is contrary to the conventional FLC of IPMSM, which linearizes the q-axis current expression by setting the d-axis current equal to zero [41]. Without a proper flux weakening operation, the controller would be saturated at high command speed and loses its controllability. The terminal voltage is related to the angular speed of the motor if the flux is constant. So at low speed the voltage constraint

does not effect the operation of the motor. But as the speed becomes higher than the rated speed the voltage constraint becomes more effective. So at higher speed (FW region) d-axis current should be controlled in such a way that it will weaken the magnetic flux by armature reaction to reduce the total air gap flux and maintain the terminal voltage constant. Thus, the conventional FLC is not capable of running the motor above the rated speed. The proposed FLC extends the operating speed range of IPMSM up to the entire field-weakening (constant power) region by properly controlling d and q axes currents.

5.2 Fundamentals of fuzzy logic controller

Fuzzy logic controllers are based on fuzzy set and fuzzy logic theory introduced by Zadeh [86]. A fuzzy control system is a control system based on fuzzy logic - a mathematical system that analyzes analog input values in terms of logical variables that take on continuous values between 0 and 1, in contrast to classical or digital logic, which operates on discrete values of either 0 and 1 (true and false). Fuzzy logic is widely used in machine control. The term itself inspires a certain skepticism, sounding equivalent to "half-baked logic" or "bogus logic", but the "fuzzy" part does not refer to a lack of rigour in the method, rather to the fact that the logic involved can deal with fuzzy concepts that cannot be expressed as "true" or "false" but rather as "partially true". Fuzzy logic has the advantage that the solution to the problem can be cast in terms that human operators can understand, so that their experience can be used in the design of the controller. This makes it easier to mechanize tasks that are already successfully performed by humans.

The fuzzy set (subset) A on the universe (set) X is defined by a membership

function, μ_A, from X to the real interval [0, 1], which associates a number $\mu_A(x) \in [0,1]$ to each element x of universe X. The membership function $\mu_A(x)$ represents the grade of the membership function of x to A, i.e., a subjective value for the degree of A-ness of x. The equation $\mu_A(x) = 0.5$ means x has A-ness of about 50%. A fuzzy singleton $S(xo) = \mu_A(x)|_{xo}$ is a fuzzy set that supports only one element x_0. Therefore, the fuzzy set is a union of fuzzy singletons of its constituents. In the fuzzy set theory, the boundaries of the fuzzy sets can be vague and ambiguous, just to make it useful for approximate systems. Fuzzy

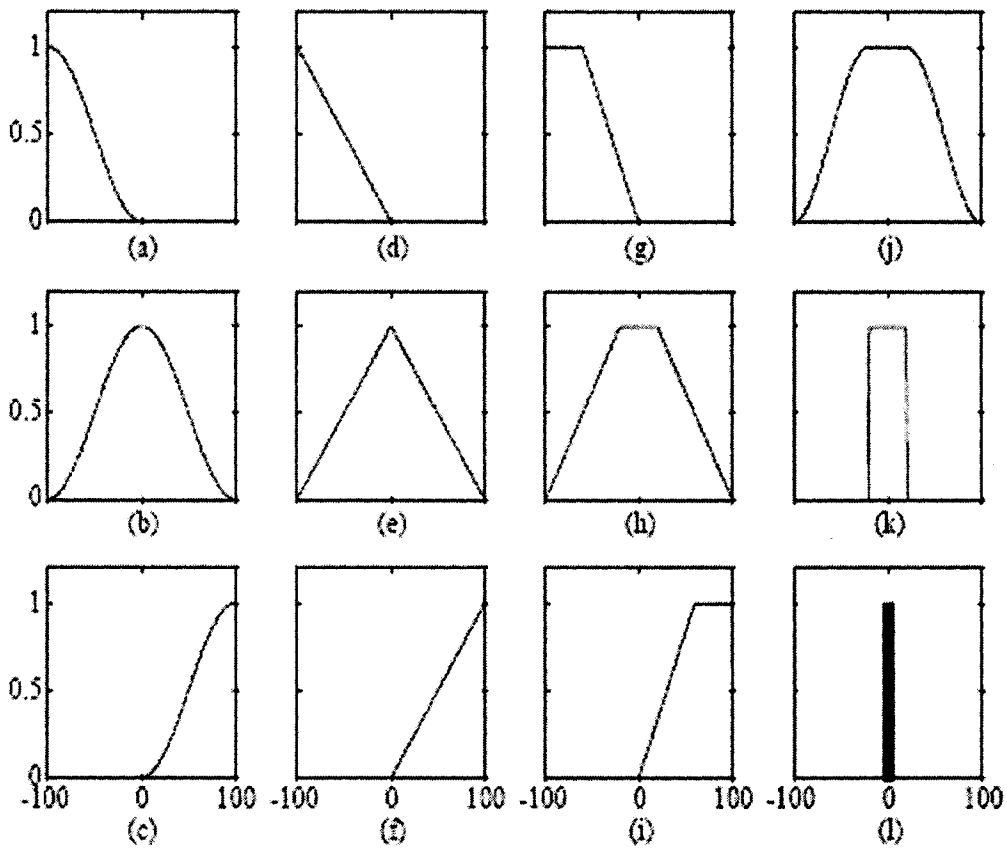

Fig.5.1: Examples of membership functions; (a) s-function, (b) Gaussian, (c) z-function, (d-f) triangular functions, (g-i) trapezoidal functions, (j) flat function, (k) rectangle function, (l) singleton function.

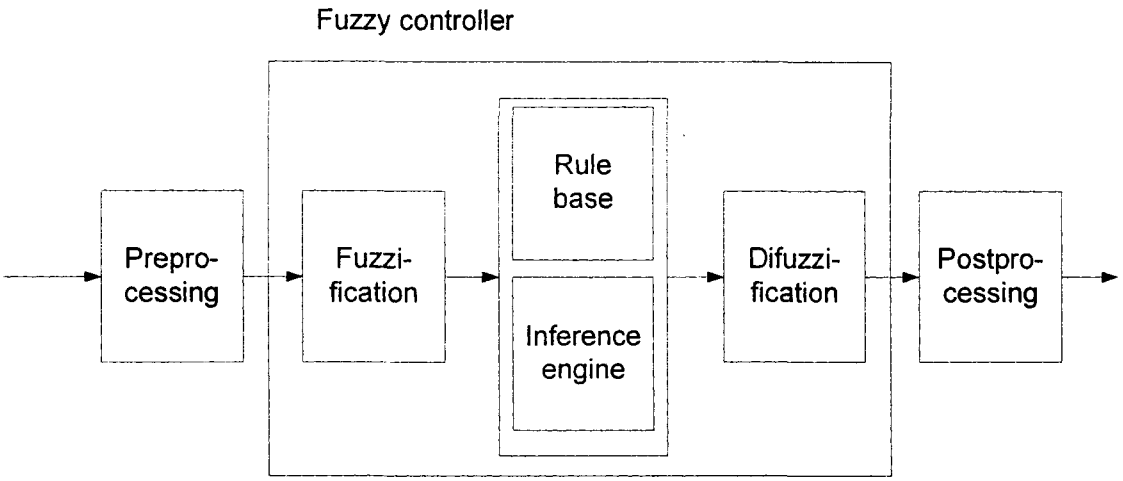

Fig.5.2: Block diagram of a fuzzy logic controller.

sets are represented graphically by means of their membership functions. There are numerous choices for the membership functions such as triangular, gaussian function, trapezoidal, singleton, etc.

The choice of fuzzy logic membership functions depends on the designer's preference and/or experience. Fuzzy logic implements human experiences and preference via membership functions and fuzzy rules. The complete process of formulating the mapping from a given input to an output using fuzzy logic is known as fuzzy inference. The block diagram of a typical FLC is shown in Fig.5.2. There are two types of fuzzy inference methods: the Mamdani type and the Sugeno type. The difference between the two methods is only in the way the output is defined. In control applications, Mamdani type fuzzy inference is the most commonly used method. In the Mamdani method the output is defined by the centroid of a two-dimensional function. Fuzzy inference is mainly based on five components which are: (1) Pre-processing (2) fuzzification, (3) fuzzy inference engine (rule base) (4) defuzzification and (5) Post-processing.

5.2.1 Pre-processing

The inputs are most often hard or crisp measurements from some measuring equipment, rather than linguistic. A pre-processor, the first block in Fig.5.2, conditions the measurements before they enter the controller. Examples of pre-processing are:

-Quantisation in connection with sampling or rounding to integers;

-Normalisation or scaling onto a particular, standard range;

-Filtering in order to remove noise;

-Averaging to obtain long term or short term tendencies;

-A combination of several measurements to obtain key indicators; and

-Differentiation and integration or their discrete equivalences.

5.2.2 Fuzzification

The first step of fuzzy inference is to take inputs and determine the degree to which they belong to each of the appropriate fuzzy sets via membership functions. The process of converting a numerical variable (real or crisp value) into a linguistic variable (fuzzy value) is called fuzzification. In the FLC, the input is a numerical value limited to the universe of the input variable and the output is fuzzy degree of membership in the qualifying linguistic set (between 0 and 1 inclusive). Mathematically, the fuzzification of an input can be obtained using a singleton fuzzifier according to the equations of pre-selected membership functions of various fuzzy sets of that input.

5.2.3 Fuzzy inference engine (rule base)

The rules may use several variables both in the condition and the conclusion of the rules. The controllers can therefore be applied to both multi-input-multi-output

(MIMO) problems and single-input-single-output (SISO) problems. The typical SISO problem is to regulate a control signal based on an error signal. The controller may actually need both the error and the change in error as inputs. To simplify, this section assumes that the control objective is to regulate some process output around a prescribed reference. Basically a linguistic controller contains rules in if-then format, but they can be presented in different formats. In many systems, the rules are presented to the end-user in a format similar to the one below,

$$\text{Rule } R_k : \text{If } \Delta\omega \text{ is } A_k \text{ and } \Delta e \text{ is } B_k \text{ then i is } C_k \tag{5.1}$$

where speed error ($\Delta\omega$) and change of speed error (Δe) are the input linguistic variables, current (i) is the output linguistic variable; and A_k, B_k, and C_k are the labels of linguistic variables $\Delta\omega$, $\Delta\omega_e$ and i, respectively. If the antecedent is true to some degree of membership, the consequent is also true to that same degree. The fuzzy operators used for fuzzy rules are AND ($\cap$), OR (U) and NOT ($\bar{}$) which can be defined as follows:

a) AND means classical intersection:

$$\mu_{A\cap B} = \min\{\mu_A(x), \mu_B(x)\} \tag{5.2}$$

b) OR means classical union:

$$\mu_{A\cup B} = \max\{\mu_A(x), \mu_B(x)\} \tag{5.3}$$

c) NOT means classical complement:

$$\bar{\mu}_A = 1-\mu_A(x) \tag{5.4}$$

Therefore, according to rule R_k, $\mu_{ck}(x)=\min(\mu_{Ak}(x), \mu_{Ak}(x))$, The fuzzy rules can be derived by using the following approaches:

a) from expert experience and control engineering knowledge

b) from the behaviour of human operators

c) from a fuzzy model of a process

d) from a learning process.

With respect to fuzzy control, Mamdani implication is the most important

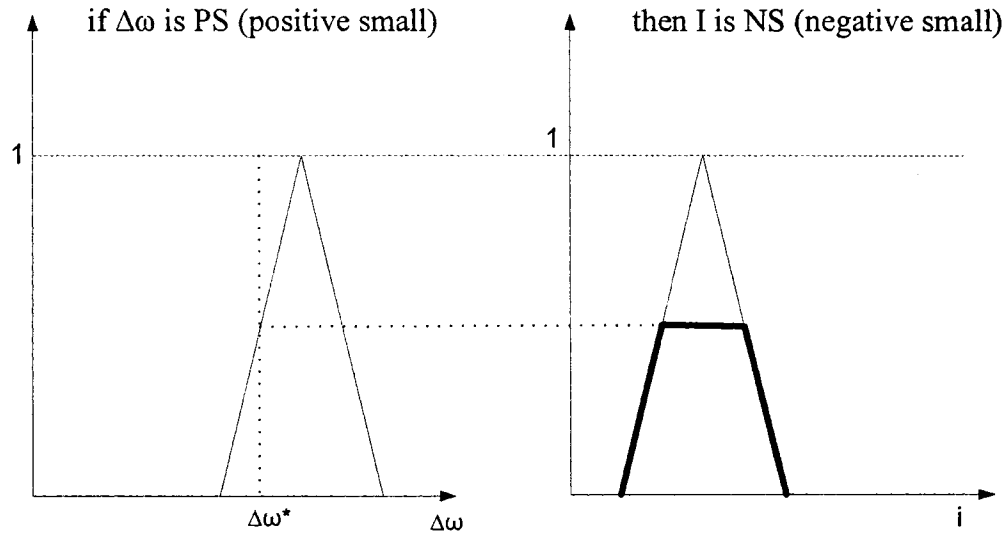

Fig.5.3: The graphical representation of the firing of a rule using Mamdani implication method.

implication known in the literature [48]. The graphical representation of Mamdani implication in order to interpret the meaning of a rule is shown in Fig.5.3. This figure shows the firing of a rule "if Δω is PS (positive small), the output 'i' is NS (negative small)". Δω* is the crisp input and the deep solid lines in the output membership function $\mu_{CNS}(i)$ indicates the modified (clipped) membership function $\mu_{CNS}(i)$. Thus according to Mamdani implication,

$$\mu_{CNS}(i) = \min(\mu_{PS}(\Delta\omega^*), \mu_{NS}(i)) \tag{5.5}$$

The process described by this equation is called rule firing. The inference engine or rule firing as described above can be of two basic types such as: (1) composition based and

(2) rule based inferences. The basic differences between them are described below:

(1) Composition based inferences: In this inference, the fuzzy relations representing the meaning of each rule are aggregated into one fuzzy relation describing the meaning of the overall set of rules. Then, inference or firing with this fuzzy relation is performed via the operation composition between the fuzzified crisp input and the fuzzy relation representing the meaning of the overall set of rules. As a result of the composition one obtains the fuzzy set describing the fuzzy value of the overall control output.

(2) Individual rule based inference: In this inference, first each single rule is fired. This firing can simply be described as: (a) computing the degree of match between the crisp input and the fuzzy sets describing the meaning of the rule antecedent and (b) clipping the fuzzy set describing the meaning of the rule consequent to which the rule-antecedent has been matched by the crisp input. Finally, the clipped values for the control output of each rule are aggregated, thus forming the value of the overall control output.

Usually, the individual rule based inference is preferred since it is computationally very efficient and saves a lot of memory. In this thesis, the individual rule based inference is used. However, the composition based inference is equivalent to the individual rule based inference in the case of Mamdani-type implication used to represent the meaning of the individual rules. In the case of individual rule based inference, the overall control output which is a combined fuzzy set from a set of rules can be mathematically expressed in [87] as

$$\mu_I(i) = \max(\mu_{CLI(1)}(i),.....,\mu_{CLI(n)}(i)) \qquad (5.6)$$

where $\mu_{CLI(k)}(i)$ (k=1,2,...,n) is the clipped value of the control output 'i' in the case of

individual (kth) rule based inference:

$$\mu_{CLI(k)}(i) = \min(\min(\mu_{A(k)}(\Delta\omega^*),\mu_{B(k)}(\Delta e^*)),\mu_{C(k)}(i)) \quad (5.7)$$

where $\mu_{A(k)}(\Delta\omega^*)$ is the degree of membership of the crisp input $\Delta\omega^*$ in fuzzy set $\mu_{A(k)}$, $\mu_{B(k)}(\Delta e^*)$ is the degree of membership of the crisp input Δe^* in fuzzy set $\mu_{B(k)}$, and $\mu_{C(k)}(i)$ is the degree of membership of the output 'i' in fuzzy set $\mu_{C(k)}$.

Figures 5.4 and 5.5 are both a graphical construction of the controller output in the core of the controller. In Fig. 5.4, each of the nine rows refers to one rule. For example, the first row says that if the error is negative (row 1, column 1) and the change in error is negative (row 1, column 2) then the output should be negative big (row 1, column 3). The picture corresponds to the rule base in (2). The rules reflect the strategy

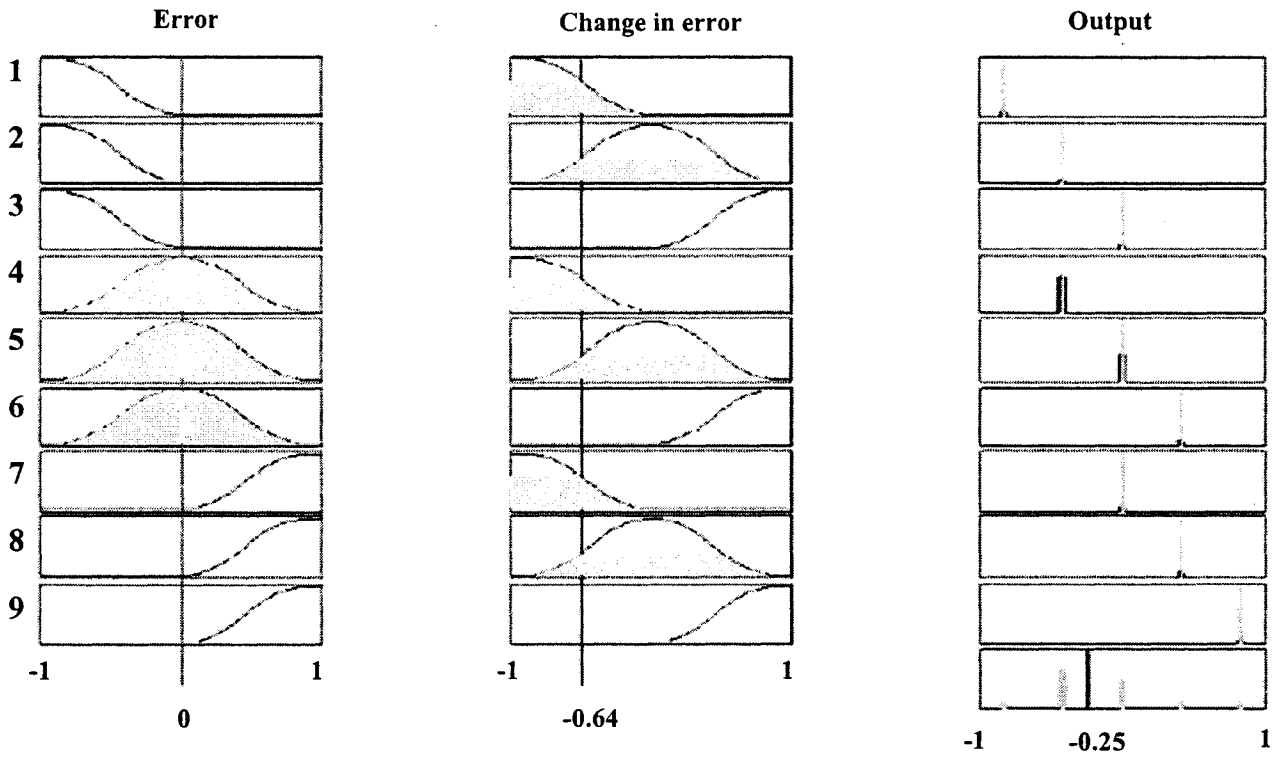

Fig.5.4: Two inputs one output rule base with singleton output sets (generated in the Matlab Fuzzy Logic Toolbox).

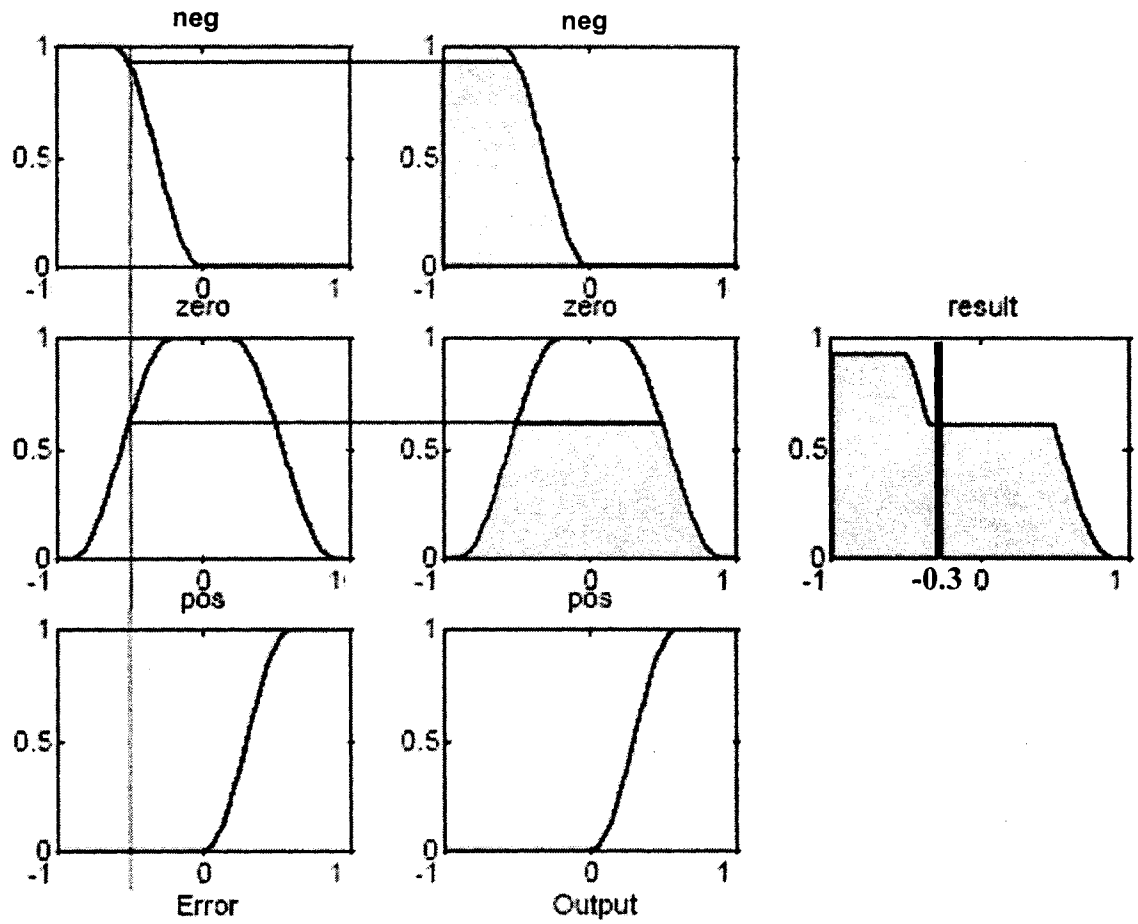

Fig.5.5: One input, one output rule base with non-singleton output sets.

that the control signal should be a combination of the reference error and the change in error, a fuzzy proportional-derivative controller.

5.2.4 Defuzzification

Defuzzification is the final process of fuzzy inference in getting the control output. The input for the defuzzification process is a fuzzy set (combined output of each rule) and the output is a single number, which is non-fuzzy i.e., a crisp value. The fuzzy set (Fig. 5.4, bottom right; Fig. 5.5, extreme right) must be converted to a number that

can be sent to the process as a control signal. This operation is called defuzzification. In Figs. 5.4 and 5.5 the x-coordinate marked by a vertical dividing line becomes the control. The resulting fuzzy set is thus defuzzified into a crisp control signal. There are several defuzzification methods. The centre of gravity or area is the most popular among all the methods of defuzzification.

Centre of Gravity: The crisp output value x (the vertical line in Figs. 5.4 and 5.5) is the abscissa under the centre of gravity of the fuzzy set,

$$u = \frac{\sum_i \mu(x_i) x_i}{\sum_i \mu(x_i)} \tag{5.8}$$

Here x_i is a operating point in a discrete universe, and $\mu(x_i)$, is its membership value in the membership function. The expression can be interpreted as the weighted average of the elements in the support set. For the continuous case, the summations will be replaced by integrals.

Some other defuzzification methods such as center of sums, center of largest area, first of maxima, middle of maxima, etc. are available. The center of gravity/area defuzzification method is used in this work. .

5.2.5 Post processing

Output scaling is also relevant. In case the output is defined on a standard universe this must be scaled to appropriate unit for instance ampere, volts, meters, or tons per hour. An example is the scaling from the standard universe [-1,1] to the physical units [-10,10] Amperes. The post processing block often contains an output gain that can be tuned, and sometimes also an integrator.

5.3 FLC design algorithms

In the design of proposed FLC incorporating flux control for a practical inverter-fed IPMSM drive the voltage and current constraints have been considered. Assume that the maximum available phase voltage amplitude and the maximum line current amplitude are V_a and I_a, respectively. Then the feasible operation range is constrained by the following inequalities:

$$(v_d)^2 + (v_q)^2 \leq V_a^2$$

$$(i_d)^2 + (i_q)^2 \leq I_a^2$$

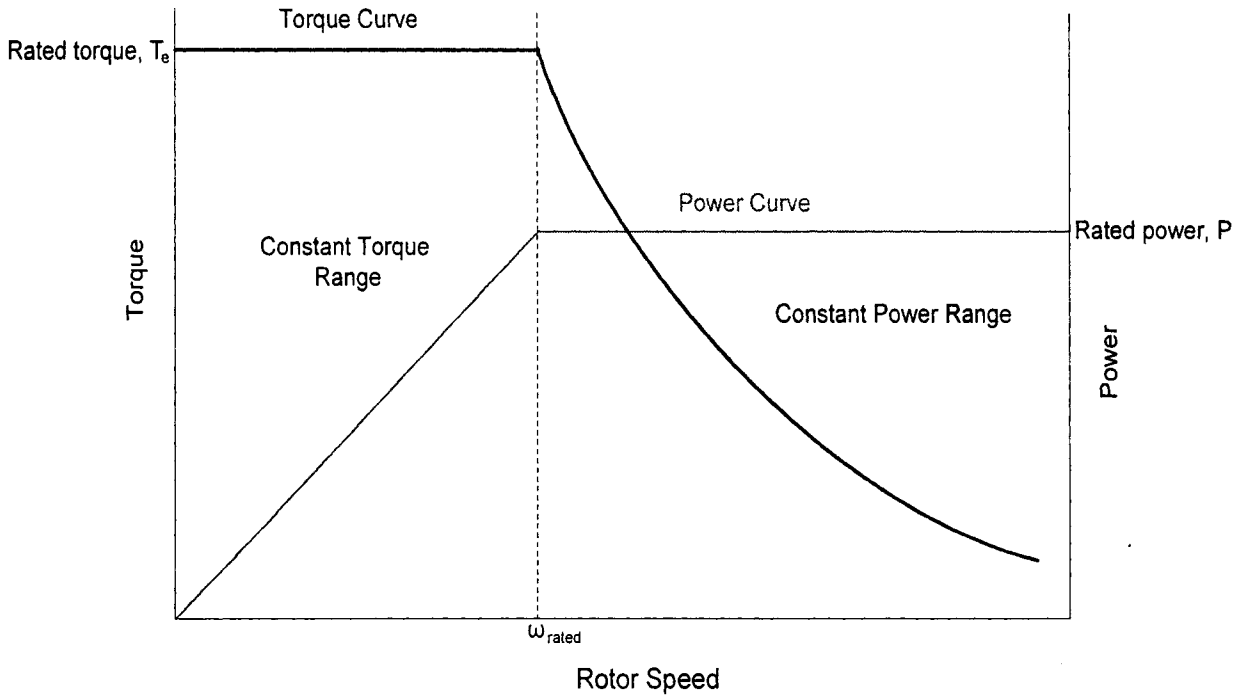

Fig.5.6: Torque curve and power curve in wide speed range.

The full operating range of the IPMSM can be divided into two regions as shown in Fig.5.6; below the rated speed where the torque is maintained constant by keeping the flux constant and above the rated speed where the power is maintained constant by field

weakening. The block diagram of the proposed controller is shown in Fig 5.7.The design of FLC for two different speed regions mentioned earlier is described below. In the proposed work a normalized FLC is designed so that the main structure of FLC will be independent of motor parameters. Thus, the normalized FLC can be used for any IPMSM motor by changing the scaling factors (k_e, k_ω, $k_{\Delta e}$, k_q, k_d) only. For both speed regions first the membership function of i_q (one output of FLC) is designed in such a way that the motor can generate the necessary torque to follow the command speed as quickly as possible. This can be done based on the knowledge of operator on fuzzy logic and motor control. Thus, the main challenge is to design the membership functions of i_d (another output of FLC), which is necessary for flux control.

5.3.1 Design of FLC in constant torque region

As the IPM motor has a saliency (L_q>L_d), as a result, the reluctance torque is available, the armature current vector is controlled according to MTPA operation. If the d-axis current, i_d is kept zero, one cannot utilize the potential reluctance torque. So in order to increase the efficiency of the IPMSM drive, the reluctance torque should be properly utilized. The dependency of MTPA curve on IPMSM saliency is shown in Fig.5.8. As shown in this figure by the arrow sign, with the increase in saliency the MTPA curve will spread out from the q-axis current line. Below the rated speed, in order to incorporate the flux control in practical IPMSM drive, conventionally i_d is calculated based on MTPA operation as [74],

$$i_d^r = \frac{\psi_m}{2(L_q - L_d)} - \sqrt{\frac{\psi_m^2}{4(L_q - L_d)^2} + i_q^{r^2}} \tag{5.9}$$

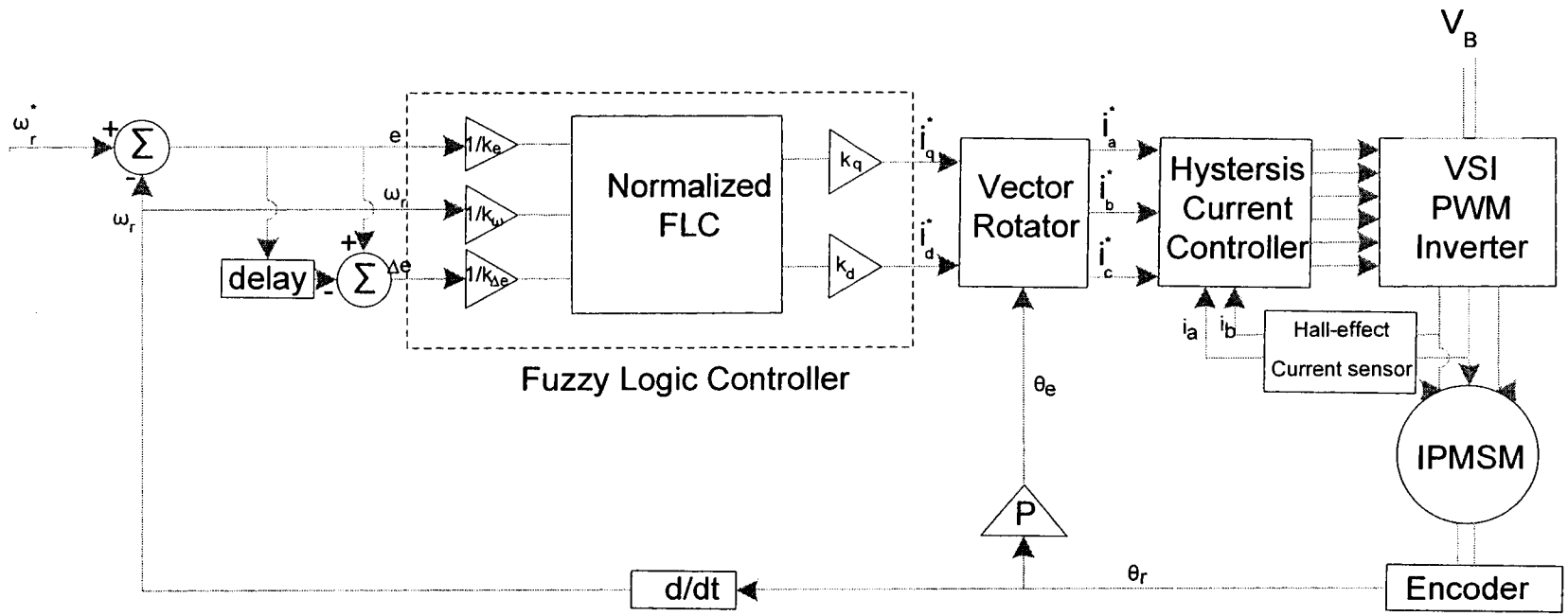

Fig.5.7: Block diagram of the proposed FLC based IPMSM drive

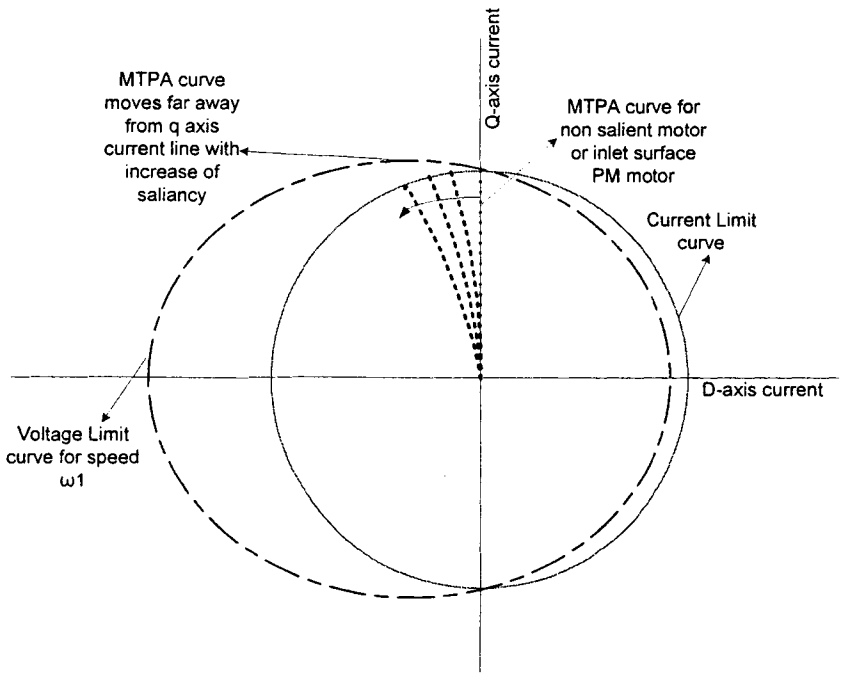

Fig. 5.8: MTPA curve for different saliency.

As the trajectories of MTPA depend on motor parameters, it can not be generalized. It is quite impossible to design a FLC considering the exact MTPA relation (5.9) as guideline. This relation can be simplified using Taylor series expansion around i_q=0 as,

$$i_d = -\frac{(L_q - L_d)}{\psi} i_q^2 + \frac{(L_q - L_d)^3}{\psi^3} i_q^4 + \ldots\ldots$$

Using the nominal value of L_d, L_q, ψ that are given in Appendix A, it is found that $\frac{(L_q - L_d)}{\psi} << 1$. Although with the increase of the order of i_q, the value of the corresponding term increases, the multiplying factor associated with i_q is very low and hence the forth and higher order terms of i_q can be neglected. Thus, the simplified relation can be written as,

$$i_d = -\frac{\left(L_q - L_d\right)}{\psi} i_q^2 \tag{5.10}$$

This simplified equation is utilized as a basis to design the membership functions of i_d below the rated speed. The scaling factor for i_q (k_q) is selected by trial and error in such a way that the motor generates rated torque at rated condition. The scaling factor for i_d (k_d) will be equal to $\frac{\left(L_q - L_d\right)}{\psi} K_q^2$ below the rated speed. So the steady point will be the point at which the MTPA curve intersects with the required torque curve as discussed in Fig.2.4 of Chapter 2. Therefore, by changing the scaling factors one can make the trajectory of the operating point of IPMSM to follow the MTPA curve even for different saliency as discussed in the Fig.5.8. The scaling factors (k_e, k_ω) at the input side of the FLC depend on the rated speed of the motor so that their normalized values lie within the limit ±2. Other scaling factor ($k_{\Delta e}$) at input side is chosen by trial and error method.

5.3.2 Design of FLC in constant power region

In case of high speed operation of IPM machine, it is constrained by linear proportionality of the back-emf and inductive voltage drop to speed. Above the rated speed, the magnetic flux must be weakened by the armature reaction of i_d, in order to maintain the stator voltage constant at its maximum value. Thus, the field weakening not only extends the operating limits of IPMSM drive but also relieves the controller from saturation that occurs at high speeds. Below the rated speed, the operating point will move through the trajectory of MTPA and above the rated speed it will follow the voltage limit curve of the corresponding speed as shown in Fig.5.9. Finally it will reach the

intersection point of voltage constraint curve with the required torque curve (T_1). In Fig.5.9, the distance between the operating point and the origin indicates the magnitude of current (I_{a1}). For high speed motoring action, the operating region is bounded by the d-axis current line, current constraint curve and voltage limit curve as shown in Fig.5.9. So the operating point should be in that part of the corresponding constant torque which is located within that bounded region as mentioned. It can be easily understood that the intersecting point of voltage limit curve with constant torque curve gives the required torque with minimum current if the MTPA point for the corresponding torque is out of the bounded region for that speed. Thus the intersecting point between the corresponding voltage limit curve and the constant torque curve becomes the best choice to achieve low copper loss. The relation between i_d and i_q for field weakening region maintaining current and voltage constraint is [74],

$$i_d^r = -\frac{\psi}{L_d} + \frac{1}{L_d}\sqrt{\frac{(V_a')^2}{P^2\omega_r^{\,2}} - L_q^2 i_q^2} \tag{5.11}$$

In order to design the structure of FLC this equation can also be simplified as follows. As shown in Fig.5.6 above the rated speed developed torque and hence the torque component current (i_q) decreases inversly with the increase in speed.

Reasonably assuming $L_q^2 i_q^2 \ll \frac{(V_a')^2}{P^2\omega_r^{\,2}}$ and hence neglecting the term $L_q^2 i_q^2$, (5.11) becomes,

$$i_d^r = -\frac{\psi}{L_d} + \frac{1}{L_d}\sqrt{\frac{(V_a')^2}{P^2\omega_r^{\,2}}} \tag{5.12}$$

where V_a' is the maximum terminal voltage neglecting stator resistance in steady-state.

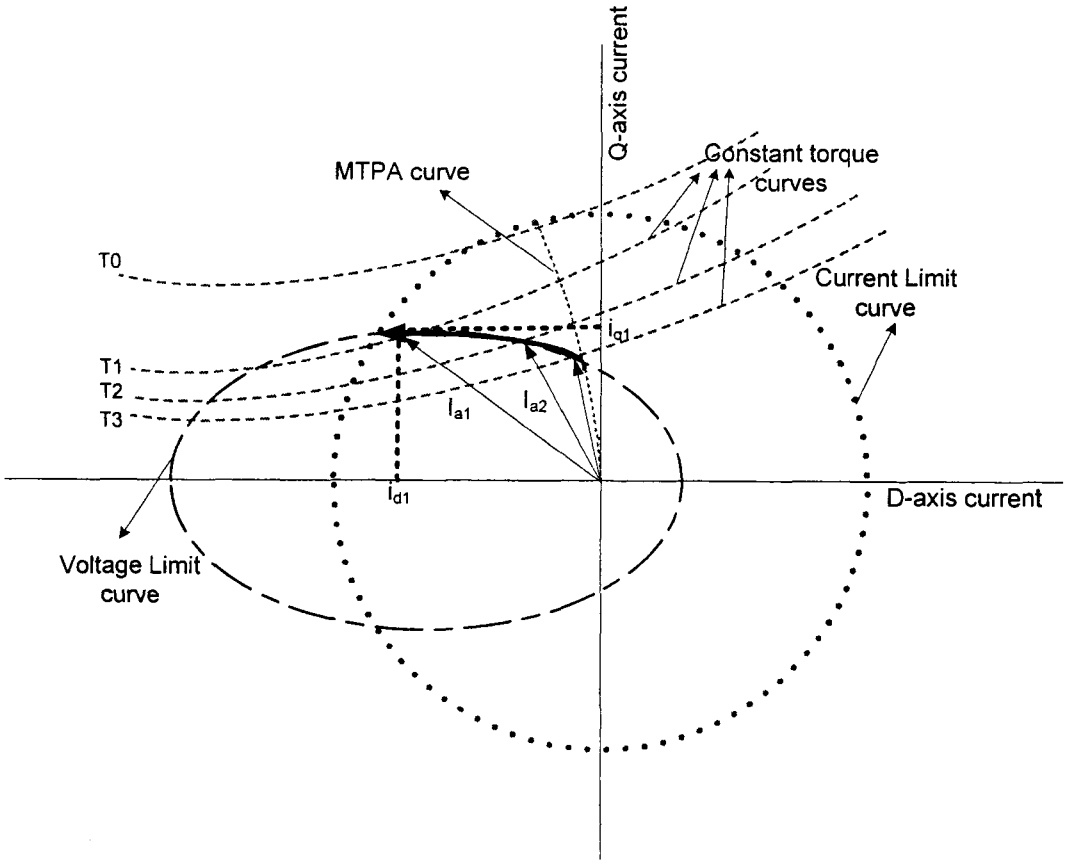

Fig.5.9: Control in constant power region.

Therefore, at rated speed V_a' can be written as,

$$(V_a')^2 \approx P^2 \omega_{r(rated)}^2 \psi^2 \tag{5.13}$$

So equation (5.12) can be simplified as,

$$i_d^r = -\frac{\psi}{L_d} + \frac{\psi}{L_d}\sqrt{\frac{\omega_{r(rated)}^{\ 2}}{\omega_r^{\ 2}}} \tag{5.14}$$

$$i_d^r = -\frac{\psi}{L_d} + \frac{\psi}{L_d \omega_{r(normalized)}}$$

$$i_d^r = \frac{\psi}{L_d}\left(-1 + \frac{1}{\omega_{r(normalized)}}\right) \tag{5.15}$$

where $\omega_{r(normalized)} = \frac{\omega_r}{\omega_{r(rated)}}$

So the scaling factor for i_d is $k_d = \frac{\psi}{L_d}$ for field weakening region. Equation (5.15) is utilized as a basis to design the membership functions of i_d above the rated speed. The membership functions for various input output variables used for the proposed FLC are shown in Fig.5.10 [88]. Once the membership functions are selected, next step is to

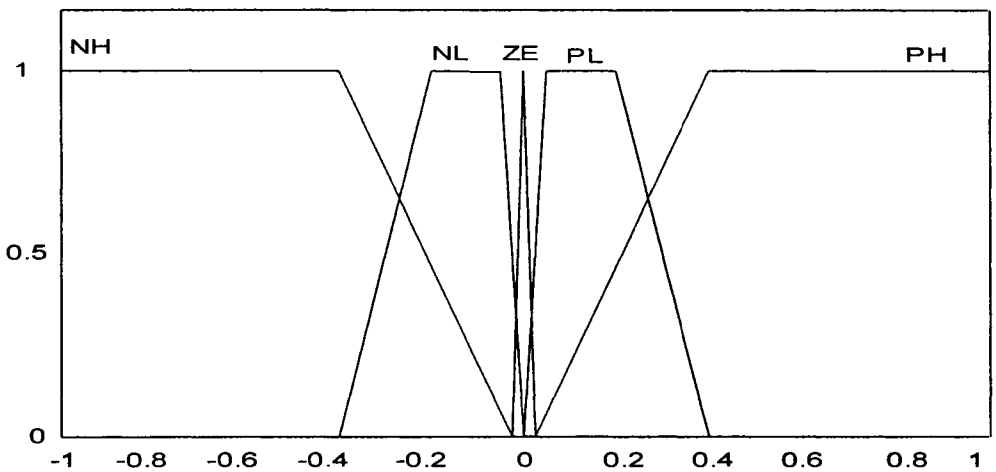

Fig.5.10(a): Membership functions for Speed error $\Delta\omega$.

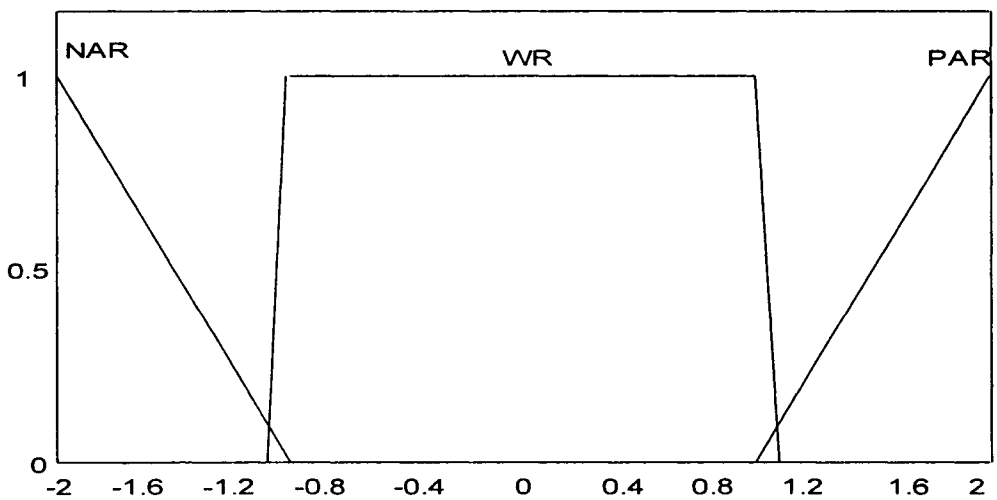

Fig.5.10(b): Membership functions for Motor speed ω_r.

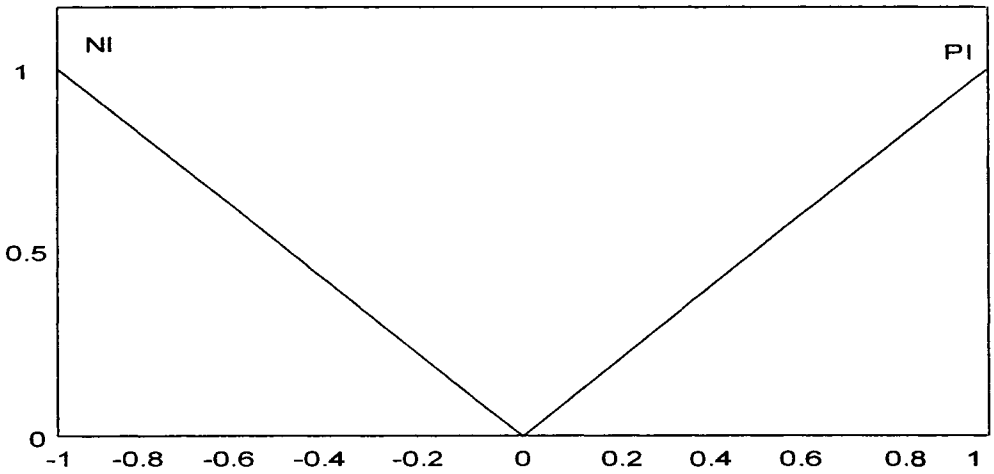

Fig.5.10(c): Membership functions for Error difference, Δe.

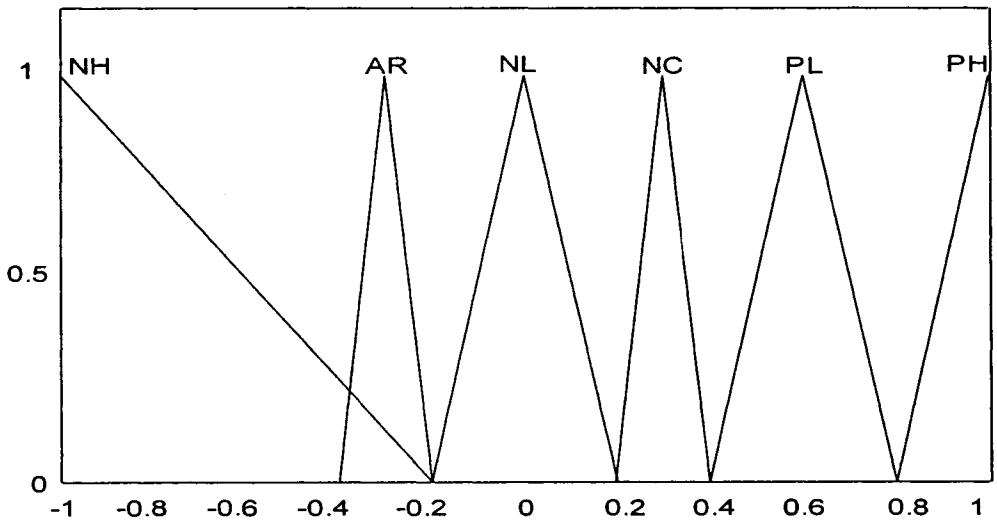

Fig.5.10 (d): Membership functions for q-axis current i_q .

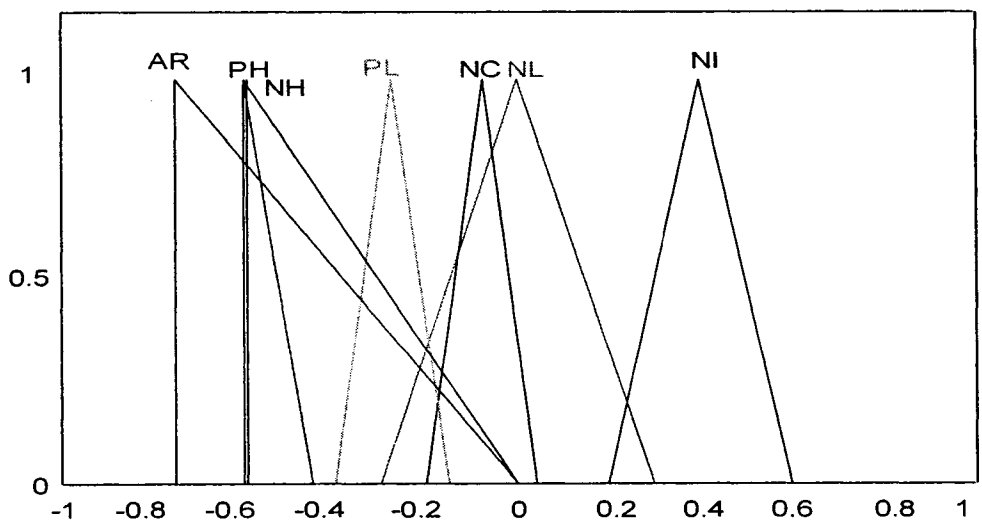

Fig.5.10 (e): Membership functions for d-axis current i_d .

choose the fuzzy rules based on the control strategies mentioned earlier. The fuzzy rules are selected by trail and error method depending on experience. The rules used for the proposed FLC algorithm is as follows [88]:

(1) if $\Delta\omega$ is PH (positive high), then i_q is PH (positive high) and i_d is PH (positive high).

(2) if $\Delta\omega$ is PL (positive low), then i_q is PL (positive low) and i_d is PL (positive low).

(3) if $\Delta\omega$ is NH (negative high), then i_q is NH (negative high) and i_d is NH (negative high).

(4) if $\Delta\omega$ is NL (negative low), then i_q is NL (negative low) and i_d is NL (negative low).

(5) if $\Delta\omega$ is ZE (zero) and ω_r is WR, then i_q is NC (not change) and i_d is NC (not change).

(6) if ω_r is PAR (positive above rated) or NAR (negative above rated), then i_q is AR (above rated) and i_d is AR (above rated).

(7) If $\Delta\omega$ is ZE (zero) and Δe is PI (positive), then i_q is PL (positive high) and i_d is PL (positive high).

(8) If $\Delta\omega$ is ZE (zero) and Δe is NI (negative), then i_q is NL (negative high) and i_d is NL (negative high).

Based on the above rules the fuzzy rule base matrix can be obtained. Mamdani type fuzzy inference is used in this work. The value of the constants, membership functions, fuzzy sets for the input output variables and the rules used in this thesis are selected in such a way that MTPA is obtained within rated speed and field weakening technique will be appeared above rated speed.

5.4 Simulation results

In order to verify the effectiveness of the proposed FLC, a computer simulation model is developed in Matlab/Simulink software and Fuzzy Logic toolbox [89]. The

values of scaling factors used in the simulation model of the FLC based IPMSM drive are k_e=(25/183), k_w=(1/183), $k_{\Delta e}$=1e-5/183, k_q=60, k_d=47.43 (below the rated speed) and 20.4 (above the rated speed). The performance of the proposed FLC is compared with conventional FLC [42] and also a conventional PI controller. The PI controller used in this chapter is the same as already used in chapter 3. The basic diagram of the conventional FLC based drive that used for comparison is shown in Fig.5.11. The model used for simulation is shown in Fig.5.12. The details of the sub-system of this model are shown in Appendix B. From the simulation results of Fig.5.13, it can be observed that the settling time is much less in the proposed FLC as compared to both PI and conventional FLC. This is because of the flux control feature of the proposed controller with MTPA technique. The conventional PI controller has a big overshoot. But the proposed FLC controller can follow the command speed with no overshoot or undershoot. The corresponding d-q axis flux linkage, line current and stator q-axis current vs stator d-axis

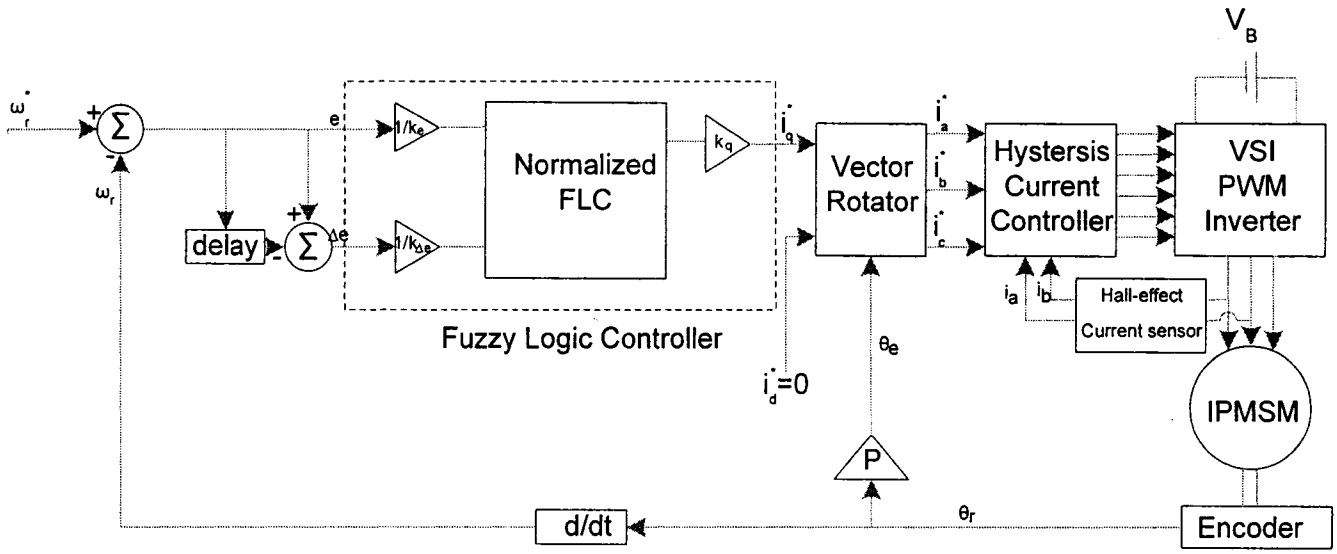

Fig.5.11: Block diagram of the conventional FLC based IPMSM drive used in simulation.

current is shown in Fig.5.14 (b)-(d). From the response of d and q axis currents it is observed that the q axis current is high enough to develop the required torque and d axis current becomes negative to develop the reluctance torque. In Fig.5.14(d), the outer circle indicates maximum value of the starting current whereas the inner circle indicates steady state current. This figure shows the stability of the controller. The developed torque for the proposed controller in the specified condition is shown in 5.15(a). The contribution of reluctance torque in the total generated torque at steady state is shown in 5.15(b). The motor used for this simulation is specially designed for constant torque region. So the difference between d and q axis inductance is not very high. Reluctance torque depends on the saliency of the motor. With increase of saliency the reluctance torque increases. The simulation results for a step command speed of 183 rad/sec at no load are shown in Figs.5.16 and 5.17 for the proposed FLC based IPMSM drive. The comparison of the developed torque vs line current trajectory between the proposed and conventional FLC are shown in Fig.5.18 (a). A ramp input of load disturbance is given to the motor while it was running at a speed of 183 rad/sec. From this figure it is observed that for a particular developed torque the magnitude of line current needed for the proposed FLC is less than the conventional one. This indicates that for any particular load, the proposed controller need less current to follow the command speed. This is because of effective utilization of reluctance torque. The comparison of the d and q axis current trajectories between the proposed and conventional FLC are shown in Fig.5.18(b). The proposed FLC follows the MTPA curve to get maximum torque while the conventional FLC is far away from the MTPA curve as the conventional FLC is designed by keeping d axis current zero. Comparison of total copper loss and rms value of line current between the proposed and

conventional FLCs at rated speed with full load is shown in Fig.5.19. The motor is started at rated load and rated speed with conventional FLC. At t = 0.5 s. the proposed FLC is activated. As the proposed controller maintains MTPA, it takes lowest line current among all these controllers. So copper loss will be minimized and hence efficiency will be maximized by utilizing the proposed FLC. This verifies the superiority of the proposed FLC as compare to conventional FLC. The results for a change of load from no load to full load (20 N-m) then to no load at rated speed for the proposed FLC based IPMSM drive are shown in Fig.5.20. The load is increased to full load from no load at t=0.5 s. then the load is released at t=1 s. The speed response is shown in Fig.5.20 (a). The speed of the motor is insensitive to increase and decrease of load. The corresponding d-q axis currents, total developed torque and magnetic, reluctance torques are shown in Figs.5.20 (b) to (d). At zero load the d-q axis current is very low as the required developed torque is very low. The torque component current (q-axis current) increases with the increase of load to supply increased load torque and the d-axis current decreases to satisfy MTPA relation. The corresponding line current and d-q axis flux linkages are shown in Fig. 5.22. The comparison of developed torque between the proposed and conventional FLCs in full speed range with the corresponding command torque is shown in Fig. 5.23. Below the rated speed both the conventional and proposed FLCs can follow the command speed. But above the rated speed, for the conventional FLC, developed torque cannot follow the command torque. It decreases quickly with speed above the rated speed, as the conventional FLC does not control flux; the controller becomes saturated quickly above rated speed. On the other hand, the proposed controller can follow the command speed even above the rated speed. The speed response of the proposed FLC for step increase of

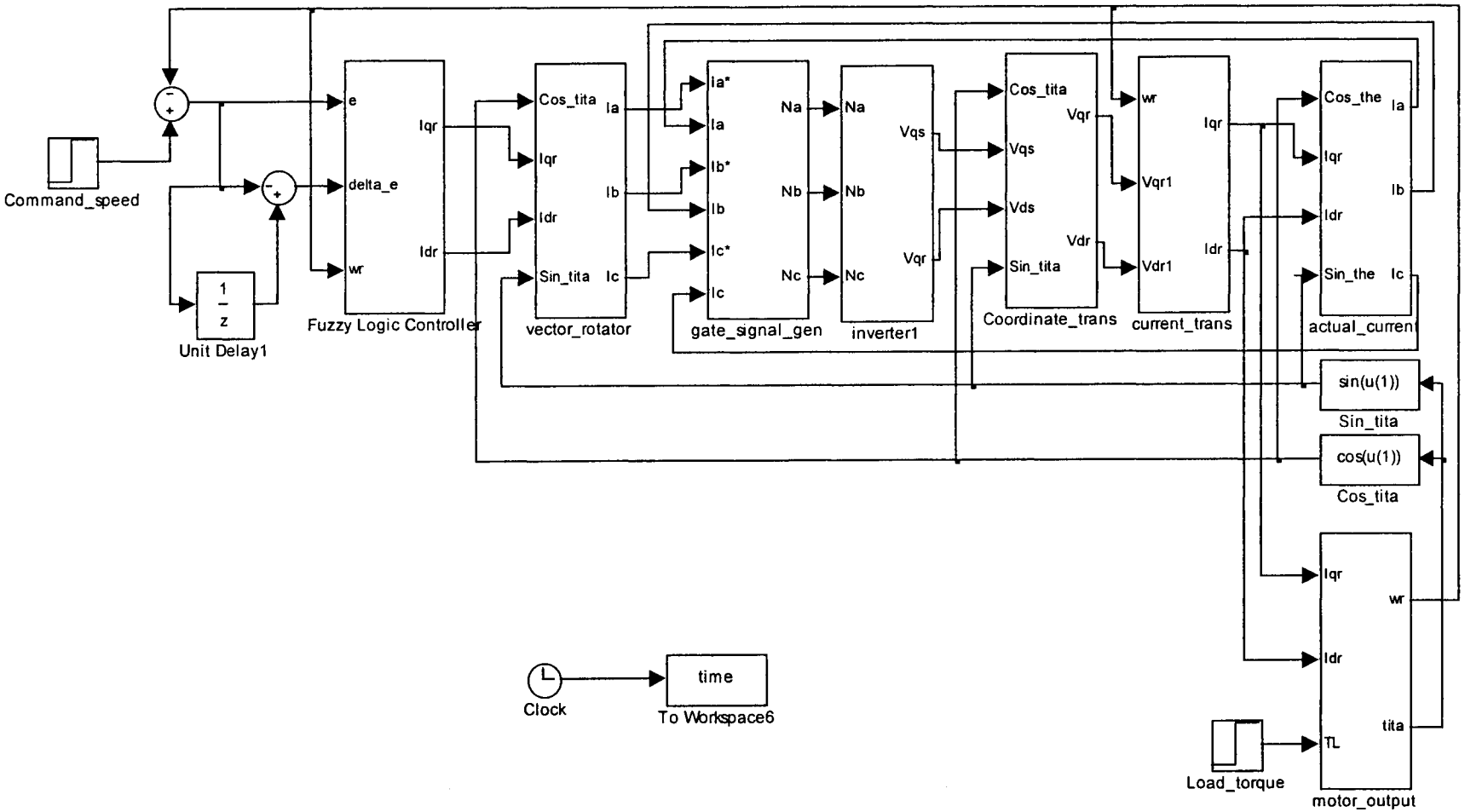

Fig.5.12: Simulink schematic of the complete proposed FLC drive for IPMSM.

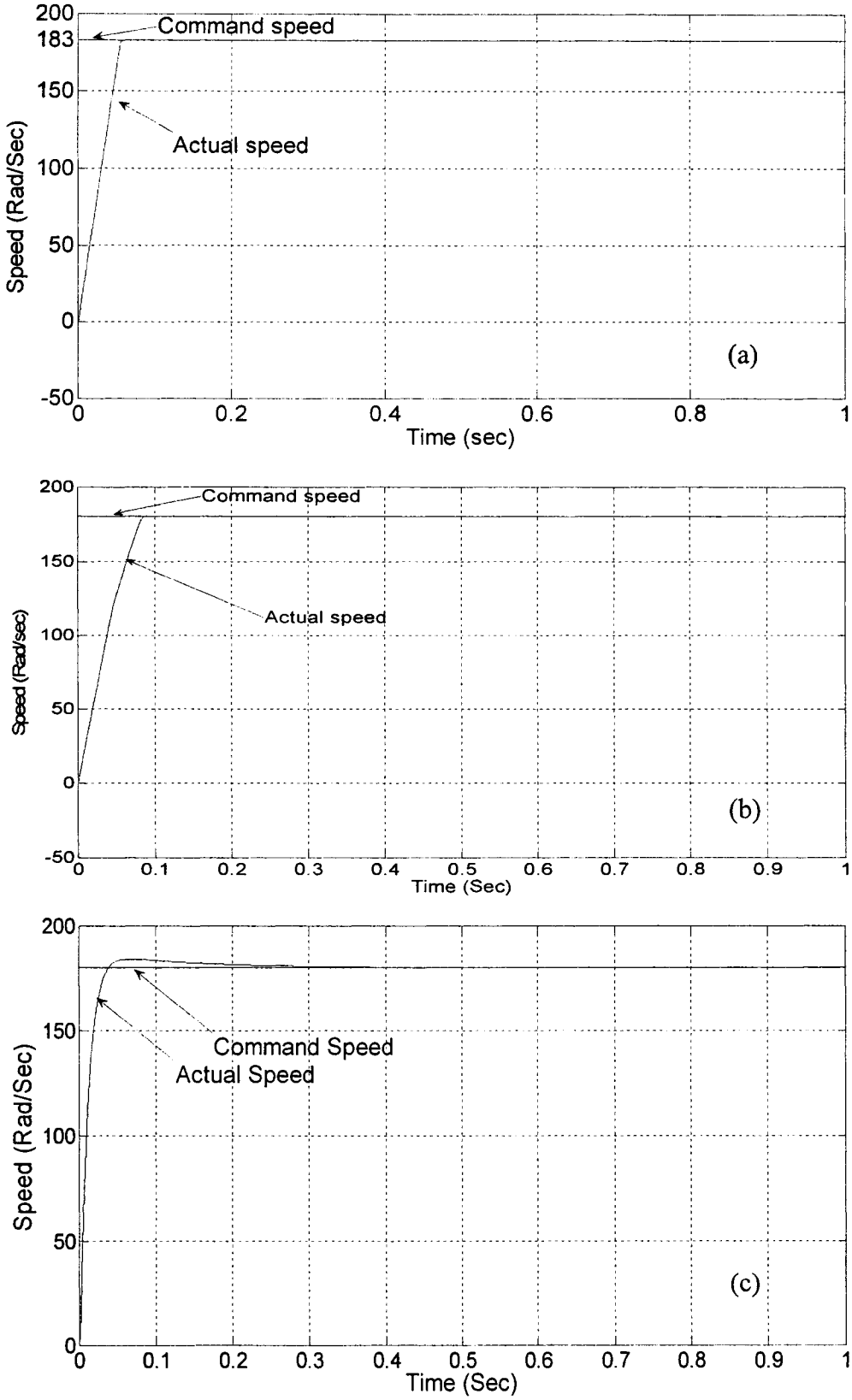

Fig.5.13: Starting speed response for a step rated speed (183 rad/s.) command with full load for; (a) Proposed FLC (b) Conventional FLC (c) PI controller.

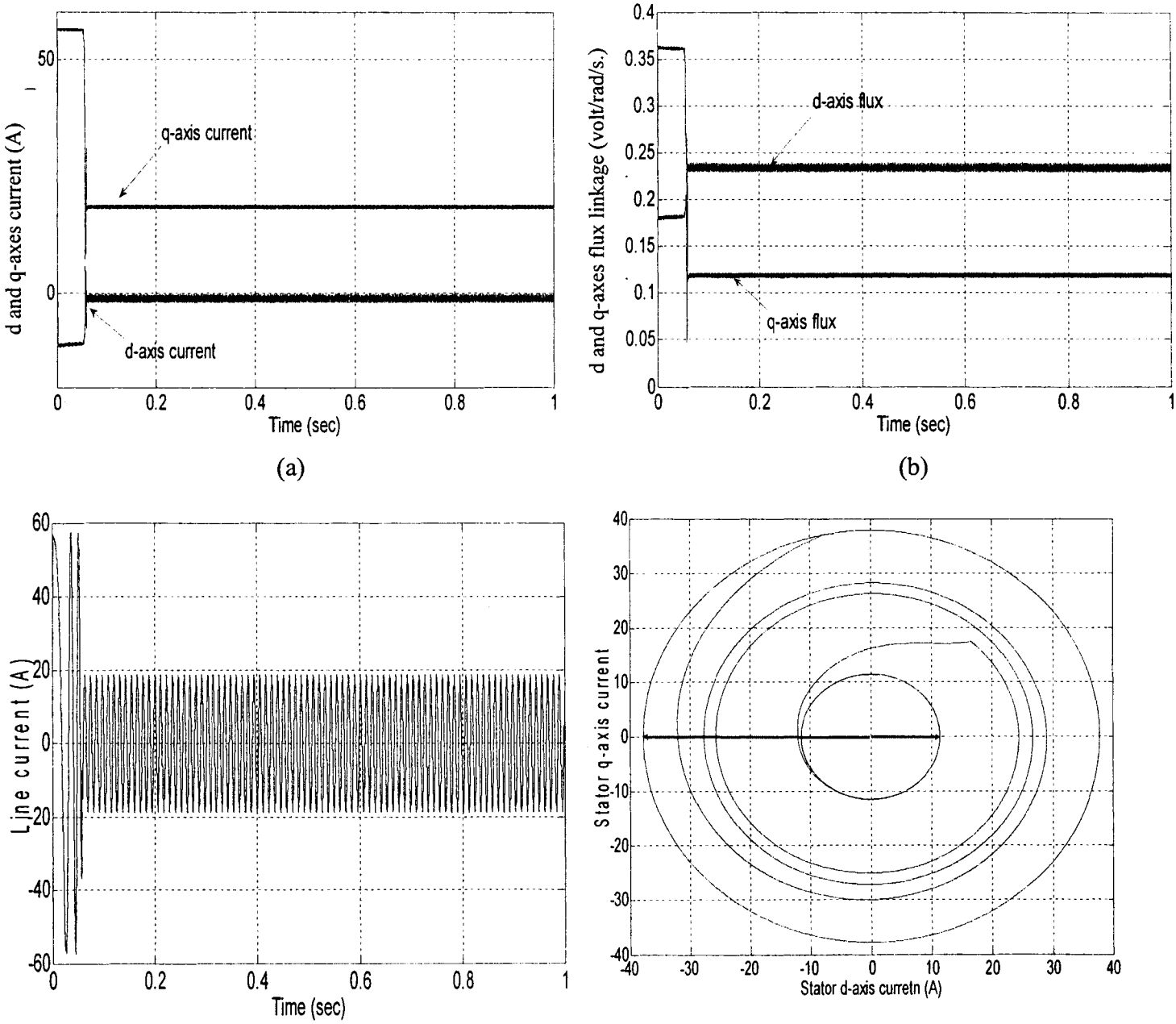

Fig.5.14: Starting speed response for a step rated speed (183 rad/s.) command with full load; (a) d-q axis current (b) d-q axis flux linkage (c) line current (d) stator q axis current vs stator d-axis current.

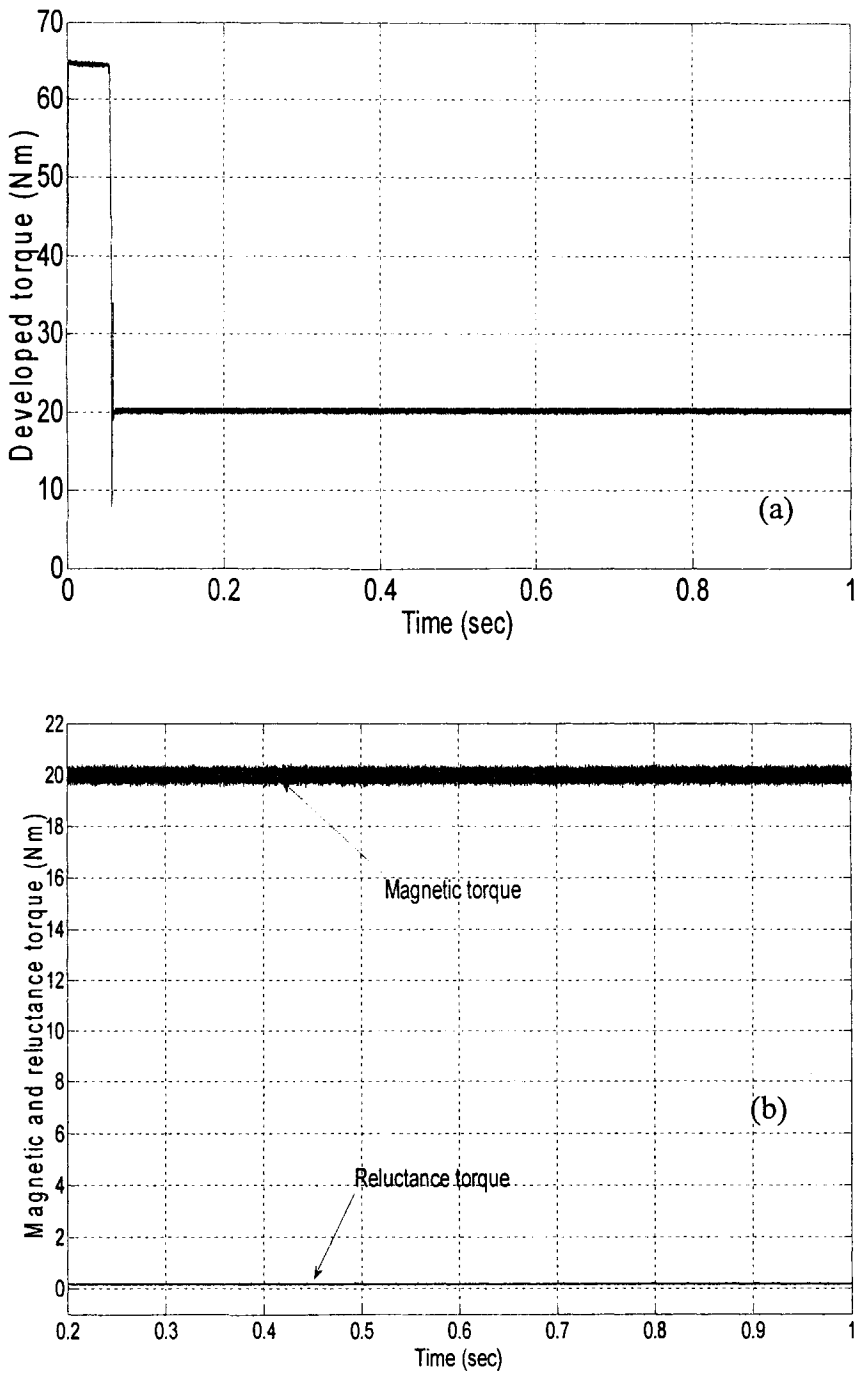

Fig.5.15: Starting speed response for a step rated speed (183 rad/s.) command with full load; (a) developed torque (b) steady state magnetic and reluctance torque.

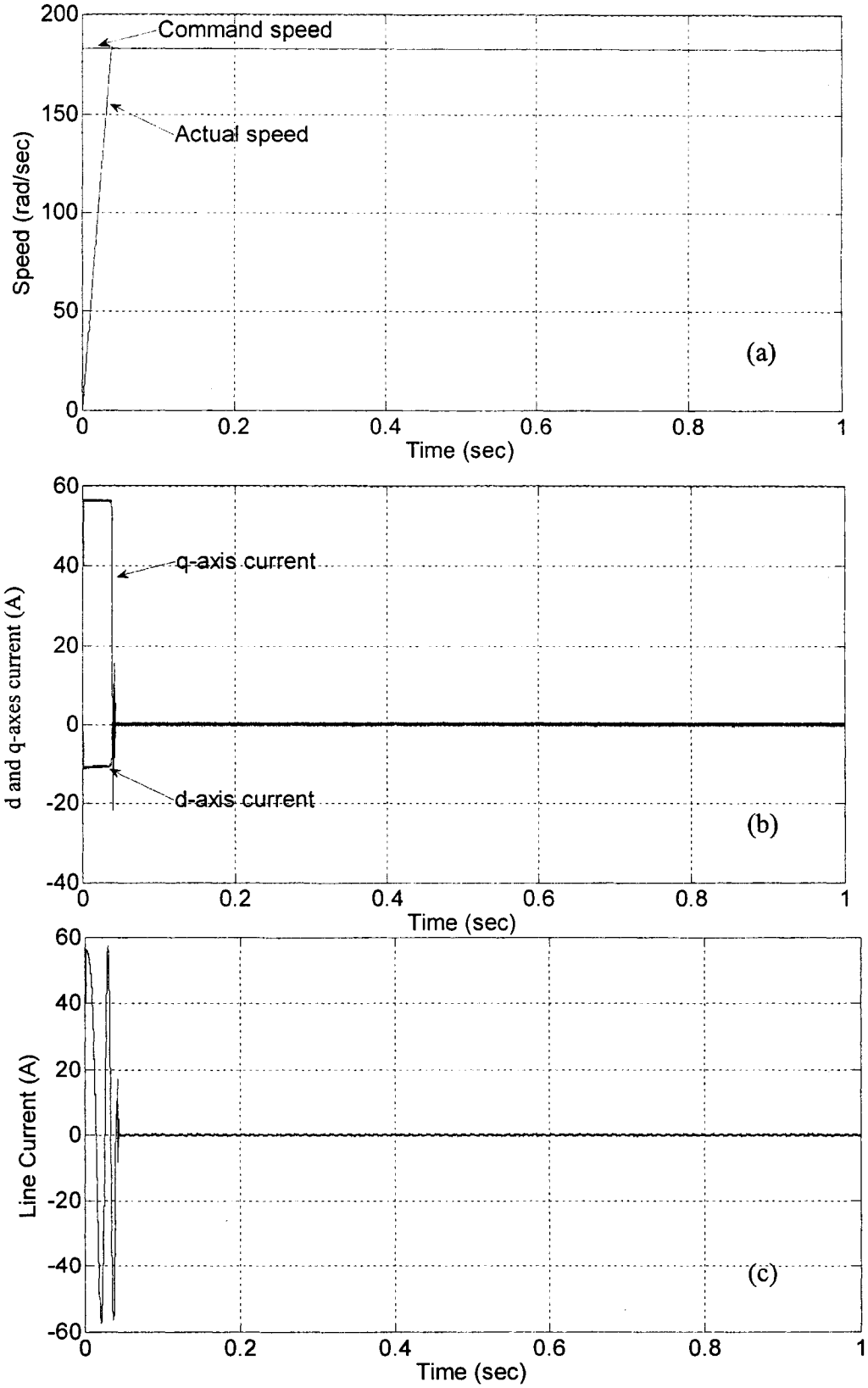

Fig.5.16: Starting speed response for a step rated speed (183 rad/s.) command with no load; (a) speed (b) d and q axis current (c) line current.

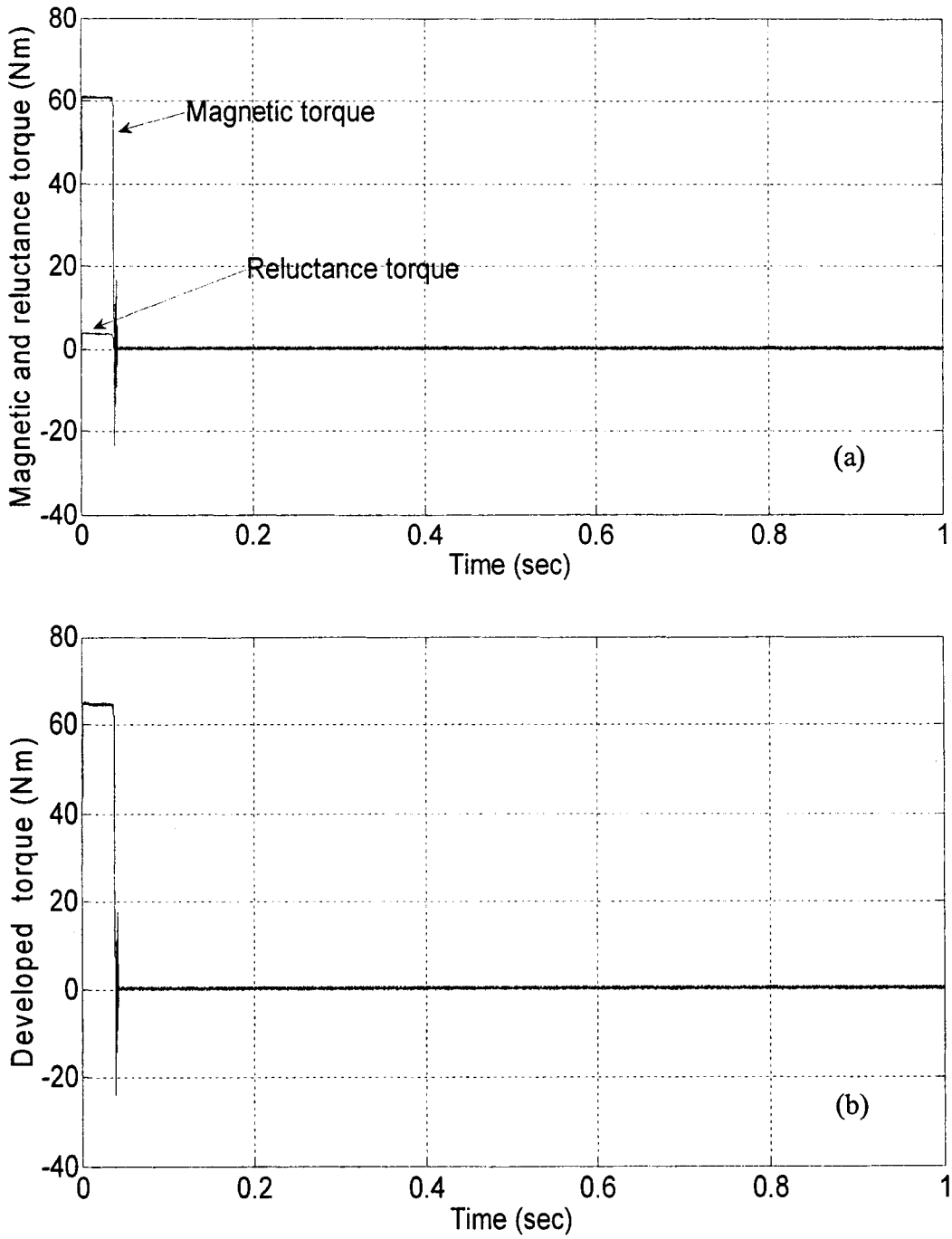

Fig.5.17: Starting speed response for a step rated speed (183 rad/s.) command with no load for the proposed FLC; (a) magnetic and reluctance torque (b) developed torque.

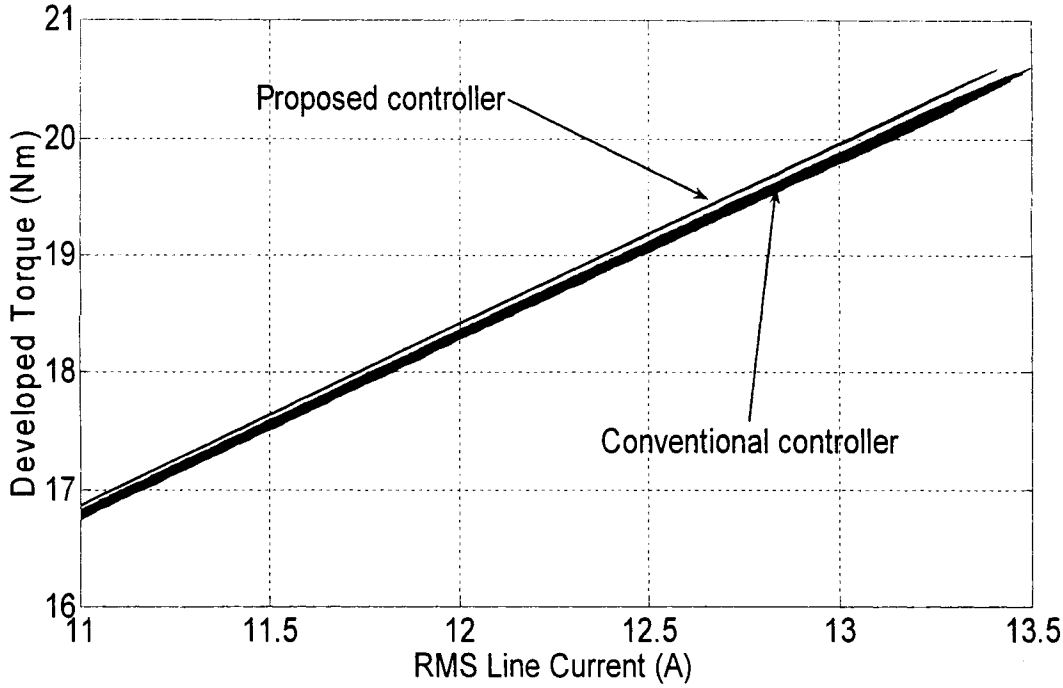

(a)

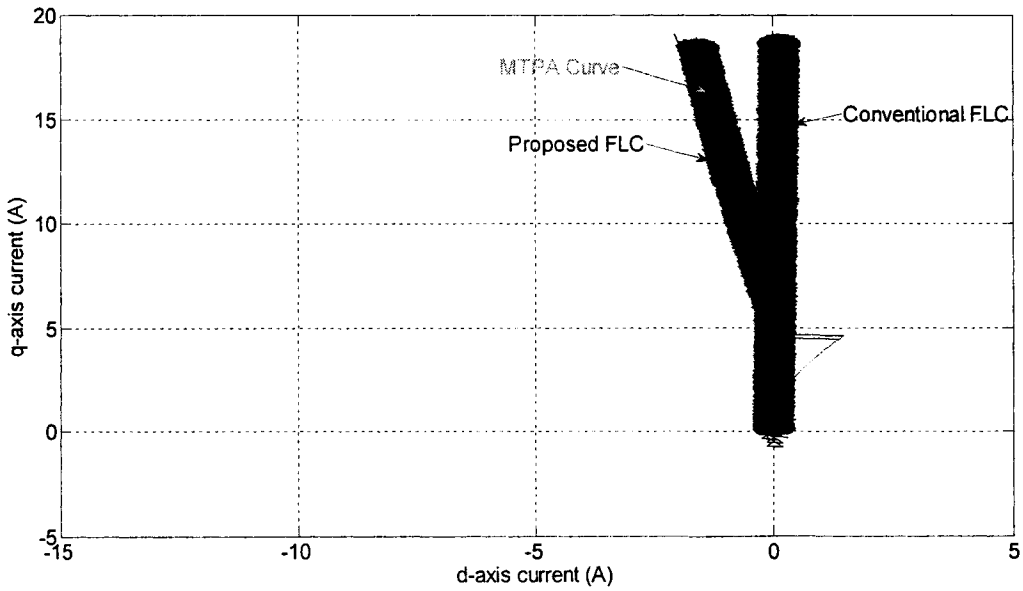

(b)

Fig.5.18: Comparison of proposed FLC with conventional FLC at different load in rated speed; (a) developed torque vs line current (b) q axis current vs d axis current.

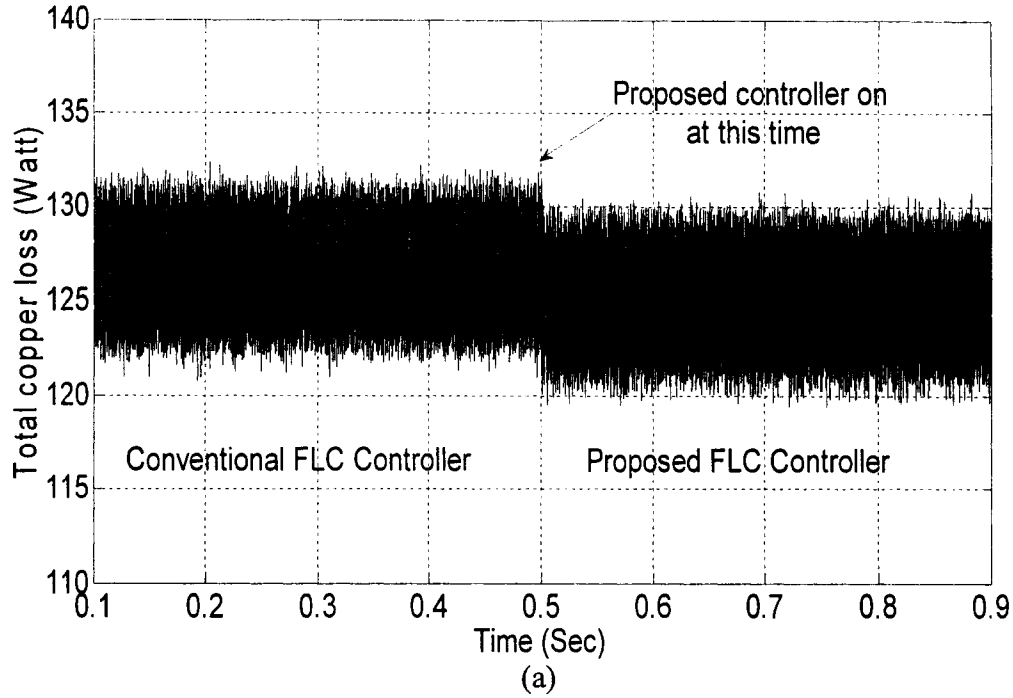

(a)

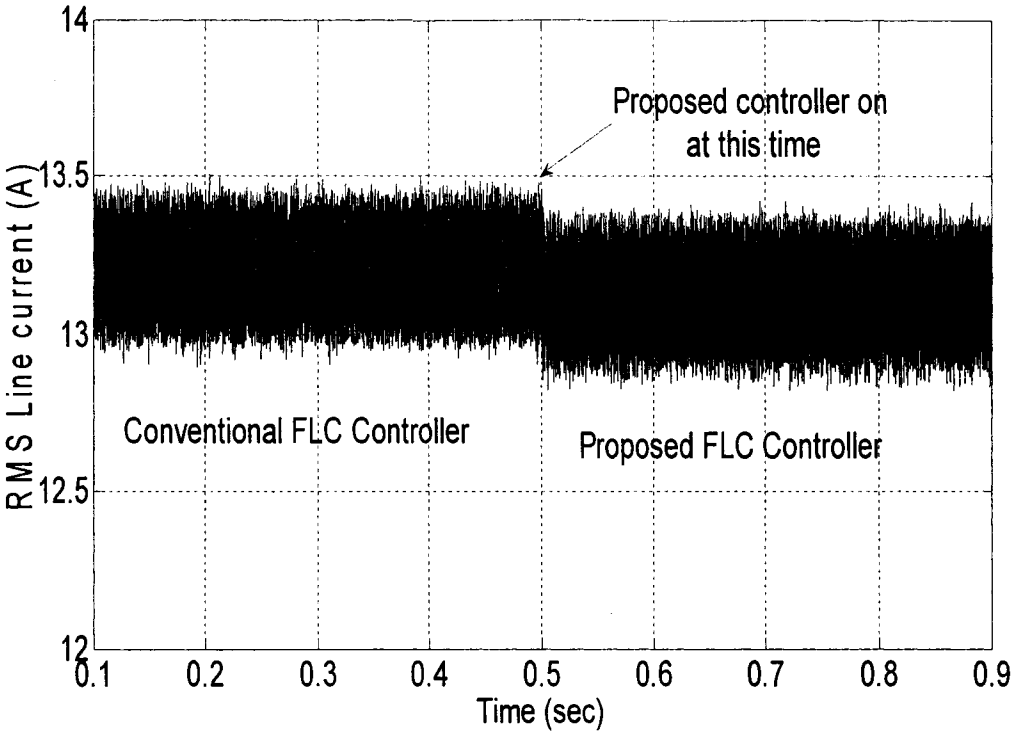

(b)

Fig.5.19: Comparison of proposed FLC with conventional FLC at rated speed with full load; (a) total copper loss (b) line current.

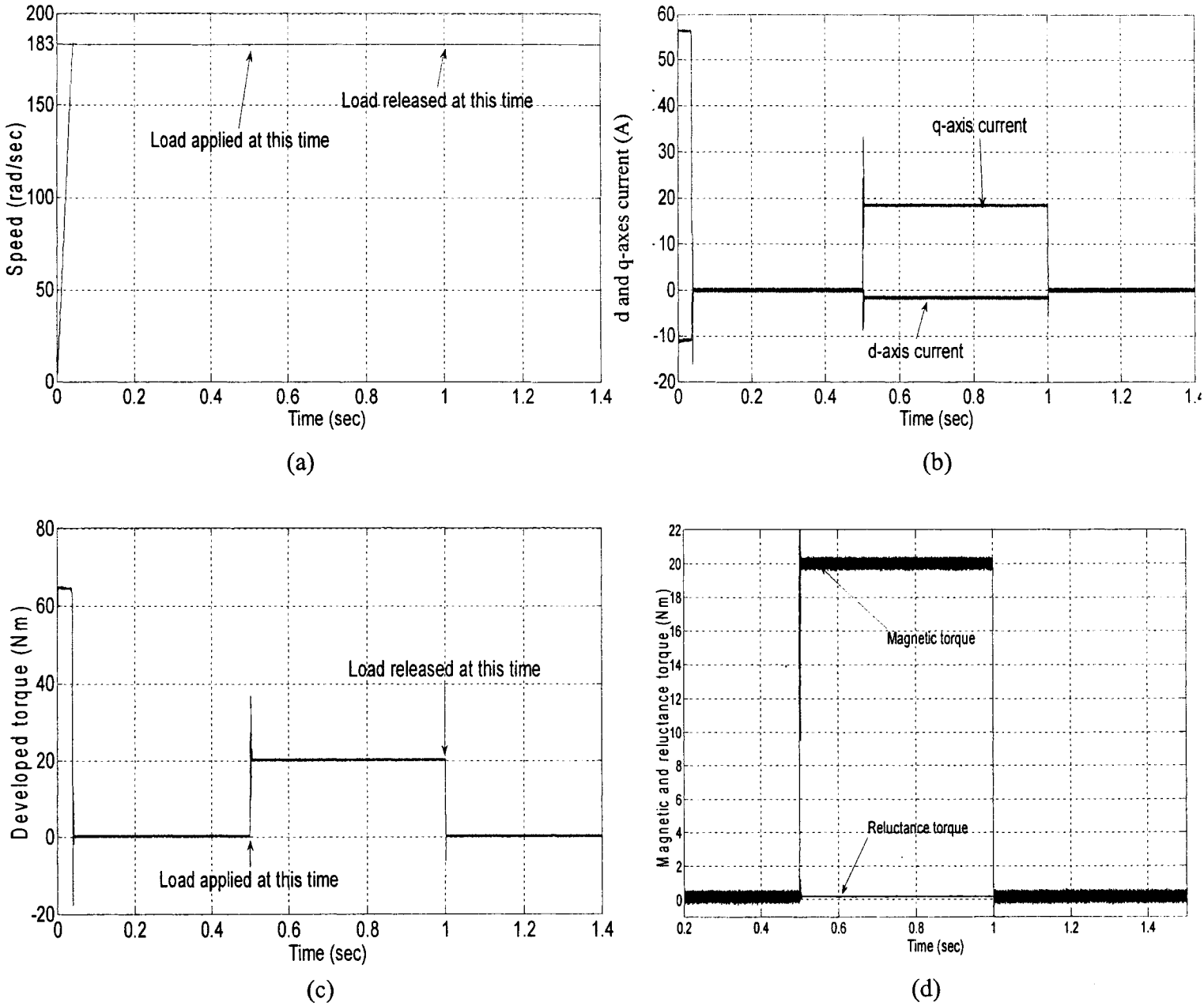

Fig.5.20: Responses of the proposed FLC based IPMSM drive with sudden change of load at rated speed; (a) speed (b) d and q axis current (c) developed torque (d) steady state magnetic and reluctance torque.

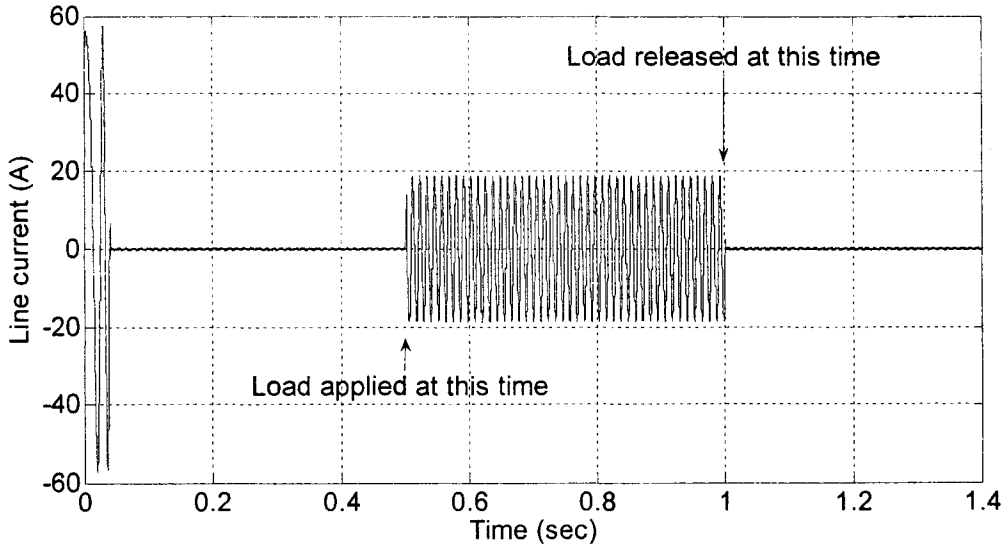

(a)

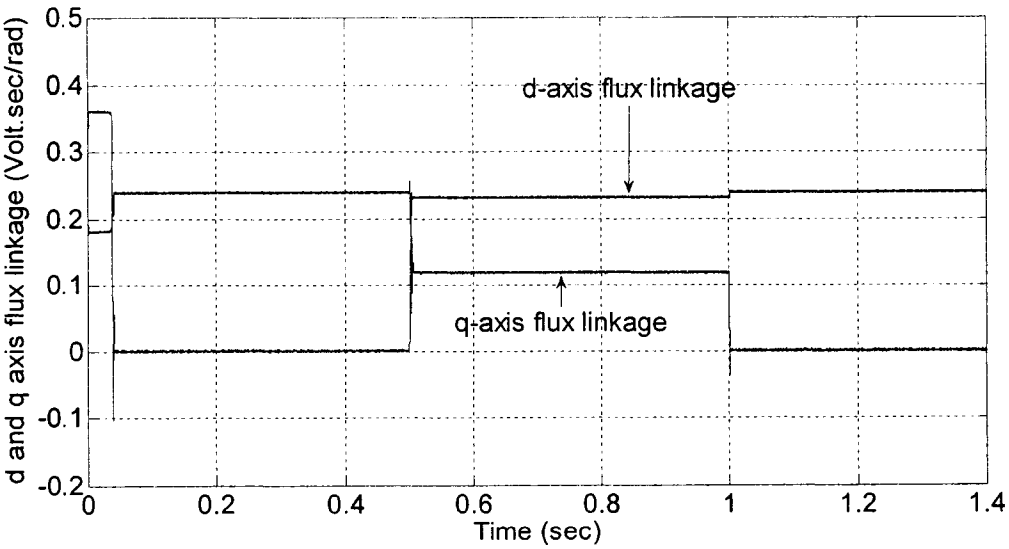

(b)

Fig.5.21: Response of the proposed controller with increase and decrease of load at rated speed; (a) line current (c) d and q axis flux linkage.

speed command from 100rad/sec to 320 rad/sec then step decreases to 30 rad/s at no load is shown in Fig.5.23. It is seen from the Fig.5.23 that the proposed drive can follow the speed command smoothly without any overshoot/undershoot and with zero steady-state error even in the field weakening region. The line current, developed torque, corresponding magnetic and reluctance torque are shown in Figs. 5.23 (b)-(d). In Fig. 5.24 (a), it is observed that d-axis current becomes more negative at high speed above rated speed (183 rad/s) to weaken the field and q-axis current remains same with the change of speed command as the load is fixed. The corresponding d-q axis flux linkages are shown in Fig. 5.24 (b). Figs.5.25 and 5.26 show the speed response of the proposed FLC based IPMSM drive under rated speed and rated load condition with doubled inertia ($J \rightarrow 2J$) and doubled friction constant ($B_m \rightarrow 2B_m$), respectively. It is evident from

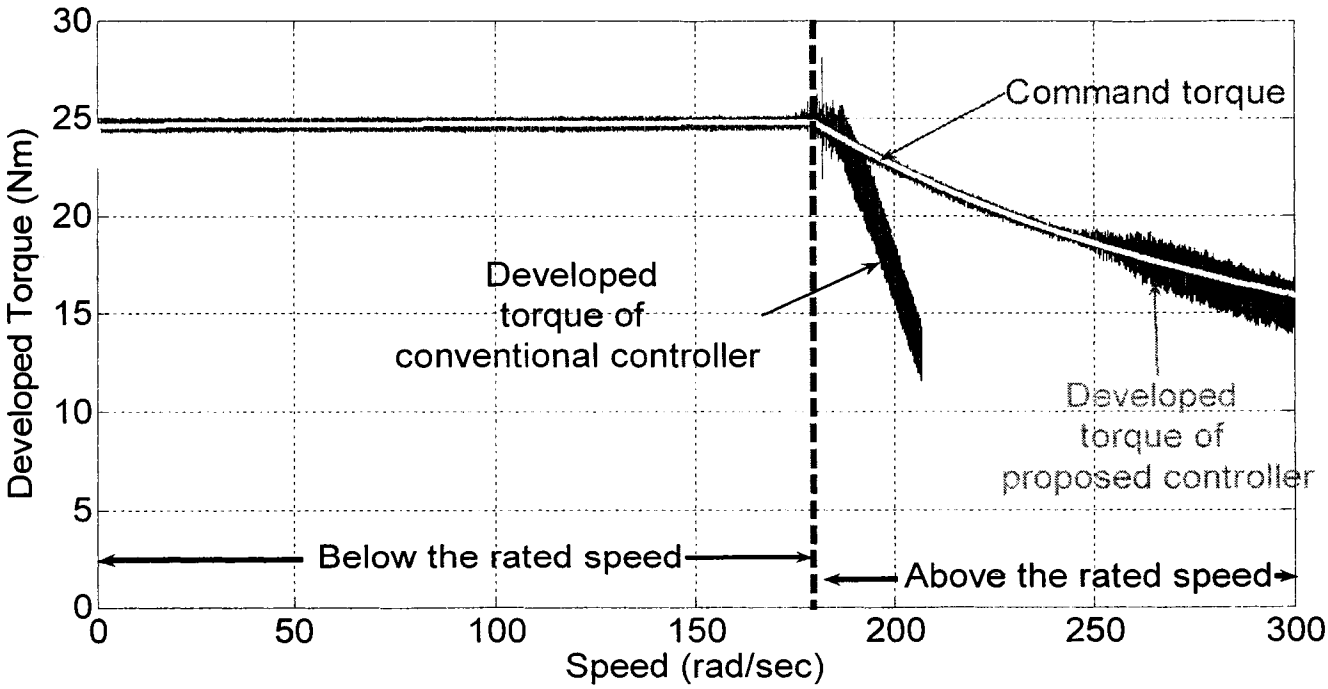

Fig.5.22: Comparison of developed torque between proposed controller and conventional controller in full speed range rated speed with command torque.

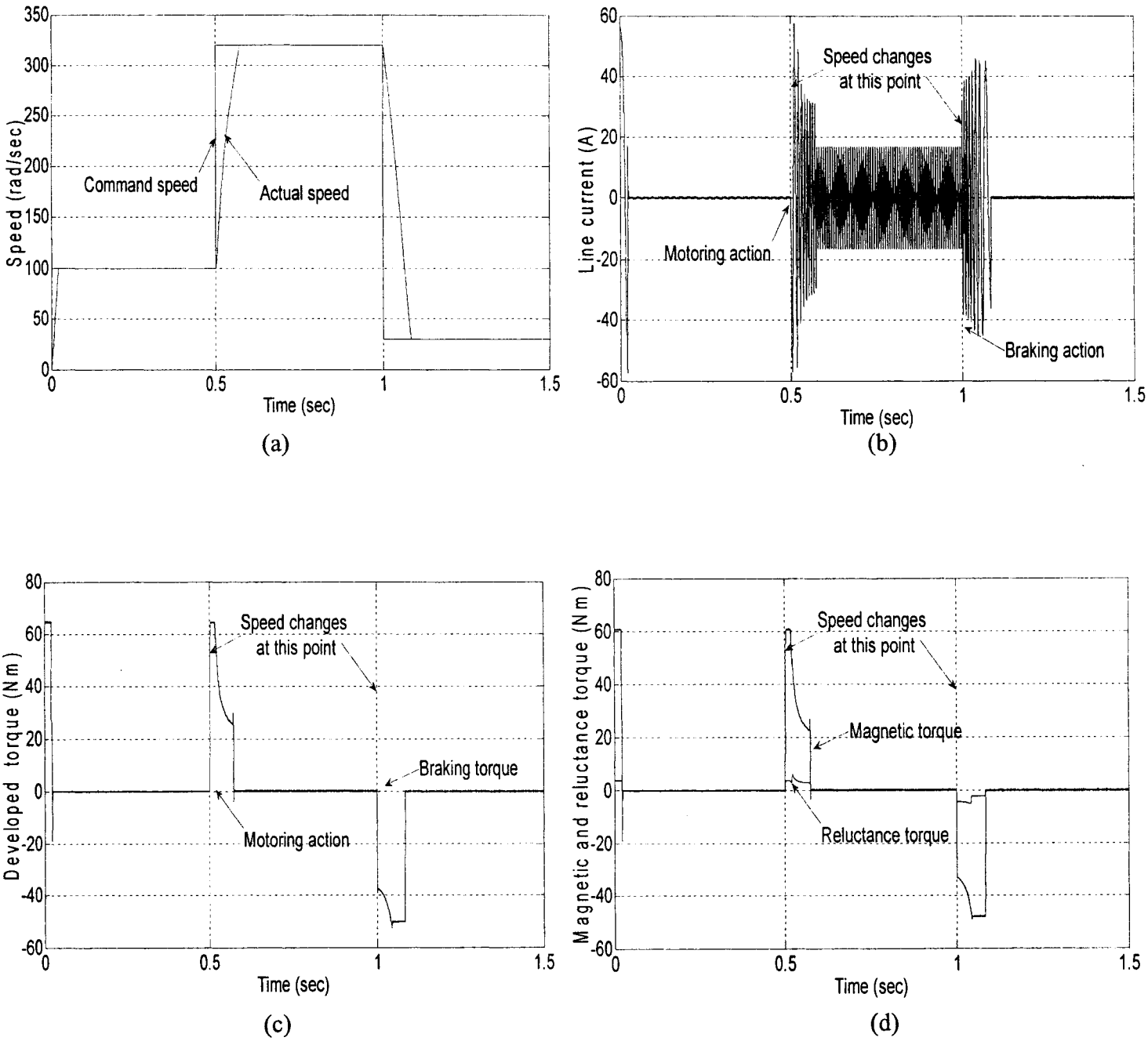

Fig.5.23: Response of the proposed controller with increase and decrease of command speed from 100rad/sec to 320 rad/sec and then to 30 rad/sec at no load; (a) speed (b) line current (c) developed torque (d) magnetic and reluctance torque.

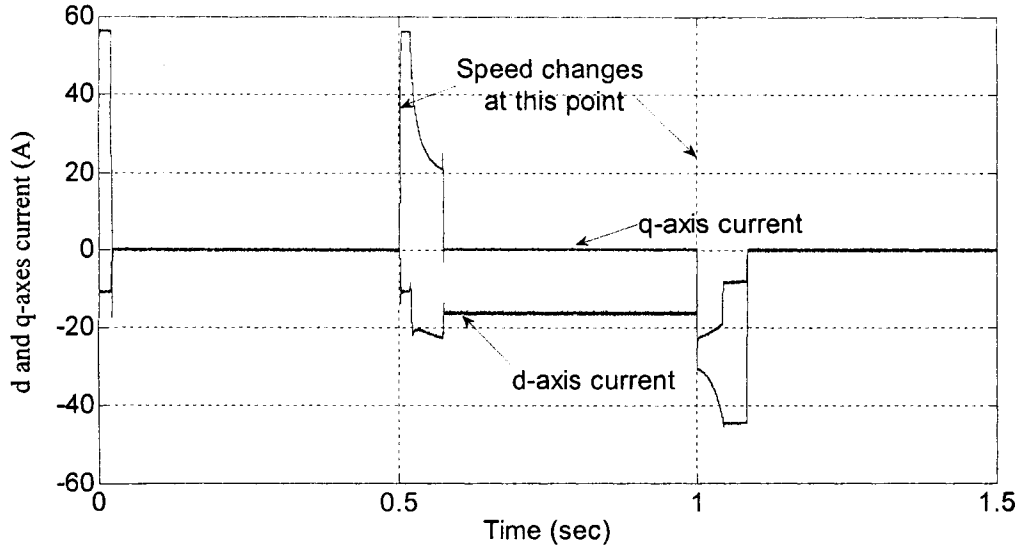

(a)

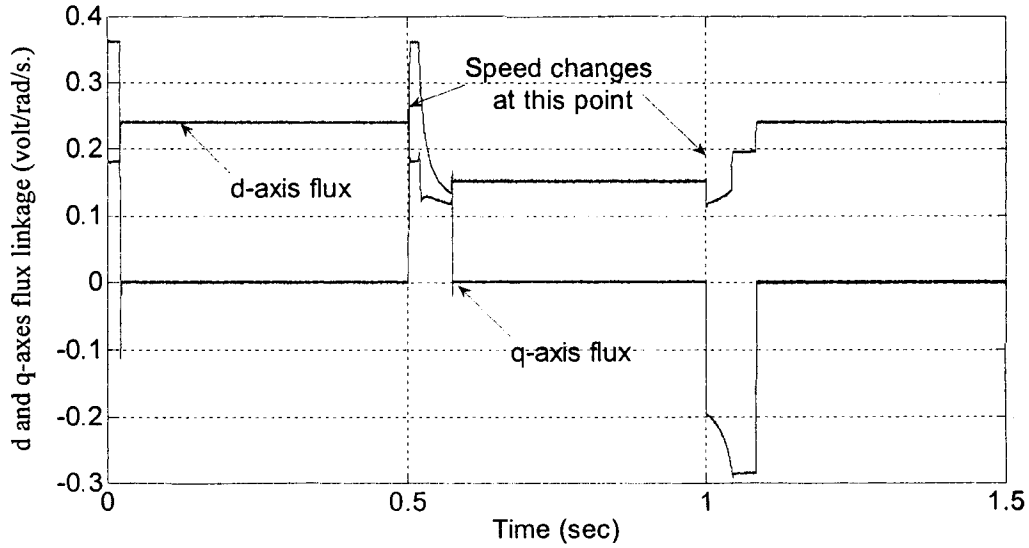

(b)

Fig.5.24: Response of the proposed controller with increase and decrease of command speed from 100rad/sec to 320 rad/sec and then to 30 rad/sec at no load; (a) d and q axis current (b) d and q axis flux linkage.

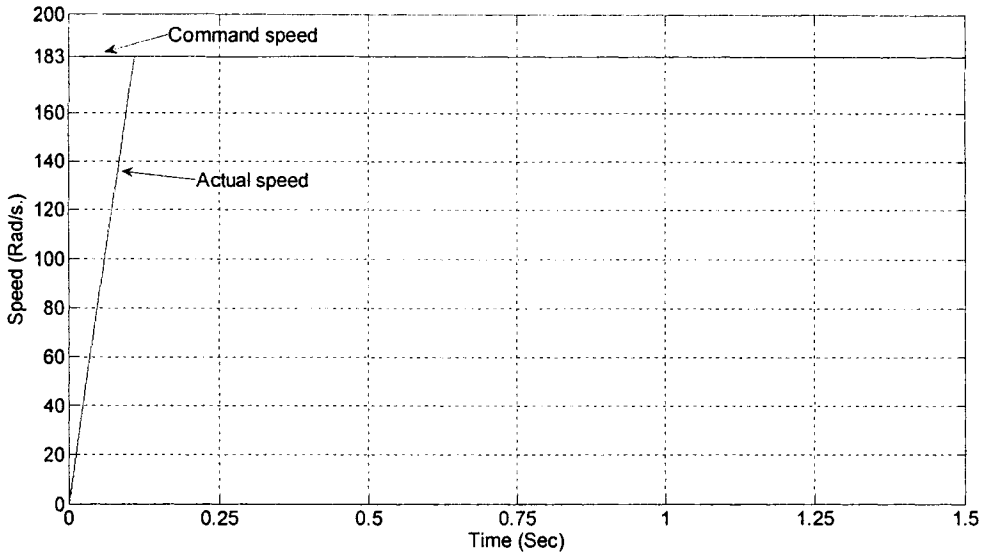

Fig.5.25: Simulated speed response of the proposed IPMSM drive system with doubled inertia (J→2J) under rated speed and load condition.

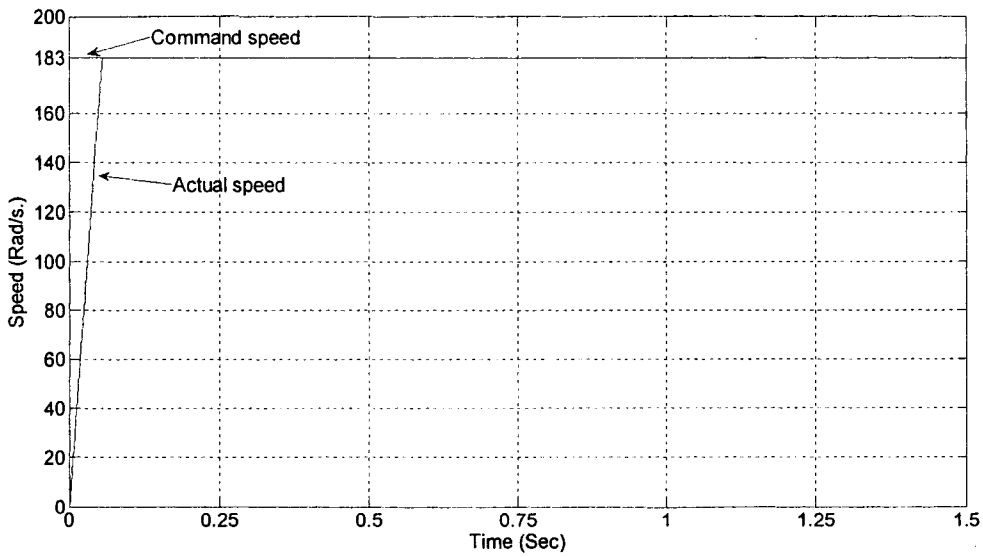

Fig.5.26: Simulated speed response of the proposed IPMSM drive system with doubled friction constant ($B_m \rightarrow 2B_m$) under rated speed and load condition.

Figs.5.25 and 5.26 that the proposed controller based IPMSM drive can follow the command speed with increased inertia and friction constant smoothly without overshoot and steady state error. The summary of the simulation results are presented in the following table:

Operating Condition	Property	Conventional FLC	Proposed FLC
Starting response for a step speed command at rated load	Overshoot	Less than 0.1%	Less than 0.1%
	Settling time	0.09 s	0.06 s
	Starting maximum current	56 A	58 A
Starting response for a step speed command at no load	Overshoot	Less than 1%	Less than 1%
	Settling time	0.05 s	0.03 s
	Starting current	56 A	58 A
Response for a step change of load	Speed deviation	Less than 2%	Less than 2%
	Settling time	0.2 s	0.2 s
	Steady state current at full load	13.3 A	13.2 A
Response at higher than rated speed	Whether follow the command torque or not	Cannot follow	Can follow

5.5 Experimental results

The effectiveness of the proposed IPMSM drive is also investigated extensively with several experiments. The experimental set-up for the proposed drive is the same as described in chapter 4. The flow chart of the software for real-time implementation of the proposed drive is shown in Fig.5.27. For a real-time implementation a real-time Simulink model is developed and then downloaded to the DSP board utilizing dSPACE ControlDesk software. The sampling frequency used in this work is found to be 5 kHz. Sample experimental results are presented below.

The experimental result for a step command speed is shown in Fig.5.28. It is observed from Fig.5.28 (a) that the motor can follow the command speed with reasonable steady state error and no overshoot/undershoot. The corresponding q-axis and d-axis currents are shown in Figs.5.28 (b) and 5.28 (c). The experimental results for step change of load is also investigated and shown in Fig. 5.29. From Fig. 5.29(a) it is found that the speed deviates from the command speed a little bit after the load changes. But it converges to the command speed rapidly. In Fig. 5.29 (b) and (c), the q-axis current increases with increase of load and the d-axis current also changes to utilize the reluctance torque. The speed response for a step change of speed from 100 rad/sec to 250 rad/sec is shown in Fig.5.30. It can be concluded that the motor can follow the command speed very smoothly without any overshoot and reasonable steady state error. The steady state speed error at the rated load and speed is shown in Fig.5.31. It is observed from that figure there is reasonable speed error at steady state condition. From these experimental results it is proved that this is a robust controller at different type of disturbance. The real-time steady state response exhibits some ripple which need further work to improve the performance of the

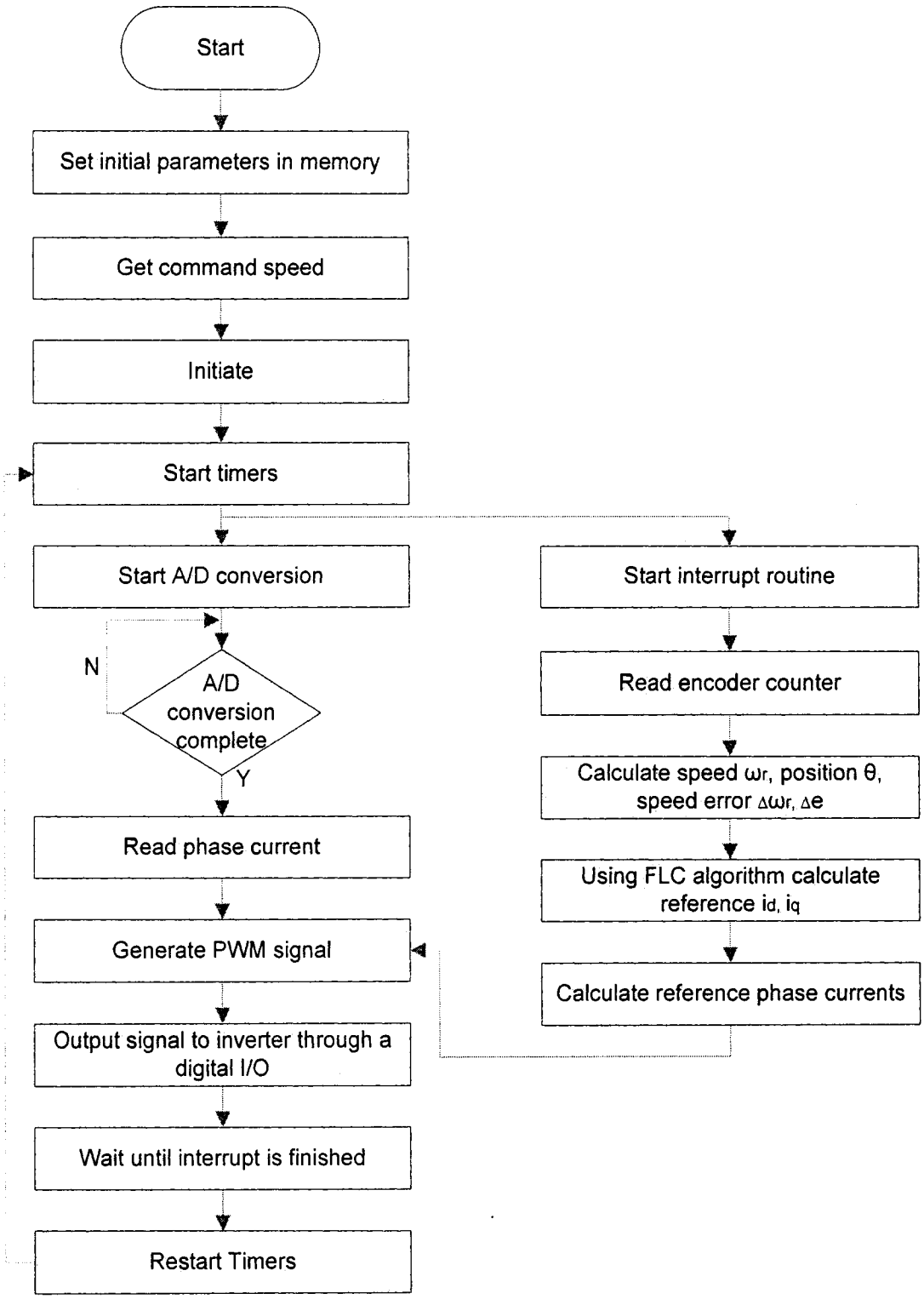

Fig.5.27: Flow chart for real-time implementation of the proposed FLC based IPMSM drive.

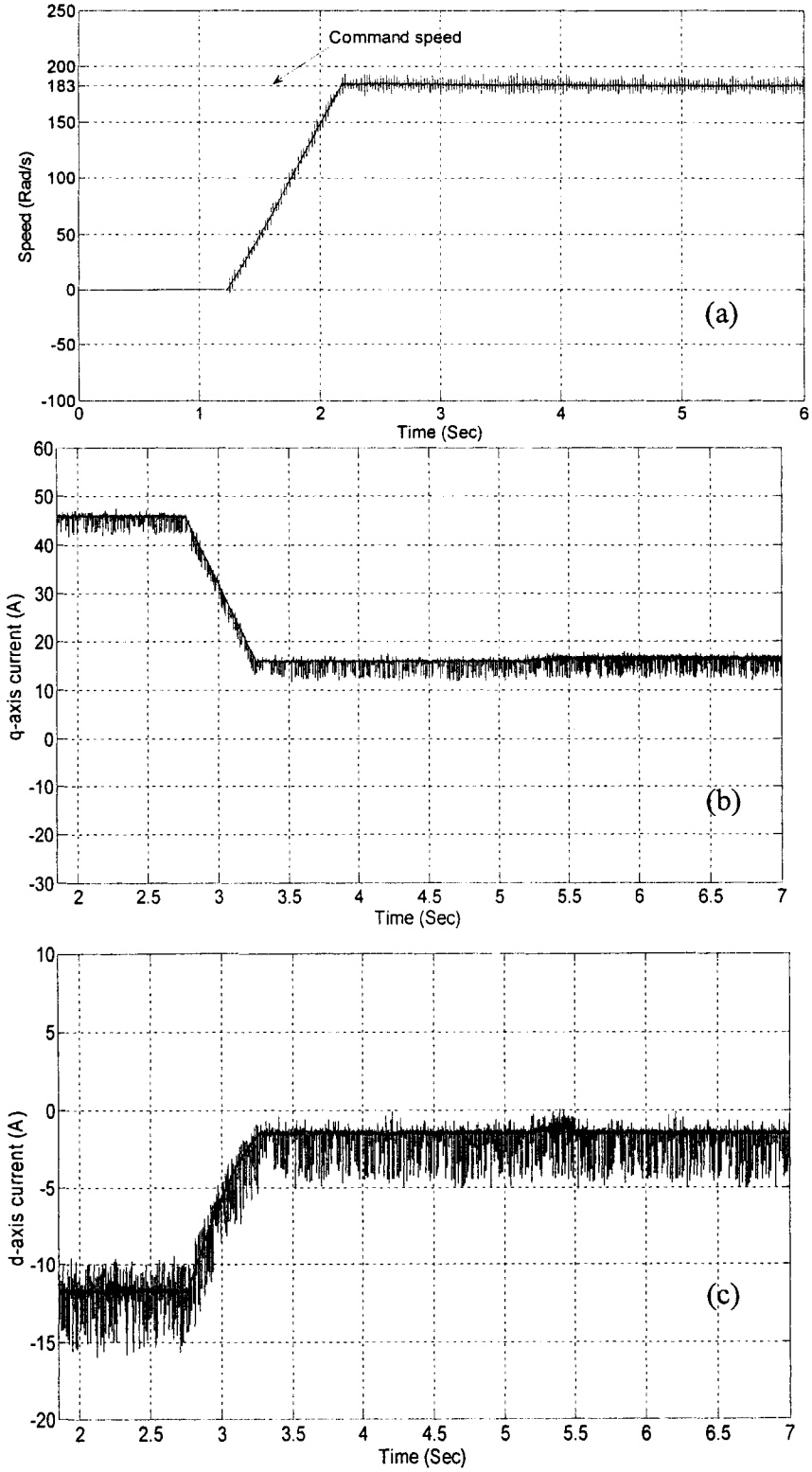

Fig.5.28: Experimental response of the proposed FLC based IPMSM drive for a step command of rated speed (183 rad/s.); (a) speed (b) q-axis current (c) d-axis current.

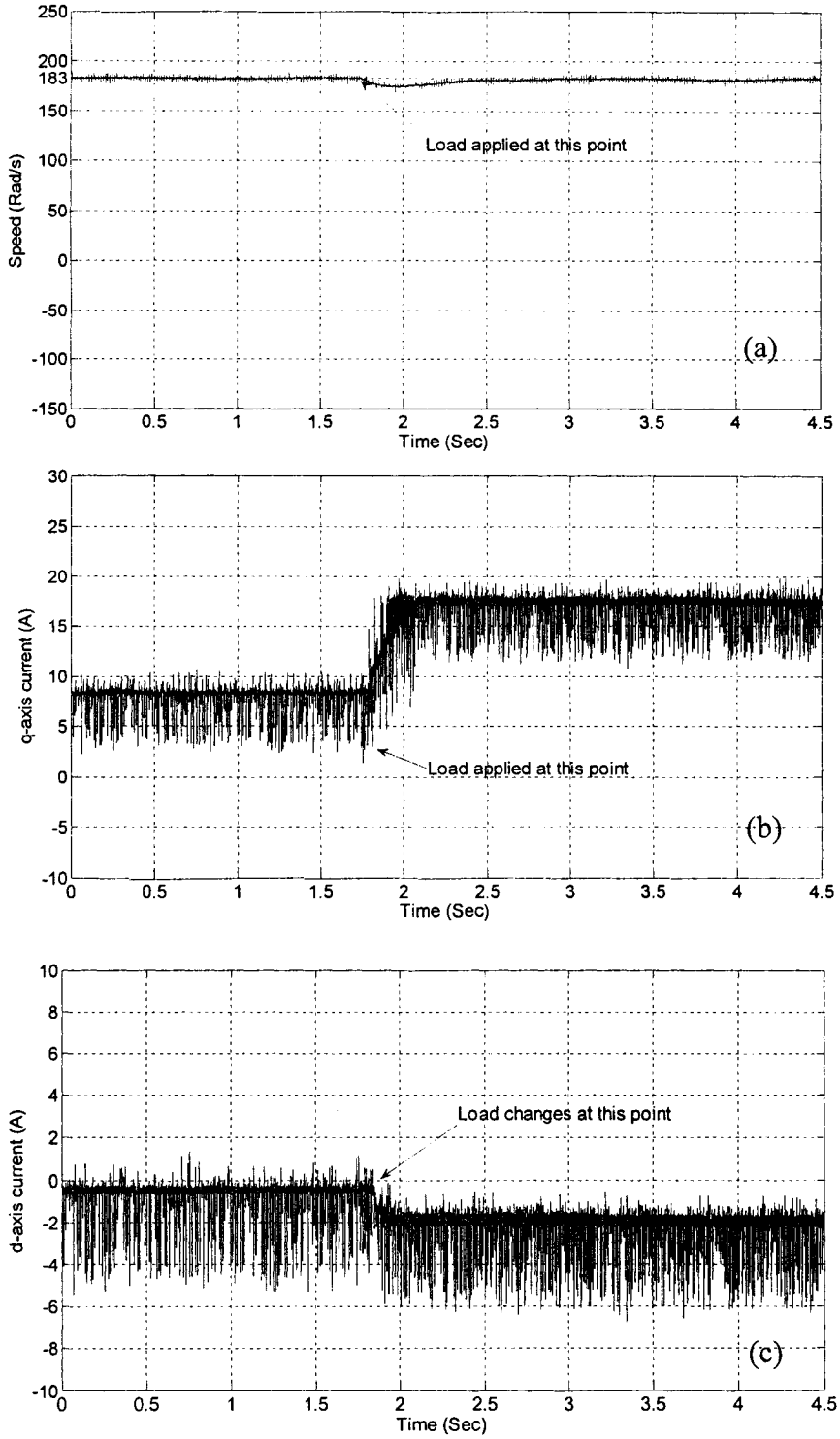

Fig.5.29: Experimental response of the proposed FLC based IPMSM drive for a step increase of load at rated speed (183 rad/s); (a) speed response (b) q-axis current (c) d-axis current.

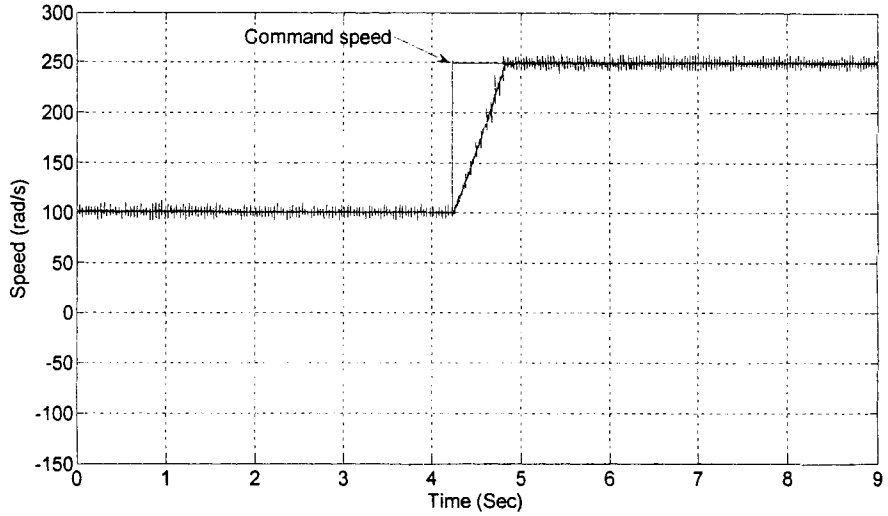

Fig.5.30: Experimental speed response of the proposed FLC based IPMSM drive for for a step change of speed command from 100rad/s to 250 rad/s.

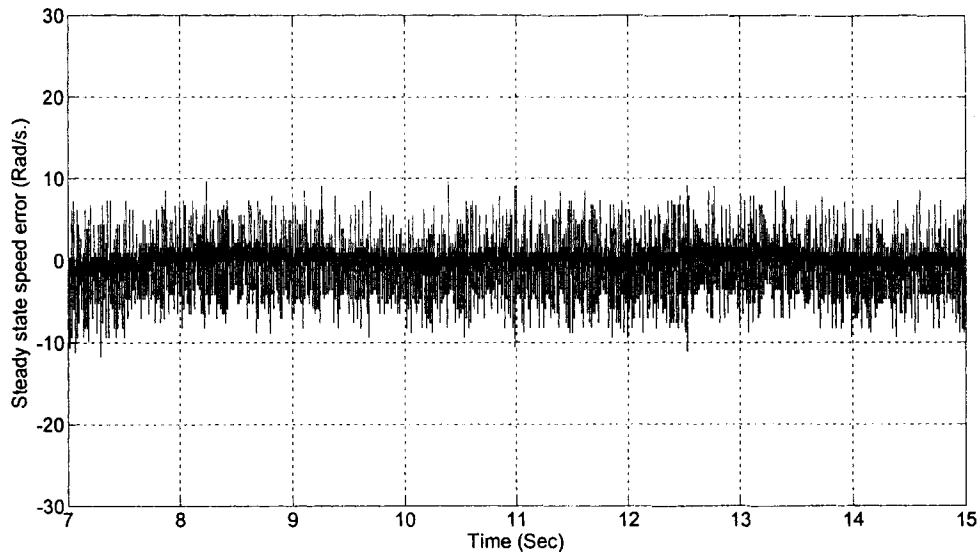

Fig.5.31: Experimental steady state speed error of the proposed FLC controller for a rated command (183 rad/s.) speed at rated load.

proposed FLC. However, due to incorporating flux control the proposed FLC extends the operating speed limit beyond the rated speed significantly as compared to conventional FLC.

5.6 Conclusion

A novel Fuzzy logic based speed control technique has been developed for an IPMSM. In this controller single FLC technique is used for both torque and flux control. The proposed field control scheme incorporates the MTPA operation in constant torque and the FW operation in constant power region. The proposed FLC based speed control through torque and field control of IPMSM drive has been experimentally implemented in real-time using digital signal processor (DSP) board DS1104 for a prototype 5 hp motor. A performance comparison of the proposed FLC based IPMSM drive with the conventional FLC has also been provided. The effectiveness of the proposed drive has been verified both in simulation and experiment at different operating conditions. The proposed FLC controller extends the operating speed limit of the IPMSM drive beyond the rated speed significantly as compared to the conventional FLC.

Chapter 6

A New ANFIS based Neuro-Fuzzy Controller of IPMSM Drive

6.1 Introduction

As mentioned earlier, the designs of intelligent controllers do not need exact mathematical model of the system. Simplicity and less intensive mathematical design requirements are the main features of intelligent controllers, which are suitable to deal with nonlinearities and uncertainties of electric motors [90]. Therefore, the intelligent controllers demand particular attention for high performance nonlinear IPMSM drive systems. However, a simple FLC has a narrow speed operation and needs much more manual adjusting by trial and error if high performance is wanted [90-92]. On the other hand, it is extremely tough to create a serial of training data for ANN that can handle all the operating modes [90-92]. The concept of NFC has emerged in recent years, as researchers have tried to combine the advantages of both FLC and ANN. The NFC

utilizes the transparent, linguistic representation of a fuzzy system with the learning ability of artificial neural networks [55-56, 68]. In [55], a NFC is applied to tune the PI controller parameters for IPMSM drive. Moreover, in those works the centers and weights of the NFC were optimized offline. In most of NFC, large number of membership functions and rules are used for designing the controller, these cause high computational burden for the conventional NFC, which is the major limitation for practical industrial applications. To the best of the author's knowledge no work has been reported on the stand alone online adaptive NFC based speed control of IPMSM drive. In this chapter, a simple online adaptive-network-based fuzzy inference system (ANFIS) is developed for speed control of IPMSM drive. Some of the advantages of ANFIS are very fast convergence due to hybrid learning and the ability to construct reasonably good input membership functions. The most striking feature of ANFIS is that it provides more choices over membership functions. It has tracking and adaptability than the other controllers. An online self tuning algorithm is also developed based on back-propagation technique in order to adjust the precondition and consequent parameters of the ANFIS. In this work a flux control algorithm is incorporated for wide speed range operation of IPMSM.

6.2 Design of proposed NFC

Fuzzy Rule-Based control systems are successfully applied to many different real-world problems recently [90-92]. Unfortunately, relatively few well-structured methodologies are available for designing them and, in many cases human experts are not able to express the knowledge needed to control a system in the form of fuzzy rules.

Takagi-Sugeno-Kang (TSK) fuzzy rule-based control systems were enunciated in defuzzification process [90]. TSK fuzzy rule based control is more accurate. In addition, if they are based on local semantic, the rules have more freedom to improve their performance at the expense of a loss of interpretability which is very useful when the main objective is the accuracy. It requires less computation than mamdani method. It is a linear defuzzification.

The neural fuzzy control systems with TSK fuzzy rules consequents are linear combination of their preconditions. The TSK fuzzy rules are in the following forms:

R^j: IF x_1 is A_1^j AND x_2 is A_2^j AND .....x_i is A_i^j .....AND x_n is A_n^j

$$\text{THEN } y = f_j = a_0^j + a_1^j x_1 + a_2^j x_2 + \ldots\ldots + a_i^j x_i + \ldots\ldots + a_n^j x_n \tag{6.1}$$

where x_i is an input variable, y is the output variable A_i^j are linguistic terms of the precondition part with membership functions $u_{Ai}^j(x_i)$, $a_i^j \in R$ are coefficient of linear equations $f_j(x_1, x_2, \ldots\ldots x_i, \ldots.x_n)$ and j=1,2,3,.....I,...n.

The inferred output

$$y^* = \frac{\mu_1 f_1 + \mu_2 f_2 + \mu_3 f_3 + \ldots\ldots + \mu_j f_j + \ldots\ldots}{\mu_1 + \mu_2 + \mu_3 + \ldots\ldots + \mu_j + \ldots\ldots} \tag{6.2}$$

where μ_j is the firing strength of R^j, j=1,2,3,4,5...

The fuzzy inference system and the corresponding ANFIS based NFC controller architecture is shown in Fig.6.1. Now the controller is designed as follows [93]:

First Layer:

This layer is called input layer. Every node in this layer just passes external signal to the next layer. For simplicity only one input is considered. The input of the proposed NFC is the normalized speed error, which is given by:

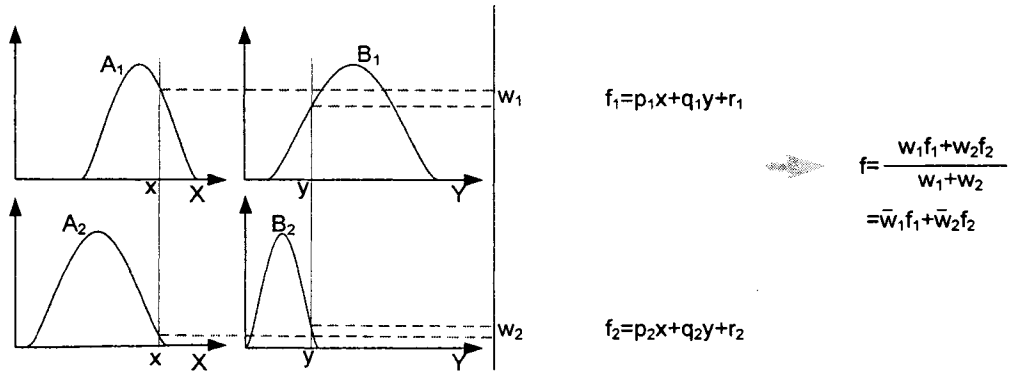

(a)

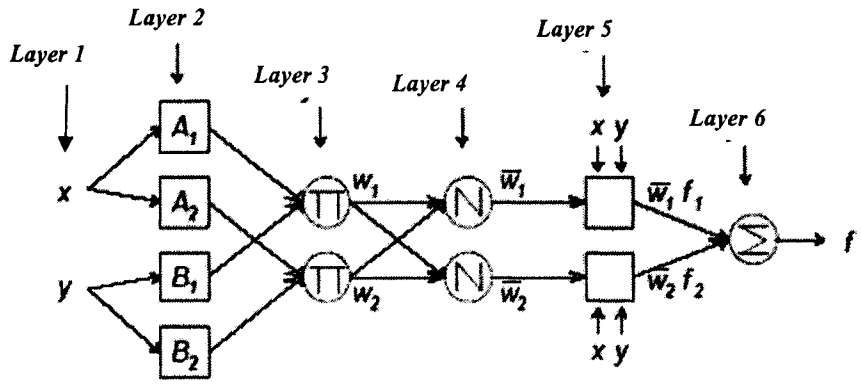

(b)

Fig.6.1: Structure of an ANFIS; (a) A fuzzy inference system (b) Equivalent ANFIS.

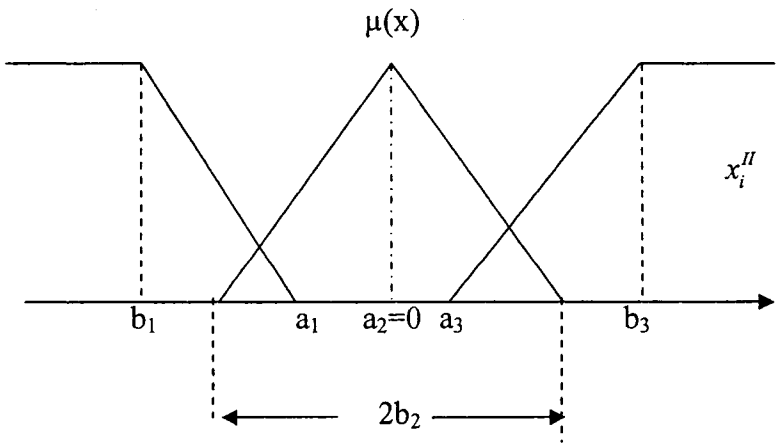

Fig.6.2: Membership functions for input.

$$x = O^{I} = \frac{\omega^{*} - \omega}{\omega^{*}} * 100\% \tag{6.3}$$

where ω is the measured speed, ω^{*} is the command speed, I denotes the 1st layer.

Second Layer:

This layer is called fuzzification Layer. Every node at this layer will act as membership function. Three membership function based fuzzy set is utilized to obtain the fuzzy number for the input. For less computational burden, triangular and trapezoidal functions are chosen as the membership functions for the proposed NFC, as shown in Fig.6.2.

The corresponding node equations are given as:

$$\mu_{A_1}^{1}(x) = \begin{cases} 1 & x \le b_1 \\ \dfrac{x - a_1}{b_1 - a_1} & b_1 < x < a_1 \\ 0 & x \ge a_1 \end{cases}, \tag{6.4}$$

$$\mu_{A_1}^{2}(x) = \begin{cases} 0 & |x| \ge b_2 \\ 1 - \dfrac{x - a_2}{b_2} & |x| < b_2 \end{cases}, \tag{6.5}$$

$$\mu_{A_1}^{3}(x) = \begin{cases} 0 & x \le a_3 \\ \dfrac{x - a_3}{b_3 - a_3} & a_3 < x < b_3 \\ 1 & x \ge b_3 \end{cases}. \tag{6.6}$$

where x is the input of the 2nd layer which is the same as the output of 1st layer. It is considered that a_2=0 in order to further reduce computational burden. Parameters in this layer are referred to as precondition parameters, which need to be tuned based on operating conditions of the motor in real-time.

Third Layer:

This layer is also called rule layer. Every node in this layer multiplies incoming signals and sends the product. The node equations in rule layer are specified as:

$$\mu_j = \mu_{A1}^j(x_1).\mu_{A2}^j(x_2).....\mu_{Ai}^j(x_i).....\mu_{An}^i(x_n) \tag{6.7}$$

But for the proposed controller this layer can be ignored as the number of input is one. So output of the second layer directly passed to the fourth layer.

$$\text{So,} \quad \mu_1 = \mu_{A1}^1(x), \mu_2 = \mu_{A1}^2(x), \mu_3 = \mu_{A1}^3(x), \tag{6.8}$$

Fourth Layer:

Every node in this layer calculates the normalized firing strength of a rule in the proposed controller.

$$\overline{\mu}_1 = \frac{\mu_1}{\mu_1 + \mu_2 + \mu_3}, \overline{\mu}_2 = \frac{\mu_1}{\mu_1 + \mu_2 + \mu_3}, \overline{\mu}_3 = \frac{\mu_1}{\mu_1 + \mu_2 + \mu_3} \tag{6.9}$$

Fifth Layer:

Every node in this layer calculates weighted consequent value $\overline{\mu}_1 f_1, \overline{\mu}_2 f_2, \overline{\mu}_3 f_3$ where f_1, f_2, f_3 are considered as linear consequent functions as,

$$f_1 = a_0^1 + a_1^1 x \tag{6.10a}$$

$$f_2 = a_0^2 + a_1^2 x \tag{6.10b}$$

$$f_3 = a_0^3 + a_1^3 x \tag{6.10c}$$

In order to make the activation functions nonlinear with time, parameters $\{a_0^1, a_1^1, a_0^2, a_1^2, a_0^3, a_1^3\}$ need to be tuned based on operating conditions of the motor. Parameters in this layer are referred to as consequent parameters.

Sixth Layer:

This layer is also called as output layer. This layer sums all the incoming inputs.

$$y = \overline{\mu}_1 f_1 + \overline{\mu}_2 f_2 + \overline{\mu}_3 f_3 \tag{6.11}$$

The output of the ANFIS controller (y) is command q-axis current (i_q^*).

The block diagram of the proposed NFC based IPMSM drive is shown in Fig.6.3.

6.3 On-line self-tuning algorithm

The algorithm of tuning of the consequent parameters can be developed using a reinforcement signal, r, which is equal to the normalized speed error of the IPMSM and is the same as x variable input to the controller. Since it is impossible to determine or calculate desired ANFIS controller output, i_q and find train data off-line covering all operating conditions, a kind of unsupervised on-line self-tuning method is employed in this project. Instead of using desired controller's output i_q as target, reinforcement signal is utilized to generate control action to produce the desired speed response. The controller's task is to minimize the objective function as defined by,

$$E = \frac{1}{2}r^2 = \frac{1}{2}\left(\omega^* - \omega\right)^2 \tag{6.12}$$

(a) Tuning of precondition parameters:

Hence, the learning rules can be derived as follows:

$$a_i(n+1) = a_i(n) - \eta_{a_i}\frac{\partial E}{\partial a_i}, \tag{6.13a}$$

$$b_i(n+1) = b_i(n) - \eta_{b_i}\frac{\partial E}{\partial b_i}, \tag{6.13b}$$

where η_{a_i}, η_{b_i} are the learning rate of the corresponding parameters. The derivatives can be found by chain rule as:

$$\frac{\partial E}{\partial a_i} = \frac{\partial E}{\partial r}\frac{\partial r}{\partial \omega}\frac{\partial \omega}{\partial y}\frac{\partial y}{\partial \mu_{A1}^i}\frac{\partial \mu_{A1}^i}{\partial a_i}, \tag{6.14a}$$

$$\frac{\partial E}{\partial b_i} = \frac{\partial E}{\partial r}\frac{\partial r}{\partial \omega}\frac{\partial \omega}{\partial y}\frac{\partial y}{\partial \mu_{A1}^i}\frac{\partial \mu_{A1}^i}{\partial b_i}, \tag{6.14b}$$

where y is the output of the ANFIS based NFC which is i_q^* for the proposed controller. The common parts of equations (6.14) are:

$$\frac{\partial E}{\partial r} = r = \omega^* - \omega, \tag{6.15}$$

$$\frac{\partial r}{\partial \omega} = -1, \tag{6.16}$$

$$\frac{\partial \omega}{\partial y} = J. \tag{6.17}$$

where J is Jacobian matrix of the system [52]. System Jacobian matrix can not easily found directly. For field oriented control, the PMSM system can be viewed as a single input single output system and then the Jacobian matrix can be estimated as a constant positive value. Considering that the effect of J is included in tuning rate parameter, the update rules can be determined from (6.12)-(6.17), as follows,

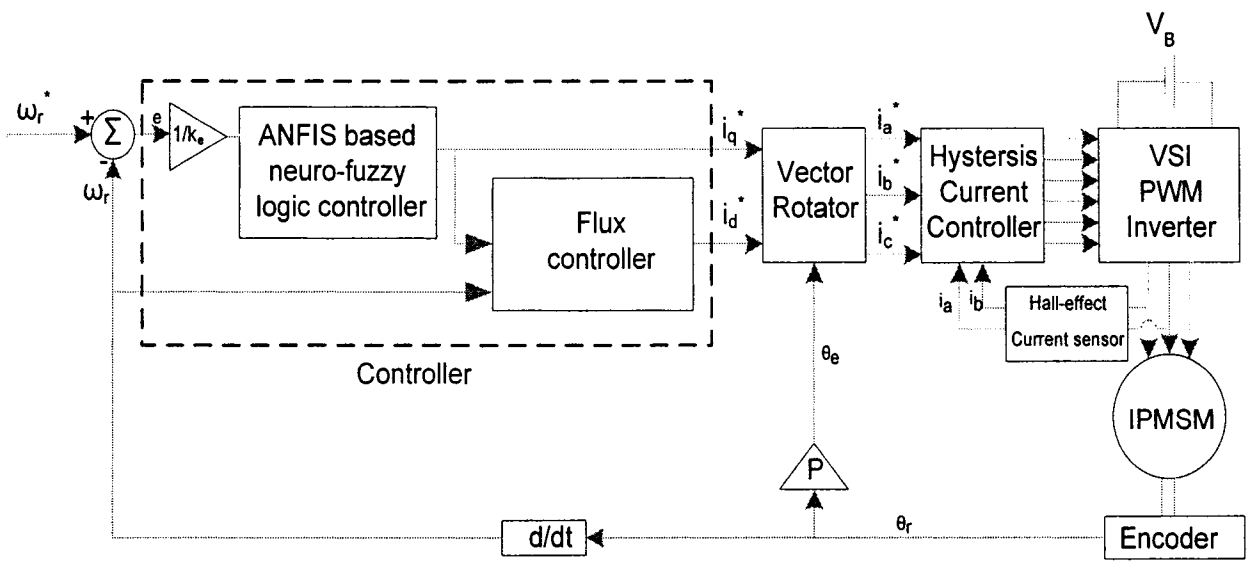

Fig.6.3: Block diagram of the proposed ABFC based IPMSM drive.

$$a_1(n+1) = a_1(n) - \eta_{a_1} r(n) \frac{f_1(n)}{\sum \mu_{A1}^i(n)} \frac{1-\mu_{A1}^1(n)}{b_1(n)-a_1(n)}, \tag{6.18a}$$

$$b_1(n+1) = b_1(n) - \eta_{b_1} r(n) \frac{f_1(n)}{\sum \mu_{A1}^i} \frac{\mu_{A1}^1(n)}{b_1(n)-a_1(n)}, \tag{6.18b}$$

$$b_2(n+1) = b_2(n) + \eta_{b2} r(n) \frac{f_2(n)}{\sum \mu_{A1}^i} \frac{1-\mu_{A1}^2(n)}{b_2(n)}, \tag{6.18c}$$

$$a_3(n+1) = a_3(n) - \eta_{a_3} r(n) \frac{f_3(n)}{\sum \mu_{A1}^i} \frac{1-\mu_{A1}^3(n)}{b_3(n)-a_3(n)}, \tag{6.18d}$$

$$b_3(n+1) = b_3(n) - \eta_{b_3} r(n) \frac{f_3(n)}{\sum \mu_{A1}^i} \frac{\mu_{A1}^3(n)}{b_3(n)-a_3(n)}. \tag{6.18e}$$

Based on these update rules, the parameters of a_1, a_3, b_1, b_2, b_3 can be tuned.

(b) Tuning of consequent parameters:

To tune the consequent parameters following updated laws are developed,

$$a_0^i(n+1) = a_0^i(n) - \eta_{a_0^i} \frac{\partial E}{\partial a_0^i}, \tag{6.19a}$$

$$a_1^i(n+1) = a_1^i(n) - \eta_{a_1^i} \frac{\partial E}{\partial a_1^i} \tag{6.19b}$$

where $\eta_{a_0^i}, \eta_{a_1^i}$ are the learning rates of the corresponding parameters. In a similar way of precondition parameters adjustment discussed earlier, the derivatives can be found by chain rule as:

$$\frac{\partial E}{\partial a_0^i} = \frac{\partial E}{\partial r}\frac{\partial r}{\partial \omega}\frac{\partial \omega}{\partial y}\frac{\partial y}{\partial a_0^i}, \tag{6.20a}$$

$$\frac{\partial E}{\partial a_1^i} = \frac{\partial E}{\partial r}\frac{\partial r}{\partial \omega}\frac{\partial \omega}{\partial y}\frac{\partial y}{\partial a_1^i}, \tag{6.20b}$$

Using equation (6.10)-(6.11),

$$\frac{\partial y}{\partial a_0^1} = \frac{\mu_1}{\mu_1+\mu_2+\mu_3}, \frac{\partial y}{\partial a_0^2} = \frac{\mu_2}{\mu_1+\mu_2+\mu_3}, \frac{\partial y}{\partial a_0^3} = \frac{\mu_3}{\mu_1+\mu_2+\mu_3} \tag{6.21a}$$

$$\frac{\partial y}{\partial a_1^1} = \frac{\mu_1 x_1}{\mu_1 + \mu_2 + \mu_3}, \frac{\partial y}{\partial a_1^2} = \frac{\mu_2 x_1}{\mu_1 + \mu_2 + \mu_3}, \frac{\partial y}{\partial a_1^3} = \frac{\mu_3 x_1}{\mu_1 + \mu_2 + \mu_3} \tag{6.21b}$$

The update laws for tuning consequent parameters can be obtained from equation (6.12), equations (6.15)-(6.17) and equation (6.19)-(6.21) are:

$$a_0^i(n+1) = a_0^i(n) + \eta_{a_0^i} r(n) \frac{\mu_i}{\mu_1 + \mu_2 + \mu_3} \tag{6.22a}$$

$$a_1^i(n+1) = a_1^i(n) + \eta_{a_1^i} r(n) \frac{\mu_i x}{\mu_1 + \mu_2 + \mu_3} \tag{6.22b}$$

So the overall tuning method can be described as [93]:

Step 1: An initial setting of fuzzy logic rules and initial values of a_1, a_3, b_1, b_2, b_3 and $\{a_0^1, a_1^1, a_0^2, a_1^2, a_0^3, a_1^3\}$ are selected.

Step 2: The normalized speed error is calculated, which is input to the controller.

Step 3: Fuzzy reasoning is performed for the normalized speed error data input using (6.1)-(6.12). The membership values are calculated for the input speed error by using (6.4)-(6.6) and output fuzzy reasoning y is calculated.

Step 4: Tuning of the a_1, a_3, b_1, b_2 and b_3 is done by substituting the measured reinforcement signal r, the membership value μ_{A1}^i and consequent value f_i into (6.18).

Step 5: Fuzzy reasoning is repeated as in step 3.

Step 6: Tune the consequent parameters $\{a_0^1, a_1^1, a_0^2, a_1^2, a_0^3, a_1^3\}$ using (6.22) by substituting the input normalized speed error data (x), measured reinforcement signal r, and calculated firing strength of rules from membership functions.

Step 7: Repeat from step 3.

6.4 Flux controller design

In order to operate the motor over wide speed range and to get the optimum performance, one can control the flux as already discussed in chapter 2. As mentioned earlier, the flux control algorithm can be categorized into three parts. If the motor speed is less than rated speed then MTPA technique is used as (2.31). If the speed is above the rated speed but below the critical speed (ω_{rc}) and the voltage constraint (2.37) is satisfied then MTPA technique is used as (2.31). If the speed is above the rated speed but below the critical speed (ω_{rc}) but the voltage constraint (2.37) is not satisfied then the field will

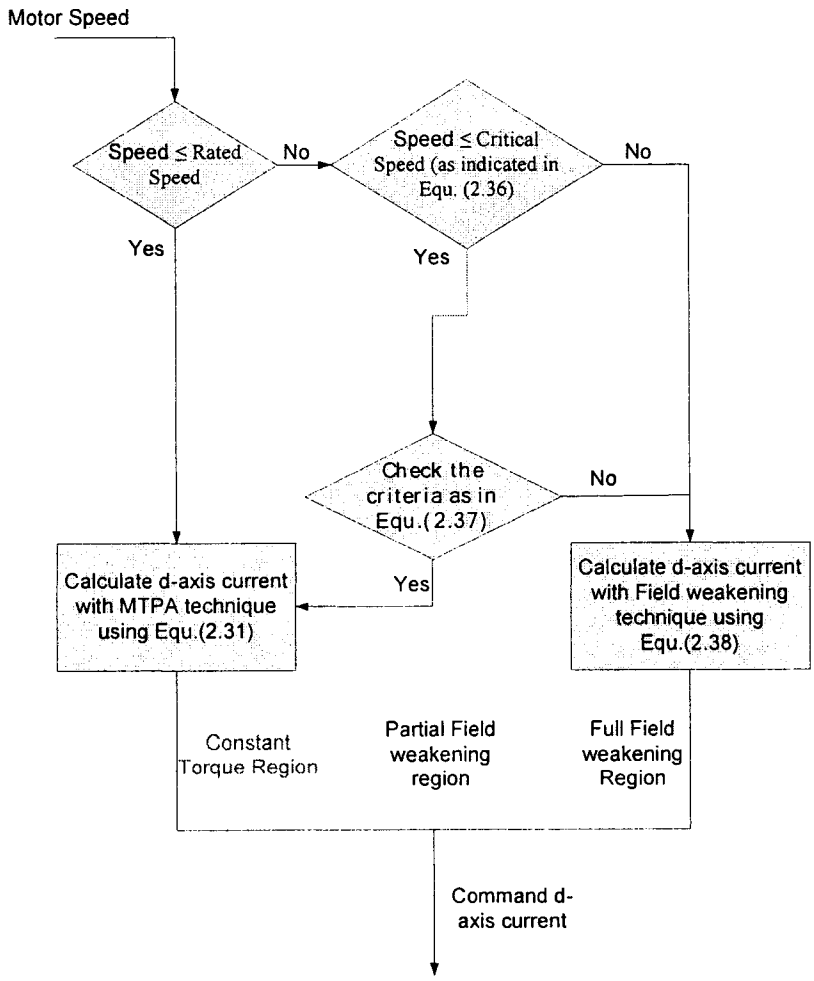

Fig.6.4: Flux component of current control algorithm.

be weakened as per (2.38). Above the critical speed field weakening technique will be applied as per (2.38). The flux control algorithms mentioned earlier can be summarized in the flow chart given in Fig. 6.4.

6.5 Simulation results

The effectiveness of the proposed simplified ANFIS based IPMSM drive is investigated extensively at first in simulation. Simulation model is developed using Matlab/Simulink. The simulation model is shown in Fig.6.5. The initial values of precondition and consequent parameters used in the simulation model are a_1=0, a_3=0, b_1=-0.5, b_2=0.001, b_3=-0.5 and $a_0^1 = 0, a_1^1 = 3, a_0^2 = 0, a_1^2 = 3, a_0^3 = 0, a_1^3 = 3$. The values of tuning rate of precondition and consequent parameters are 3e-7 and 0.05 respectively. The details of the model are shown in Appendix B. Sample results are presented below.

Fig.6.6 shows the simulated starting speed and current response of the proposed ANFIS based NFC for IPMSM drive at full load. It is shown from this figure that the performance for the proposed controller is fast and smooth. It is also seen that the drive can follow the command speed without overshoot or undershoot. The corresponding total developed torque as well as magnetic and reluctance torque are shown in Fig. 6.7 (a) and (b), respectively. It shows that the reluctance torque due to nonzero d-axis current contribute a part to the total developed by the drive. The trajectory of stator q-axis current and d-axis current is shown in Fig.6.7(c). The trajectories are bounded by a circle which indicates the stability of the drive. Fig. 6.8(a) shows the speed response of the proposed controller and drive system for a step change in reference speed from 0 rad/sec to 183 rad/sec at no load. The actual speed converges with the reference speed in a very short

time with minimal overshoot and no steady state error. The corresponding d-q axis motor currents, the magnetic torque, reluctance torque and line current are shown in Figs 6.8(b), (c), (d), respectively. The effectiveness of the proposed drive is also tested for a step increase in load from no load to full load at rated command speed in Fig. 6.9. With the increase of load the q axis current increases and d axis current decreases to maintain MTPA as shown in Fig. 6.9(b), while the speed response is almost insensitive as shown in Fig.6.9(a). The corresponding total developed torque, magnetic and reluctance component of the torque are shown in Fig.6.9(c) and (d), respectively. The effect in line current and d-q axes flux linkage are shown in Fig.6.10(a) and (b), respectively. The responses of the proposed NFC based IPMSM drive for step changes of command speed from 100rad/sec to 350 rad/sec and then to 50 rad/sec at no load are shown in Fig. 6.11. From the Fig.6.11(a), it is observed that the motor can follow the command speed over a wide speed range almost without any overshoot/undershoot and with zero steady-state error. The d-q axes current are shown in Fig.6.11(b). When the motor speed increases from 100 rad/s to 350 rad/s, the d-axis was determined by MTPA up to the rated speed in transient state, then it moves to field weakening technique. Magnetic and reluctance torque as well as total developed torque is shown in Figs 6.12(a) and (b). From these results it is observed that reluctance torque contributes to total torque. The simulated d-q axis current vector trajectories for different speed regions are shown in Figs.6.13 - 6.15, which validate the flux control algorithms shown in section 6.5. In Fig.6.13, the vector trajectories outside current circle represent the starting transient current which follows MTPA curve. From this figure it is observed that at rated speed the drive can follow MTPA technique at different load condition. In Fig.6.14, the vector trajectories outside

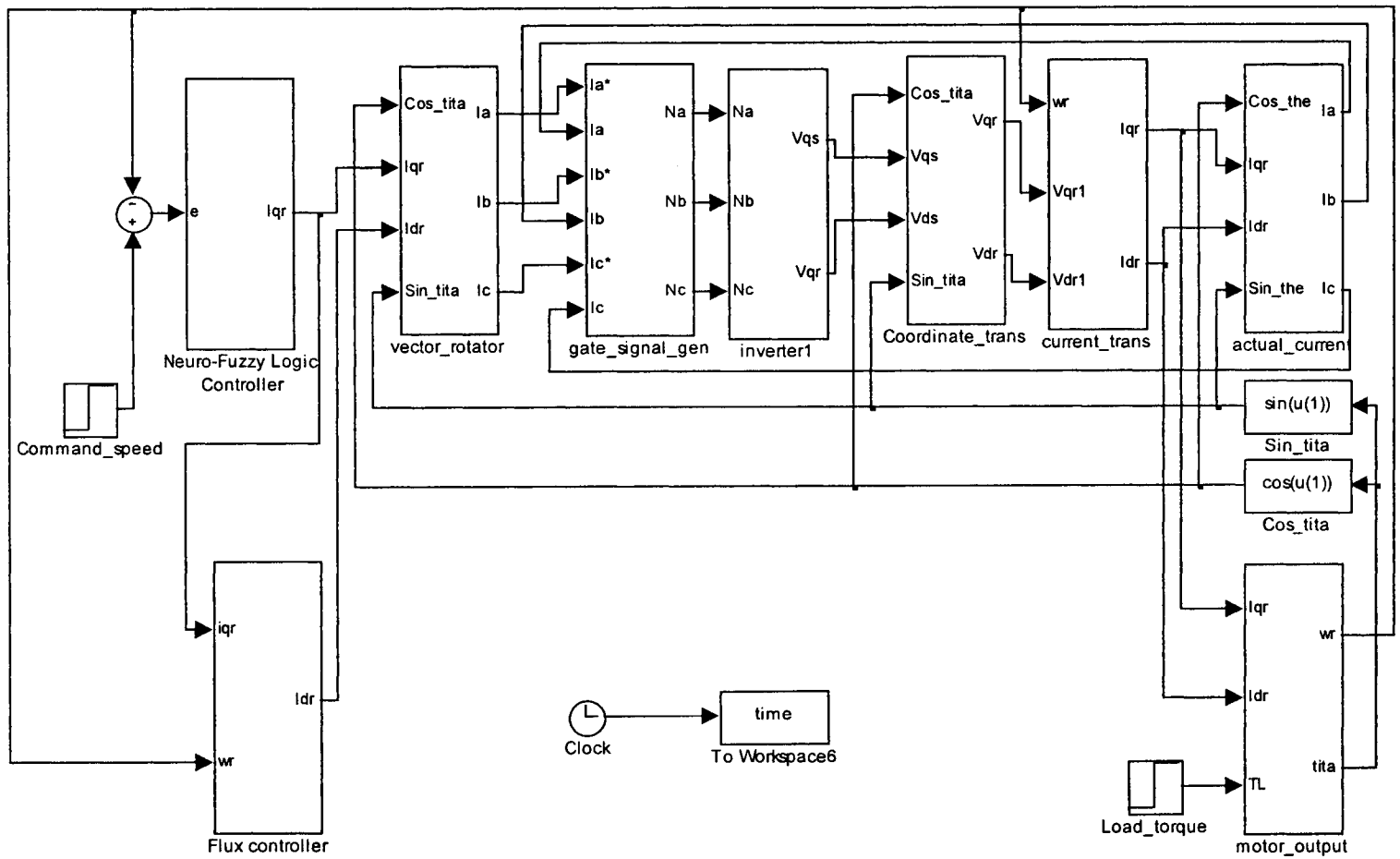

Fig.6.5: Simulink schematic of the complete ANFIS based NFC drive for IPMSM.

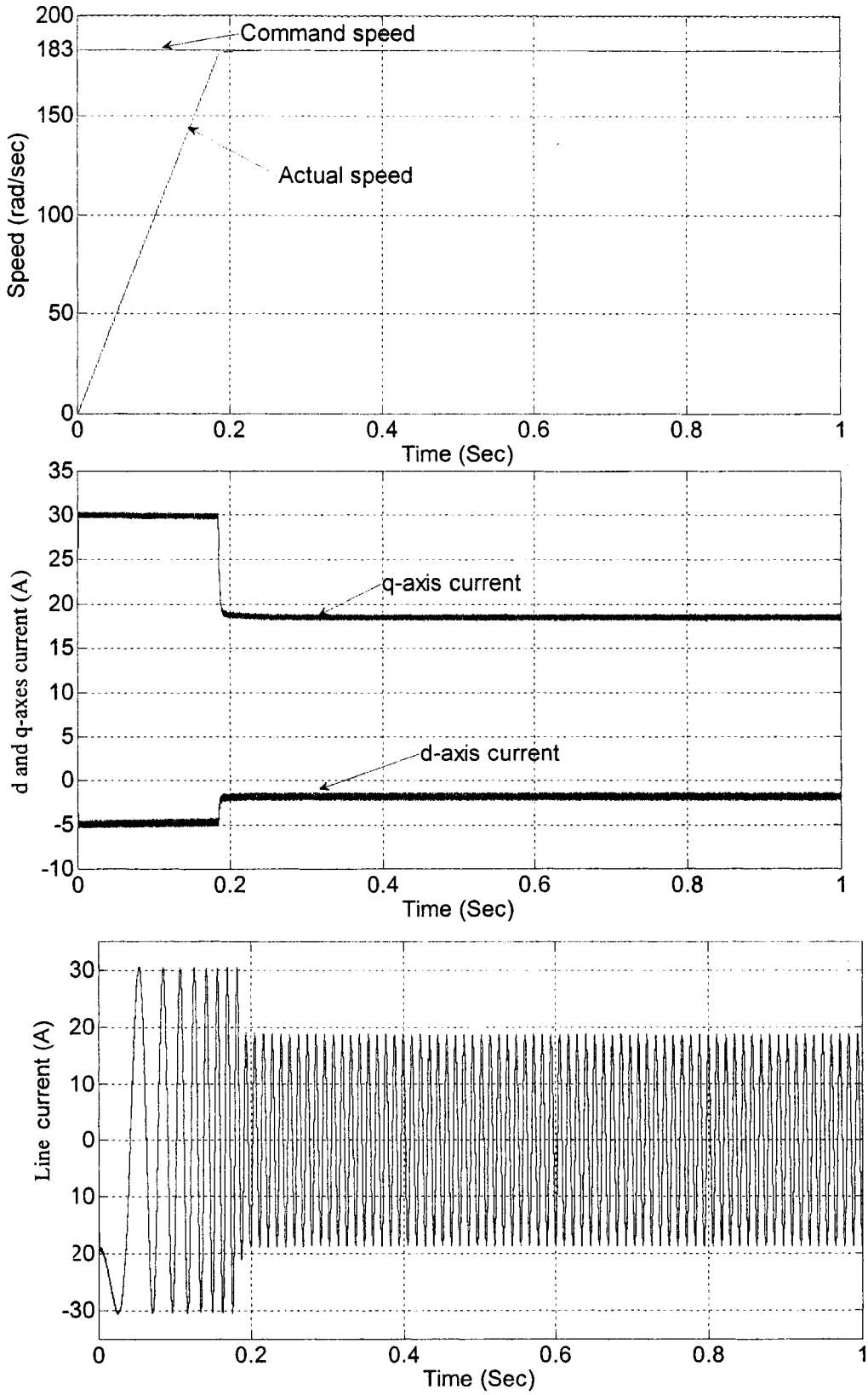

Fig.6.6: Starting response with full load for a step command of rated speed; (a) speed (b) d-q axis current (c) line current.

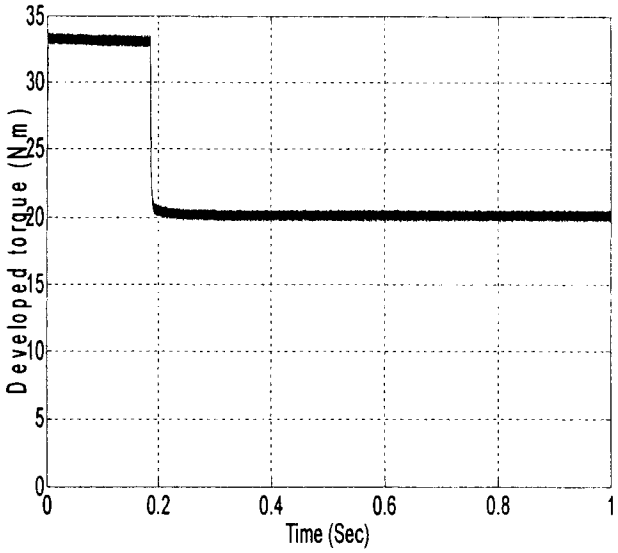

(a)

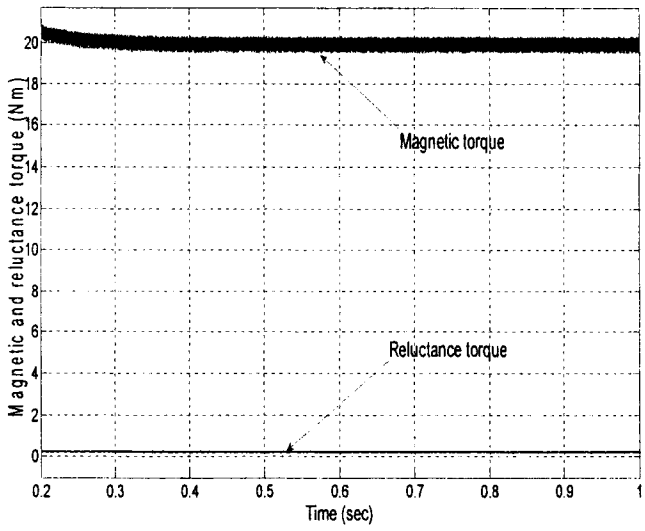

(b)

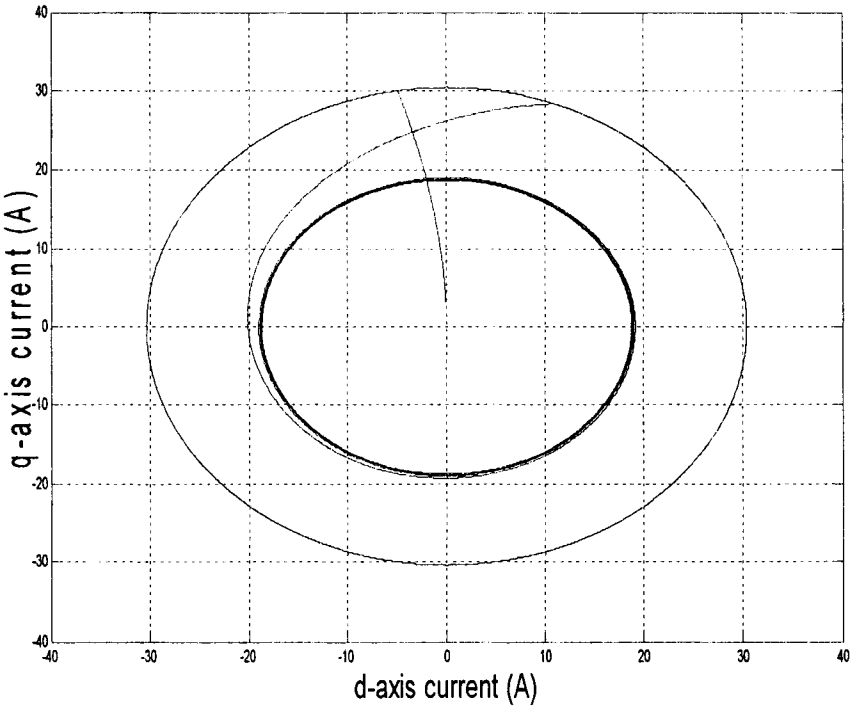

(c)

Fig.6.7: Starting response with full load for a step command of rated speed; (a) developed torque (b) steady state magnetic and reluctance torque (c) stator q axis current vs stator d-axis current.

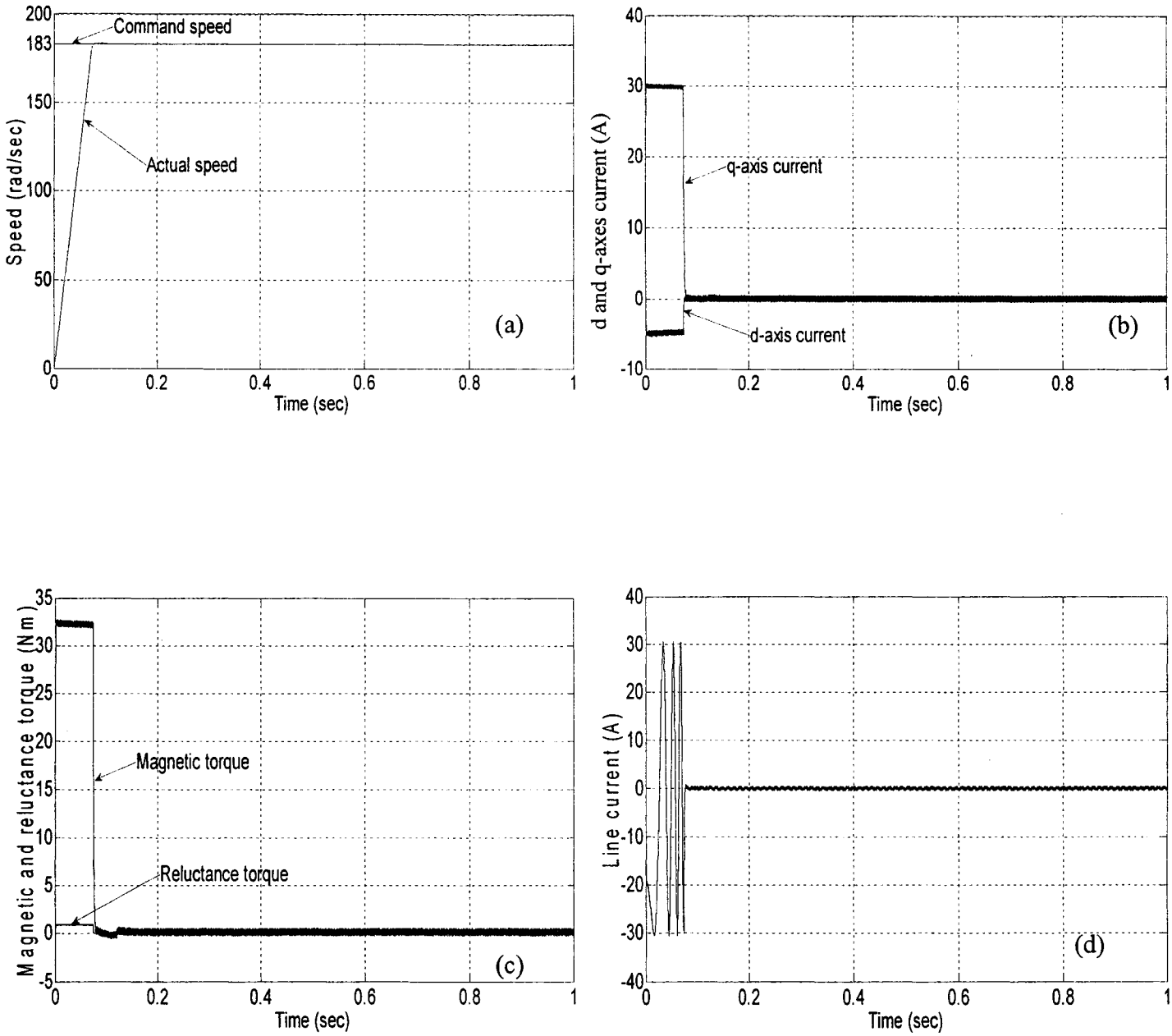

Fig.6.8: Starting response with no load for a step command of rated speed; (a) speed (b) d-q axis current (c) magnetic and reluctance torque (d) Line current.

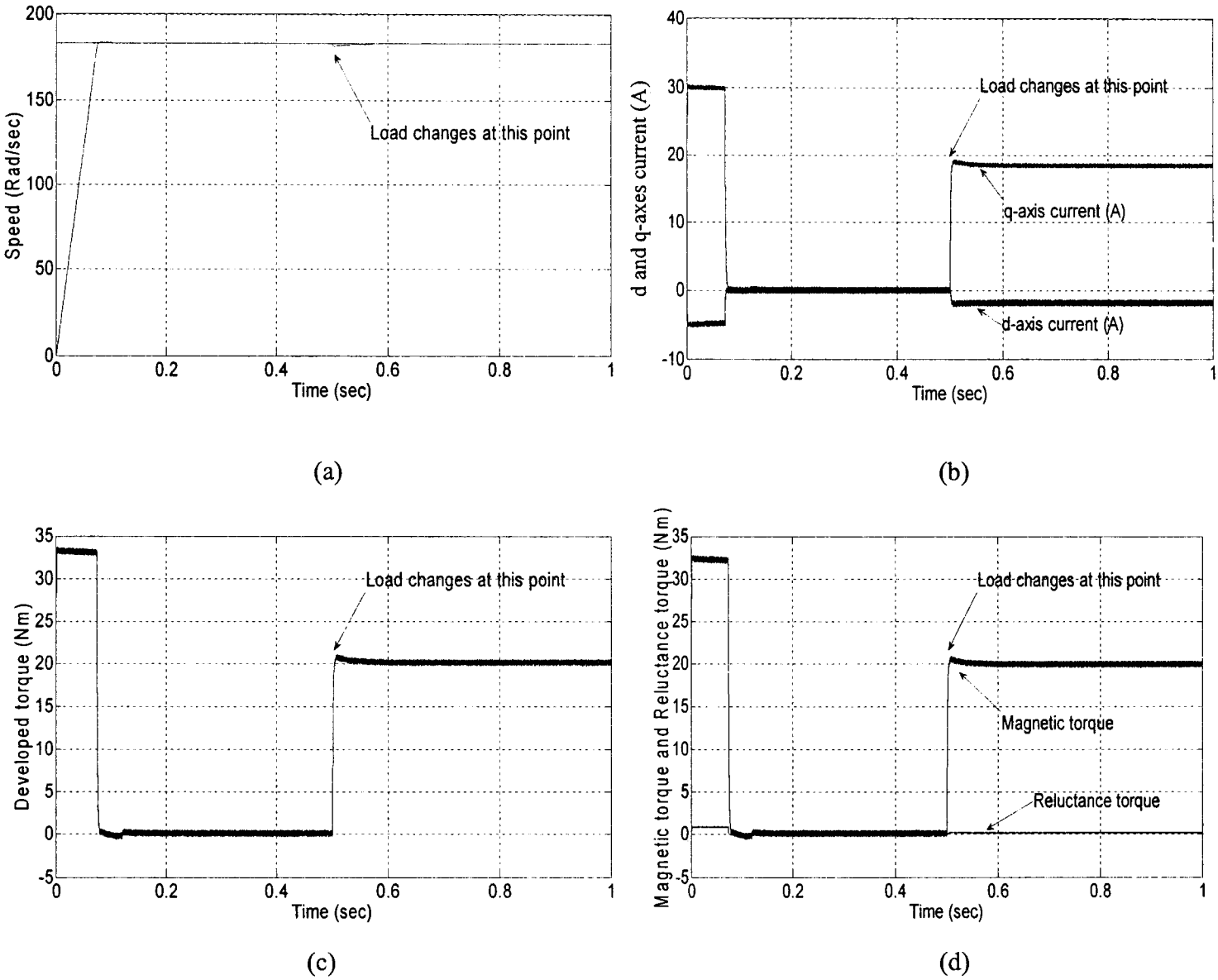

Fig.6.9: Response of the proposed controller with change of load at rated speed; (a) speed (b) d and q axis currents (c) developed torque (d) magnetic and reluctance torques.

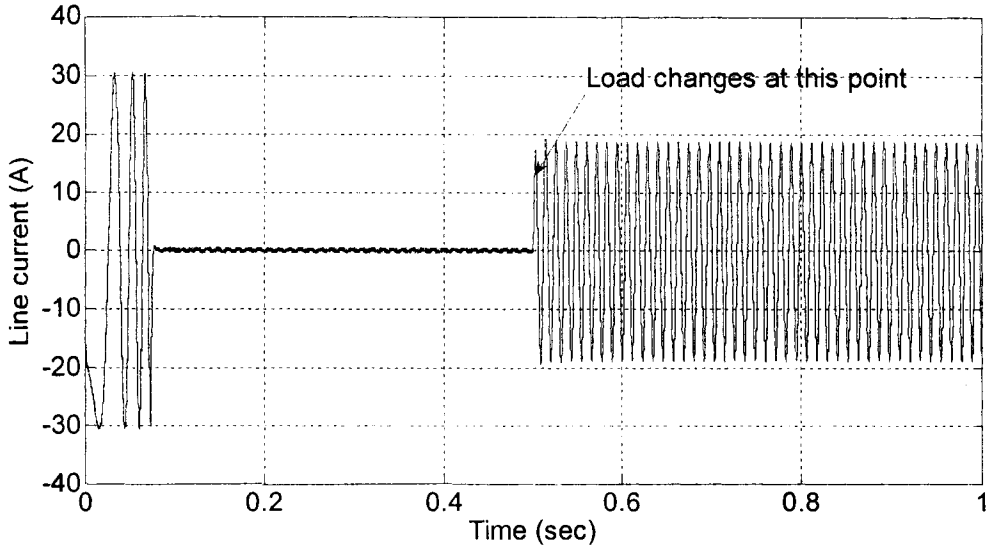

(a)

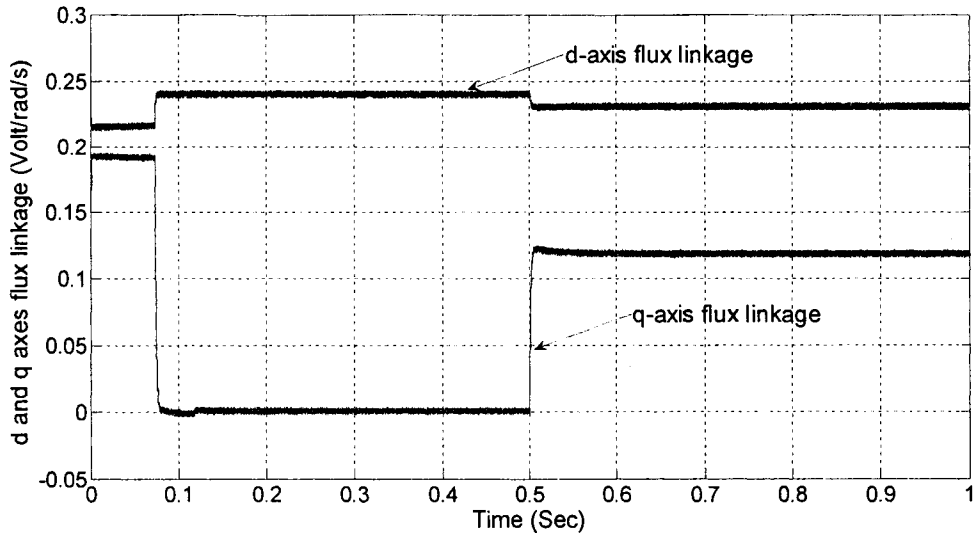

(b)

Fig.6.10: Response of the proposed controller with increase of load at rated speed; (a) line current (b) d and q axis flux linkages.

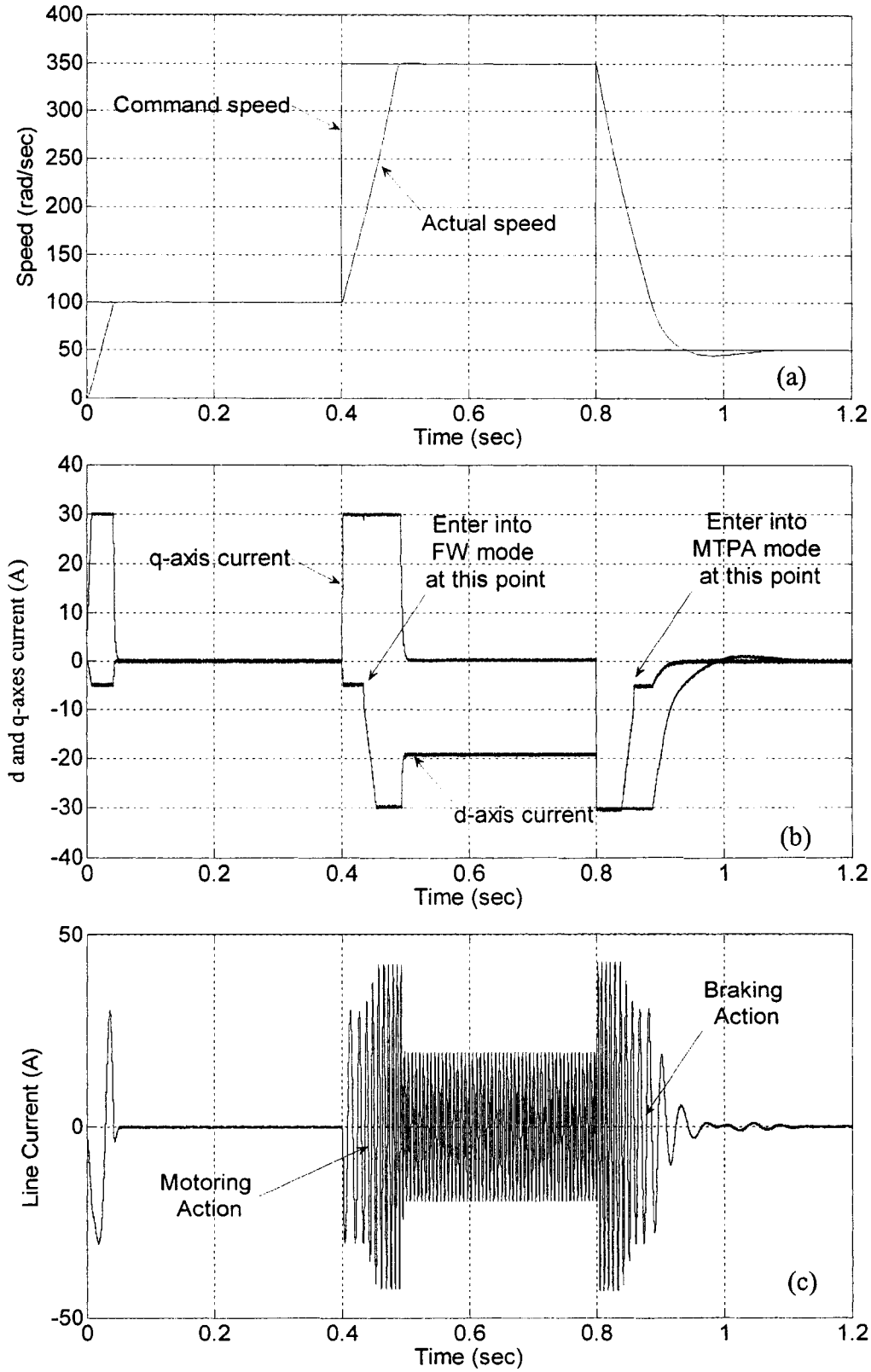

Fig.6.11: Response of the proposed controller with increase of command speed from 100rad/sec to 350 rad/sec and then decrease to 50 rad/sec at no load; (a) speed (b) d and q axis current (c) line current.

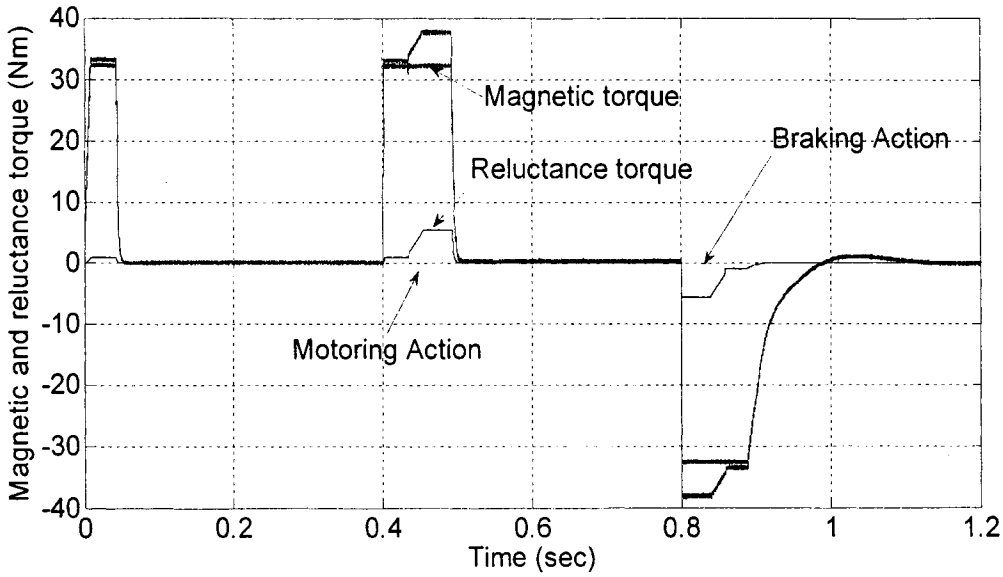

(a)

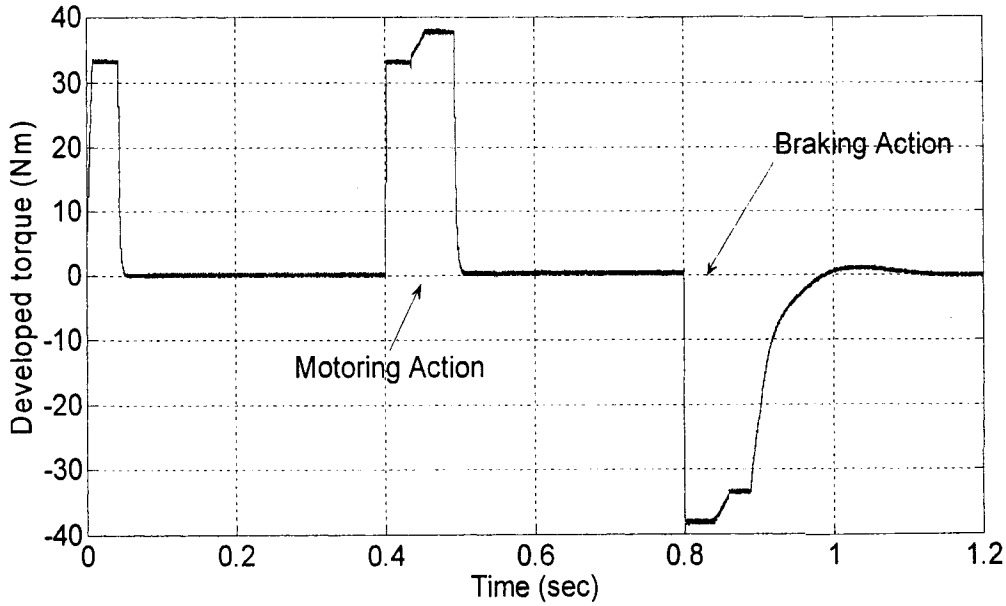

(b)

Fig.6.12: Response of the proposed controller with increase of command speed from 100rad/sec to 350 rad/sec and then decrease to 50 rad/sec at no load; (a) magnetic and reluctance torques (b) developed torque.

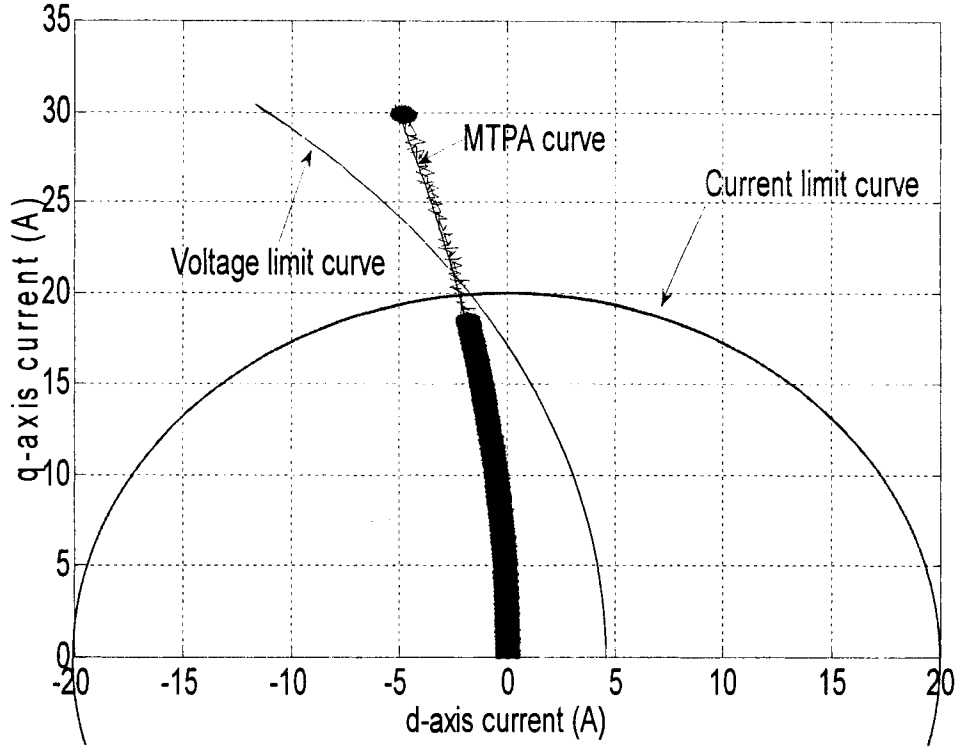

Fig.6.13: Current vector trajectory for a ramp load disturbance of the proposed controller at rated speed (183 rad/s.) in constant torque mode control.

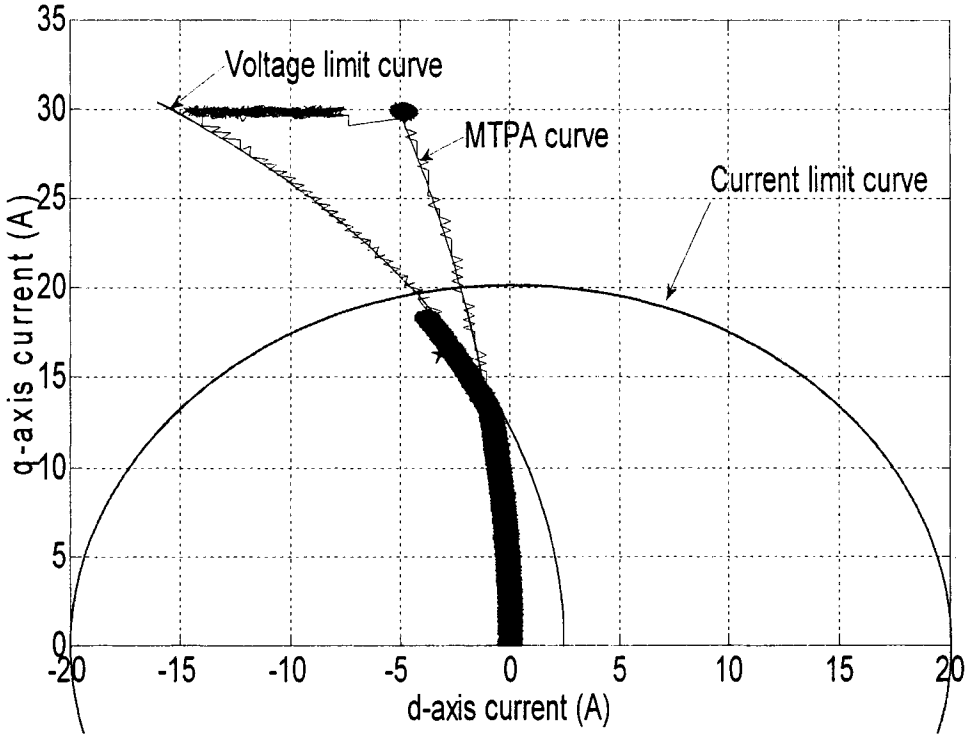

Fig.6.14: Current vector trajectory for a ramp load disturbance of the proposed controller at 190 rad/s. which is above rated speed (183 rad/sec) but below the critical speed (208 rad/sec) in transition mode control.

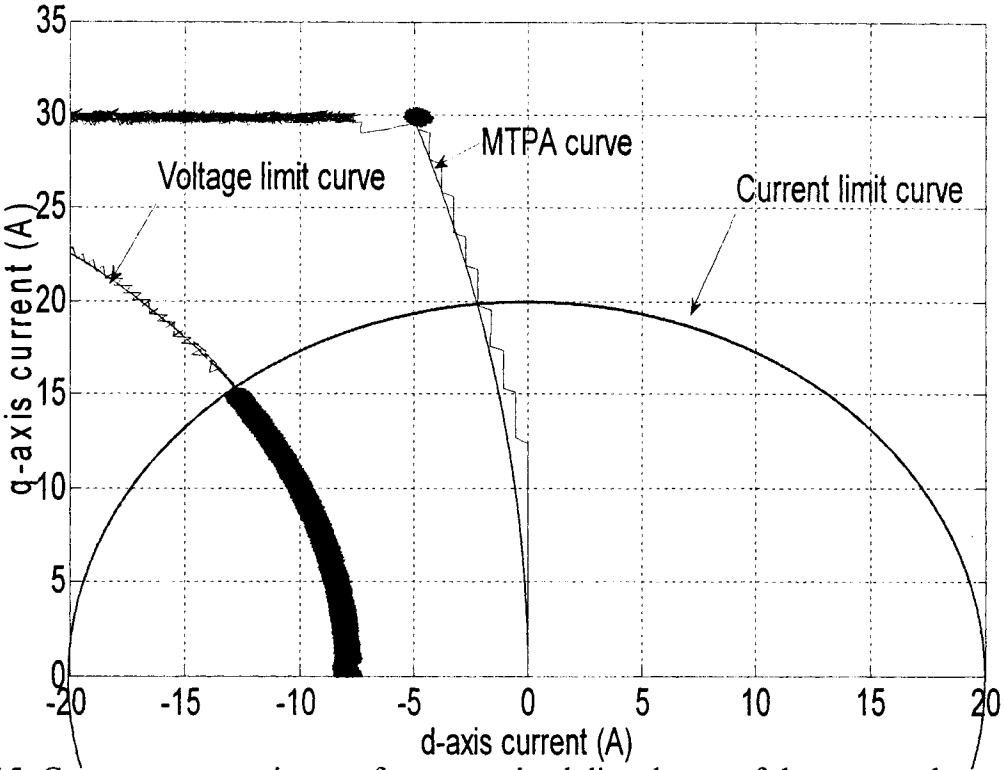

Fig.6.15: Current vector trajectory for a ramp load disturbance of the proposed controller at 250 rad/s. which is above the critical speed and in constant power mode control.

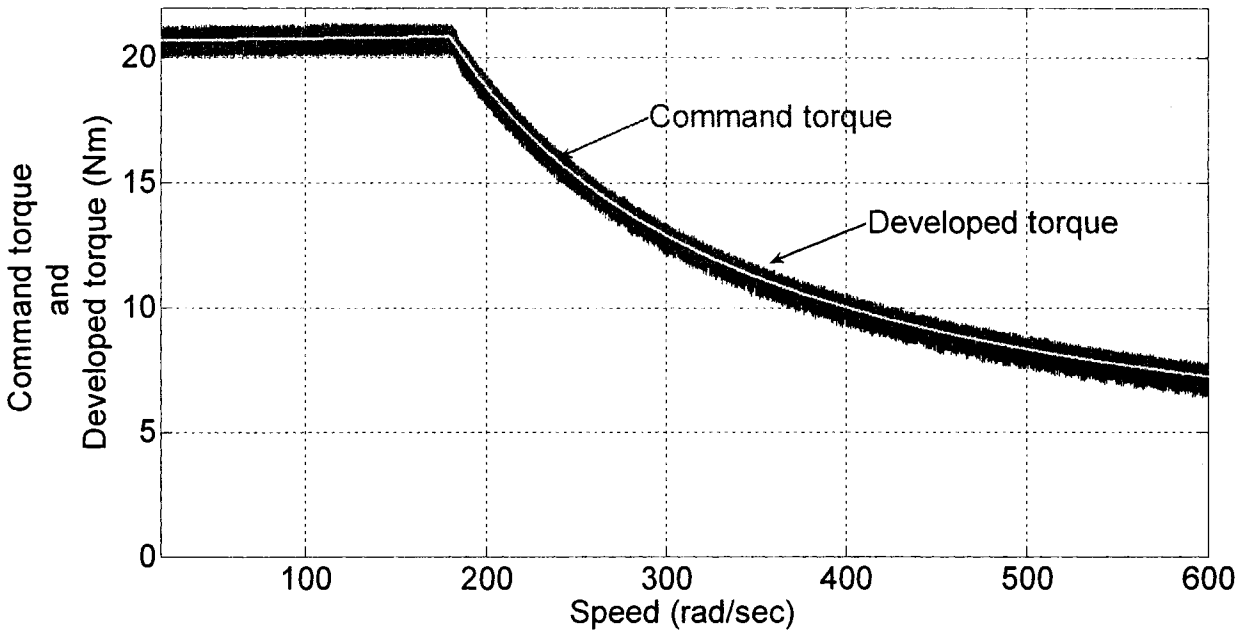

Fig.6.16: Developed torque of proposed controller in full speed range rated speed with command torque.

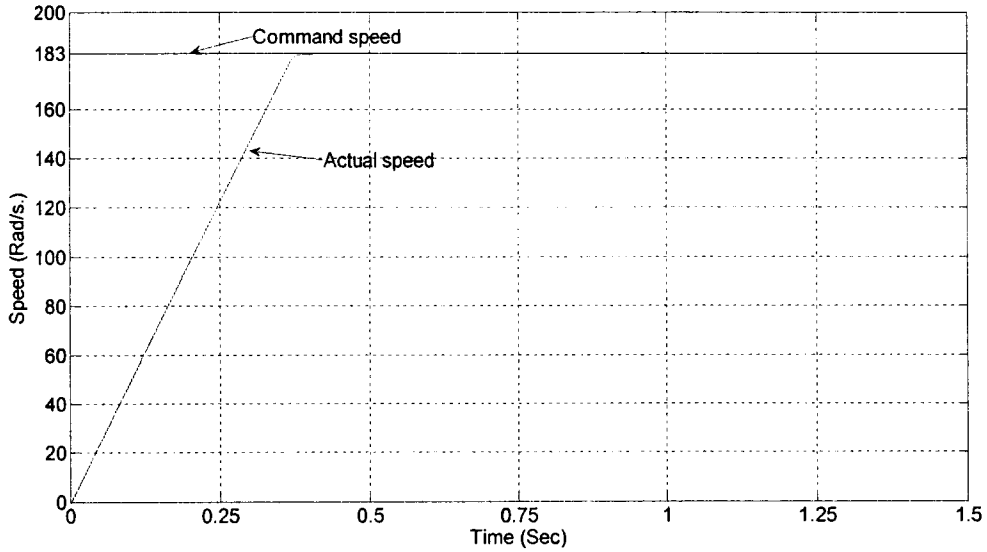

Fig.6.17: Simulated speed response of the proposed IPMSM drive system with doubled inertia (J→2J) under rated speed and load condition.

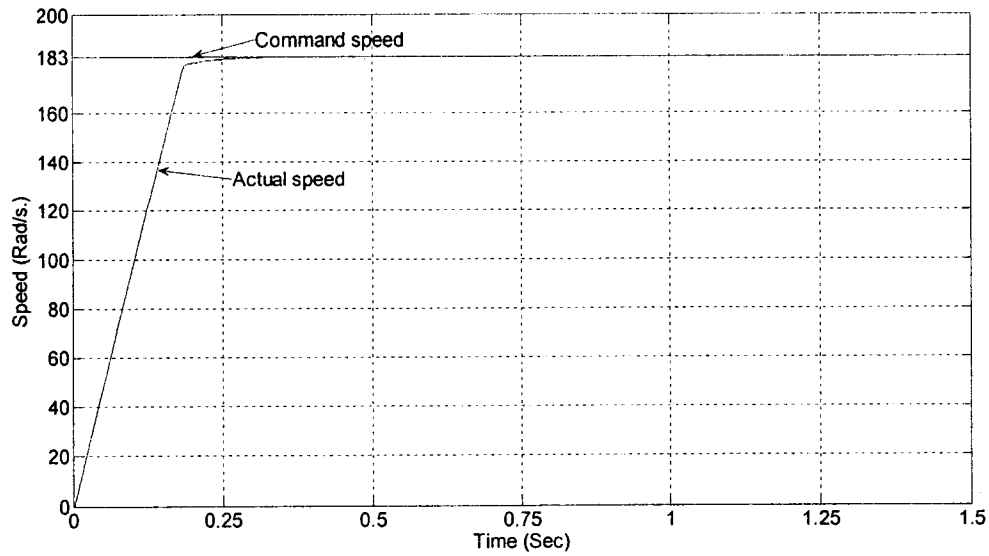

Fig.6.18: Simulated speed response of the proposed IPMSM drive system with doubled friction constant ($B_m \rightarrow 2B_m$) under rated speed and load condition.

current circle represent the starting transient current which follows MTPA curve till the motor achieves rated speed. Then it goes to field weakening technique in transient state. From this figure it is observed that below the critical speed the drive can follow MTPA technique up to a certain load condition and above that load the drive is transferred to field weakening technique at steady state condition. In Fig.6.15, the vector trajectories outside current circle represent the starting transient current which follows MTPA curve till the motor achieves rated speed. Then it goes to field weakening technique in transient state. From this figure it is observed that above the critical speed the drive can follow field weakening technique at steady state condition. Developed torque of proposed controller in full speed range rated speed with command torque is shown in Fig.6.16. It is observed that this drive can follow the command torque over a wide speed range. Figs.6.17 and 6.18 show the speed response of the proposed ANFIS based NFC controller of IPMSM drive under rated speed and rated load condition with doubled inertia ($J \rightarrow 2J$) and doubled friction constant ($B_m \rightarrow 2B_m$), respectively. It is evident from Figs.6.17 and 6.18 that the proposed controller based IPMSM drive can follow the command speed with increased inertia and friction constant smoothly without overshoot and steady state error.

6.6 Experimental results

The same experimental set up as described in chapter 4 is used for real-time implementation. The flow chart of real-time implementation algorithm of the proposed speed controller is shown in Fig.6.19. The sampling frequency used for this experiment is 10 kHz. The experimental starting speed response of the proposed controller for a step

command speed of 183 rad/s is shown in Fig.6.20(a). The motor can follow the command speed with reasonable steady state error and without overshoot or undershoot. The corresponding d-q axis currents and line current are shown in Fig.6.20(b)-(d). It is seen from Fig.6.21(a) that the motor can follow the command speed with a negligible dip in

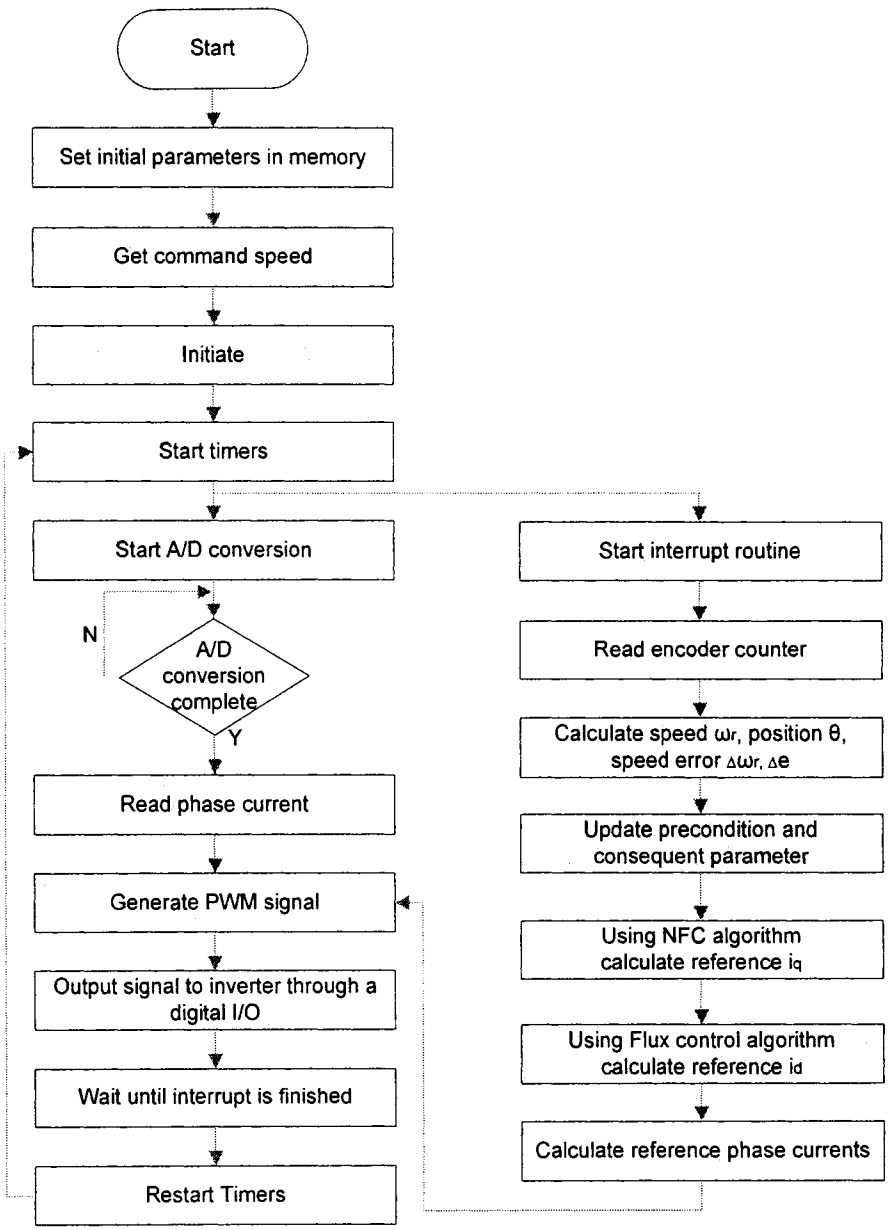

Fig.6.19: Real-time implementation algorithm of the proposed speed controller.

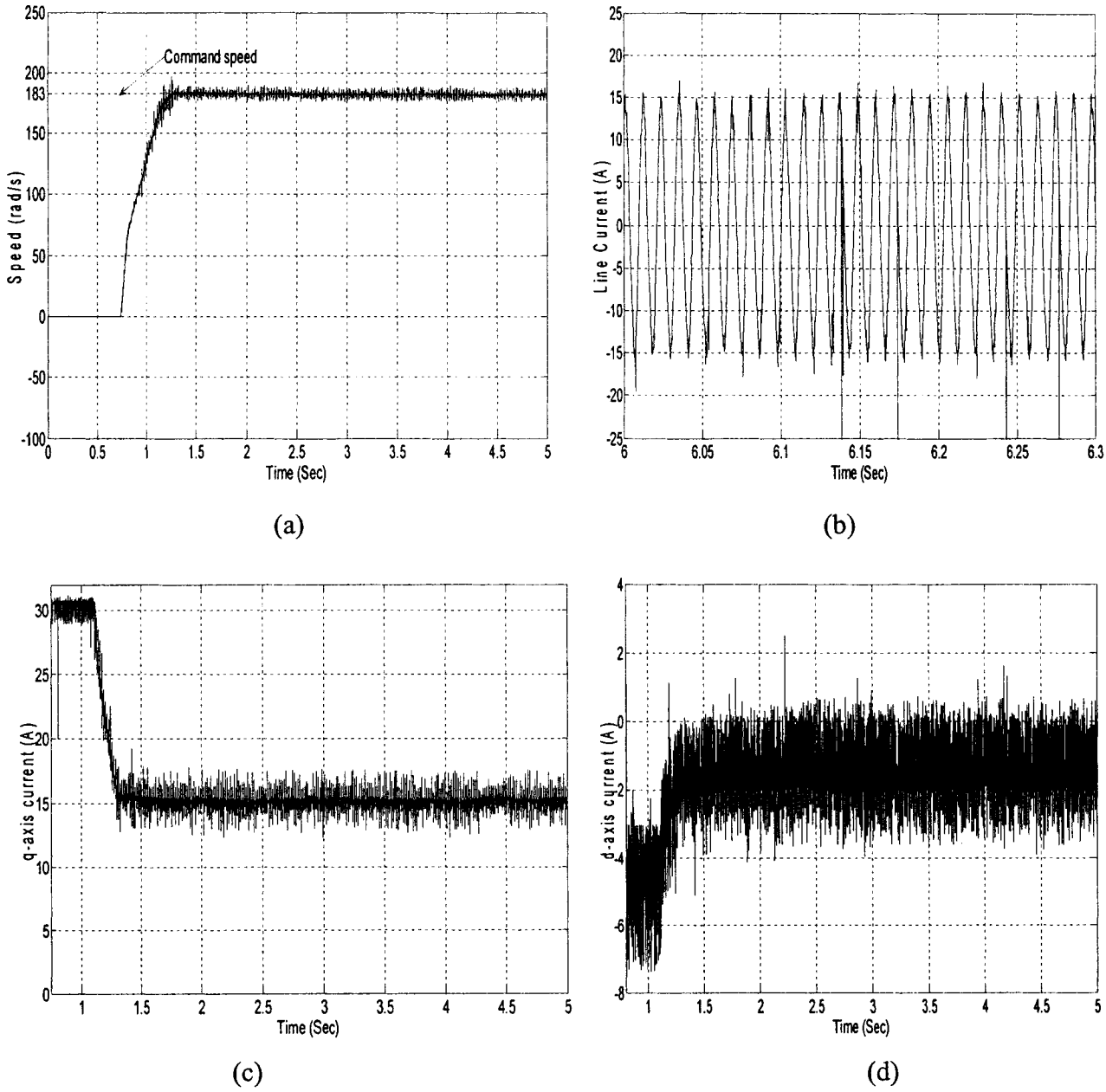

Fig.6.20: Experimental starting speed response of the proposed ANFIS based NFC drive (a) speed (b) q-axis current (c) d-axis current (d) line current.

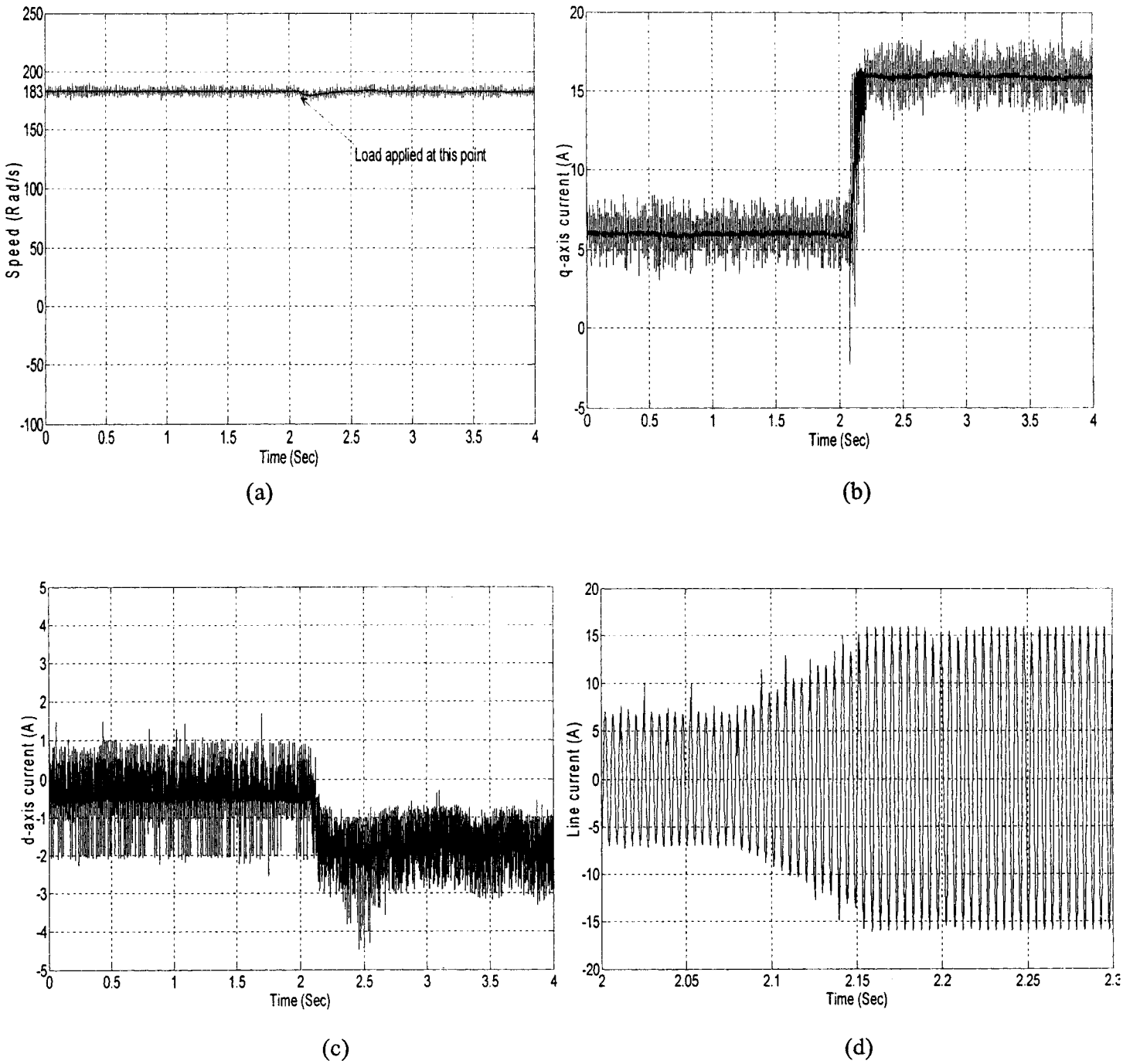

Fig.6.21: Experimental response of the proposed NFC controller for a step increase in load at rated speed (183 rad/s); (a) speed (b) q-axis current (c) d-axis current (d) line current.

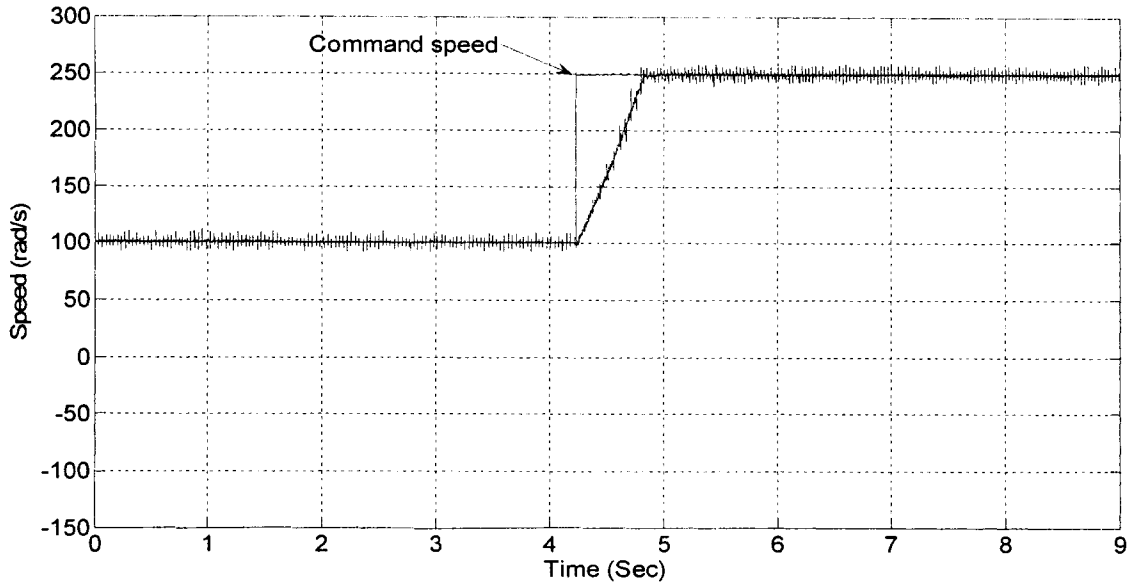

Fig.6.22: Experimental response of the proposed NFC controller for a step increase in speed from 100 rad/s to 250 rad/s.

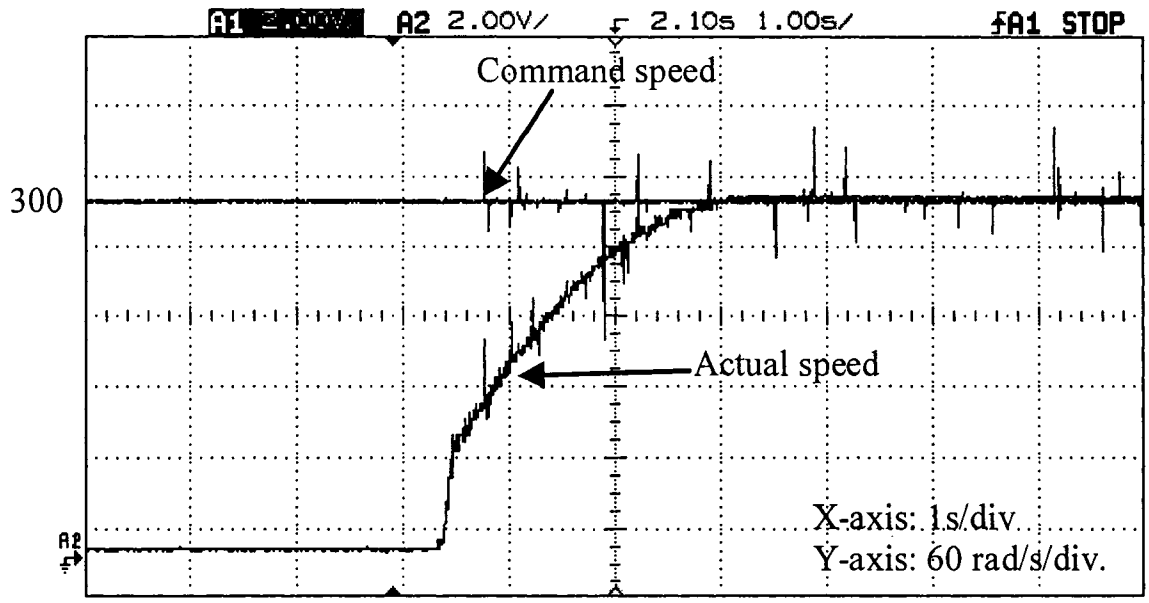

Fig.6.23: Experimental response of the proposed NFC controller for a step command speed 300 rad/s.

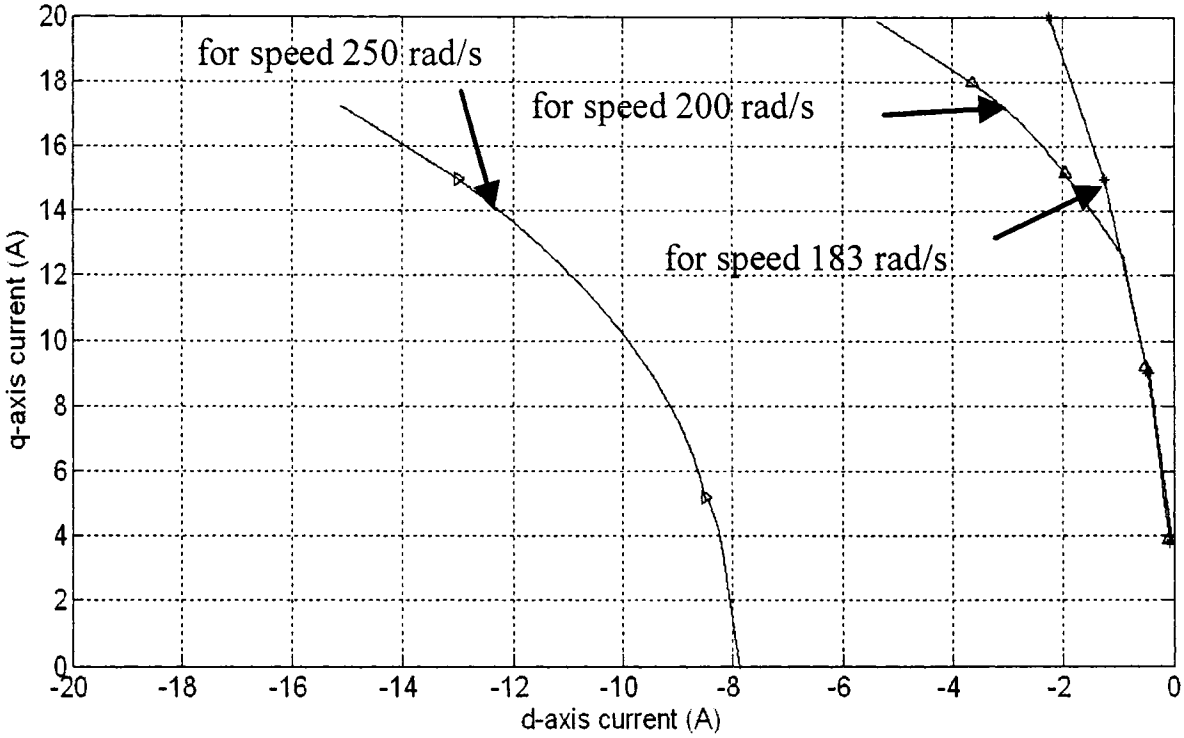

Fig.6.24: Experimental d-q axes current vector trajectories at different load of the proposed NFC at different speed regions ('*'-183 rad/s, 'Δ'-200 rad/s and '▶'-250 rad/s).

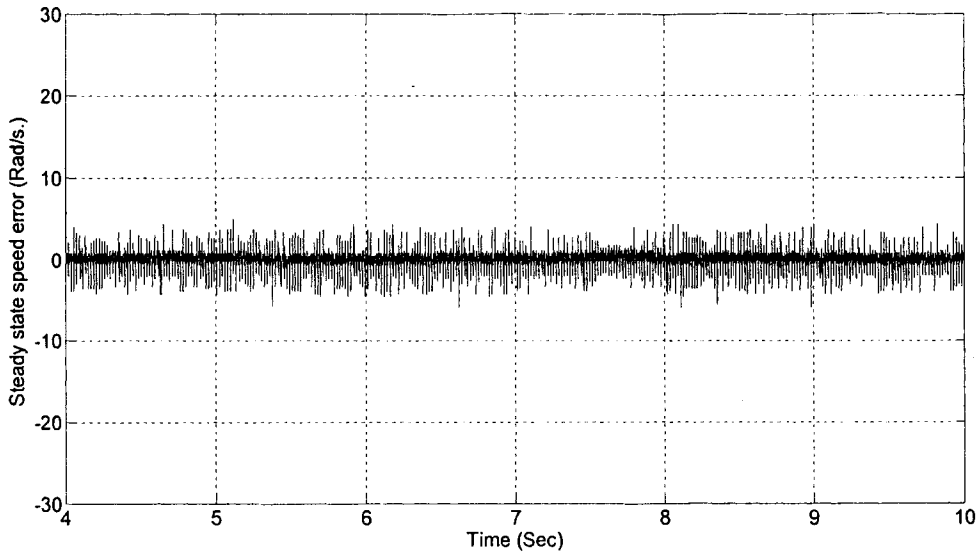

Fig.6.25: Experimental steady state speed error of the proposed NFC based IPMSM drive for a rated command speed at rated load

speed for a step increase in load. With change of load the value of d and q axis currents change to generate more torque as shown in Fig.6.21(b) and (c). The effectiveness of the proposed controller is further verified by another experimental speed response for a step change of command speed from 100 rad/s to 250 rad/s, which is shown in Fig. 6.22. It is shown in Fig.6.22 that the motor can follow the command speed even with online step increase of speed. The speed response for a step command speed 300 rad/s is shown in Fig.6.23 to see the effectiveness of the drive at high speed condition. From this result it should be noted that the proposed controller gives stable operation with acceptable performance even at pure field weakening region. The proposed drive can follow the command speed smoothly with negligible speed ripple, without any overshoot/undershoot and with zero steady-state error. Fig.6.24 shows the experimental d-q axes current vector trajectories for three different regions. To show these vector trajectories the motor was run by the proposed controller at 183 rad/s (for below rated speed region), 200 rad/s (for partial field weakening region) and 250 rad/s (pure field weakening region) at different loads. The average values of d and q axes current are taken to plot these trajectories. Thus, these results verify the flux control theory and simulations. The steady state speed error is shown in Fig.6.25 for rated speed command at rated load. It is observed that there is no steady state speed error at rated condition. In real-time the speed response exhibits negligible ripple, which needs further work to eliminate or minimize. The summary of the results of the three proposed controller is presented in the following table.

Comparison of the three proposed controllers:

Operating Condition	Property	Proposed ABNC	Proposed FLC	Proposed NFC
Starting response for a step speed command at rated load	Overshoot	Less than 0.5 %	Less than 0.1%	Less than 0.2%
	Settling time	0.4s	0.06 s	0.2 s
	Starting maximum current	60 A	58 A	30 A
Starting response for a step speed command at no load	Overshoot	Less than 2%	Less than 1%	Less than 0.5%
	Settling time	0.65s	0.03 s	0.08 s
	Starting current	60 A	58 A	30 A
Response for a step change of load	Speed deviation	Less than 2.5%	Less than 2%	Less than 3%
	Settling time	0.7s	0.2 s	0.1 s
	Steady state current at full load	13.2 A	13.2 A	13.2 A
High Speed operation	Speed range	Up to critical speed	Up to double of rated speed	Up to extreme speed
	Computation	High	Very high	Lower than others
	Ripple	High	High	Less than others
	Controller Design	Depend on mathematical model	Does not depend on mathematical model	Does not depend on mathematical model

6.7 Conclusion

An ANFIS based novel and simplified neuro-fuzzy logic controller (NFC) has been proposed in this paper. Neuro-fuzzy technique has been used to get both the good feature of FLC and ANN controller. The proposed NFC is simple and hence low computational burden. A flux control technique for different speed regions is also incorporated to achieve optimum efficiency and good speed response over the entire speed range. The simulation and experimental results verify the feasibility of the proposed drive for real life industrial drive applications.

Chapter 7

Conclusions

In addition to the control of torque component of stator current, the control of flux component of stator current is also important to achieve high performance, wide speed range control and efficient operation. From the review of previous works as in chapter 1, the IPMSM is a good choice for high performance variable speed drives in industry in view of performance and economy. However, the performance of the drive depends on the type of controllers used. Although using simple controller with the assumption of i_d=0, the control of IPMSM becomes easier with the cost of reluctance torque and high speed operation. It was found that sometimes it can not even reach the rated speed at rated condition.

In Chapter 1, the review of the previous works has been discussed in this thesis. From this review, it is observed that although field control is very important to get a

better performance of IPMSM, only few works have been reported considering flux control. So in this thesis, attention was being paid to develop various controllers incorporating flux control in order to get optimum performance below the rated speed and to operate the motor at high speed condition particularly, above the rated speed.

In chapter 2, the equivalent circuit model of IPMSM is investigated and the operation of the IPMSM analyzed. In order to incorporate the flux control algorithm, the operating region of an IPMSM is divided into three regions such as constant torque region, partial field weakening region and full field weakening region. The flux control algorithm for these three regions is investigated in this chapter.

The fixed gain controller suffer from overshoot, undershoot, steady state error and sometimes instability although they are easy to implement in real field. Some adaptive controllers as done in previous works require complex algorithms, as well as accurate system model parameters. Adaptive controller such as model reference controller, sliding mode controller and self tuning regulator requires a lot of computation, which makes those difficult and cumbersome to design and implement. Moreover, a large number of parameters are associated with these types of controllers which make it more expensive. Uncertainty and nonlinearity from the motor mechanical load sometimes cause the drive system to become unstable in the absence of proper control.

In chapter 3, an adaptive backstepping based nonlinear controller has been developed for IPMSM drive incorporating flux control. The adaptive backstepping based nonlinear controllers have been found to be capable to follow the command speed smoothly and quickly maintaining the global stability. Besides it has negligible speed ripple. Chapter 4 provides details of the implementation and experimental result of the

proposed adaptive backstepping based vector control of IPMSM. After discussions of the various elements of the experimental set up and DSP controller board, the experimental results have been presented which verify the simulation results that shown in chapter 3.

One of the disadvantages of adaptive backstepping based nonlinear controller is that it depends on the motor model and it requires huge computation. In recent years intelligent controllers such as FLC, ANN, NFC become popular for control of electric motors due to their inherent properties of generalization, parameter insensitivity, parallel processing and nonlinear mapping between input and output. The problem of controlling the electric motors in HPD is uncertainty of the motor model parameters. The intelligent controller adjusts the control output with different dynamic conditions with its inherent adaptive nature. In chapter 5, a FLC is developed to control both torque and flux component such that the motor can be run efficiently. In order to verify the efficacy of the FLC in high performance application, a vector control scheme of the IPMSM incorporating the FLC has been simulated and implemented in real-time. However the FLC showed good transient response but suffers from steady state ripple.

For further improvement of the intelligent controller performance, an ANFIS based NFC is developed with tuning the membership function in chapter 6. The tuning procedure of the membership functions of the neuro fuzzy logic controller discussed in this chapter. The NFC is designed in such a way that the computational burdens remain low which is suitable for real-time implementation. For the proposed NFC, the flux control algorithm has also been incorporated to operate the motor with efficient utilization of torque below the rated speed and to control the motor above the rated speed within rated capacities of motor/inverter.

7.1 Major contribution of this thesis

The major contributions of this thesis are listed below:

- Detail analysis of flux control algorithm for an IPMSM has been provided. Above the rated speed control below the critical speed, up to a certain level of load torque MTPA technique can be used. As mentioned earlier it is better to use MTPA technique as long as possible in view of efficiency and low loss. Selection of either MTPA or field weakening depends on the load torque which is unknown. It is a problem in choosing either MTPA or the flux weakening control technique in partial field weakening region. The criteria of choosing flux control technique have been derived in this thesis.

- The flux control algorithm has been developed in such a way that IPMSM will give its optimum performance and efficiency over the whole operating region maintaining voltage and current constraint.

- An adaptive backstepping based nonlinear control technique incorporating MTPA operation has been developed for IPMSM. Stability of the ABNC based IPMSM drive has been proved using Lyapunov's stability theory. Besides control laws, mechanical parameter estimation update laws have also been developed using Lyapunov function.

- A stand alone multi output FLC has been developed for controlling of flux and torque from a single controller block. In deign of the controller MTPA and field-weakening algorithms have been taken into consideration.

- Conventional FLC controls only torque component of current, which may be used only for constant torque region. In the proposed stand alone FLC developed in this thesis enhances the speed region above the rated speed.

• An ANFIS based noble and simple NFC has been developed. The performance of the controller has been investigated both in simulation and experiment at different operating conditions. The performance of the proposed NFC has been found as superior to other controllers presented in this thesis as the membership functions as well as weights were tuned online for NFC.

• In development of an ANFIS based NFC, an algorithm for tuning of the memberships functions and weights have been developed. Tuning of weights were performed indirectly by tuning precondition and consequent parameters.

7.2 Future work

This thesis develops different types of speed controller for high performance IPMSM drive.

• For developing the MTPA relation, d axis current calculated in terms of q axis current for MTPA control. The MTPA was achieved by differentiating developed torque equation with respect to i_q and setting it to zero considering a constant line current. In the differentiation, d and q axis inductances are considered constant with respect to d and q axis current. In practice that is not true. So in future work, MTPA relation can be calculated considering the variation of d and q axis current.

• In the development of the adaptive controller, only the mechanical parameters were estimated. d and q axis inductances are varying with different operating condition. So future work can be done with the estimation of electrical parameters too.

• In the neuro fuzzy logic controller design, tuning of membership functions was done online. But there was still ripple in speed. These ripple caused by the ripple in

command q-axis current. A filter can be designed and used to optimize the speed ripple. But this might make the controller slow.

- A NFC can be developed to control both torque and flux. This intelligent controller can be designed in such a way that it will maintain MTPA by tuning the membership function of i_d. So the parameter dependency of the controller for optimum performance can be omitted.

- Many research studies are being reported using the speed sensorless approach. This will eliminate the need for a position encoder as well as any difficulties associated with it.

7.3 Conclusion

In this thesis a survey on the state of the art work on IPMSM drive has been presented at the beginning. The detail analysis of flux control for different speed region of IPMSM drive has also been presented. An adaptive backstepping based nonlinear controller incorporating flux control has been developed and implemented. The detailed experimental implementation procedure for the IPMSM drive incorporating different controllers has also been presented. In order to get better performance with independent of motor model an FLC controller has been developed. The proposed FLC has been found to be more robust as compared to conventional FLC. This controller also enhances the operating speed range. To improve the performance membership function has been tuned according to operating condition using NFC. The proposed ANFIS based NFC provides an efficient, robust and easy way to control speed. Initial set of weights and membership functions are updated online which provide a unique feature of adaptive

controller. The performance of this ANFIS based NFC controller has been found better than the proposed FLC and ABNC.

References

[1] Richard M. Crowder, *Electric Drives And Their Controls*, Clarendon Press, 1995.

[2] S.J. Chapman, *Electric Machinery Fundamentals*, New York, NY: Mcgraw-Hill, 1999.

[3] Eugene C. Lister and Michael R. Golding, *Electric Circuits and Machines*, Mcgraw-Hill Ryerson Limited, 1987.

[4] W. Shepherd and L. N. Hulley, *Power Electronics and Motor Control,* Cambridge University Press, 1987.

[5] *Super Energy Saving Variable Speed Drives Manual LITERATURE NO.* KAE-S686-15D, Yaskawa Electric Inc.

[6] T.A. Lipo, "Comparative Analysis of Permanent Magnet AC Machines in Variable Speed Applications." *University of Wisconsin-Madison, ECE Dept.,* WEMPEC Research Report No. 82-12, Sept. 1982.

[7] R.S. Colby, "Classification of Inverter Driven Permanent Magnet Synchronous Motors." *Conference Record of IEEE Industry Applications Society Annual Meeting,* 2-7 Oct. 1988, Vol.1, pp.1 – 6.

[8] J.T. Boys, S.J. Walton, "Scalar Control: An Alternative AC Drive Philosophy" *IEE Proceedings-Electric Power Applications.* May, 1988, Vol. 135, No. 3, pp. 151 – 158.

[9] R. H. Park, "Two-reaction theory of synchoronous machines – generalized method of analysis part 1," *AIEE Transactions,* Vol. 52, June, 1933, pp. 352-355.

[10] B.K. Bose, P.M. Szczesny, "A Microcomputer-Based Control And Simulation of an Advanced IPM Synchronous Machine Drive System for Electric Vehicle Propulsion." *IEEE Transactions on Industrial Electronics*; Vol. 35, No. 4, Nov. 1988, pp.547 – 559.

[11] A. V. Gumaste and G. R. Slemon, "Steady State Analysis of a Permanent Magnet Synchronous Motordrive With Voltage Source Inverter", *IEEE Transactions on Industrial Applications,* Vol. IA-17, No. 2, March/April 1981, pp. 143-151.

[12] G. R. Slemon and A. V. Gumaste, "Steady State Analysis of a Permanent Magnet Synchronous Motordrive With Current Source Inverter", *IEEE Transactions on Industrial Applications,* Vol. IA-19, No. 2, March/April 1983, pp. 190-197.

[13] S.R. Macminn, T.M. Jahns, "Control Techniques for Improved High-Speed Performance of Interior PM Synchronous Motor Drives", *IEEE Transactions on Industry Applications,* Vol. 27, No. 5, Sept.-Oct. 1991, pp. 997 – 1004.

[14] T. M. Jahns, G. B. Kliman and T. W. Neumann, "Interior Permanent Magnet Synchronous Motors for Adjustable Speed Drives," *IEEE Transactions on Industry Applications*, Vol. IA-22, No. 4, July-Aug. 1986, pp. 738-47.

[15] T. M. Jahns, "Flux-Weakening Regime operation of an Interior Permanent Magnet Synchronous Motors Drive," *IEEE Transactions on Industrial Applications,* Vol. IA-23, No.4, 1987, pp. 681–689.

[16] P. Pillay and R. Krishnan, "Control Characteristics and Speed Controller Design for a High Performance Permanent Magnet Synchronous Motor Drive," *In Proc. IEEE PESC*, 1987, pp. 598–606.

[17] S. Ogasawara, H. Akagi, "Implementation and Position Control Performance of a Position-Sensorless IPM Motor Drive System Based on Magnetic Saliency" *IEEE Transactions on Industry Applications,* Vol. 34, No. 4, July-Aug. 1998, pp. 806 – 812.

[18] Y. Kazunori, S. Ogasawara, H. Akagi, "Performance Evaluations of a Position-Sensorless IPM Motor Drive System Based on Detection of Current Switching Ripples" *IEEE 31st Annual Power Electronics Specialists Conference*, 18-23 June, *2000.* Vol. 2, pp. 873 – 878.

[19] J. Oyama, K. Ogawa, T. Higuchi, E. Rashad, M. Mamo, M. Sawamura, "Sensorless Vector-Control of IPM Motors over Whole Speed Range" *IEEE International Conference Proceedings on Power Electronics And Drive Systems,* 22-25 Oct. 2001, Vol. 2, , pp.448 – 451.

[20] C. Mademlis, V.G. Agelidis, "A High-Performance Vector Controlled Interior PM Synchronous Motor Drive with Extended Speed Range Capability" *Annual Conference of IEEE Industrial Electronics Society,* 29 Nov.-2 Dec. 2001, Vol. 2, pp.1475 – 1482.

[21] Ting-Yu Chang, Ching-Tsai Pan, J.H. Liaw, S.M. Sue, "A Hall-Sensor-Based IPM Traction Motor Drive." *Proceedings of The IEEE International Symposium on* Industrial Electronics. 26-29 May, 2002, Vol. 3, pp.840 – 843.

[22] S. Bolognani, L. Tubiana, M. Zigliotto, "EKF-Based Sensorless IPM Synchronous Motor Drive for Flux-Weakening Applications", *IEEE Transactions on Industry Applications*, Vol. 39, No. 3, May-June, 2003, pp.768 – 775.

[23] M. Morimoto, K. Aiba, T. Sakurai, A. Hoshino, M. Fujiwara, "Position Sensorless Starting of Super High-Speed PM Generator for Micro Gas Turbine" *IEEE Transactions on Industrial Electronics,* Vol. 53, No.2, April 2006, pp. 415 – 420.

[24] S. Morimoto, M. Sanada And Y. Takeda, "Effects and Compensation of Magnetic Saturation in Flux-Weakening Controlled Permanent Magnet Synchronous Motor Drives," *IEEE Transactions on Industry Applications*, Vol. 30, No. 6, Nov./Dec. 1994, pp. 1632-1637.

[25] M. F. Rahman, L. Zhong And K. W. Lim, "A Direct Torque-Controlled Interior Permanent Magnet Synchronous Motor Drive Incorporating Field Weakening" *IEEE Transactions on Industry Applications,* Vol. 34, No. 6, Nov./Dec. 1998, pp. 1246-1253.

[26] S. Vaez, V.I. John, M.A. Rahman, "An On-Line Loss Minimization Controller for Interior Permanent Magnet Motor Drives" *IEEE Transactions on Energy Conversion*, Vol. 14, No. 4, Dec. 1999, pp.1435 – 1440.

[27] I. Choy, T. Yoon, K. Kim and M. Park, "Microprocessor based Permanent Magnet Synchronous Motor Drives using MRAC.", *IPEC Conference Record, Tokyo, Japan*, 1990, pp. 481-488.

[28] E. Cerruto, A. Raciti and A. Testa, "A Robust Adaptive Controller for PM Motor Drives in Robotic Applications", *IEEE Transactions on Power Electronics*, Vol. 10, No. 1, Jan. 1995, pp. 62-70.

[29] Y. Sozer and D. A. Torrey, "Adaptive Flux Weakening Control of Permanent Magnet Synchronous Motors", *IEEE/IAS Annual Meeting Conference Record*, 1998, pp. 475-482.

[30] C. Namudri and P. C. Sen, "A Servo-Control System using a Self-Controlled Synchronous Motor (SCSM) with Sliding Mode Controller." *IEEE/IAS Annual Meeting Conference Record*, 1987 , pp. 283-295.

[31] A. Consoli and Antonio, "A DSP Based Sliding Mode field oriented control of an interior permanent magnet synchronous motor drive," *IPEC Conference record, Tokyo, japan*, 1990, pp. 263-303.

[32] M. Ghirby and H. Le-huy, "Optical control and Variable structure combination using permanent magnet synchronous motor.", *IEEE/IAS Annual Meeting Conference Record.* 1994, pp. 408-415.

[33] R.B. Sepe and J. H. Lang, "Real-time adaptive control of the permanent magnet synchronous motor." *IEEE/IAS Annual Meeting Conference Record*, 1990, pp. 545-552.

[34] M. A. Rahman, M. Vilathgamuwa, M.N. Uddin, K. Tseng "Nonlinear Control of Interior Permanent-Magnet Synchronous Motor" *IEEE Transactions on Industry Applications*, Vol. 39, No.2, March/April 2003, pp. 408-416.

[35] P. Zhou, M. A. Rahman, M. A. Jabbar; "Field circuit analysis of permanent magnet synchronous motors" *IEEE Transactions on Magnetics*, Vol. 30, No. 4, Part 2, Jul 1994, pp. 1350 – 1359.

[36] Z. Ibrahim And E. Levi. "A Comparative Analysis of Fuzzy Logic and PI Speed Control in High Perfbrmance AC Drives Using Experimental Approach". *IEEE Transactions on Industrial Application,* Vol. 38, No. *5,* Sept./Oct 2002, pp. 1210-1218.

[37] C. Butt, M.A. Rahman, "Limitations of Simplified Fuzzy Logic Controller for IPM Motor Drive." *IEEE/IAS Annual Meeting Conf. Record*, 3-7 Oct.2004, Vol. 3, pp.1891 – 1898.

[38] Y. Tang And L. Xu, "Fuzzy Logic Application for Intelligent Control of a Variable Speed Drive," *IEEE Transactions on Power Electron.*, Vol.12, Nov. 1997, pp. 1028-1039.

[39] C. C. Lee, " Fuzzy Logic In Control System: Fuzzy Logic Controller – Part I, II. " *IEEE Transactions on System, Man And Cybernetics.* Vol.20, No-2, 1990. pp. 404-435.

[40] S. Y. Yi and M. J. Chung, "Robustness of Fuzzy Logic Control for an Uncertain Dynamic System," *IEEE Transactions on Fuzzy Syst.,* Vol. 6, May 1998, pp. 216–224.

[41] M N Uddin and M A Rahman. "Fuzzy Logic Based Speed Control of an IPM Synchronous Motor Drive". *Journal of Advanced Computational Intelligence*, Vol. 4, No. 3, 2000, pp. 212-219.

[42] C. Butt, M.A. Hoque, M.A. Rahman, "Simplified Fuzzy Logic Based MTPA Speed Control of IPMSM Drive." *IEEE Transactions on industry applications,* 2004. Vol. 40, No.6, pp. 1529– 1535.

[43] M. N. Uddin, M. A. Abido and M. A. Rahman, "Real-Time Performance Evaluation of a Genetic Algorithm Based Fuzzy Logic Controller for IPM Motor Drives", *IEEE Transactions on Industry Applications*, Vol. 41, No. 1, Jan./Feb. 2005, pp. 246-252.

[44] K. Zawirski, "Fuzzy Robust Speed Control for Permanent Magnet Synchronous Motor Servo Drive" *Proc. Of 8th Int. Power Electronics & Motion Control Conference, Prague*, 8-10 Sept, 1998.

[45] S Bolognani And M. Zigliono. "Fuzzy Logic Control of a Switched Reluctance Motor Drive''. *IEEE Transactions on Industry Applications*. Vol. 32. No. 5, Sept./Oct. 1996, pp. 1063-1068.

[46] Yen-Shin Lai and Juo-Chiun Lin, "New Hybrid Fuzzy Controller for Direct Torque Control Induction Motor Drives." *IEEE Transactions on Power Electronics,* Vol.18, No. 5, Sept. 2003, pp.1211 – 1219.

[47] P. Stewart, D. A. Stone And P. J. Fleming. "Design of Robust Fuzzy-Logic Control Systems by Multi-Objective Evolutionary Methods with Hardware in the Loop." *Engineering Application of Artificial Intelligence*, Vol. 17, No. 3, April 2004, pp. 275-284

[48] M. N. Uddin, T. S. Radwan, M. A. Rahman, "Performances of fuzzy-logic-based indirect vector control for induction motor drive." *IEEE Transactions on Industry Applications,* Vol. 38, No. 5, Sept.-Oct. 2002, pp. 1219 – 1225.

[49] M A Rahman. M Nasir Uddin. And M. A. Abido. "An Anificial Neural Network for Online Tuning of a Genetic Based PI Controller for Interior Permanent Magnet Synchronous Motor Drive", *Canadian Journal of Electrical & Computer Engineering,* Vol. 31, No. 3, July 2006, pp. 159-165.

[50] Yang Yi, D.M. Vilathgamuwa, M.A. Rahman, "Implementation of an Artificial-Neural-Network-Based Real-Time Adaptive Controller for an Interior Permanent-

Magnet Motor Drive." *IEEE Transactions on Industry Application,* Vol. 39, No. 1, Jan.-Feb. 2003, pp. 96 – 104.

[51] M.A Rahman and M.A. Hoque, "On-Line Adaptive Artificial Neural Network Based Vector Control of Permanent Magnet Synchronous Motors".*IEEE Transactions on Energy Conversion.* Vol. 13, No. 4, 1998, pp. 311-318.

[52] M.E Elbuluk, L Long and I Husain, "Neural Network Based Model Reference Adaptive Systems for High-Performance Motor Drives and Motion Controls". *IEEE Transactions on Industry Applications.* Vol. 38. May/June 2002, pp. 1063-1068.

[53] N. Urasaki, T. Senjyu, K. Uezato, "Neural Network Based High Efficiency Drive for Interior Permanent Magnet Synchronous Motors Compensating EMF Constant Variation." *Power Conversion Conference,* Osaka, Japan, April, 2002, Vol. 3, pp. 1273 - 1278 .

[54] M.A El-Sarkawi. A.A El-Samahy and M L El-Sved. "High Performance Drive of DC Brushless Motors Using Neural Network." *IEEE Transactions on Energy Conversion,* Vol. 9. No. 2. June 1994, pp. 317-322.

[55] M. N Uddin. M A Abido and M. A Rahman. "Development and Implementation of a Hybrid Intelligent Controller for Interior Permanent Magnet Synchronous Motor Drive" *IEEE Transactions on Industry Applications*, Vol. 40, No. 1, Jan./Feb. 2004, pp. 68-76.

[56] A.Rubaai, D.Ricketts and M.D.Kankam, "Development and Implementation of an Adaptive Fuzzy-Neural-Network Controller for Brushless Drives," *IEEE Transactions on Industrial Application*, Vol. 38, Mar./Apr.2002, pp. 441–447.

[57] C. T. Lin, "A neural fuzzy control system with structure and parameter learning," *Fuzzy Sets Syst.*, vol. 70, 1995, pp. 183–212.

[58] Faa-Jeng Lin,Chih-Hong Lin, and Po-Hung Shen "Self-Constructing Fuzzy Neural Network Speed Controller for Permanent-Magnet synchronous Motor Drive" , *IEEE Transactions on Fuzzy Systems*, Vol 9, no. 5, Oct. 2001 pp:751 – 759.

[59] K. Inoue, Y. Takakado and M. Nakaoka, "Auto Tuning Technology for Fuzzy Algorithms based DC Brushless Servo System", *IEEE/PESC Conference Record*, 1993,pp. 446-450.

[60] T. Fukuda and T. Shibata, "Theory and Applications Of Neural Networks for Industrial Control Systems", *IEEE Transactions on Industrial Electronics,* Vol. 39, No. 6, 1992, pp. 472-489.

[61] K.S. Narendra and K. Parthasarathy ,"Identification and Control of Dynamical Systems Using Neural Networks", *IEEE Transactions on Neural Networks,* Vol. 1, No. 1, 1990, pp. 1-27.

[62] G. S. Buja and F. Todesco, "Neural Network Implementation of Fuzzy Logic Controller," *IEEE Transactions Industrial Electronics*, Vol. 41, Dec.1994, pp. 663–667.

[63] A.K. Nandi and D. K. Pratihar. "An Expert System Based on FBFN Using a GA to Predict Surface Finish in Ultra-Precision Turning." *Journal of Materials Processing Tech.*, Vol. 155-156, 30 Nov., 2004, pp.1150-1156.

[64] M. Chiaberge, G. Di Bene, S. Di Pascoli, B. Lazzerini, A. Maggiore, L.M. Reyneri, "An Integrated Hybrid Approach to the Design of High-Performance

Intelligent Controllers." *International IEEE/IAS Conference on Industrial Automation And Control: Emerging Technologies,* 22-27 May, 1995, pp.436 – 443.

[65] M. Kadjoudj, M.E.H. Benbouzid, C. Ghennai, D. Diallo, "A Robust Hybrid Current Control for Permanent-Magnet Synchronous Motor Drive" *IEEE Transactions on Energy Conv.* Vol. 19, No. 1, March,2004, pp.109 – 115.

[66] B.N. Mobarakeh, F. Meibody-Tabar, F.M. Sargos, "A Self Organizing Intelligent Controller for Speed and Torque Control of a PMSM." *IEEE Conference on Industry Applications,* 8-12 Oct.,2000. Vol. 2, pp. 1283 – 1290.

[67] M. Tursini, F. Parasiliti, and D. Zhang, "Real-Time Gain Tuning of PI Controllers for High-Performance PMSM Drives," *IEEE Transactions on Industrial Applications*, Vol. 38, July/Aug. 2002, pp. 1018–1026.

[68] Faa-Jeng Lin and Rong-Jong Wai "Robust Recurrent Fuzzy Neural Network Control for Linear Synchronous Motor Drive System" *Neurocomputing*, Vol. 50, January 2003, pp. 365-390.

[69] R. Mohammdi-Milasi, C. Lucas, B. Nadjar-Arrabi, "Speed Control of an Interior Permanent Magnet Synchronous Motor Using Belbic (Brain Emotional Learning Based Intelligent Controller)." *World Automation Congress,2004. Proceedings,* 28 June - 1 July, 2004, Vol.16, pp.280 – 286.

[70] M. R. Emami, I. B. Turksen and A. A. Goldenburg, "Development of a Systematic Methodology of Fuzzy Logic Modeling," *IEEE Transactions on Fuzzy Systems*, Vol. 6, Aug. 1998, pp. 346–361.

[71] B Singh, V. K.Shanna and S. S Murthy, "Perlormance Analysis of Adaptive Fuzzy Logic Controller for Switched Reluctance Motor Drive System". *IEEE IAS Annual Meetting,* 1998, pp. 571-579.

[72] C. Cavallaro, M. Coco, A. Raciti, A. Testa, "A neuro-fuzzy approach to design adaptive control systems for PM motor drives" *Proceedings of the IEEE International Caracas Conference onDevices, Circuits and Systems,* 12-14 Dec. 1995. pp. 225 – 229.

[73] Z. Koviac, S. Bogdan and P. Crnosija, "Fuzzy Rule-Based Model Reference Adaptive Control of Permanent Magnet Syncronous Motor", *IEEE/IECON Conference Record,* 1993, pp.207-212.

[74] M.N Uddin, T.S. Radwan, M.A. Rahman "Performance of Interior Permanent Magnet Drive over Wide Speed Range" IEEE Transactions on Energy Conversion, Vol 72, No.1, March 2002, pp. 79-84.

[75] J. Wai, T.M. Jahns, "A New Control Technique for Achieving Wide Constant Power Speed Operation with an Interior PM Alternator Machine" *Thirty-Sixth IAS Annual Meeting. Conference Record of IEEE Industry Applications,* 30 Sept.-4 Oct. 2001, Vol. 2, pp.807 - 814.

[76] Longya Xu and Shengming Li, "A Fast Response Torque Control for Interior Permanent-Magnet Synchronous Motors in Extended Flux-Weakening Operation Regime" *IEEE International Electric Machines and Drives Conference,* 2001. pp.33 – 36.

[77] C. T. Pan and S. Sue, "A Linear Maximum Torque Per Ampere Control for IPMSM Drive over Full-Speed Range" *IEEE Transactions on Energy Conversion*, Vol. 20, No.2, June 2005, pp. 359-366.

[78] B. Sneyers, D.W. Novotny and T. A. Lipo, "Field-Weakening in Buried Permanent Magnet AC Motor Drives," *IEEE Transactions Industrial Applications*, Vol. IA-21, Mar./Apr. 1985., pp. 398–407.

[79] Md. M. I. Chy. and M. N. Uddin "Detail Analysis of Flux Control for IPMSM drive over Wide Speed Operation." accepted for *LESCOPE Conference*, Montreal, Canada, Oct, 2007..

[80] Rouche, Nicolas, "*Stability Theory By Liapunov's Direct Method*" New York : Springer-Verlag, 1977.

[81] J. Soltani and M. Pahlavaninezhad "Adaptive Backstepping Based Controller Design For Interior Type PMSM Using Maximum Torque Per Ampere Strategy" *International Conference on Power Electronics And Drives Systems*, 28-01 Nov. 2005, Vol. 1, pp. 596 – 601.

[82] D.F. Chen, T.H. Liu and C.K. Hung, "Nonlinear Adaptive Backstepping Controller Design for a Matrix-Converter Based PMSM Control System" *Conf. Rec. IEEE-IES Annual Meeting*, 2003, Vol. 1, pp.673-678.

[83] Md. M. I. Chy. and M. N. Uddin "Development of a Nonlinear Speed Controller of IPMSM Drive Incorporating MTPA with Mechanical Parameter Estimation." *IEMDC*, Antalya, Turkey, May, 2007.

[84] *Matlab, Simulink User Guide*, The Math Works Inc., 2004.

[85] *dSPACE*, "Digital Signal Processing and Control Engineering", Implementation Guide, Paderborn, Germany, 2003.

[86] L. A. Zadeh, "Outline of a new approach to analysis of a complex system and decision process", *IEEE Transactions on System, Man and Cyber*, vol. SMC-3, 1973, pp.28-44.

[87] T. Takagi and M. Sugeno, "Fuzzy identification of systems and its applications to modeling and control," *IEEE Transactions on System, Man and Cyber*, Vol-15(1), 1885, pp. 116–132.

[88] Md. M. I. Chy. and M. N. Uddin "A Novel Fuzzy Logic Controller Based Torque and Flux Controls of IPM Synchronous Motor." accepted for *IEEE/IAS Annual Meeting*, New Orleans, Louisiana, USA, 2007.

[89] *Fuzzy Logic Toolbox User Guide*, The Math Works Inc., March, 2004.

[90] Chin-Teng Lin and C. S. George Lee "*Neural Fuzzy Systems, A Neuro-Fuzzy Synergism to Intelligent Systems"*, Prentice Hall P T R publication company, 1996.

[91] H.Dmathur and S. Ghosh, "A Comprehensive Analysis of Intelligent Controllers for Load Frequency Control" *Power India Conference, IEEE,* 10-12 April, 2006. pp. 5.

[92] D. Driankov, H. Hellendoorn and M. Reinfrank, "An introduction to fuzzy control," second edn, *Springer-Verlag, Berlin.* 1996.

[93] Md. M. I. Chy. and M. N. Uddin "Development and Implementation of a New Adaptive Intelligent Speed Controller for IPMSM Drive." accepted for *IEEE/IAS Annual Meeting*, New Orleans, Louisiana, USA, 2007.

[94] S. Brock, J. Deskur, K. Zawirski, "Robust Speed and Position Control of PMSM." *Proceedings of The IEEE International Symposium on Industrial Electronics*, ISIE. 12-16 July 1999, Vol. 2, pp. 667 –672.

[95] A. Zilouchian And M Jamshidi, *Intelligent Control Systems Using Soft. Computing Methodologies*. CRC. 2001.

[96] C. C. Lee, "Fuzzy logic in control systems: Fuzzy logic controller." *IEEE Transactions on Systems, Mand & Cybernetics,* Vol-20(2), 1990, pp. 404–435.

[97] M. Mizumoto, "Realization of PID controls by fuzzy control methods," *IEEE (ed.), first int. Conf. On Fuzzy Systems,* San Diego, USA, 1992, , pp. 709–715.

[98] W. Pedrycz, *Fuzzy control and fuzzy systems*, second edn, Wiley and Sons, New York, 1993.

[99] W. Qiao and M. Mizumoto "PID type fuzzy controller and parameters adaptive method," *Fuzzy set and systems,* Vol-78, 1996, pp. 23–35.

[100] W. Siler and H. Ying "Fuzzy control theory: The linear case," *Fuzzy set and systems,* Vol- 33, 1989. pp. 275–290.

Appendix -A

IPMSM Parameters

Number of phases = 3

Number of poles = 6

Rated Frequency = 87.5 Hz

Rated power = 5 HP

Rated input line-to-line voltage = 183 V

q-axis inductance, L_q = 6.42 mH

d-axis inductance, L_d = 5.06 mH

Stator resistance per phase R = 0.242 ohm

Inertia constant $J = 0.0133 kg.m^2$

Rotor damping constant $B_m = 0.001(Nm)/rad./\sec$

Permanent magnet flux linkage $= 0.24 volts/rad./\sec$

Appendix – B

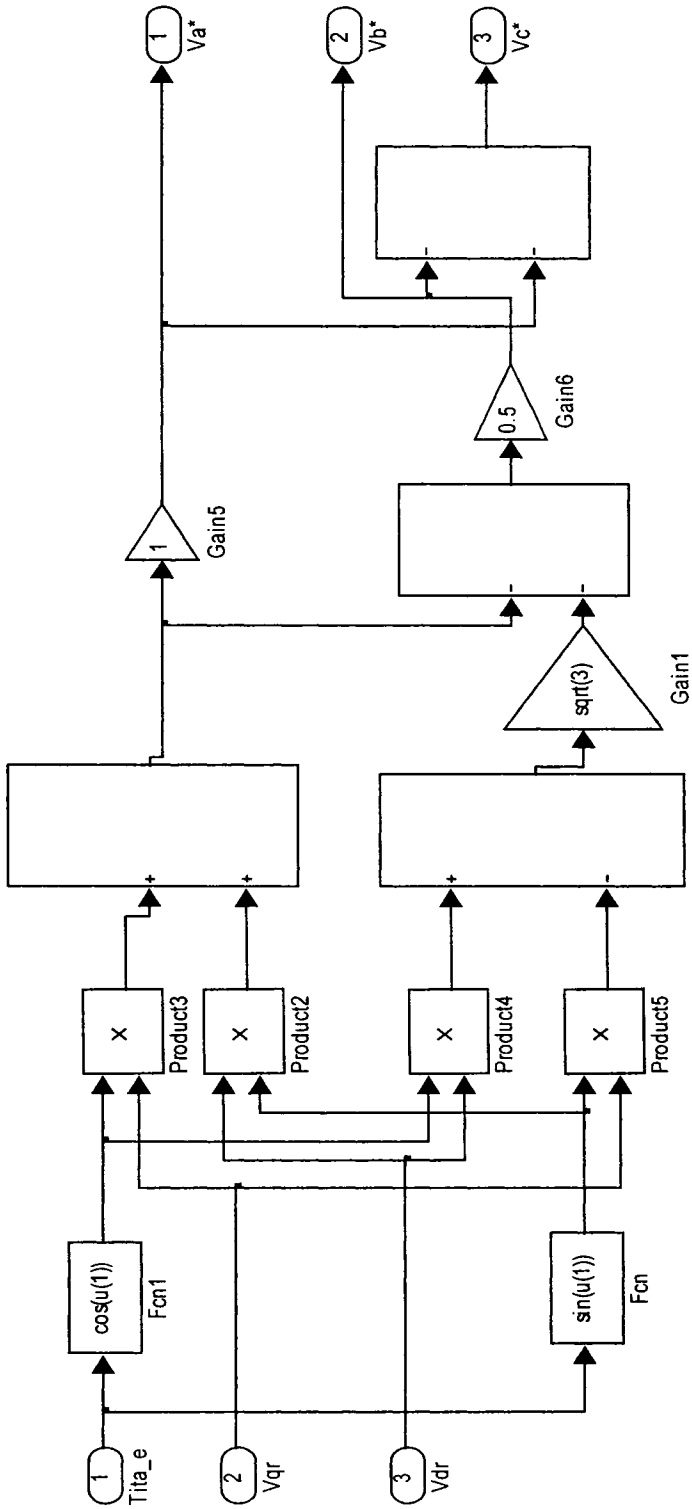

B1. DQ/ABC Vector Rotator

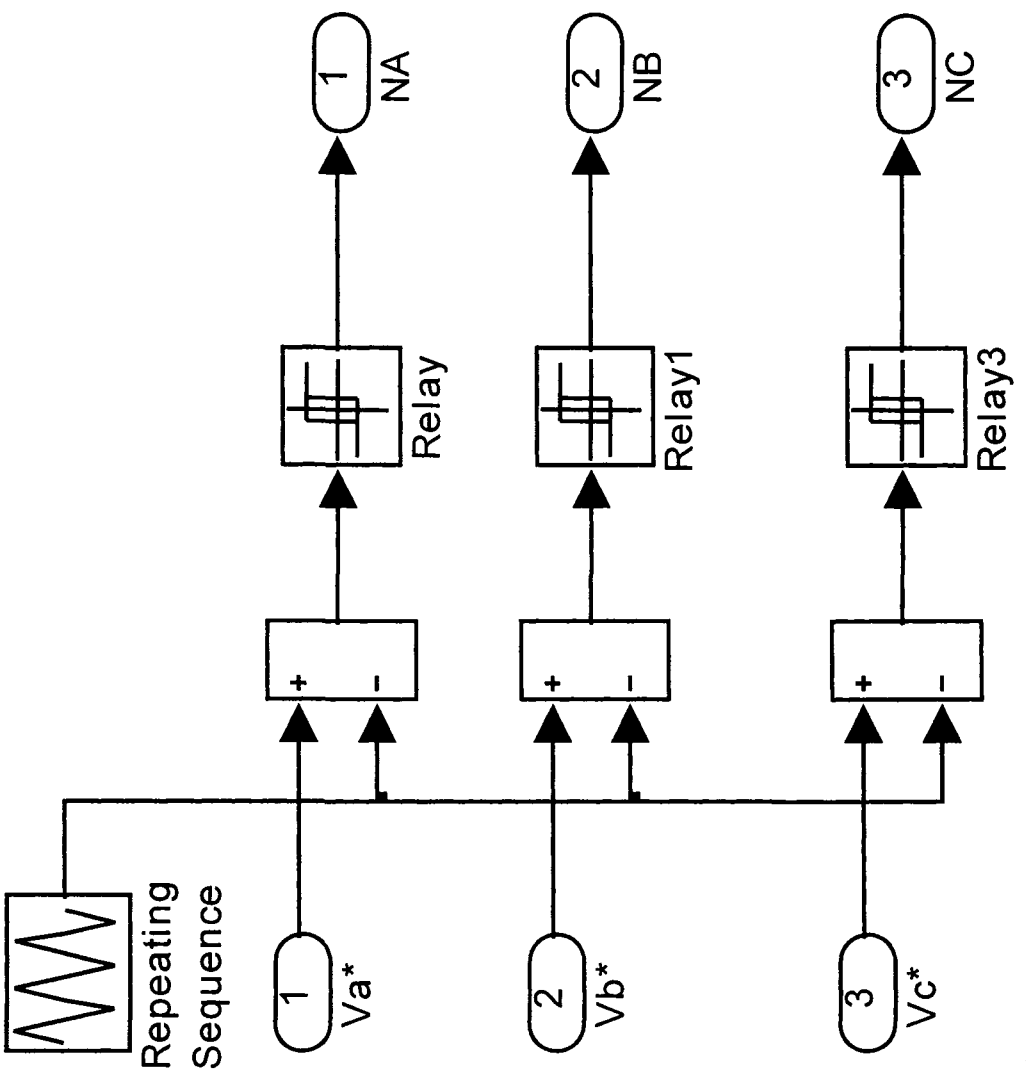

B2. PWM Signal Generator

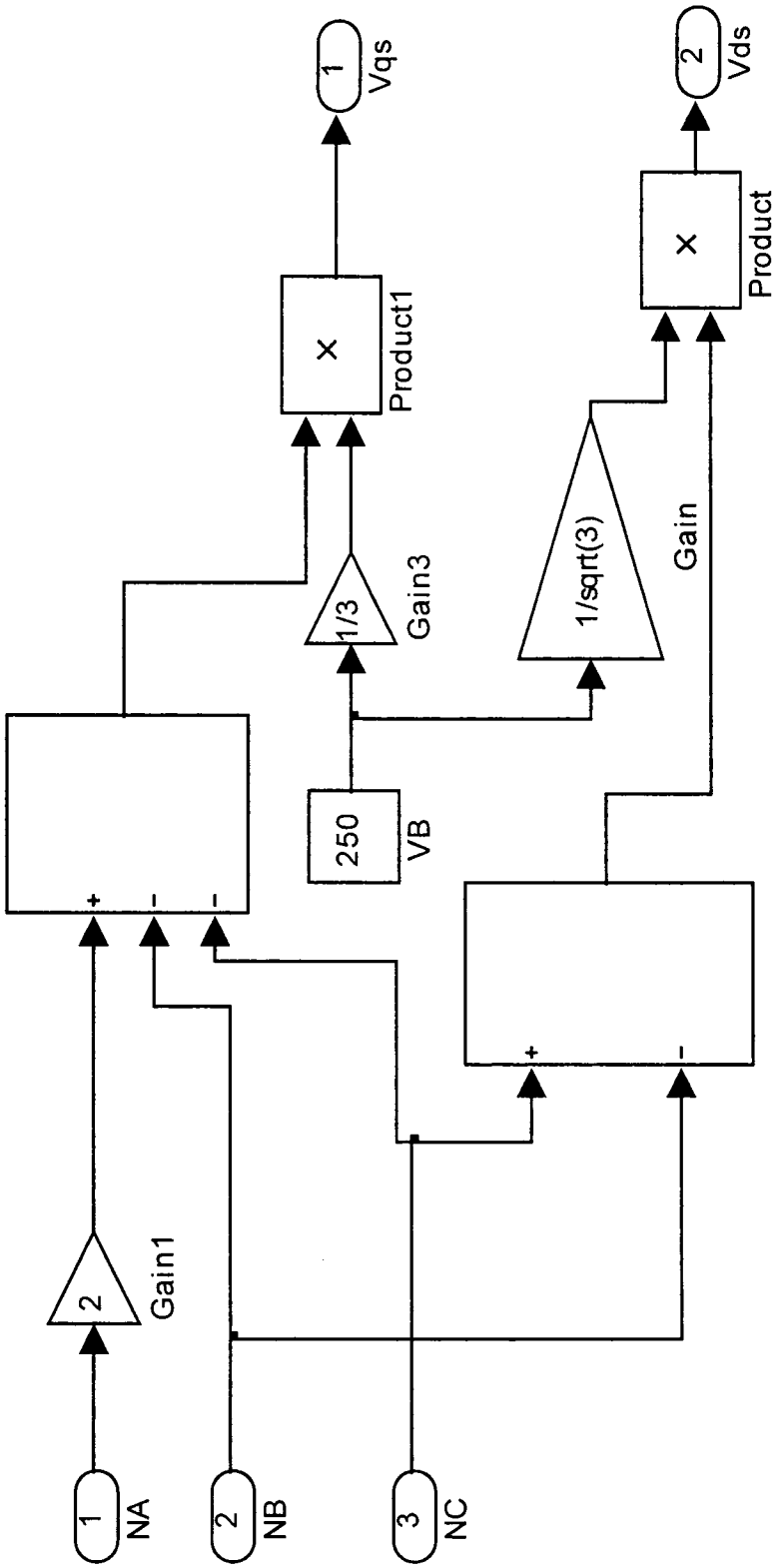

B3. 3-Phase Inverter

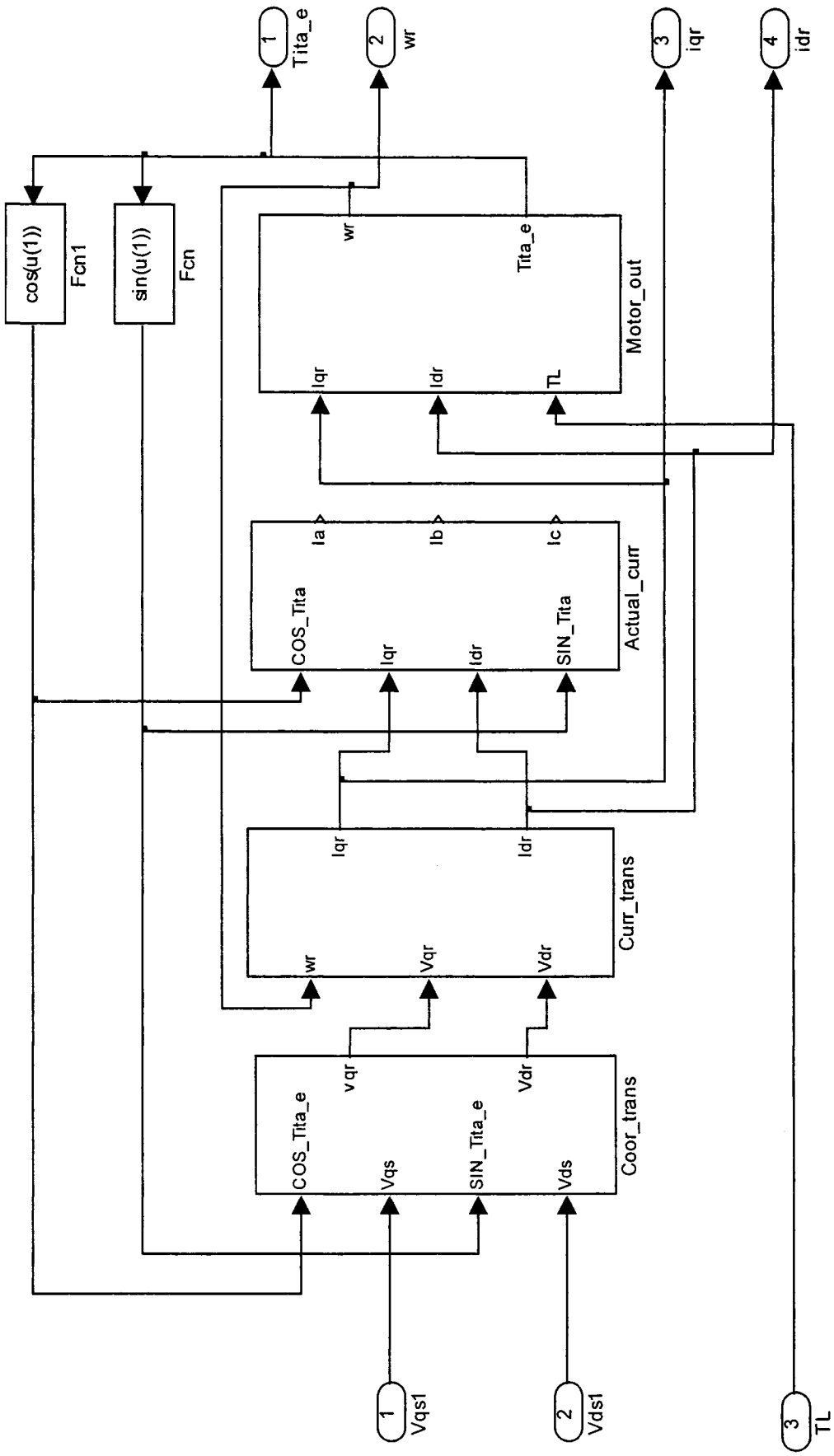

B4. Motor Subsystem

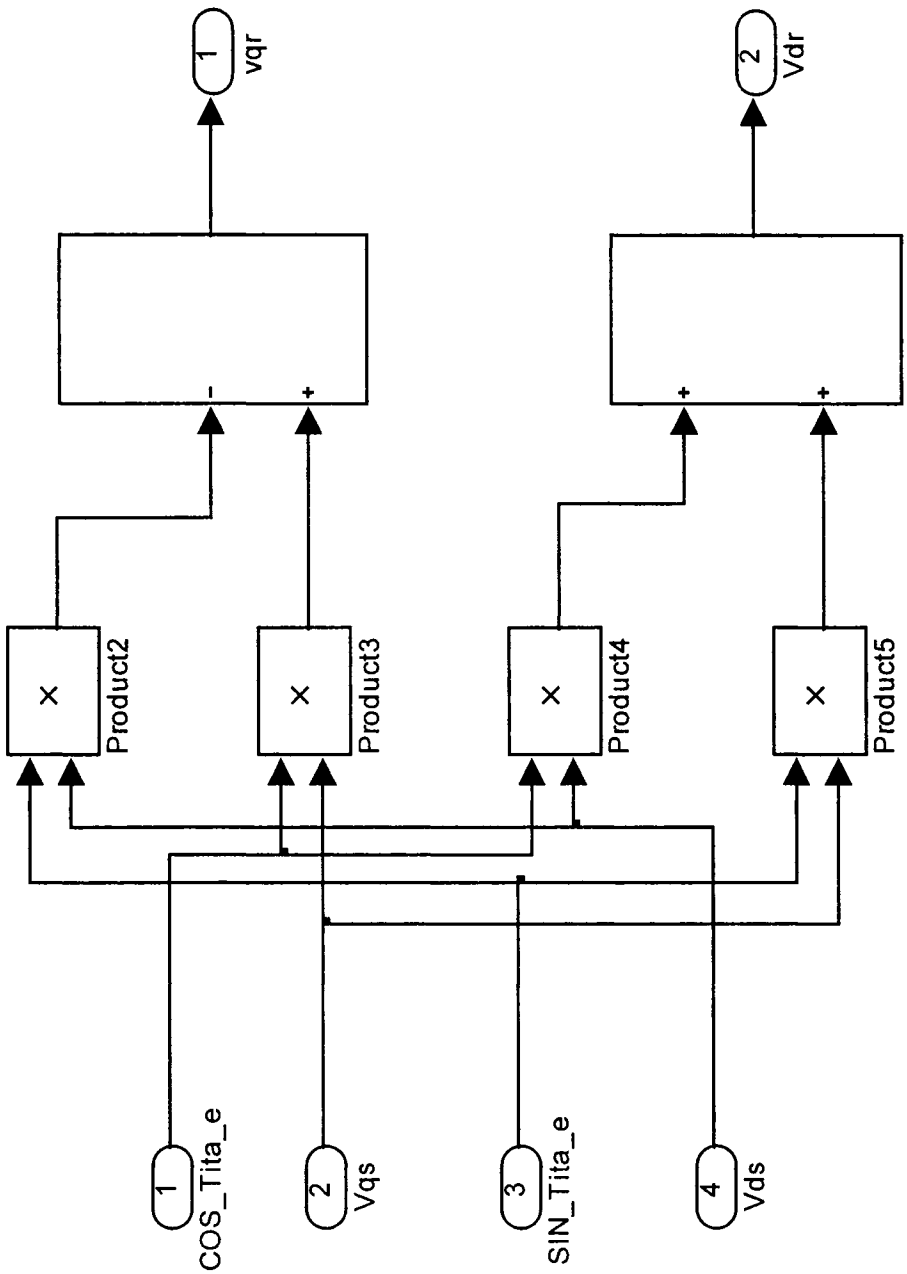

B4.1. Co-ordinate Transformer Subsystem (Coor_trans)

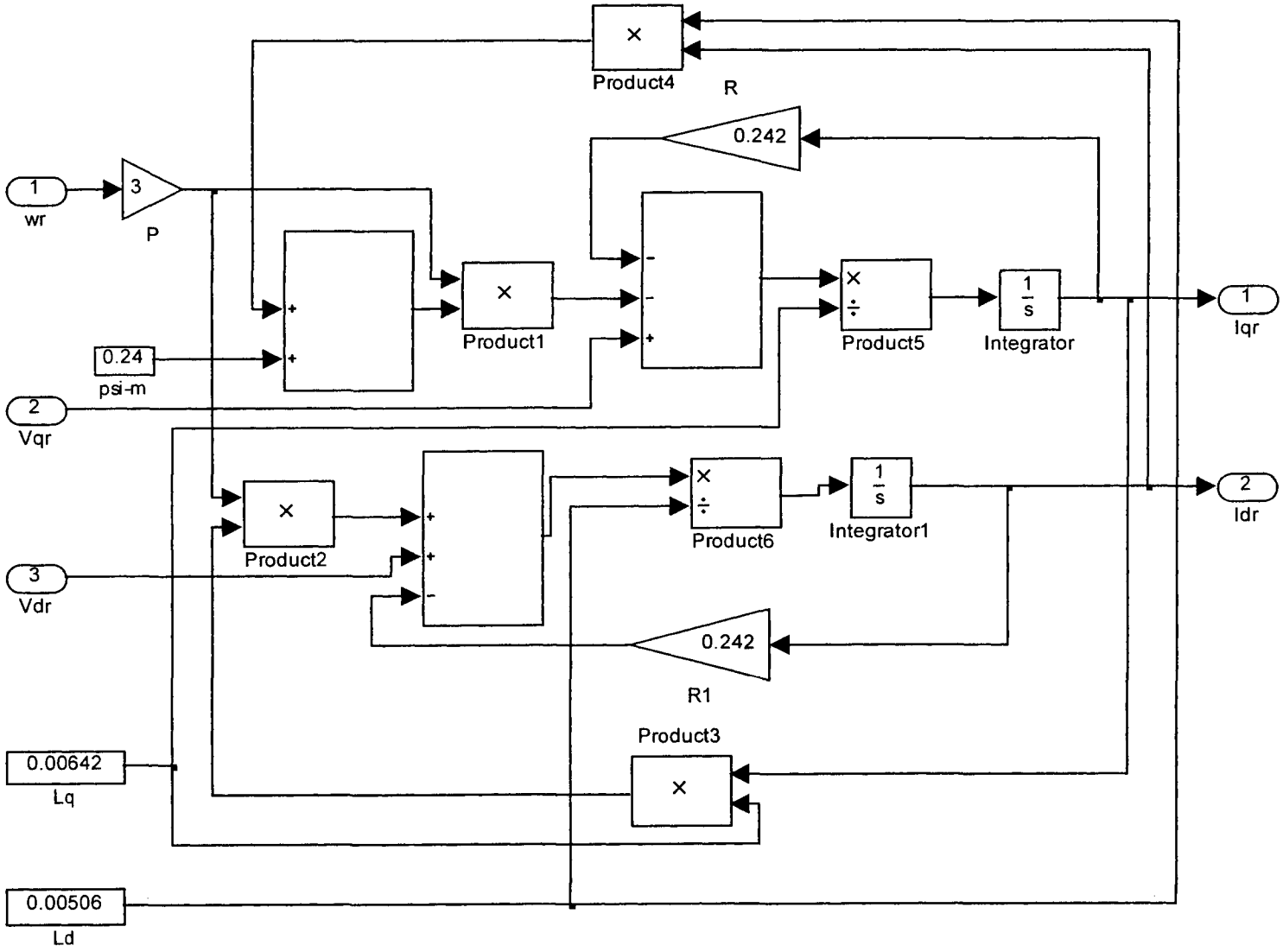

B4.2. Current Transformer Subsystem (Curr_trans)

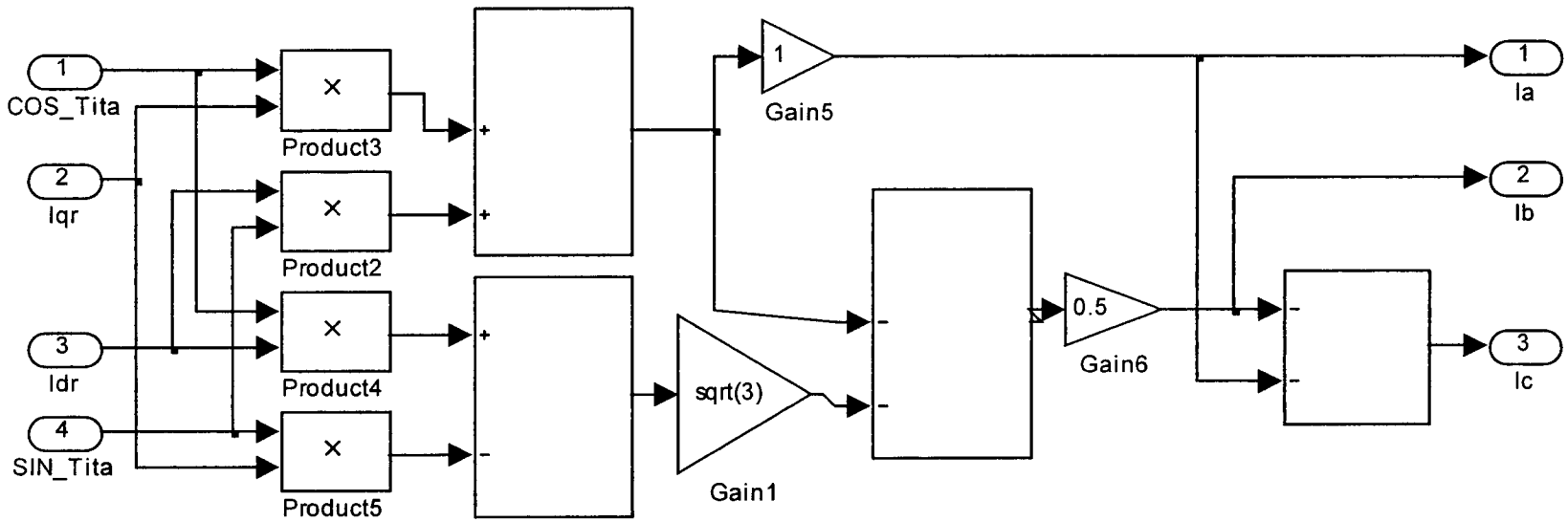

B4.3. Vector Rotator Subsystem (Actual_curr)

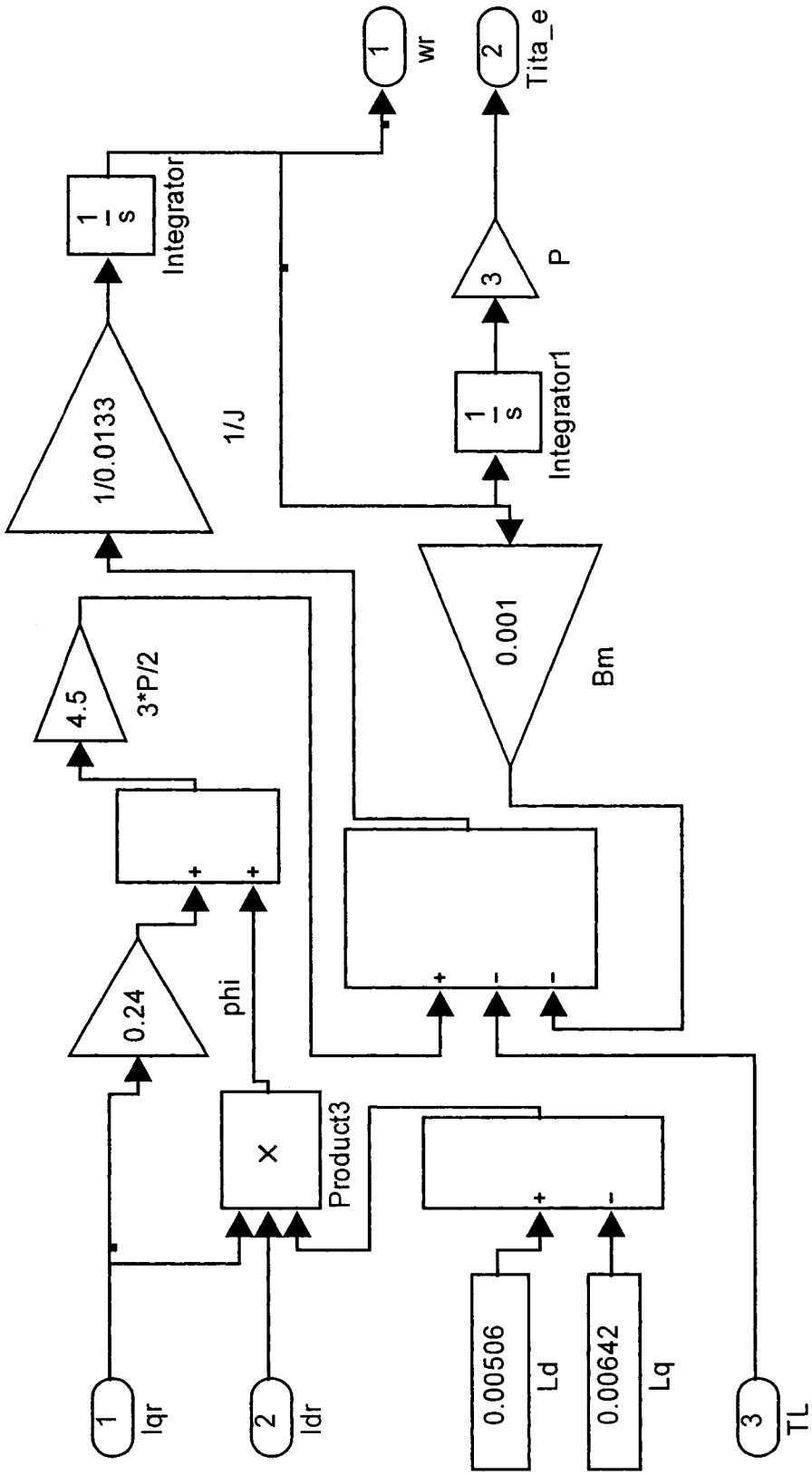

B4.4. Motor Output Subsystem (Motor_out)

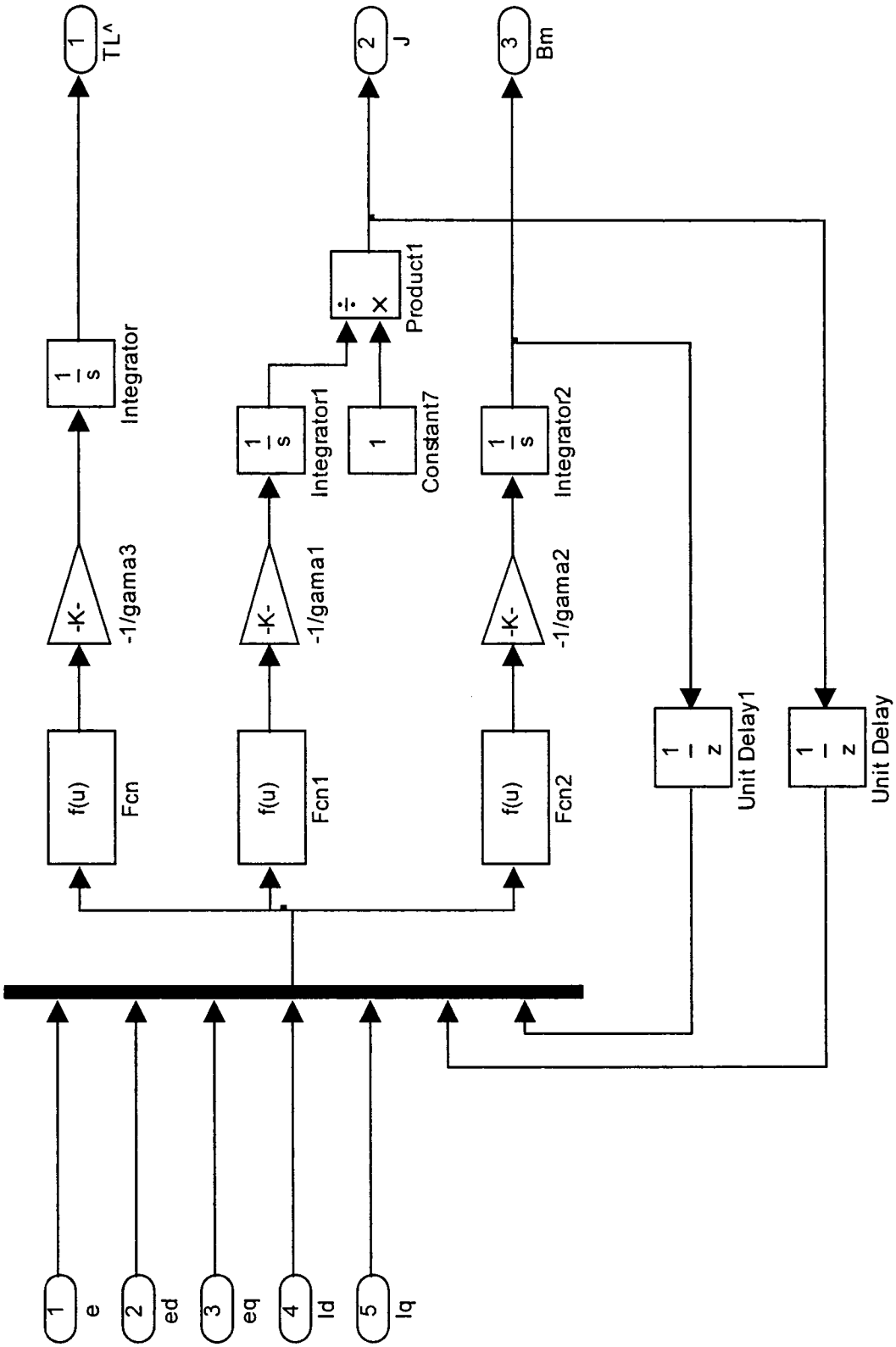

B.5. Parameter Estimator

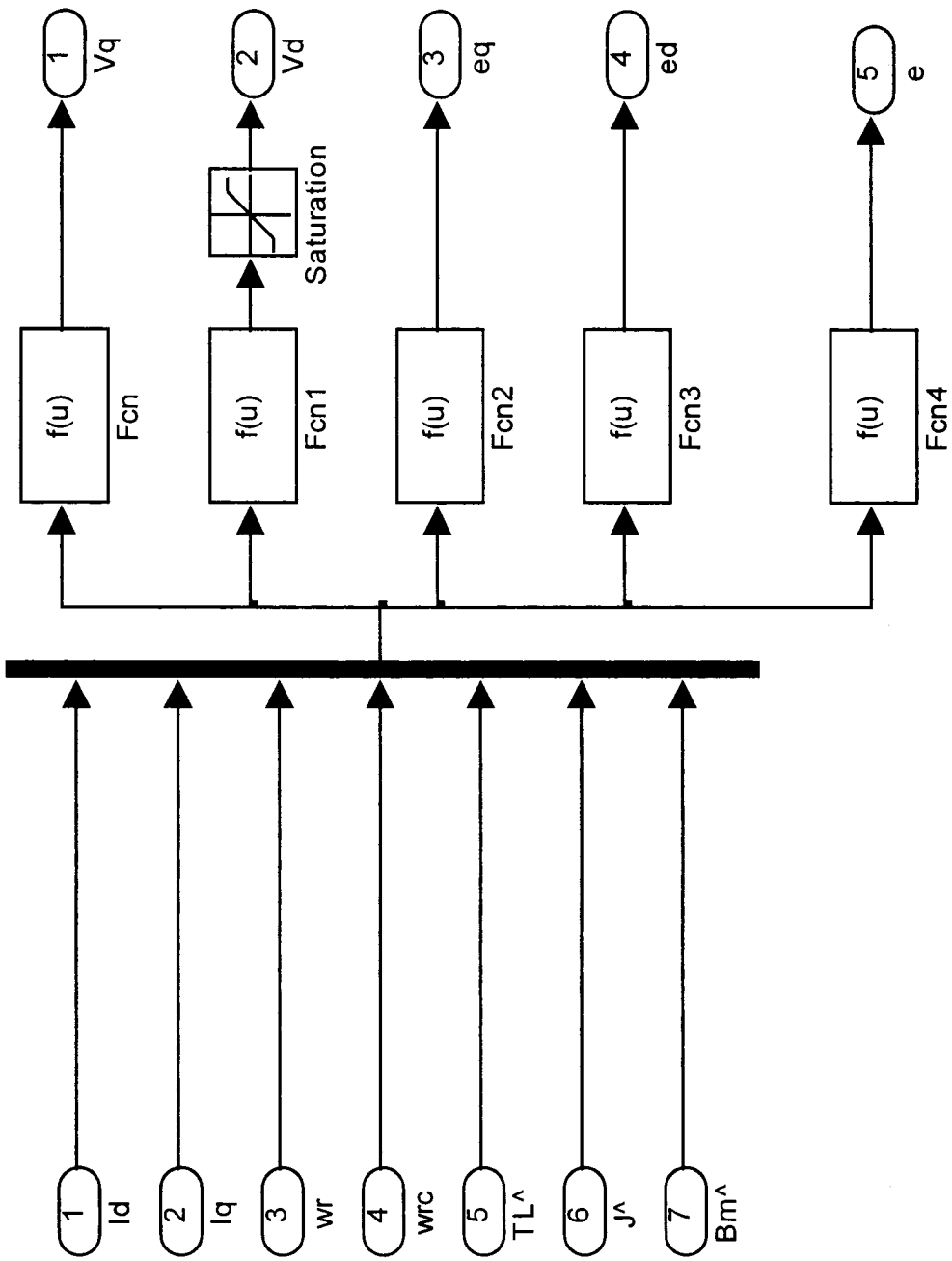

B.6. Adaptive Controller

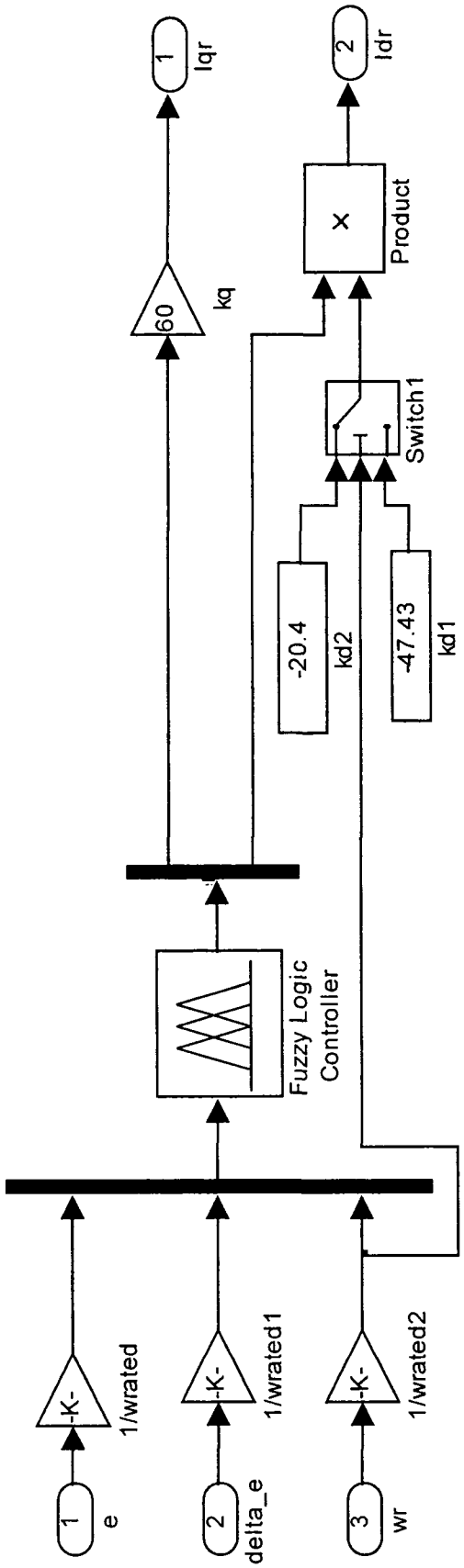

B.7. Fuzzy Logic Controller (Proposed)

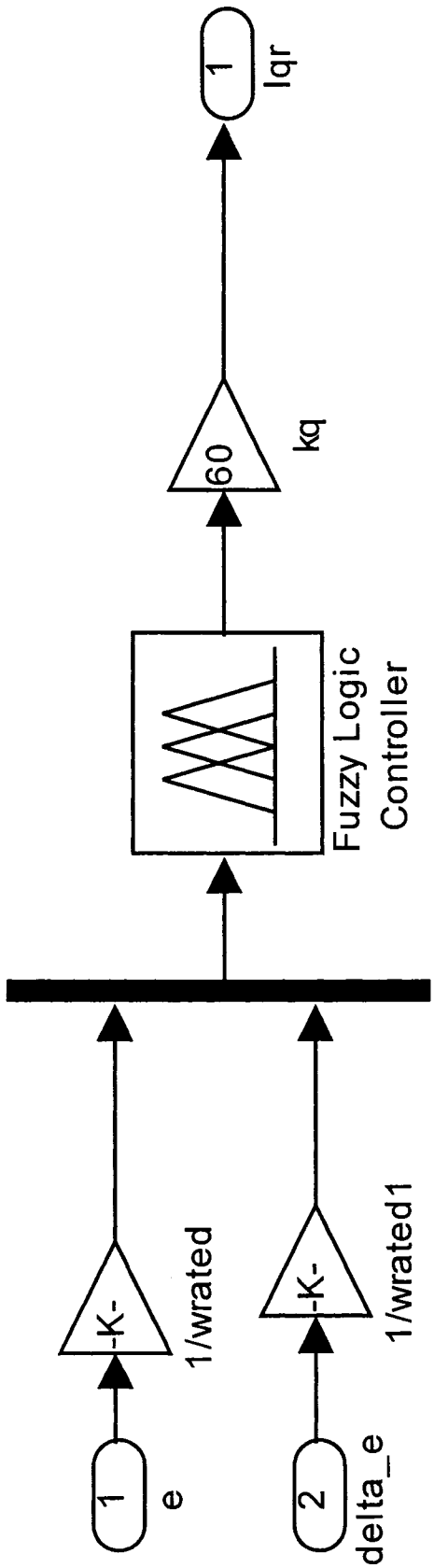

B.8. Fuzzy Logic Controller (Conventional)

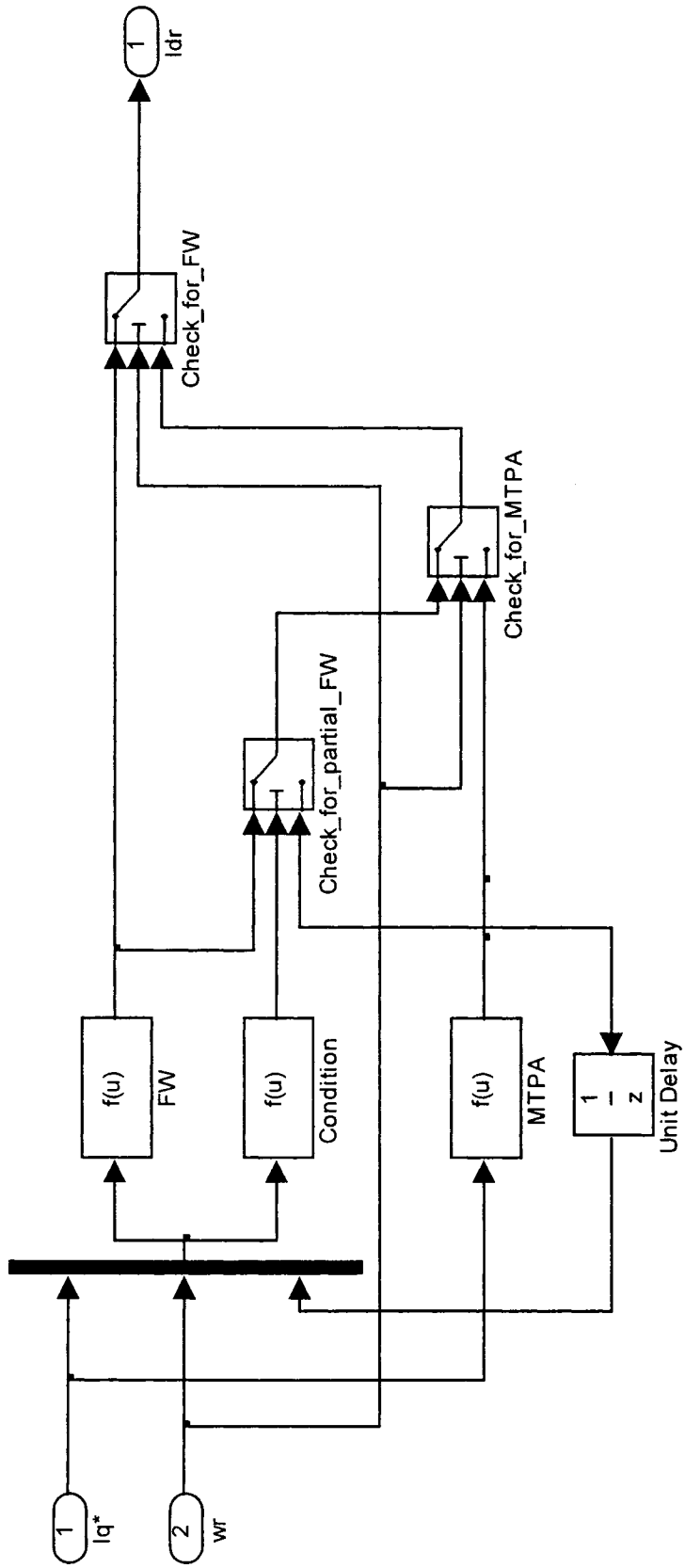

B.9. Flux Controller

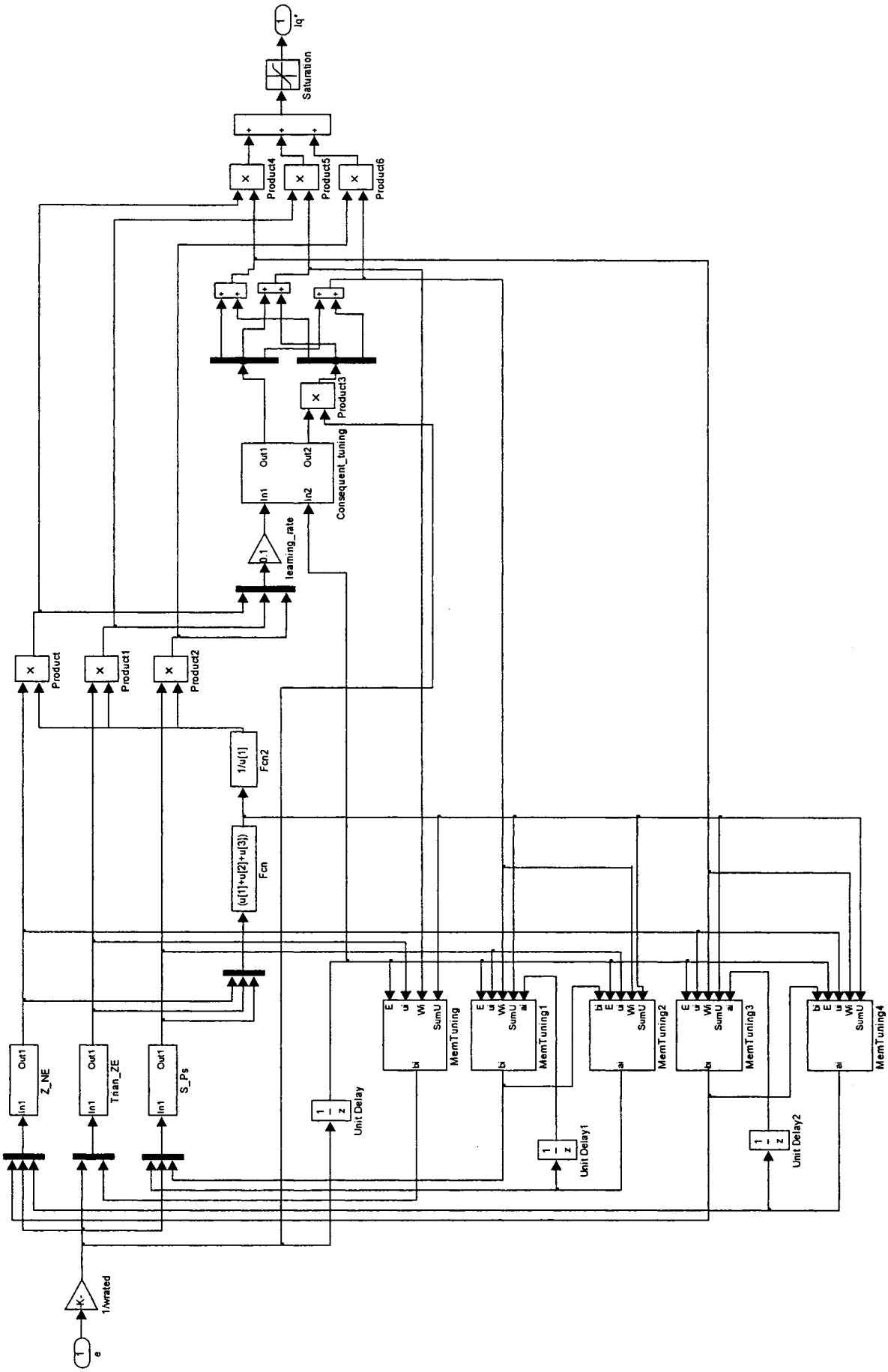

B.10. Neuro-Fuzzy Logic Controller

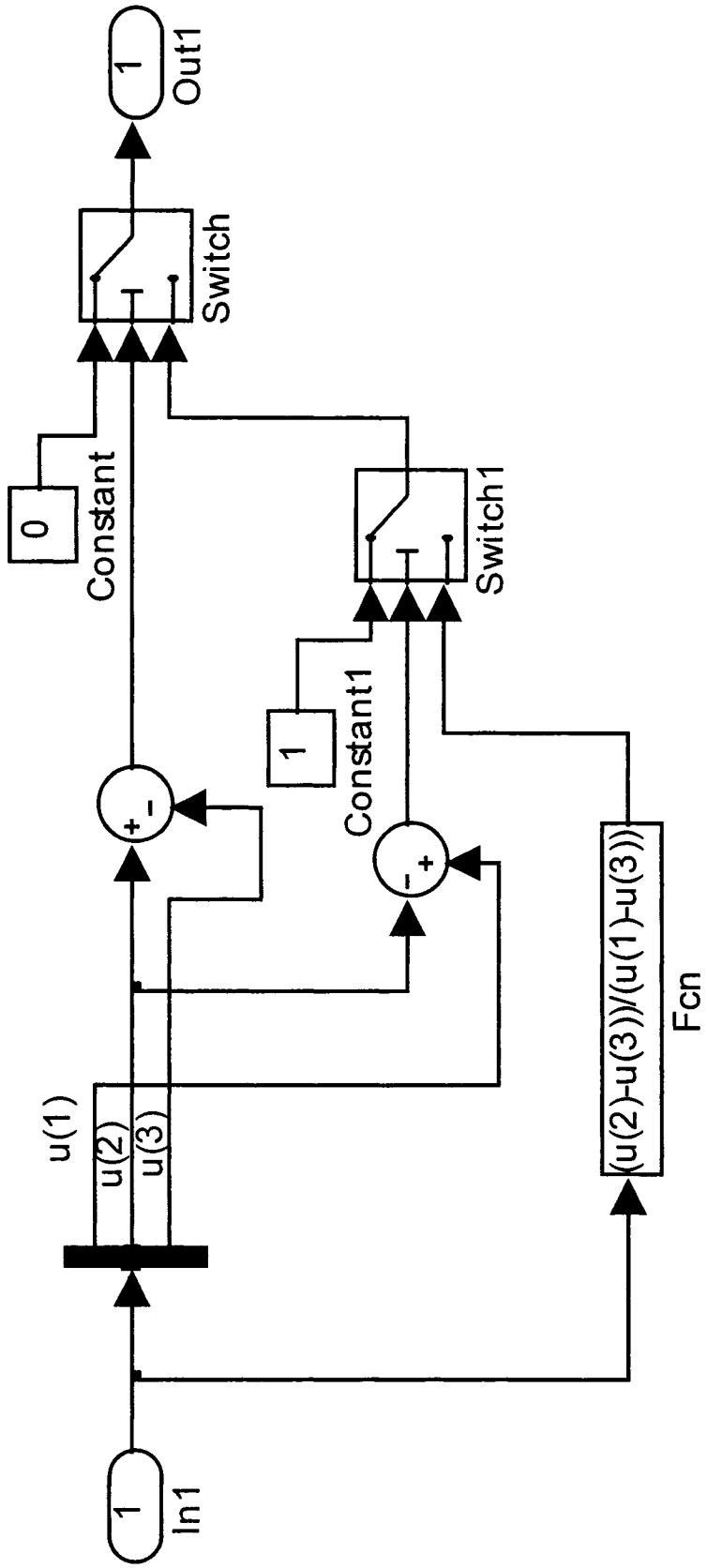

B.10.1. Fuzzy Value Calculator Subsystem for Z function (Z_NE)

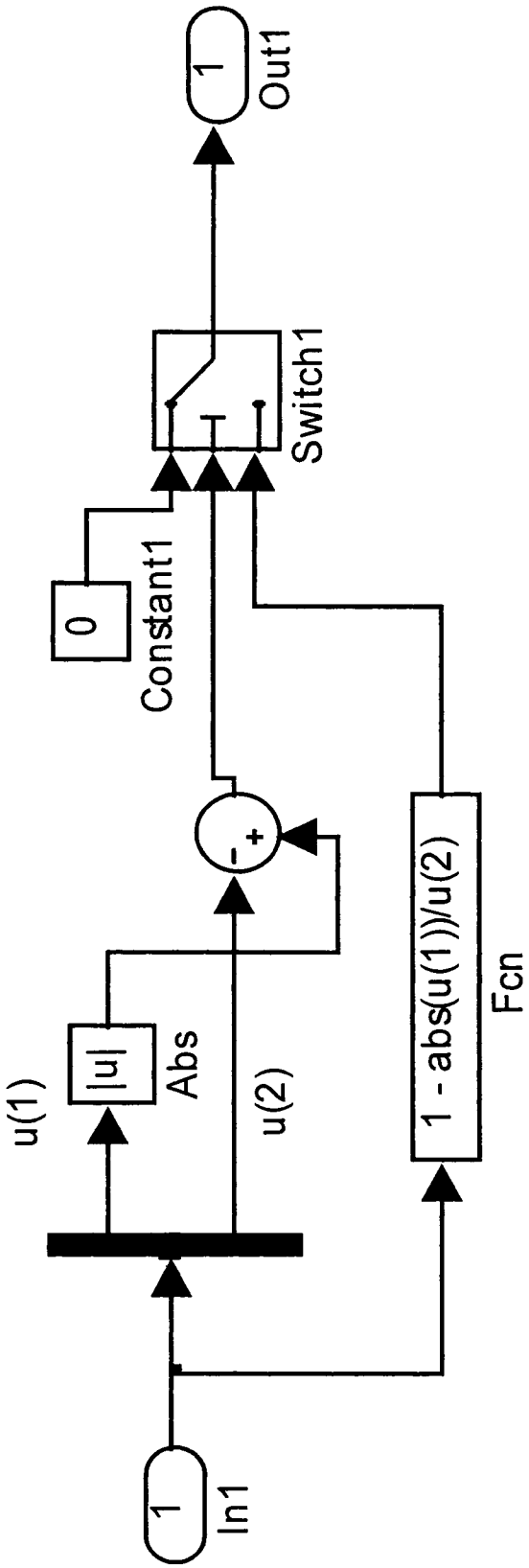

B.10.2. Fuzzy Value Calculator Subsystem for Triangle function (Trian_ZE)

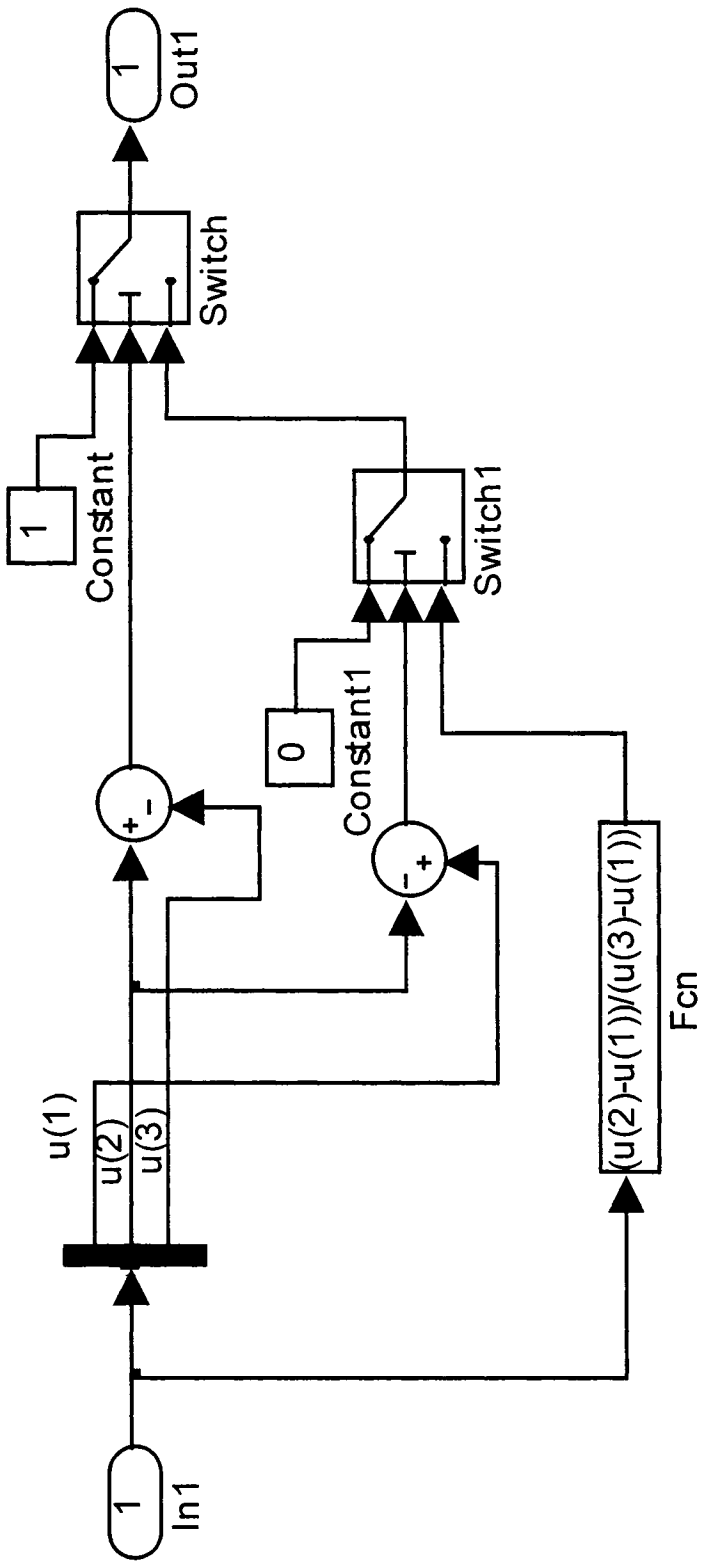

B.10.3. Fuzzy Value Calculator Subsystem for S function (S_PE)

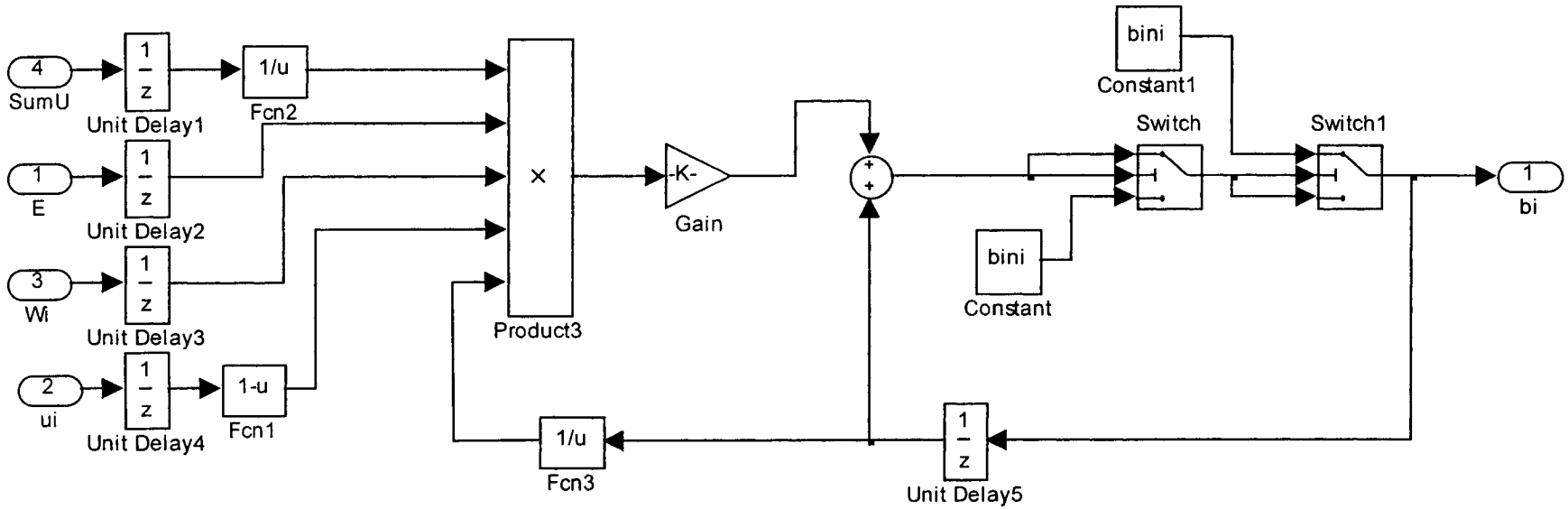

B.10.4. Membership Tuning Subsystem for b_2 (MemTuning)

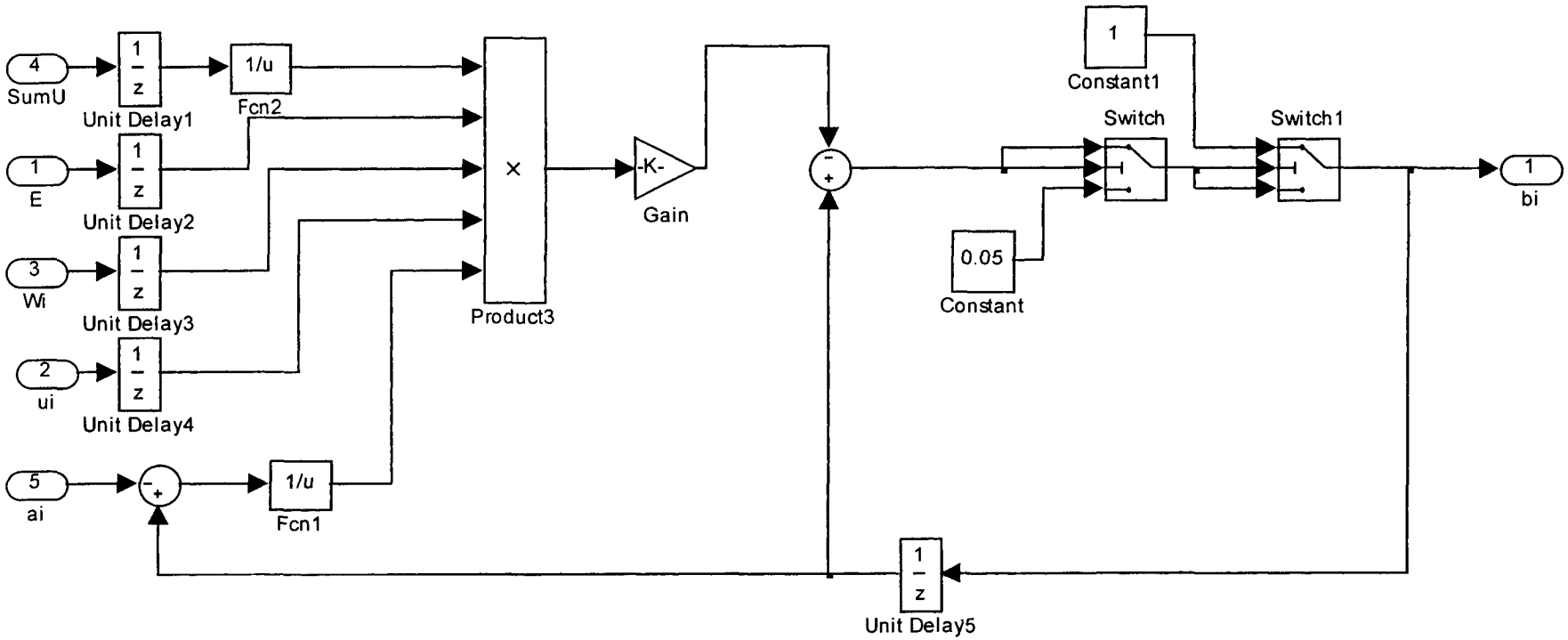

B.10.5. Membership Tuning Subsystem for b_3 (MemTuning1)

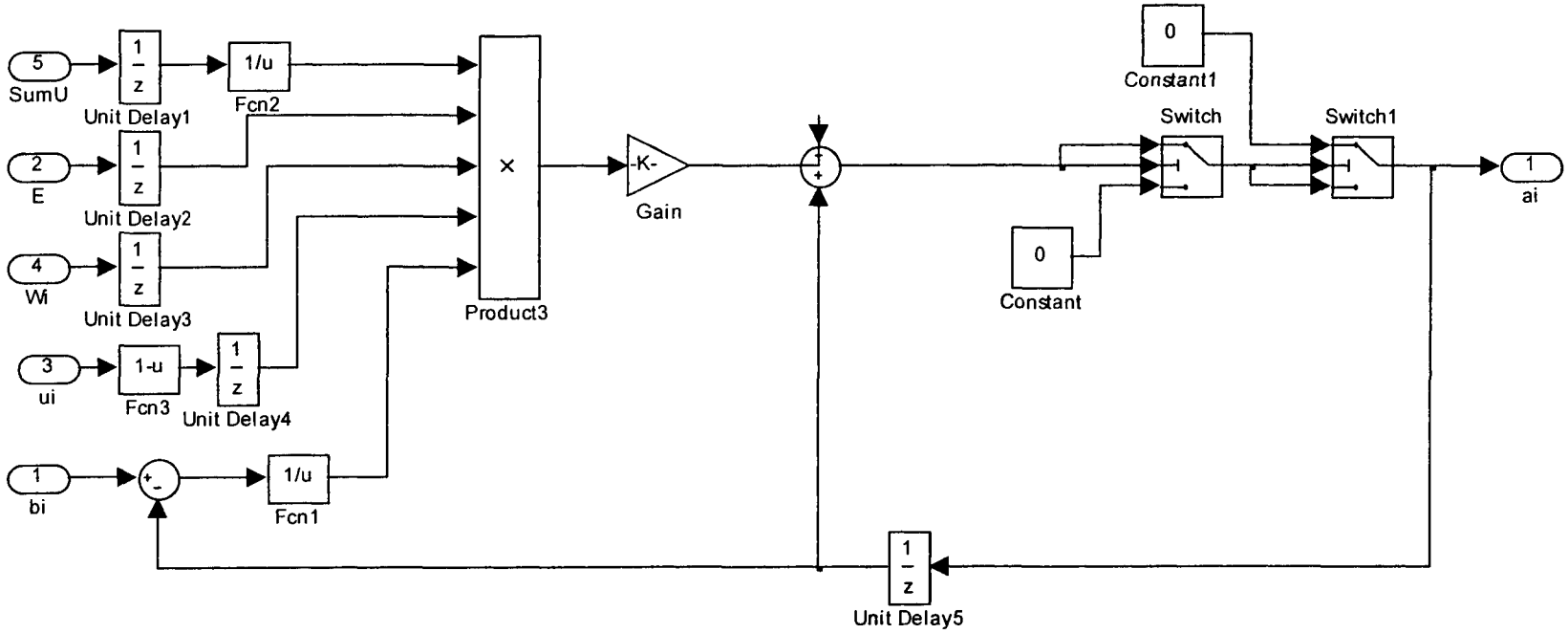

B.10.6. Membership Tuning Subsystem for a_3 (MemTuning2)

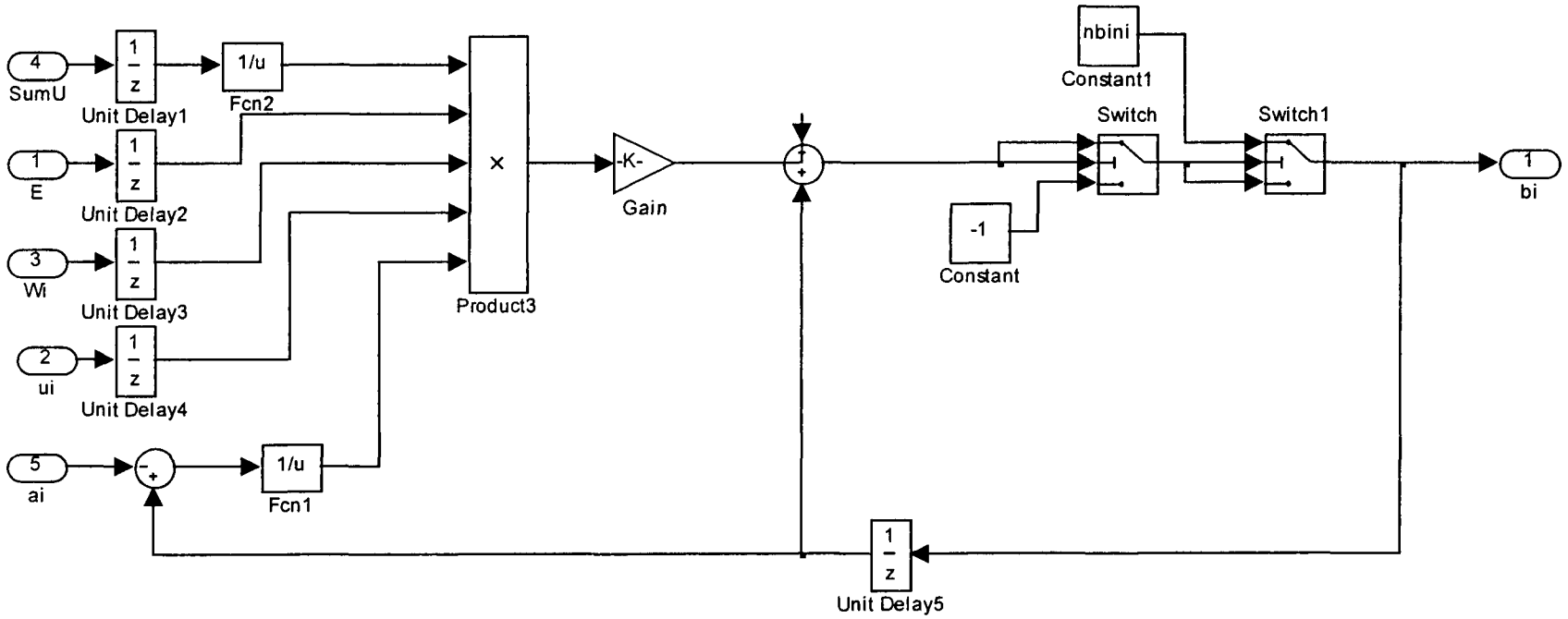

B.10.7. Membership Tuning Subsystem for b_1 (MemTuning3)

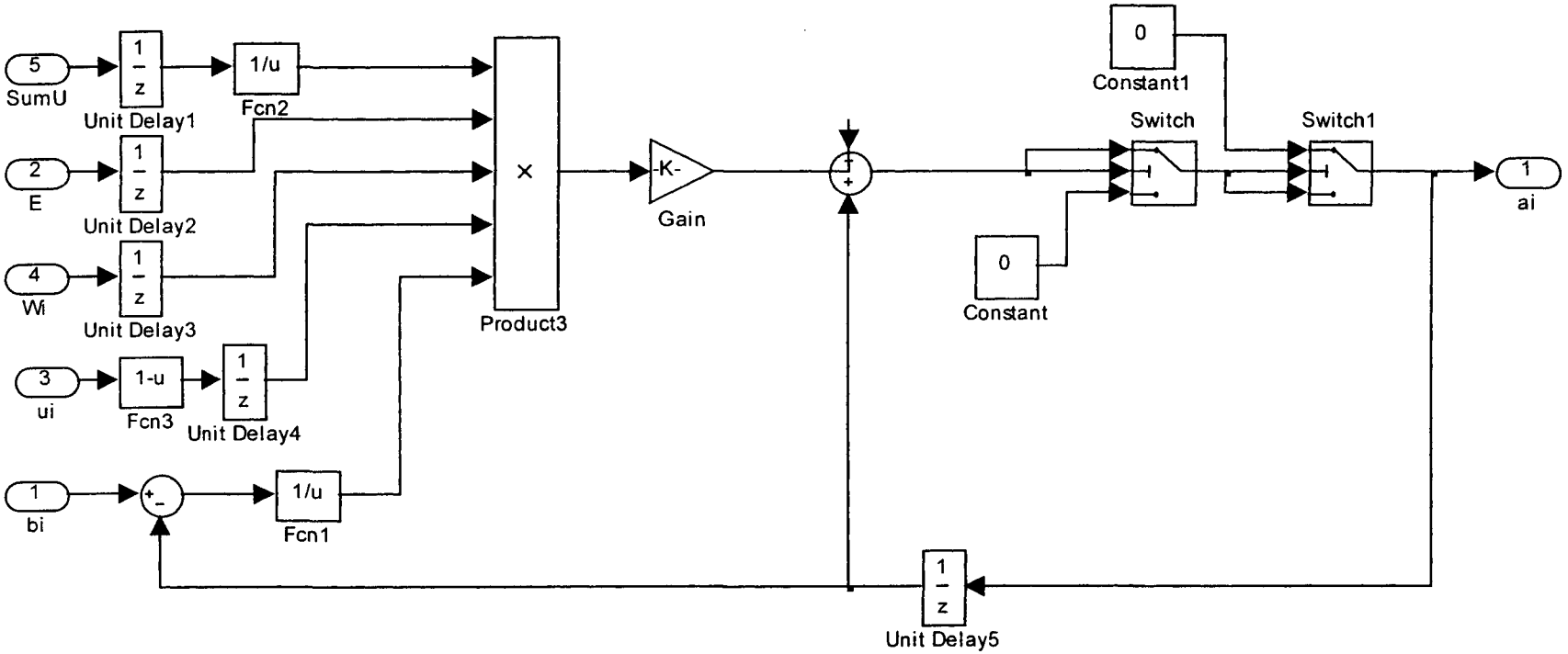

B.10.8. Membership Tuning Subsystem for a_1 (MemTuning4)

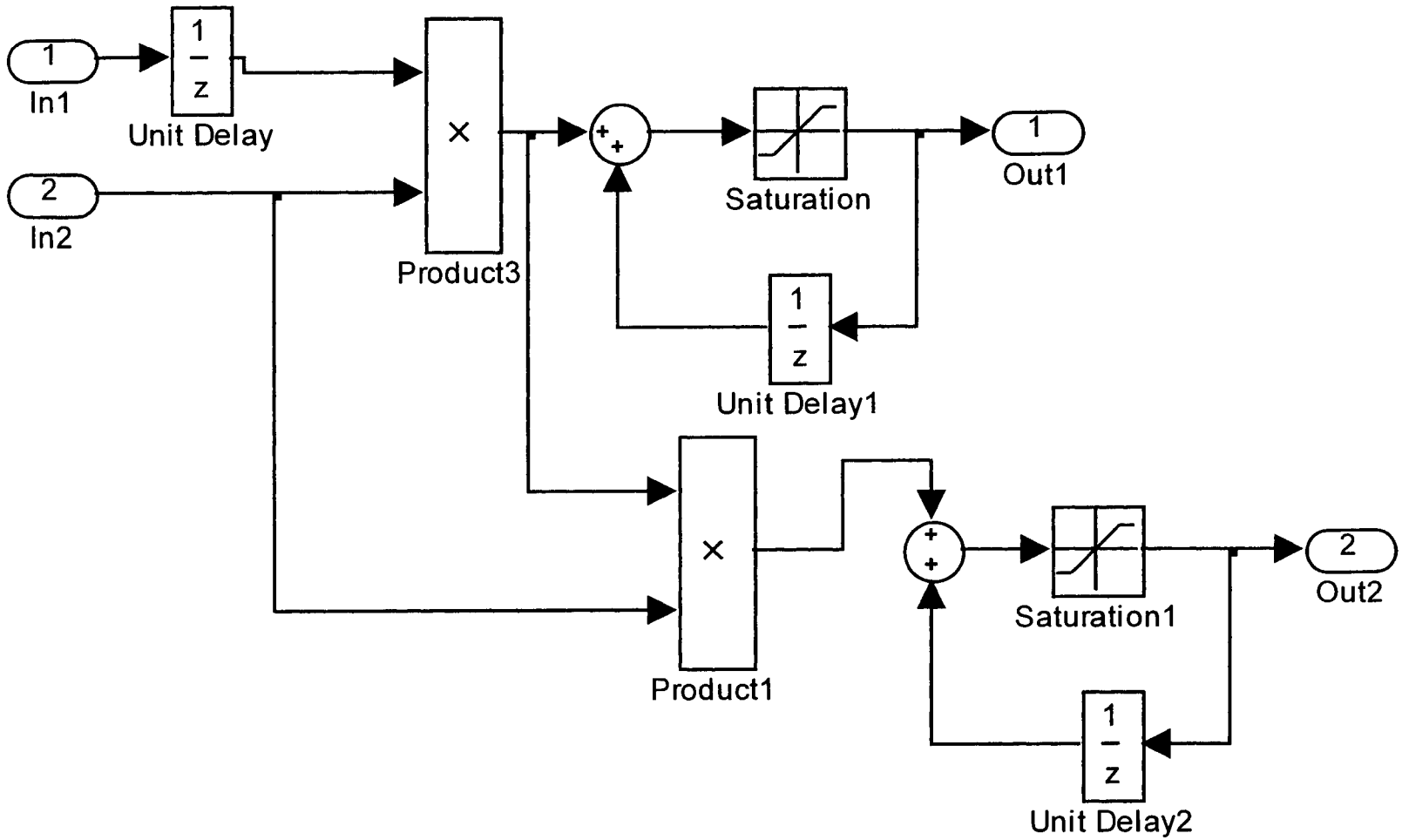

B.10.9. Tuning Subsystem for Consequent Parameter (Consequent_tuning)

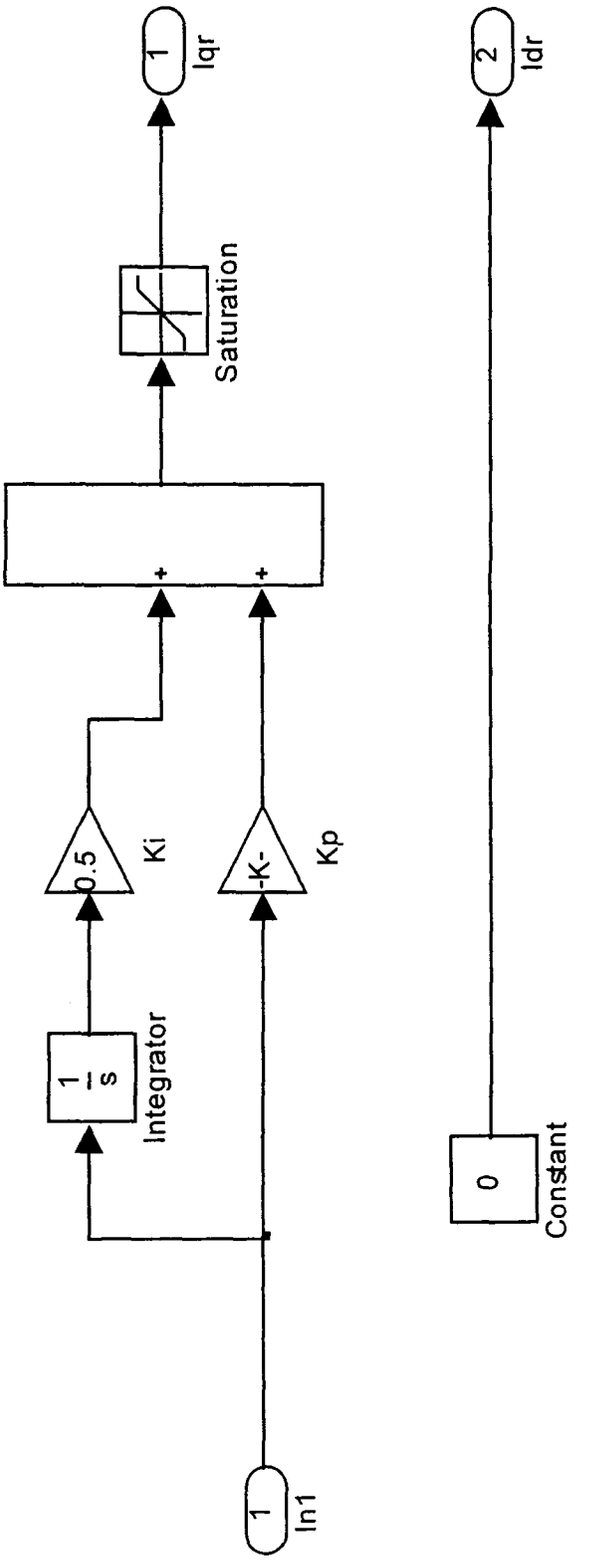

B.11. PI Controller

Appendix C

Base drive circuit for the inverter and interface circuit for the current sensor

R1= R2 = R3 = R4 = R5 = R6 = 1.5k

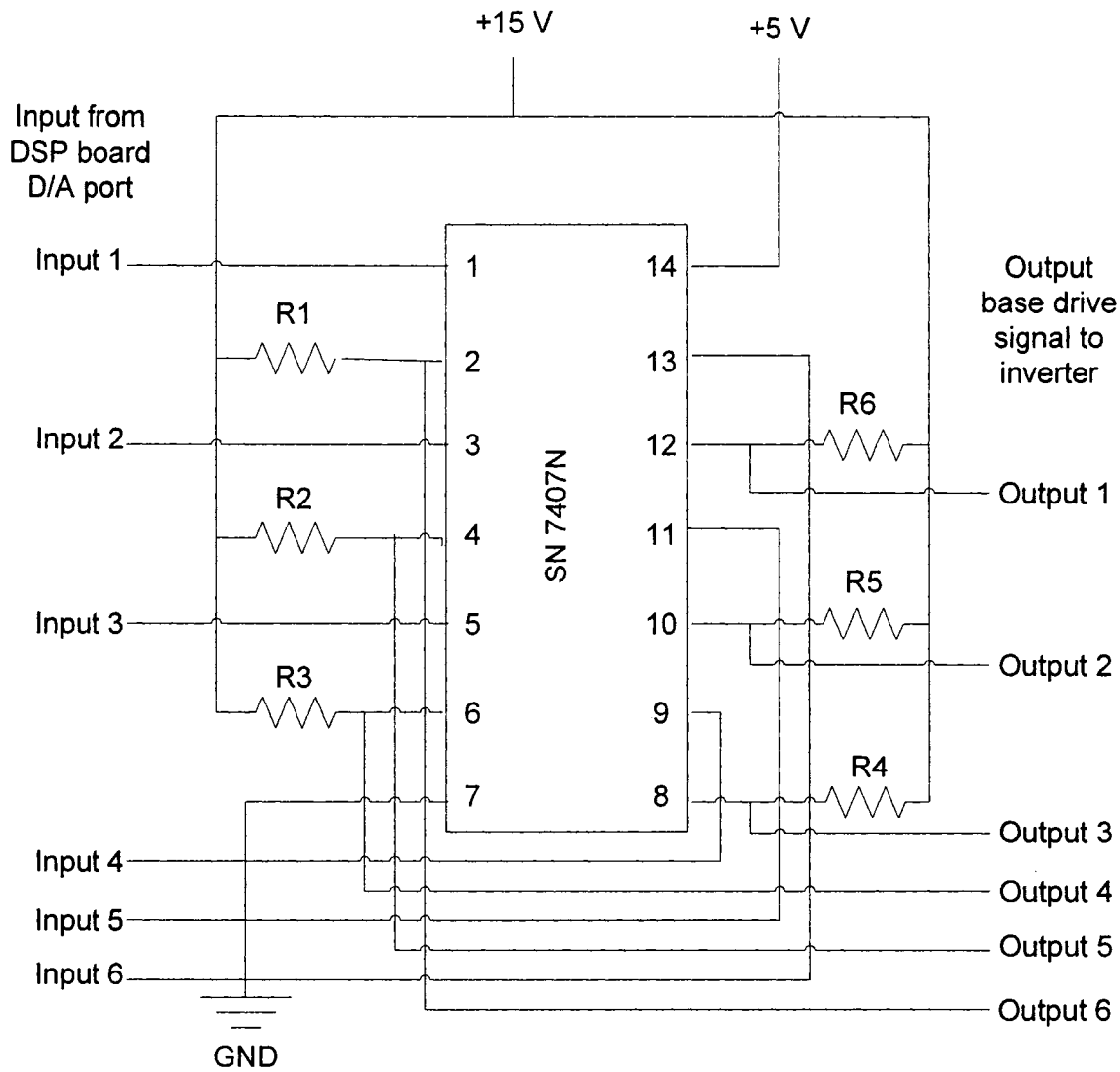

C.1. Base drive circuit for the inverter

Gain of Op-Amp (741CN) = 1+R3/R2

Magnitude of resistors:

	Current sensor for phase 'a'	Current sensor for phase 'b'
R1	98.7 ohm	99 ohm
R2	1.8 k	2 k
R3	5.5 k	5.1 k

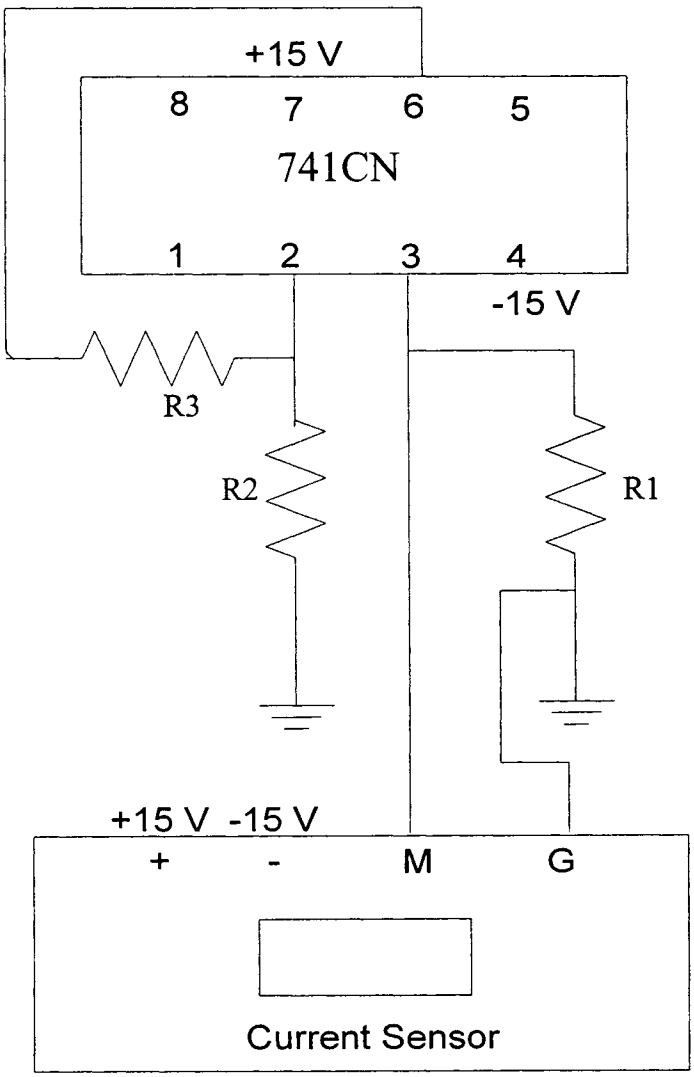

C.2. interface circuit for the current sensor

Appendix D
Real-Time Simulink Model

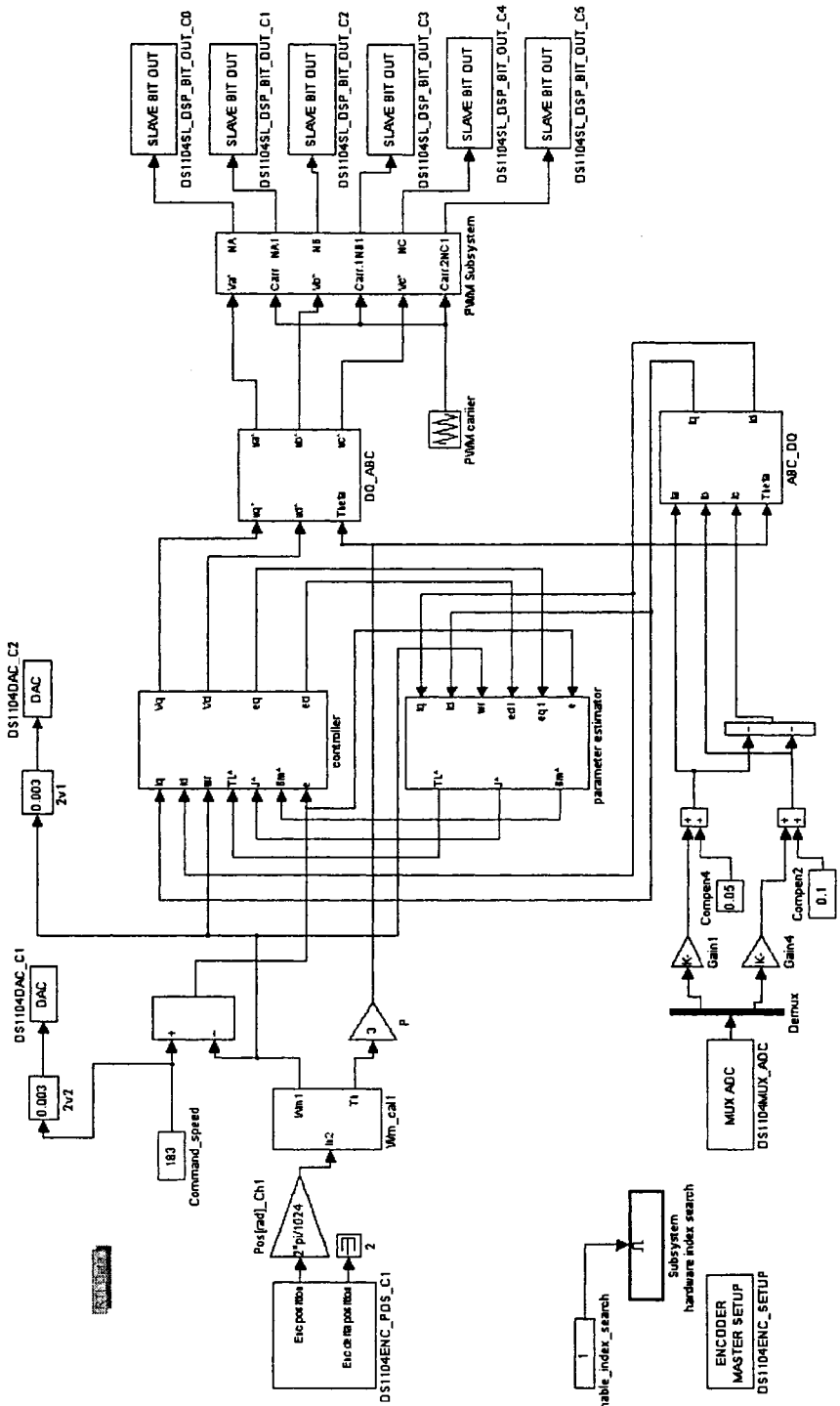

D1. Real-time Simulink model for the ABNC based IPMSM drive

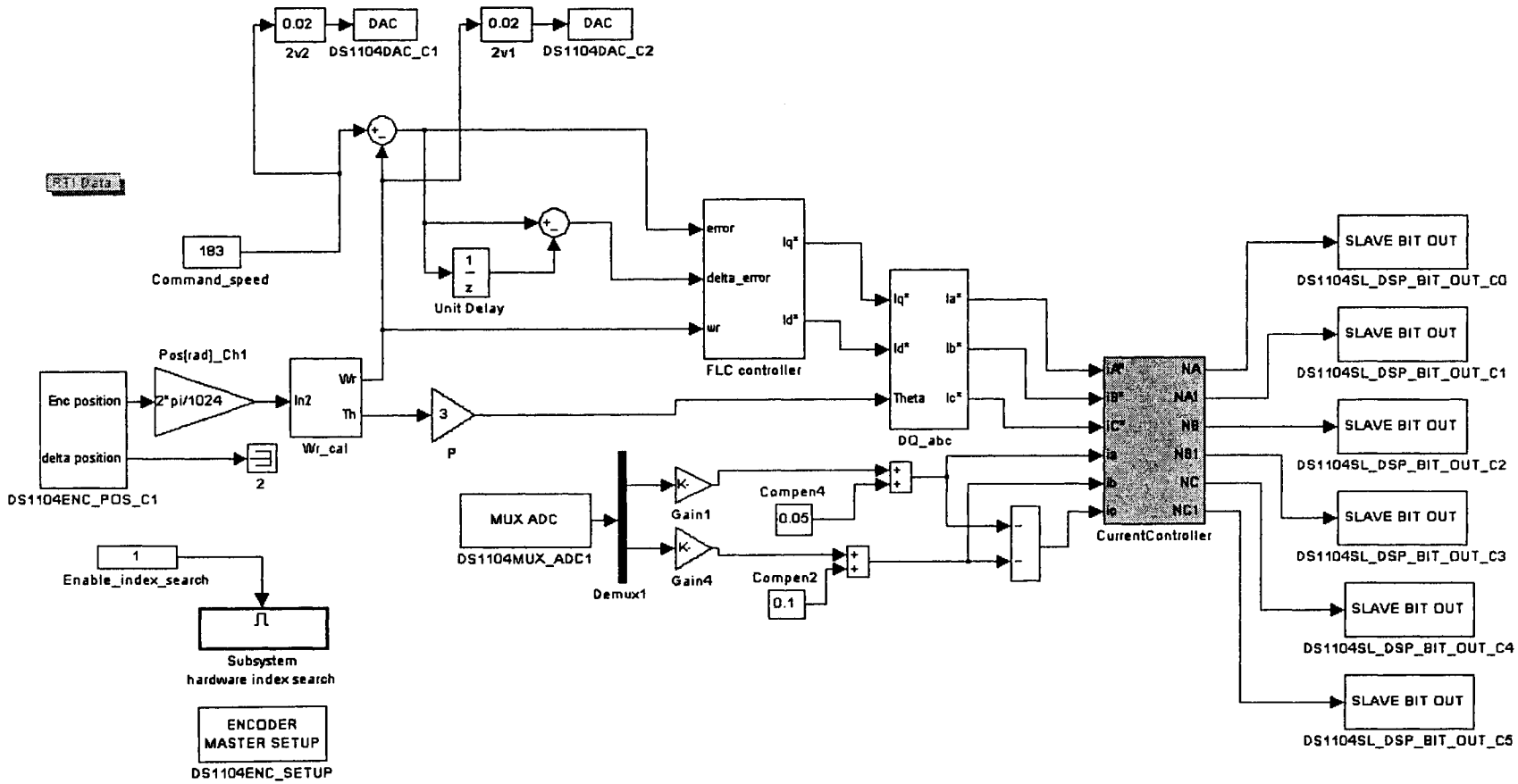

D2. Real-time Simulink model for the FLC based IPMSM drive

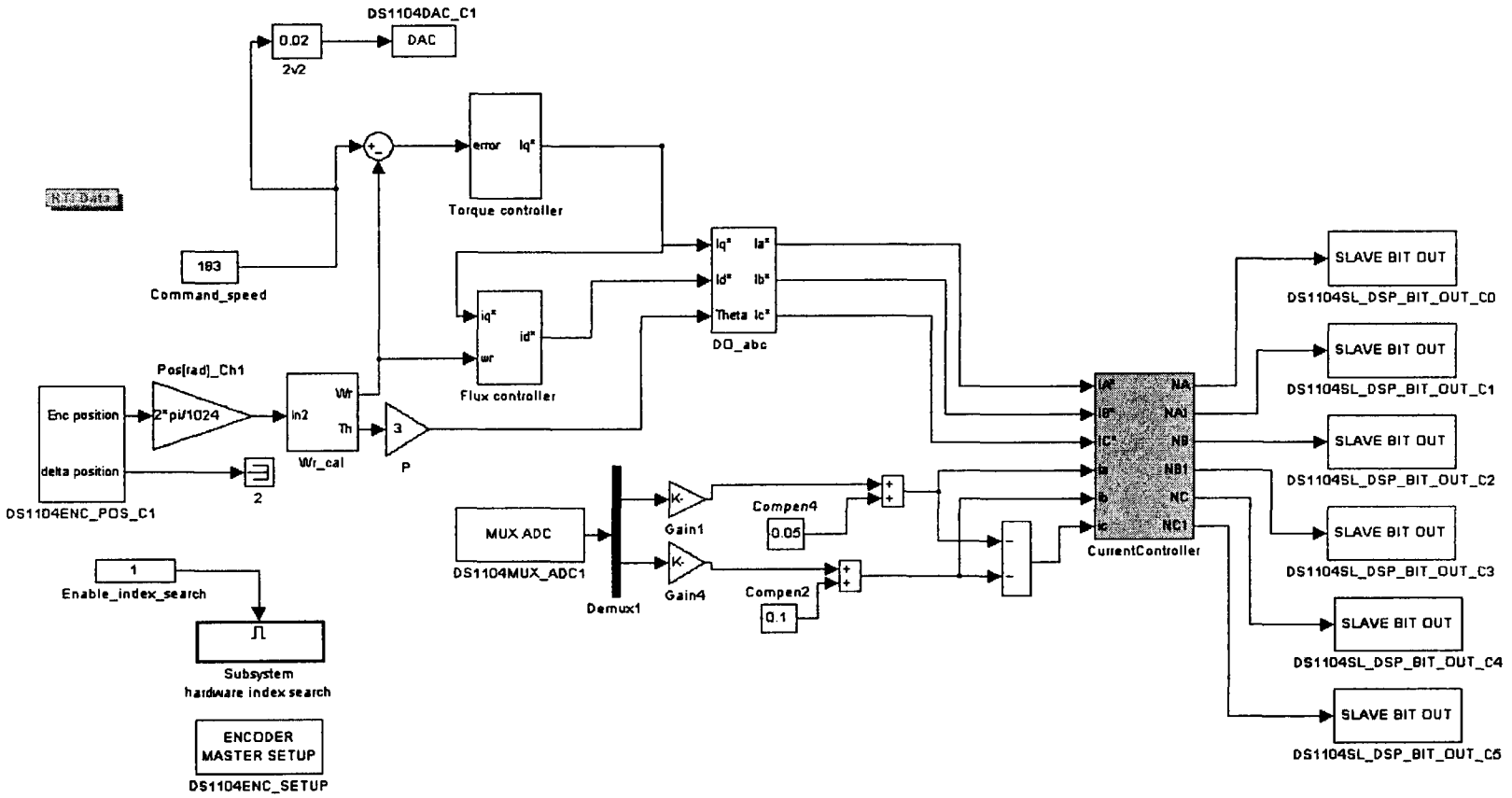

D3. Real-time Simulink model for the ANFIS based NFC controller of IPMSM drive